2013

Mechanism of Translational Control by the Fragile X Mental Retardation Protein and Creation of the FMRP CTAG Mouse

Sarah Van Driesche

MECHANISM OF TRANSLATIONAL CONTROL BY THE FRAGILE X MENTAL RETARDATION PROTEIN AND CREATION OF THE FMRP CTAG MOUSE

A Thesis Presented to the Faculty of

The Rockefeller University

in Partial Fulfillment of the Requirements for

the degree of Doctor of Philosophy

by

Sarah Van Driesche

June 2013

MECHANISM OF TRANSLATIONAL CONTROL BY THE FRAGILE X MENTAL RETARDATION PROTEIN AND CREATION OF THE FMRP CTAG MOUSE

Sarah Van Driesche, Ph.D.
The Rockefeller University 2013

The Fragile X Mental Retardation Protein (FMRP) is a neuronal RNA-binding protein that is predominantly associated with polyribosomes. Loss of FMRP results in Fragile X Syndrome, characterized by mental retardation, autism and epilepsy. FMRP was recently found to be associated with a specific set of mRNAs with key roles in neuronal function and to physically interact with targeted mRNAs along their entire coding sequences (Darnell 2011). Here, we find that FMRP inhibits translation on these target transcripts by stalling ribosomes, both *in vivo* and in rabbit reticulocyte lysate programmed with endogenous brain polyribosomes. In these systems, loss of FMRP function resulted in increased ribosome runoff after treatment with puromycin, a drug that acts specifically on translocating ribosomes. In addition to genetic loss-of-function models, FMRP-dependent relief of ribosome stalling could be induced by acute biochemical removal of FMRP from polysomes, indicating reversibility of stalling. FMRP was also directly visualized on stalled polysomes by immunoelectron microscopy. Together, these results suggest a model in which FMRP actively regulates translation of target mRNAs by stalling ribosomes. To further advance our understanding of FMRP function, we have created the FMRP cTAG mouse, a knock-in model in which FMRP can be conditionally tagged with AcGFP in a Cre-dependent manner while maintaining wt FMRP expression in all Cre-negative cells. The cTAG mouse will be a valuable tool in the study of cell type-specific FMRP function.

ACKNOWLEDGEMENTS

I am deeply grateful for the help and support of many people during the last seven years. First and foremost, I would like to thank my advisors, Bob and Jen Darnell, for their unwavering support. They are very good at doling out encouragement and a kick in the pants at the right doses and at the right times, to good effect. Their mentorship has been instrumental in helping me to mature as a scientist. Second, I would like to thank the skilled and dedicated technicians that our lab is lucky to have, as well as our saintly lab managers, Jeff Smith and Brian Houck-Loomis. In particular, I would like to thank Sharon Hung for handling all the radioactive steps of my CLIP experiments during my pregnancy. Sharon is unbelievably hard working and pays meticulous attention to detail; qualities that will serve her very well as she embarks on her own PhD journey at Harvard next fall. Third, I would like to thank Chaolin Zhang for his endless patience in answering my bioinformatics questions. I am sure he has better things to do with his time. Fourth, I would like to thank Eleana Sphicas for her help with using the electron microscope and the members of the Gene Targeting Facility for their help in design and targeting of the FMRP cTAG mouse. Fifth, I would like to thank the members of my committee: Nat Heintz, Mike Rout and Eric Klann, for their advice, discussions and valuable time. Sixth, I would like to thank all of my labmates, for their advice, support and camaraderie. You guys are a great bunch.

Last but not least, I owe an enormous amount of thanks to my family. Over the years, I have eaten many delicious dinners and spent many nights at my grandmother's house, which was a nice way to end a long day. I would like to thank my mom and dad, for letting me keep a number of fish tanks and a snapping turtle in the house way back when I was getting interested in science. I would like to thank our new baby, Avni Jaya Mandal, for putting up with a thesis-writing mama from the moment she entered this world. And finally, I would like to thank my wife, Purnima Mandal. We came to New York together ten years ago with dreams of becoming a doctor, getting a PhD, and becoming parents. This year, all three of those things have come true and I am unbelievable happy.

Table of Contents

List of Figures

List of Tables

LIST OF ABBREVIATIONS

APRA	Antibody Positioned RNA Amplification
BWB	Bead Wash Buffer
CLIP	Crosslinking and Immunoprecipitation of RNA-Protein complexes
cTAG	Conditional TAG
DHPG	Dihydroxyphenylglycine
DIV	Days *In Vitro*
EJC	Exon Junctioin Complexes
ER	Endoplasmic Reticulum
FXG	FXR- containing Granule
FXS	Fragile X Syndrome
HITS	High-Throughput Sequencing
IEGs	Immediate Early Genes
IP	Immunoprecipitation
IVT-EBP	*In vitro* Translation of Endogenous Brain Polysomes
KH	K-homology
LTD	Long-Term Depression
LTP	Long-Term Potentiation
MECS	Maximal Electroconvulsive Shock
NMD	Nonsense-Mediated Decay
PC	Purkinje Cell
PSD	Post-Synaptic Density
RBPs	RNA Binding Proteins
RIP-CHIP	coIPed RNAs
RPKM	Reads Per Kilobase of transcript per Million mapped reads
RRS	Retained Ribosome Score
SPR	Signal Recogntion Particle
uORF	Upstream Open Reading Frame

Chapter I. General Introduction

Fragile X Syndrome and FMRP

Fragile X Syndrome (FXS) is the most common form of inherited mental retardation and the leading known single-gene cause of autism, occurring in 1:4500 males and 1:9000 females (O'Donnell and Warren, 2002), (Hagerman et al., 2010). Fragile X syndrome is characterized by mild to severe intellectual disability, sensory hypersensitivity, seizures, and autistic features such as poor eye contact and social anxiety, as well as by a mild craniofacial phenotype and macroorchidism. FXS is caused by expansion of a tandem CGG repeat region in the 5'UTR of the *Fmr1* gene, resulting in methylation and silencing of the locus (O'Donnell and Warren, 2002). Normal individuals have fewer than 50 of these CGG repeats, while those with FXS have 200 or more.

The protein that is absent in Fragile X syndrome, FMRP (fragile X mental retardation protein), is predominantly expressed in neurons and testes and is primarily associated with polyribosomes. FMRP was first characterized as a polysome-associated protein in non-neuronal cell lines (Eberhart et al., 1996), (Khandjian et al., 1996), (Feng et al., 1997a), (Corbin et al., 1997), (Ceman et al., 2003). FMRP was shown to comigrate with polyribosomes on sucrose gradients, and to shift to light fractions when polysomes were disrupted by RNAse or EDTA. FMRP could also be removed from polysomes by treatment with 0.5M KCl, a condition that leaves the majority of ribosomes still associated with mRNA (Corbin et al., 1997). Establishment of FMRP as a polysome-binding protein in brain initially met with some resistance due to technical issues with fractionating polysomes from neuronal tissue and an early report that FMRP was not associated with brain polysomes (Zalfa et al., 2003). However, improved methods of polysome preparation from brain later clearly showed that the majority of neuronal FMRP is polysome-associated, and that this association is sensitive to EDTA, RNAse and sodium deoxycholate as in earlier cell studies (Stefani et al., 2004), (Khandjian et al., 2004). Our lab routinely prepares polysomes from mouse brain with 90% of cellular FMRP on heavy polysomes.

RNA binding properties of FMRP

FMRP has three well-characterized RNA-binding domains: two hnRNP K homology (KH) domains and an RGG box (Siomi et al., 1993b). KH domains were first discovered in the hnRNP K proteins (Siomi et al., 1993a) and are present in many other RNA binding proteins (RBPs) such as the Nova proteins, which contain three KH domains that mediate RNA splicing (Teplova et al., 2011), (Licatalosi et al., 2008). The importance of the KH domains to FMRP function was first indicated by a severe case of FXS associated with an I304N point mutation in the KH2 domain of FMRP (De Boulle et al., 1993). Cocrystallization of the Nova KH3 domain with a bound stem-loop YCAY RNA predicted that the *Fmr1* I304 residue should lie directly within the RNA-binding pocket of the FMRP KH2 domain (Lewis et al., 2000). *In vitro* RNA selection studies found that the FMRP KH2 domain bound to a kissing complex RNA motif (kcRNA) (Darnell et al., 2005a) and the RGG box bound to a G-quadruplex motif (Darnell et al., 2001), (Phan et al., 2011) though the *in vivo* significance of these interactions is not yet understood. Biochemical evidence also suggested that FMRP interactions with polysomal RNA were primarily mediated through the KH domains, since RGG box deletion mutants maintained normal polysome association in neuroblastoma cells, while I304N FMRP did not (Darnell et al., 2005b). In addition, kcRNA disrupted FMRP association with polyribosomes in brain extracts, while G quartet RNA did not (Darnell et al., 2005a). Finally, creation of the I304N knock-in mouse confirmed that endogenously expressed I304N FMRP was not associated with polysomes in brain (Zang et al., 2009). Critically, the I304N mutant mouse also exhibited several phenotypes associated with FMRP loss-of-function, linking loss of polysome association to FXS pathology. Collectively, these results underscore the centrality of polysome association to FMRP function.

FMRP has two paralogs in mammals and fish, FXR1P and FXR2P, collectively termed the FXRPs. FXR1P and FXR2P are also polysome-associated and contain KH1 and KH2 domains, although the FMRP KH2 domain contains an extended variable loop not present in the FXR1P or FXR2P domains (Price et al., 1996), (Blonden et al., 2005). Interestingly, this expansion loop is only found in mammals, suggesting that mammalian FMRP may have unique properties. In addition, the region containing the RGG box is

significantly diverged among the three family members and only FMRP recognizes G quartet RNA with high affinity (Darnell et al., 2009). The KH domains are also conserved in the single ancestral FXR that exists in Drosophila, dFMR (Wan et al., 2000). dFMR binds kcRNA with the same affinity as mammalian FXRPs, but does not bind G quartet RNA (Darnell et al., 2009). Overall, the data suggest that the most ancient function of FMRP involves its KH domains (and therefore presumably is related to polysome association), and the currently enigmatic function of the RGG box evolved more recently.

Synaptic plasticity and translational control in neurons

The overall organizational principle governing brain function is one of nested sub-modules, such that incoming information is successively broken down into discrete bits that can be processed by local circuitry, and output from these local circuits is then successively reintegrated at higher and higher levels until a response is achieved that unifies output from disparate brain regions. Individual neurons integrate signals from several to hundreds of thousands of synapses, responding by an all-or-none decision to fire or not to fire. Thus, synaptic signaling underpins complex multilayer neuronal circuitry.

Synapses are not static "input-output" devices: the properties of both signaling and reception can be modulated at many stages, with effects on plasticity that last from milliseconds to years. One of many examples of short-term plasticity is paired pulse facilitation, in which the postsynaptic potential produced by a stimulus is increased if a previous stimulus has just occurred. This is due to residual presynaptic calcium from the first stimulus augmenting vesicle release during the second stimulus. This type of plasticity adds a layer of richness to signaling dynamics, but does not persist beyond a few seconds. In order for learning and memory to occur, the brain must possess mechanisms by which certain stimuli can result in long-term changes to synaptic efficacy. The first such example of long-term synaptic plasticity was discovered by Bliss and Lomo in 1973. They found that a short, high frequency stimulation of perforant path inputs onto granule neurons in the dentate gyrus resulted in increased synaptic strength

and an increased likelihood that the granule neurons would fire in response to a stimulus of a given strength (Bliss and Lomo, 1973). These phenomena, which were termed long-term potentiation (LTP), lasted several hours, suggesting that these long-term changes in synaptic strength had properties consistent with the support of learning and memory. This conjecture has been substantiated over the years, with studies linking long-term changes in synaptic strength evoked by experimental manipulation to outcomes in learning tasks (reviewed in (Ito, 1986), (Lynch, 2004), (Collingridge et al., 2010).

Neurons also have special requirements for control of protein synthesis, due both to their complex morphology and to the need for rapid and dynamic control of events at the synapse (Cajigas et al., 2010). Forty years ago, studies that originally suggested the importance of protein synthesis to learning and memory showed that injection of the protein synthesis inhibitor puromycin into mouse brain 1-3 days after learning an avoidance task blocked the ability of the animal to later remember its training (FLEXNER et al., 1963), while increased radiolabeling of brain proteins was observed in goldfish recently trained in a learning task (compared to untrained fish), indicating that *de novo* protein synthesis was increased after learning (Shashoua, 1976). These avenues of research converged with those concerning long-term plasticity several years later, when it was discovered that increased radiolabeling of proteins occurred in the CA1 region of hippocampal slices after induction of LTP at CA1 synapses (Duffy et al., 1981) and that blockade of protein synthesis inhibited LTP at these synapses (Stanton and Sarvey, 1984). Together, these studies demonstrated a requirement for protein synthesis during synaptic plasticity. This link was later substantiated by genetic studies in which manipulations that either increased or decreased translation resulted in alterations in the translation-dependent late phase of LTP and defects in learning and memory tasks (Kelleher et al., 2004), (Banko et al., 2005). Finally, protein synthesis has been shown to be necessary for the expression of other forms of synaptic plasticity, in particular long-term depression (LTD), a form especially relevant to the FMRP literature (Linden, 1996), (Huber et al., 2000), (Bear et al., 2004), (Collingridge et al., 2010).

Neurons employ diverse mechanisms of translational control. For example, translation can trigger regulated mRNA turnover in transcripts that contain an intron within their 3'UTR. During splicing, exon junction complexes (EJCs) are deposited upstream of exon-exon boundaries and are displaced during the pioneer round of translation. These EJCs serve a surveillance function, recruiting mRNA degradation factors to transcripts that retain EJCs due to nonsense mutations that prematurely terminate translation (Chang et al., 2007). However, EJCs deposited within 3'UTRs are not displaced during translation and remain to recruit components of the nonsense-mediated mRNA decay (NMD) pathway. The time lag between when translation begins and when the message is degraded allows a brief burst of translation to occur. Knockdown of a core EJC component, eIF4AIII, resulted in increased translation of the dendritically localized mRNA *Arc* as well as defects in synaptic plasticity, suggesting that the EJC-NMD mechanism is important for the control of protein synthesis at synapses (Giorgi et al., 2007). Synaptic plasticity can also be regulated by miRNA-mediated translational control. For example, binding of *Limk1* mRNA by the brain-specific miRNA miR-134 decreased Limk1 synthesis and was associated with changes in dendritic spine volume, although it should not be concluded that *Limk1* is the sole executor of miR-134 function with relation to spine dynamics (Schratt et al., 2006). In a third example, short open reading frames upstream of the main start codon (uORFs) can regulate translation of certain proteins. These mechanisms depend on the fact that ribosomes that finish translating a uORF can resume scanning and reinitiate on downstream open reading frames if they reacquire the requisite initiation factors in time. Formation of the required initiation factor complex, consisting of the initiation factor eIF2a, GTP and initiator methionine tRNA, is prevented by phosphorylation of eIF2a. Thus, when eIF2a phosphorylation levels are high, the eIF2a initiation complex is in short supply and scanning ribosomes travel further before they acquire it. Depending on the relative spacing of uORFs and the main open reading frame, scanning ribosomes may reinitiate either at a second, downstream uORF or at the main open reading frame, with profound consequences for expression of the encoded protein. In the case of ATF4, a transcription factor linked to synaptic plasticity and memory (Chen et al., 2003a), increased levels of eIF2a phosphorylation facilitate translation of the main open reading frame (Vattem and

Wek, 2004). Specific deletion of the eIF2a kinase PERK in mouse forebrain resulted in decreased ATF4 expression without detectable changes in global translation, and also resulted in impaired cognitive function (Trinh et al., 2012). While it was not shown whether restored ATF4 expression could rescue observed defects in cognitive function, a reduction in ATF4 expression was noted in schizophrenic patients, suggesting that regulation of *ATF4* translation plays a role in neuronal function and cognition. Finally, local translation at synapses is important for the expression of various forms of synaptic plasticity. In an early example, BDNF-induced LTP was shown to require protein synthesis and yet be inducible in hippocampal slices in which both the presynaptic and postsynaptic neurites were severed from their cell bodies (Kang and Schuman, 1996). In another example, genetic restriction of CaMKIIa expression to neuronal soma by mutation of the dendritic targeting signal in the *CaMKIIa* 3'UTR caused a reduction in hippocampal late phase LTP and impairments in learning and memory (Miller et al., 2002). CaMKIIa is a major constituent of the postsynaptic compartment and these results suggest that transport of this protein from the soma is insufficient to support normal synaptic function.

Historic efforts to identify FMRP-associated mRNAs

As it became clear that polysome association was essential to FMRP function, identification of the mRNAs associated with FMRP became a major priority, although originally it was unknown whether FMRP was a general translation factor or regulated a specific subset of mRNAs. In an early approach, FMRP immunoprecipitation (IP) from wt and *Fmr1* KO mouse brains under stringent conditions was followed by microarray analysis of coIPed RNAs (RIP-CHIP), resulting in identification of more than 400 mRNAs enriched at least four-fold in the wt IP (Brown et al., 2001). A second approach at target identification used RNA SELEX, a method in which an RNA pool is passed over an immobilized protein ligand and the bound fraction is then eluted and passed again over the ligand again in repeated cycles. Each successive cycle enriches for RNAs that bind the ligand with greatest affinity. RNA SELEX has previously been used in our lab to show that the neuronal protein Nova binds YCAY motifs on target mRNAs (Buckanovich and Darnell, 1997), (Jensen et al., 2000), although the YCAY motif was

not sufficiently complex for *de novo* identification of unknown targets. A similar approach was undertaken to discover binding motifs for FMRP. A library of RNAs containing 52 nt of random sequence was selected against full-length FMRP for eight rounds, with all resulting sequences containing a G-quartet motif, which bound FMRP with an affinity of 10-30nM Kd in a filter binding assay (Darnell et al., 2001). Binding activity was mapped to the RGG domain of FMRP using truncation constructs. This experiment was later repeated under conditions designed to select for lower affinity aptamers specific for the KH domains (in detail, the 52 nt library was selected for six rounds over full-length FMRP, followed by eight additional rounds of selection over a KH1-KH2 fragment) resulting in identification of a consensus kissing complex motif that bound FMRP with an affinity of 30-100nM Kd (Darnell et al., 2005a). However, secondary structure of this motif was too complicated to permit bioinformatic target prediction. To try to circumvent this problem, Chen et al employed SELEX using a full-length cDNA library from human brain (Chen et al., 2003b). Selection was limited to three rounds in order to preserve complexity; however, this had the unavoidable downside of limiting enrichment. Fifty-seven mRNAs were cloned that corresponded to cDNA sequences, many of which contained U-rich elements. Finally, a third approach used antibody-positioned RNA amplification (APRA) to assess target binding by FMRP in fixed primary hippocampal neuron culture (Miyashiro et al., 2003). Anti-FMRP antibodies were used to position a degenerate priming oligo next to endogenous FMRP, such that nearby exposed, single-stranded RNA could be transcribed *in situ*. Purified sequences were characterized by microarray, identifying more than 800 mRNAs bound by FMRP.

Each of the assays presented above has advantages and limitations. *In vivo* protein-RNA interactions are determined by a number of factors including binding affinities, dissociation constants, exposure or masking of epitopes due to interaction with other binding partners, and physical compartmentalization within the cell. When cells are lysed, these factors change due to differences between buffer composition and cytosolic composition and physical disruption of the cell, and protein:RNA complexes may reassort according to the new equilibrium conditions *in vitro*. This was demonstrated by

mixing separate cell lysates expressing either the protein HuR or its target mRNA, *c-fos*, and comparing an IP from the combined lysates to an IP from a single lysate expressing both HuR protein and *c-fos* mRNA (Mili and Steitz, 2004). Nearly equal amounts of *c-fos* mRNA associated with HuR protein in both IPs, indicating that the IPs reflected the equilibrium binding state of these two factors *in vitro*, and not their *in vivo* interactions. Thus, assays such as RIP-CHIP that rely on IP in the absence of crosslinking likely contain interactions that are not found *in vivo*. In particular, the very high affinity RNA aptamers identified by the SELEX assay may or may not have *in vivo* relevance. The APRA approach attempts to circumvent this problem by performing reverse transcription *in situ* without lysing cells. However, the positioning of the priming oligo relative to the protein of interest is not very precise due to the size of the antibody and the flexibility of the oligo, and mRNAs *in vivo* can exist in large multiprotein, multi-mRNA complexes. These factors may allow the oligo to prime mRNAs that are not directly bound by the protein of interest. Alternatively, the protein of interest may bind RNA in a physical context not accessible to the oligo, for example in a region containing secondary structure or other RNA-binding proteins.

HITS-CLIP of polysomal FMRP

An assay developed in our lab termed CLIP (crosslinking and immunoprecipitation of RNA-protein complexes) offers significant improvement over previous methods (Jensen and Darnell, 2008). In CLIP, immediate UV_{254} crosslinking captures *in vivo* binding interactions in intact cells or tissue. Crosslinking forms covalent bonds between proteins and nucleic acids, but only sparsely and only if the two molecules are within a bond length, thus providing tight spatial specificity without generating extensively crosslinked macrocomplexes. Limited RNAse treatment generates ~100nt RNA fragments (termed "tags"), some of which are covalently crosslinked to a protein of interest. Such protein:RNA complexes can then be stringently purified, starting with immunoprecipitation and stringent washes. Specificity of the IP is also promoted by preclearing of lysate, limiting the time of IP, and using magnetic beads from which 100% of supernatant/buffer can be easily removed.

While protein:RNA complexes are still bound to antibody-coupled beads, they are treated with alkaline phosphatase to remove any 3' phosphate groups left by RNAse digestion, as well as exposed 5' phosphates. An RNA linker is then ligated to the 3' end of the RNA tag (the linker has a blocked 3' end to prevent linker-linker concatamerization during ligation, and the tag cannot self-ligate due to earlier removal of 5' phosphates). Linker ligation is followed by T4 polynucleotide kinase treatment to re-phosphorylate and ^{32}P -label the 5' end of the tag.

Protein:RNA complexes are then boiled in SDS, separated on a polyacrylamide gel and transferred to nitrocellulose. This step offers significant further purification of desired complexes, as contaminating complexes that bound nonspecifically during the IP are likely to migrate at different molecular weights on the gel, and any RNA not crosslinked to protein will pass through the nitrocellulose during transfer. Desired complexes can be visualized on film as a smear approximately 30kD larger than the protein of interest. A band containing this smear is cut out and treated with proteinase K to free RNA from protein. The RNA is then extracted and precipitated by standard methods.

After resuspension, a 5' linker is ligated to the RNA tag. All tags now have linkers of known sequence at either end. The RNA is then DNAse treated to remove any trace contaminants prior to reverse transcription and PCR amplification. PCR amplification is titrated so that the minimum number of cycles need to successfully sequence the products is used, in order to not to skew tag abundance ratios by over-amplification. For this same reason, the entire cDNA pool is amplified (except 20% reserved for –RT control) so that rare transcripts are not missed. PCR products are then further purified on a denaturing acrylamide gel to select for products of ~175nt (length of tag plus linker sequences) and analyzed by high-throughput sequencing (HITS). Sequencing data are bioinformatically filtered and mapped to the annotated genome of interest. A typical experiment may return up to a million unique sequences, each ideally representing a discrete site of *in vivo* RNA binding by the protein of interest.

Recent HITS-CLIP analysis of polysomal FMRP has identified 842 mRNAs associated with FMRP in mouse brain (Darnell et al., 2011). Satisfyingly, the number of CLIP tags per target mRNA was uncorrelated with neuronal mRNA abundance, suggesting that FMRP regulates a discrete subset of mRNAs. Surprisingly, FMRP CLIP tags were distributed across the entire exonic sequences of target mRNAs, with higher tag densities in coding sequences than in UTRs. This differed from CLIP data for other RBPs such as Nova and Hu, which have discrete binding peaks in particular regions of transcripts (eg, introns or 3'UTRs) (Licatalosi et al., 2008), (Darnell et al., 2011) and suggested that FMRP may be associated with a processive factor such as a helicase or the ribosome (see later chapters for discussion). The FMRP CLIP targets were characterized bioinformatically using the DAVID database (Huang da et al., 2009) and Ingenuity software to identify enriched gene ontology (GO) categories and enriched signaling pathways, respectively. GO analysis revealed that the FMRP targets were enriched for genes involved in synaptic transmission and small GTPase signaling, while Ingenuity analysis identified the most enriched signaling pathways as those involved with neuronal CREB, synaptic long term potentiation, Huntington's disease, glutamate receptors, neuropathic pain and axonal guidance. The CLIP dataset was also overlapped with datasets representing the postsynaptic (Croning et al., 2009) and presynaptic (Abul-Husn et al., 2009) proteomes and genes linked to autism (Basu et al., 2009). Substantial overlap was found with each, suggesting that FMRP regulates the translation of a specific set of genes with roles in synaptic function. However, the mechanism of translational control by FMRP remained a mystery.

Chapter II. Experimental Procedures

Preparation of mouse brain extracts

Mice were sacrificed by brief isoflurane anesthesia and decapitation. The brain was removed and placed in ice-cold polysome buffer (20mM HEPES pH 7.3, 150mM NaCl, 5mM $MgCl_2$). Cortex, hippocampus and cerebellum were dissected free of underlying white matter, homogenized in 1 ml polyribosome lysis buffer (polysome buffer plus 0.5 mM dithiothreitol, 0.1 mg/ml CHX [Sigma C-7698, made fresh in methanol], 1X Complete EDTA-free protease inhibitor cocktail [Roche], 40 U/ml RNAsin [Promega]) per brain, with 10 strokes at 900 rpm in a motor-driven Teflon-pestle 5 ml glass homogenizer (Wheaton). NP-40 was added to a final concentration of 1% from a 10% stock (Calbiochem) and lysate was allowed to sit on wet ice for 10 min. The homogenate was spun at 2,000 x g for 10 min at 4°C. The supernatant (S1) was respun at 20,000 x g for 10 min at 4°C. The resulting supernatant (S2) was used for Western blot or loaded over sucrose gradients.

SDS-PAGE and Western blotting

Proteins from sucrose gradient fractions or S2 lysates were TCA-precipitated from 50-200 ul and analyzed by Western blot. Samples were run on handcast 10% or commercial 4%–12% gradient SDS-polyacrylamide gels (BioRad) and transferred to Immobilin-P PVDF membranes (Millipore) by standard methods. Membranes were blocked for 1hr at room temperature in 5% non-fat dry milk (Carnation) in PBS followed by addition of primary antibody for 1 hr at room temperature or overnight at 4 degrees. Blots were washed 3x10 min with Western blot wash buffer (23mM Tris, pH 8.0, 190mM NaCl, 0.1% w/v BSA, 1 mM EDTA, 0.5% Triton X-100, 0.02% SDS) after each antibody incubation. HRP-conjugated secondary antibodies (Jackson Immunochemicals) were used at 1:10,000 in 5% milk/PBS for 1 hr at RT, washed as before, and HRP signal was detected by Enhanced ChemiLuminescence (Western Lightning detection kit, Perkin Elmer) and detected on film (Kodak MR).

Antibodies

The following antibodies were used for Western blotting:

anti-FMRP 17722 at 1:1000 (Abcam ab17722)
anti-FMRP 27455 at 1:1000 (Abcam ab27455)
anti-FMRP 2F5 at 1:1000 (obtained from the Developmental Studies Hybridoma Bank)
anti-FXR1P ML13 at 1:20,000 (a gift from Dr. Eduoard Khandjian)
anti-FXR2P 1G2 ascites at 1:100 (obtained from the Developmental Studies Hybridoma Bank)
anti-rpP0 at 1:20,000 (polysomes) or 1:5000 (whole cell lysate) (US Biological R2031-25)
anti-GFP B-2 (HRP-conjugated) at 1:200 (Santa Cruz sc-9996 HRP)
anti-GFP 19C8 at 1:1000 (developed by Nat Heintz, produced in Monoclonal Antibody Core Facility)
anti-GAPDH 6C5 at 1:25,000 (Abcam ab8245)
anti-NeUN A60 (biotinylated) at 1:1000 (Abcam ab77315)
anti-calnexin at 1:1000 (Abcam ab13504)
anti-hnRNP C1/C2 at 1:1000 (Abcam ab10294)
anti-histones at 1:500 (Millipore mab052)
anti-eIF2a at 1:1000 (Cell Signaling 9722)
anti-eIF2a [pS^{52}] (phosphospecific) at 1:1000 (Invitrogen 44728G)
anti-eEF2 at 1:1000 (Cell Signaling 2332)
anti-eEF2 (Thr56) (phosphospecific) at 1:200 (Cell Signaling 2331)
HRP-conjugated anti-rabbit, anti-mouse and anti-human secondaries at 1:10,000 (Jackson Immunoresearch)
Neutra-Avidin secondary at 1:1500 (Abcam ab77315)

The following antibodies were used for immunoprecipitations:

anti-FMRP ab17722 (Abcam)
anti-FMRP ab27455 (Abcam)
anti-FMRP 7G1-1 ascites developed by Drs. Ceman and Warren (Brown et al., 2001), obtained from the Developmental Studies Hybridoma Bank
anti-GFP 19C8 (developed by Nat Heintz, produced in Monoclonal Antibody Core Facility)
anti-GFP 19F7 (developed by Nat Heintz, produced in Monoclonal Antibody Core Facility)

The following antibody was used for immuno-electron microscopy:

anti-GFP (Abcam ab6556)

Immunoprecipitations

Amounts of beads and antibodies for CLIP

40uL of Protein A Dynabeads (Invitrogen) loaded with 12ug 17722 or 27455 FMRP antibodies, 20ug mixed 19C8/19F7 anti-GFP monoclonals (mixed, yet specific, monoclonals were used to markedly increase avidity), or 20uL rabbit anti-mouse secondary (2.3 mg/ml IgG, Jackson ImmunoResearch 315-005-008, for preclearing) were used per 1 brain-equivalent (nuclei from 1 brain was estimated to be 0.1 brain-equivalents). For beads loaded with anti-GFP monoclonals, beads were pre-coated with rabbit anti-mouse secondary for use as a bridging antibody (5uL secondary per 20uL beads. 20uL beads can hold 5ug antibody, so beads will be saturated by secondary).

Loading beads with antibody for CLIP

Protein A Dynabeads were washed 3X with 0.1 M Na-phosphate buffer, pH 8.1, plus 0.01% Tween-20 (bead wash buffer, BWB). Antibodies were then added to beads in amounts indicated above, in total volume of 100uL with BWB. Beads plus antibodies were rotated for 1 hr at 4°C (for primaries) or 30 minutes at RT (for secondaries), followed by 3X wash with BWB (1 ml each time) and final suspension in 100uL BWB. Loaded beads were stored on ice or at 4°C until use.

Immunoprecipitations for CLIP

DNAse- and RNAse-treated samples precleared by addition of 40uL Protein A Dynabeads loaded with 20uL rabbit anti-mouse secondary as described above and rotating at 4°C for 1 hour. Samples were then rotated with primary antibody-loaded beads at 4°C for 1 hour. Following IP beads were washed sequentially (1 ml washes) with high stringency buffer (15 mM Tris-HCl, pH 7.5, 5 mM EDTA, 2.5 mM EGTA, 1% Triton X-100, 1% Na-deoxycholate (DOC), 0.1% SDS, 120 mM NaCl, 25 mM KCl), high salt buffer (15 mM Tris-HCl, pH 7.5, 5 mM EDTA, 2.5 mM EGTA, 1% Triton X-100, 1% Na-DOC, 0.1% SDS, 1 M NaCl) and twice with low salt buffer (15 mM Tris-HCl, pH 7.5, 5 mM EDTA) followed by one wash with NT-2 buffer (50 mM Tris-HCl pH 7.4, 150 mM NaCl, 1 mM MgCl2, and 0.05% NP-40). After each capture on the magnet beads, the beads were resuspended by end-over-end rotation for a few minutes. Resuspended beads were transferred to new microfuge tubes once during the protocol,

and throughout the washes tubes were treated in a random order to diminish the chance of artifacts. Throughout the CLIP protocol 1.5 ml SlickSeal microfuge tubes (National Diagnostics) were used to reduce non-crosslinked RNA binding to tubes.

IP-Westerns from mouse brain

FMRP antibody 7G1 was covalently coupled to Affiprep Protein A beads (Biorad). 7G1 antibody was purified from ascites using Pierce ImmunoPure (A Plus) IgG Purification Kit, exchanged into 0.1M phosphate buffer using PD-10 columns (Biorad) and concentrated using Amicon Ultra 50mL concentrators. 30uL beads were washed 2X in 0.1M Na-phosphate buffer pH 8.1, sedimenting beads by gravity and removing supernatant by needle vacuum. 600uG purified 7G1 was added to washed beads (1X the molar saturation of the beads) and rotated at RT for 30 min. Beads were then washed 2X in 0.2M Na-borate buffer pH 9.0 and resuspended in the same buffer plus 20mM dimethyl pimelimidate (a crosslinking reagent – note all reagents must be azide-free for successful crosslinking) and rotated at RT for 30 min. Beads were washed 2X in 0.2M ethanolamine pH 9.0 and then resuspended in this same buffer and rotated at RT for 2 hours to quench the crosslinking reaction. Beads were then washed in polysome buffer and kept on ice.

100uL aliquots of wt or *Fmr1* KO S2 brain lysates were treated as described in Figure 11 with either 200nM kc7 RNA, 15uL of 1ug/uL RNAse A plus 4uL 1U/uL RNAse T1, 30mM EDTA or untreated. For the kcRNA and RNAse treatments, lysate was incubated at RT for 15 minutes. Each aliquot of lysate was then combined with 5uL beads (as prepared above, containing approximately 100ug 7G1) and rotated at 4°C for 1 hour. Beads were then washed 3X in polysome buffer and proteins were eluted by rotating with 0.5M ammonium hydroxide plus 0.5mM EDTA at RT for 20 min. The eluant was then frozen in an ethanol/dry ice bath, speedvac'ed to dryness, and resuspended in SDS sample buffer. Samples were separated by SDS-PAGE and blotted with FMRP antibody 2F5.

***In vitro* transcription of kcRNA**

Transcription templates for kcRNA and $kcRNA_{C50G}$ were prepared by PCR and purified over G-25 columns as follows. *In vitro* transcription reactions included 80uL of DNA template, 80uL of 5X transcription buffer (Stratagene), 50uL of 100mM NTP mix (Amersham), 24uL 0.1M DTT, 4.8uL 1M $MgCl_2$, 4uL of RNAsin (Promega), 16uL of T7 RNA polymerase (Stratagene) and RNAse-free water to 400uL. Reactions were incubated overnight at 37°C. RNA was treated with 5uL of RQ1 DNase at 37°C for 45 minutes, concentrated in Amicon concentrators (10,000 kD cutoff), heated in gel loading buffer at 75°C for 10 minutes and gel purified on 8% urea-polyacrylamide gels followed by UV shadowing, excision and precipitation. Quality was checked by end labeling with T4PNK and γ-P^{32}-ATP and running on 8% urea-polyacrylamide gels, drying, and exposure to Kodak MR film.

RNA preparation and QPCR analysis from whole brain

Half brains from ten littermate pairs of P10-P15 *Fmr1*$^{-/-}$, *Fxr2*$^{-/-}$ and *Fmr1*$^{+/+}$, *Fxr2*$^{+/-}$ mice were mashed in 1mL Trizol (Invitrogen) in Eppendorf tubes using 1mL syringe plungers. Samples were blinded to genotype. Samples were extracted in chloroform and precipitated in isopropanol. Pellets were washed once in 75% EtOH, resuspended in water and RNA was recovered using RNAeasy spin columns (Qiagen) with on-column DNAse treatment. 3ug of RNA was then reverse transcribed using random hexamers and Superscript III (Invitrogen) and digested with RNAse H. cDNAs were amplified by QPCR using iTaq SYBR Green Supermix with ROX (Biorad), a 1:100 dilution of cDNA and 200 nM primers (sequences included in following section). QPCR was performed on an iQ5 Multicolor Real-Time PCR Detection System (Biorad) using a 58°C annealing temperature. Melt curves and (-)RT controls were performed. A panel of 16 control genes (listed below) were screened against all 20 samples and results were analyzed using GeNorm software to select the best internal controls (Vandesompele 2002). A normalization factor was calculated using GeNorm based on the data from *Hprt1*, *TBP* and *B2M*. The efficiencies for all primers were calculated using four 5X serial dilutions. To calculate efficiency, the $\log_{10}$ value of ng input (assuming 1:1 RNA:cDNA correspondence) was plotted against the Ct value (y-axis); efficiency (E) then equals

$10^{\wedge\text{-}(1/\text{slope})}$, and the amount of product is $E^{\wedge Ct}$.

Preparation of RNA from cTAG mouse brains was done by homogenization of brain in polysome lysis buffer followed by addition of Trizol LS (Invitrogen) and chloroform:isoamyl alcohol per manufacturor's instructions. Extracted samples were precipitated with 1uL glycoblue and 1 volume isopropanol and washed 2X in cold 75% EtOH. Pellets were resuspended in water and RNA was purified using High Pure RNA isolation kit (Roche) with on-column DNAse digest. 1ug of RNA from each sample was reverse transcribed using random hexamers and Superscript III (Invitrogen). cDNAs were amplified by QPCR using FastStart SYBR master mix (Roche), using a 1:50 dilution of cDNA and 400nM each primer. QPCR was performed on an iQ5 Multicolor Real-Time PCR Detection System (Biorad) using a 58°C annealing temperature. Melt curves and (-)RT controls were performed. Primers amplified either from *Fmr1* exon 16 to exon 17 (133nt amplicon) or from *Fmr1* exon 16 to AcGFP (177nt amplicon).

QPCR primers used for cTAG mouse
Exon 16 (forward): 5'-ccaagagaggctaaaggaagaacagct-3'
Exon 17 (reverse): 5'-gttgcagcccatctacgctgtctg-3'
AcGFP (reverse): 5'-cacgatgccggtgaacagctc-3'

QPCR Primers screened for use as internal controls (for others, see list below):

B2M beta-2-microglobulin (NM_009735)
F: CTGACCGGCCTGTATGCTAT; R: TGCATGCTATCTGAGCCATC

GAPDH glyceraldehyde-3-phosphate dehydrogenase (NM_008084)
CATGGCCTTCCGTGTTCCTA
GCGGCACGTCAGATCCA

HMBS hydroxymethyl-bilane synthase variant 1 (NM_013551)
F: TGCACGATCCTGAAACTCTG; R: TGCATGCTATCTGAGCCATC

HPRT1 hypoxanthine phosphoribosyl-transferase-1 (NM_013556)
F: AAGCTTGCTGGTGAAAAGGA; R: TTGCGCTCATCTTAGGCTTT

SDHA succinate dehydrogenase complex, subunit A (NM_023281)
F: GATTACTCCAAGCCCATCCA; R: GCACAGTCAGCCTCATTCAA

TBP TATA box binding protein (NM_013684)
F: GGGAGAATCATGGACCAGAA; R: CCGTAAGGCATCATTGGACT

YWHAZ tyrosine 3-monoxygenase 1 tryptophan 5-monoxygenase activation protein, zinc polypeptide (NM_011740)
F: TTGAGCAGAAGACGGAAGGT; R: GAAGCATTGGGGATCAAGAA

GUSB beta-glucoronidase (NM_010368)
F: TCAGCTCTGTGACCGATACG; R: GCCACAGACCACATCACAAC

IPO8 importin8 NM_(001081113)
F: CGTGACAACATTGTGGAAGG; R: GTAAACTGCCAAGCCAGCTC

PGK1 phosphoglycerate kinase (NM_008828)
F: CAAGGCTTTGGAGAGTCCAG; R: TGTGCCAATCTCCATGTTGT

PPIA peptidylprolyl isomerase A (NM_008907)
F: AGCATACAGGTCCTGGCATC; R: TTCACCTTCCCAAAGACCAC

TFRC transferrin receptor (NM_011638)
F: TCCGCTCGTGGAGACTACTT; R: ACATAGGGCGACAGGAAGTG

Tubg1 Gamma-tubulin (NM_134024)
F: GCCGAGAGAAATCATCACCCTAC; R: TAGACTGTCACTGCCATCTGCCTC

GfaP glial fibrillary acidic protein (NM_010277)
F: AGAAAACCGCATCACCATTC; R: AGAAAACCGCATCACCATTC

RPL13A ribosomal protein large subunit A (NM_009438)
F: CCCTCCACCCTATGACAAGA; R: TTCTCCTCCAGAGTGGCTGT

RPS6 ribosomal protein small subunit 6 (NM_009096)
F: AAGCTCCGCACCTTCTATGA; R: CATGGGAAAACCTTGCTTGT

Polyribosome analysis (mouse brain and cells)

Supernatants from mouse brain (S2 lysates) or cells (S1 lysates) were loaded onto a 20%–50% w/w linear density gradient of sucrose in gradient buffer (20 mM HEPES-KOH pH 7.4, 150 mM NaCl, and 5 mM MgCl2) prepared using a Gradient Master 107 (BioComp), in 14x3x89 mm polyallomer ultracentrifuge tubes (Beckman 331372). Gradients were centrifuged at 40,000 rpm for 2 hrs at 4°C in a Beckman SW41 rotor and sixteen fractions of 0.72 ml volume were collected with continuous monitoring at 254 nm using an ISCO UA-6 UV detector.

RNA preparation and QPCR analysis from polysome gradients

RNA from polyribosome fractions was extracted using Trizol LS Reagent according to manufacturer's instructions (Invitrogen) and then back-extracted in chloroform:isoamyl alcohol (49:1) and spun at 10,000 3 g for 15 min. The aqueous phase was precipitated with 15 mg glycoblue (Ambion) and 1 volume isopropanol. RNA was pelleted at 20,000 x g for 10min at 4°C, washed twice with cold 75% ethanol and resuspended in water. Samples were digested with RQ1 DNase (Promega) for 1 hr at 37°C, extracted with phenol-chloroform, back-extracted with chloroform:isoamyl alcohol, precipitated with glycoblue in 2 volumes of 1:1 ethanol:isopro- panol and washed as before. cDNA was prepared with equal volumes of RNA from each fraction, using random hexamers (Roche) and Superscript III Reverse Transcriptase (Invitrogen) according to manufacturer's instructions. cDNAs were amplified by qPCR using iTaq SYBR Green Supermix with ROX (Biorad) and 200 nM primers (sequences included in following section). qPCR was performed on an iQ5 Multicolor Real-Time PCR Detection System (Biorad) using a 58°C annealing temperature. Relative RNA levels were calculated using a Ct threshold of 100 and the formula $2^{(40-Ct)}$. Normalization to an internal control was not necessary. For each gene, polyribosome fractions were plotted as percentages of the total amount of the gene on the gradient (obtained by summing values of individual fractions). Error bars refer to technical replicates of qPCR measurements within single experiments. Primers were checked for single products of correct size by separating amplified products from pooled polysome fractions on an agarose gel.

Primer sets used for QPCR in runoff assays (intron spanning)

Bsn Bassoon (NM_007567)
F: GGAGCACTCCTCTACGTTGC; R: GCTGCTGCTTTGCTTCTTCT

Kif1a Kinesin 1A (NM_008440)
F: ACCAGAGTGGGCAGAGAAGA; R: TGTGTCTGCTCCTTCACAGG

Adcy1 Adenylate cyclase 1 (NM_009622)
F: CTTACCAGGGAAGGTCCACA; R: GGCTGGTTTGATATCCGAGA

Cyfip2 Cytoplasmic FMRP-interacting protein 2 (NM_133769)
F: CGGTCTTGGACGAGCTAAAG; R: CACTGGGTGATCCTGTTGTG

Mtap1b Microtubule-associated protein 1B (NM_008634)
F: CGGACAGTGCTTTGAGAACA; R: GTGGTGCTTAGGAGCTCACC

Nisch Nischarin (NM_022656)
F: GACAGGTGGCCTCTGATGAT; R: CTGAGGCGCTGGATAAAGTC

Bai2 Brain-specific angiogenesis inhibitor 2 (NM_173071)
F: GGGACCTGCTCTTCTCTGTG; R: AATCCACCATGAAGCTCACC

Atp1a3 ATPase, Na+/K+ transporting, alpha 3 (NM_144921.1)
F: CCATTGTCACTGGTGTGGAG; R: CAATGCAGAGGATGGTGATG

Bat2 HLA-B associated transcript 2 (NM_020027)
F: CCTACCCCAACACCAGAGAA; R: TGGTTCAGGACCCTCTTTTG

Pde2a Phosphodiesterase 2a (NM_001008548)
F: GGGAGTCCAGACTGGTGTGT; R: CAGGGGTATGACCAGCACTT

Camk2a Ca/Calmodulin dep. kinase IIa (NM_009792.3)
F: TCTGAGAGCACCAACACCAC; R: CCATTGCTTATGGCTTCGAT

Grik5 Kainate receptor subunit 5, KA5 (NM_008168.2)
F: AGTACGAGACCACGGACACC; R: CGAAGCGAAGGTACTGAAGG

Grin2b NMDAR subunit 2B (NM_008171)
F: TGCGCTCTCCCTTAATCTGT; R: GCCAACACCAACCAGAACTT

Lingo1 Leucine-rich repeat and IgG domain-containing-1 (NM_181074.4)
F: CCTGAGGATCCATCCAGAAA; R: AGCCTGTAGCAGAGCCTGAC

Dlg4 PSD-95 (NM_007864.2)
F: AACAGAGGGGGAGATGGAGT; R: CAAACAGGATGCTGTCGTTG

Dlgap3 SAPAP3 (NM_198618)
F: TCAGATGGTAGCCCCAAGAC; R: TGTAGCCAGGGATGGAACTC

Grin2a NMDAR subunit 2A (NM_008170)
F: GGTTCTGCATCGACATCCTT; R: GAACGCTCCTCATTGATGGT

Pctk1 PCTAIRE protein kinase 1 (NM_011049.4)
F: GCTAGACAAGCTGGGTGAGG; R: AGTACAGGGTGCCCCTTCTT

Ndrg4 NDRG family member 4 (NM_145602.2)
F: CAGCCATCCTCACCTACCAT; R: TGGCACACCACAAAGTGTTT

Gnb1 G protein, beta polypeptide 1 (NM_008142.4)
F: GCGGGACACACAGGTTATCT; R: CAGTCTGGTGTCAGGAGCAA

Ttyh3 Tweety homolog 3 (NM_175274.4)
F: GGAGGTGCTAGCTGAACAGG; R: AGACCCCAACCAAGATACCC

Arc Arg3.1/Arc (NM_018790)
F: GAGAGCTGAAAGGGTTGCAC; R: GCCTTGATGGACTTCTTCCA

Pabpc1 polyadenylate binding protein (NM_008774.3)
F: GAGACCAGCTTCCTCACAGG; R: GGACTCCCGCAGCATATTTA

Gria1 AMPAR subunit GluR1 (NM_008165.3)
F: ACCACTACATCCTCGCCAAC; R: TCACTTGTCCTCCACTGCTG

Hyou1 Hypoxia upregulated 1 (NM_021395.4)
F: TACCAAACTTGGCAACACCA; R: GGCTCTCCTCTTCCTCCTGT

Clcn6 Chloride channel 6 (NM_011929.2)
F: CTGGAGGTGTTGGAGACCAT; R: ACGTTTGAACCACTCCGAAC

Sae1 SUMO1 activating enzyme subunit 1 (NM_019748)
F: CTGCTGCAGATACGGAATGA; R: CCAACCACAGCACATACTGG

Hprt1 Hypoxanthine phosphoribosyltrans. 1 (NM_013556)
F: AAGCTTGCTGGTGAAAAGGA; R: TTGCGCTCATCTTAGGCTTT

Eif3a Eukaryotic initiation factor 3a (NM_010123.3)
F: ACTCCCTGGGTCAAGTTCCT; R: CACATAGCTTGCGGAACTCA

Tcerg1 Transcription elongation regulator 1 (NM_001039474.1)
F: TTCGAGAACGGGAAAGAGAA; R: CCGGAGGGTCCTCCTAGTAT

Npepps Aminopeptidase puromycin sensitive (NM_008942.2)
F: CAAAAGAATGCTGCCACAGA; R: GGTCCACTGGCACAAAACTT

Gria2 AMPAR subunit GluR2 (NM_001039195)
F: AACGGCGTGTAATCCTTGAC; R: CACCAGGGAGTCGTCGTAGT

Vldlr Very low density lipoprotein receptor (NM_013703.2)
F: ACGGCCAGTGTGTTCCTAAC; R: ATTTTCACCATCGCATCTCC

Canx Calnexin (NM__001110499.1)
F: GCCTGAAGATTGGGATGAAA; R: CAATCCTCTGGCTTCTCTGC

Glrb Glycine receptor, beta (NM__010298.5)
F: TGTGGTTCTCTCCTGGCTCT; R: CAGCGCCTTCACATAAGACA

Slc35f1 Solute carrier family 35, member F1 (NM_178675)
F: CGGTCAACCTTTCTCTGCTC; R: GGGGATCCTGGGCTATGTAT

St8sia3 ST8 a-N-Ac-neuraminide a-2, 8-sialyltransf. 3 (NM_009182.2)
F: CGGACAGCGTTTTTACATCA; R: AGCAGGGACCGGAAGTTATT

Atp6ap2 ATPase, H+ transp., lysosomal acc. prot.2 (NM_027439.3)
F: TTTGGATGAACTTGGGAAGC; R: CACAAGGGATGTGTCGAATG

Tmem65 Transmembrane protein 65 (NM_175212.4)
F: CATCTACAGCCTGCACTCCA; R: GCGTTATCCAAAAAGCCAAA

IVT-EBP system and ribosome runoff assays

Two- to three-week old wild-type mice (CD1, FVB or C57Bl6/J, both sexes) or paired littermates (*Fmr1* KO versus WT (FVB background) or I304N versus WT (C57Bl6/J background) (Zang et al., 2009), only males) were sacrificed by isoflurane anesthesia and decapitation. Postnuclear supernatants (S1) of cerebral cortex and cerebellum, dissected free from white matter, were prepared by homogenizing 2 mouse brains in 1 ml polyribosome lysis buffer (without addition of NP-40 or CHX) and yielded 300uL of S1 following a 10 min, 2000xg spin at 4°C. ATP was added to 2 mM, 15 ml each of the (-)Met and (-)Leu amino acid mixtures (1mM stocks, Promega nuclease-treated RRL kit L4960) and 150 ml of the nuclease-treated rabbit reticulocyte lysate (RRL, Promega L4960) were added to 300uL of S1 and incubated at 30°C in the presence of puromycin (7.2 ug/ml) for the indicated times. 75uL reactions were terminated by addition of 1 ml polysome lysis buffer including 1% NP-40 and 0.1 mg/ml CHX, on ice (10 min) followed by a 20,000 x g spin (10 min, 4°C) and S2 was applied to 20%–50% sucrose gradients to frationate polysomes. Where indicated, *in vitro* transcribed RNAs (1.0 uM final concentration; unlabeled) were added to the S1 lysate (after heating RNA to 75 degrees for 10 min and bench cooling for 5 min in 1X SBB buffer (Selex binding buffer, 50 mM Tris acetate, pH 7.7, 200 mM potassium acetate, 5 mM Mg-acetate) as previously described for filter binding assays (Darnell et al., 2009) at the start of the incubation.

In one set of experiments, kcRNA or mutant kcRNA was added after puromycin run-off, as follows. Brains from three WT FVB mice aged P14 were dissected of white matter and homogenized together in 750 ml polyribosome lysis buffer (without addition of NP-40 or CHX). Polyribosome run-off was conducted in the presence of puromycin as above, for 20 min at 30°C, and then placed on ice water. 1.2 mM CHX and 0.2 mM anisomycin were added for 10 min on ice water, followed by 1 uM kcRNA or 1 uM mutant kcRNA. Samples were incubated on ice water for 20 min, then diluted in 2.5 volumes gradient buffer containing protease inhibitors, RNAsin Plus, 1.2 mM CHX, 0.2 mM anisomycin and 1% NP-40. Samples were incubated on ice 10 min, then loaded onto 20%–50% (w/w) sucrose gradients.

EDTA treatment during puromycin runoff

FVB P15 brain lysate was prepared for the IVT-EBP assay, and run-off was performed in the presence of ATP, amino acids, and RRL as described above. Samples were split into 3 aliquots and treated with either 1 uM kcRNA, 1 uM kcRNA + 30 mM EDTA, or 1 uM $kcRNA_{C50G}$. Puromycin was then added and each reaction was allowed to run off for 20 min at 30°C. Reactions were stopped by the addition of 1 ml of lysis buffer containing CHX and 1% NP-40. Samples were incubated on ice for 10 min and then loaded onto sucrose gradients for analysis.

FXRP knockdown and puromycin runoff in N2A cells

A mouse siGENOME ON-TARGETplus SMARTpool (Fisher Dharmacon) containing 4 siRNAs was used for each gene (*Fmr1*, *Fxr1* and *Fxr2)*. N2A cells were transfected at 30% confluence in OptiMEM-I + GlutaMax medium (Invitrogen), with 11.7nM of each of the three oligo pools using Lipofectamine (Invitrogen) according to manufacturer's instructions. Medium was changed after 4-6 hrs and knockdown was repeated the same way on the subsequent day. 15 hrs after the second knockdown, cells were treated with 0.5 mg/ml puromycin (Sigma) for 1 hr, and then with 0.10 mg/ml cycloheximide for 20 min. Cells were washed twice in PBS to remove RNAse-containing medium and cells were scraped in 1mL in polysome lysis buffer containing RNAsin and CHX. Cells were

Dounce homogenized and lysates were spun at 5000xg for 10 min at 4°C and supernatants were loaded over 20-50% gradients for polysome separation.

siRNA pools (Dharmacon):

FXR1H (NM_008053)
Sense: CUAAUUACACCUCCGGUUAUU
Anti-Sense: 5'-P UAACCGGAGGUGUAAUUAGUU

Sense: CGGACGAAGUUGAUGCUUAUU
Anti-Sense: 5'-P UAAGCAUCAACUUCGUCCGUU

Sense: UAGAGUAUCACAUCGCUUAUU
Anti-Sense: 5'-P UAAGCGAUGUGAUACUCUAUU

Sense: UGAAGACACCGGAACGUUUUU
Anti-Sense: 5'-P AAACGUUCCGGUGUCUUCAUU

Fmr1 (NM_008031)
Sense: GAUGAGCAGUUGCGACAAAUU
Anti-Sense: 5'-P UUUGUCGCAACUGCUCAUCUU

Sense: CCAGAAGAUUUACGACAAAUU
Anti-Sense: 5'-P UUUGUCGUAAAUCUUCUGGUU

Sense: GCACCAAGUUGUCUCUUAUUU
Anti-Sense: 5'-P AUAAGAGACAACUUGGUGCUU

Sense: GAUCAUUCCCGAACAGAUAUU
Anti-Sense: 5'-P UAUCUGUUCGGGAAUGAUCUU

FXR2H (NM_011814)
Sense: CAUCAGUGGAGACCGCCAAUU
Anti-Sense: 5'-P UUGGCGGUCUCCACUGAUGUU

Sense: UGGAUGAGAAGGCGUAUUUUU
Anti-Sense: 5'-P AAAUACGCCUUCUCAUCCAUU

Sense: CCGCCGUAAUCGUGGUAACUU
Anti-Sense: 5'-P GUUACCACGAUUACGGCGGUU

Sense: CCUUGGAGUUGGGUAGUUUUU
Anti-Sense: 5'-P AAACUACCCAACUCCAGGUU

Estimation of Ribosomes/mRNA Per Sucrose Gradient Fraction

A representative gradient from a CHX-treated sample was used to quantify the number of ribosomes per gradient fraction. Individual ribosome peaks on the A_{254} trace were resolved between fractions 4 and 9, allowing polyribosome size to be directly counted up to 10 ribosomes. Polyribosome sizes in fractions 10-16 were extrapolated by fitting a polynomial trend line to the resolved data in fractions 4-9 ($y = 0.125x2 + 0.025x – 0.8$). To verify that the sucrose gradient was linear, the concentration of sucrose in each fraction of a blank gradient was measured using a sucrose refractometer (Hanna Instruments).

Selection of FMRP Targets and Nontargets for Analysis

Genes were selected for validation as FMRP targets on the basis of total number of CLIP tags. Because many top targets have long coding sequences compared to nontargets, several targets of moderate CDS length were included. Nontargets were required to have few CLIP tags, moderate to high representation in polyribosome fractions (measured by Affymetrix Exon Array) and strong neuronal expression (based on the neuronal transcriptome previously described (Cahoy et al., 2008)). Special effort was made to include nontargets of long CDS length.

Calculation of Ribosome Retention Score (RRS) and Ribosome Load

In order to quantify the FMRP-dependent effect on ribosome stalling we devised a means of estimating ribosome occupancy on mRNA in polyribosome gradient fractions, and weighting the differences in polyribosome profiles from WT and *Fmr1* KO fractions for this ribosome occupancy. By counting the number of ribosomes in each fraction from A_{254} traces and extrapolating, the average number of mRNA-associated ribosomes in each gradient fraction can be estimated based on linearity of the sucrose gradients. Multiplying the percentage of mRNA in each fraction by the number of ribosomes in that fraction and summing over the gradient puts a value on total ribosome occupancy (‘‘ribosome load’’) under any one condition. The difference between this value of stalled ribosomes from WT and the corresponding FMRP loss-of-function model value (*Fmr1* KO, I304N, or kcRNA-treated) after puromycin run-off yields an FMRP-dependent

ribosome retention score.

Electron Microscopic Analysis of Sucrose Gradient Fractions Containing Stalled Polyribosomes

Negative staining with uranyl acetate was performed by the Rockefeller University Electron Microscopy Resource Center as follows: 10 ul of fraction 9-10 from a WT puromycin-treated IVTEBP experiment sucrose gradient was deposited on a glow discharged, carbon-coated grid (EMS Cat#CF400-Cu-50) for 30 s to 1 min. After washing the sample quickly by passing over two drops of dd-H2O, the grid was then treated with 2 drops of 2% uranyl acetate (Fisher Cat#79853) for a total of 30 s. Excess stain was removed by touching the edge of the grid carefully to a filter paper wedge. After air drying the grid was viewed with a TecnaiSpiritBT Transmission Electron Microscope (FEI) at 80 KV and pictures were taken with Gatan 895 ULTRASCAN Digital Camera.

Immunogold-electron microscopy to detect polyribosomes by localization of EGFP-tagged ribosomal protein L10a was performed following 20%–50% sucrose gradient purification of cerebellar extracts, prepared as described above, from Bac transgenic Purkinje cell-specific *Pcp2* promoter driven EGFP-tagged rpL10a adult male mice (provided by Dr. Nat Heintz, Rockefeller University). Sucrose gradient fraction 9 or 10 was fixed in suspension using concentrated paraformaldehyde (PF) (16%) to reach a final concentration of 4% PF on ice. 10 ul of sucrose fraction 9 or 10 was deposited on a glow discharged and carbon-coated grid for 1 min and fixed again in 0.08% glutaraldehyde for 10 min at RT. After PBS washes and blocking in 1% BSA/PBS the polyribosomes were incubated first with anti-GFP antibody (Abcam #ab6556, 1:1000 dilution) and then with 6nm or 12nm colloidal gold conjugated to goat anti-rabbit IgG (H+L) for 30 min. The grids were washed and negatively stained with 2% uranyl acetate (Fisher Cat#79853) for a total of 30 s. Excess stain was removed by touching the edge of the grid carefully to a filter paper wedge. After air drying the grid was viewed with a TecnaiSpiritBT Transmission Electron Microscope (FEI) at 80 KV and pictures were taken with Gatan 895 ULTRASCAN Digital Camera.

In experiments using transfected EGFP-FMRP in cultured cells, 20 ug of pEGFP-C1 (negative control expressing only EGFP) or pEGFP-iso7-hFMRP (Darnell et al., 2005b) was transfected using FuGene 6 into 6 100 mm tissue culture plates of HEK293T cells at 30% confluence and allowed to express for 48 hr. Plates were treated with 1 mM puromycin or vehicle alone for 1 hr in the incubator, followed by 0.1 mg/ml cycloheximide for 20 min. Plates were washed twice with warm PBS and post mitochondrial cell lysates were prepared and fractionated on 20%–50% (w/w) linear sucrose gradients as described above. 10 ul of each fraction number 10 was fixed in 4% PF at 4_C overnight. 10 ul was deposited on a glow discharged and carbon-coated grid for 1 min and fixed again in 0.095% glutaraldehyde for 10 min at RT. The remainder of the protocol was performed as in the previous paragraph with 12 nm colloidal gold conjugated to goat anti-rabbit IgG (H+L).

Expression of GFP-FMRP in 293T cells

A sequence containing the human *Fmr1* cDNA seqeunce with a Kozak/ATG site and the TAA stop codon replaced by a Gly-Pro-Val swivel (contains AgeI site) was cloned in-frame to AcGFP in pAcGFP1-N1 by Jen Darnell (Clontech). Note that this construct does not contain the 3'UTR of *Fmr1*, since AcGFP is C-terminal to FMRP. The final plasmid was maxiprepped using an EndoFree kit (Qiagen) and transfected into 293T cells using FuGene (Promega) according to manufacturer's instructions. One plate of cells was transfected with 18ug of plasmid. Cells were grown 24 hours and were then treated with 0.1mg/mL CHX for 20 min. Cells were washed 2X with PBS to remove RNAse-containing medium and scraped in 1mL polysome lysis buffer containing RNAsin and CHX. Cells were Dounce homogenized and lysates were spun at 5000xg for 10 min at 4°C and supernatants were loaded over 20-50% gradients for polysome separation.

Purification of BAC DNA

A single colony was innoculated into 2mL TB medium and grown overnight at 37°C shaking at 250rpm. Cells were pelleted and resuspended in 0.3mL of P1 buffer (15mM Tris pH 8, 10mM EDTA, 100ug/mL RNAse A) by vortexing. 0.3mL of P2 buffer was then added (0.2N NaOH, 1% SDS), gently shaken and incubated 5 min at RT. 0.3mL of

P3 buffer (3M KOAc pH 5.5) was then slowly added while gently shaking to mix, and then incubated on ice for at least 5 min. Lysates were spun on benchtop microfuge at 10,000rpm for 10 min at 4°C. Supernatant was transferred to 1.5mL tube containing 0.8mL cold isopropanol and incubated on ice for at least 5 min or -20°C overnight. DNA was precipitated by spinning in benchtop microfuge at max speed for 15 min. DNA was washed twice in 0.5mL of 70% EtOH, dried on benchtop to a translucent color (not overdried) and resuspended in 40uL TE. Important: DNA was not vortexed or pipetted at any stage, and resuspension was achieved by soaking DNA in TE for about an hour, occasionally tapping tube.

Recombineering protocol

An overnight 5mL culture of the desired strain (SW106 or SW102, containing target plasmid as appropriate) was grown at 32°C, plus antibiotic as appropriate. Note that it is critical not to grow these cells any higher than 32°C, because the recombination genes are temperature-controlled. The overnight culture was added at approximately 1:50 ratio to 50mL LB (plus antibiotic as appropriate) and grown 2-3 hours at 32°C to an OD_{600} of 0.6. 10mL of culture was put on a slush of ice+water as the uninduced control. Another 10mL was transferred to a small Erylenmeyer flask and swirled in a 42°C water bath for 15 min (to induce recombination genes), and then swirled in the ice slush for 2 min and left on ice. Both sets of cells were spun down at 4000xg for 6 min at 4°C. Pellets were resuspended in 0.9mL ice-cold water by extremely gentle pipetting. Cells were washed twice more, spinning down in benchtop centrifuge at max speed for 20 sec, being careful to remove all the supernatant so residual salt did not ruin electroporation. Cells were resuspended extremely gently in 40uL ice-cold water. DNA was then added to cells (50ng linearized retrieval vector, 6ug BAC DNA, or 300ng lox-neo-lox PCR product was used) and 50uL of cells were put in a 0.1cm electroporation cuvette on ice. Electroporation was done at 1.7kV, 25uF, 200Ω. Cells were recovered in 1mL LB at 32°C for 1 hour and then plated and grown at 32°C for 18-24hrs. Cells containing correctly recombineered constructs were miniprepped and plasmid was retransformed to obtain a pure clone (since not all copies of plasmid recombine in each cell originally). To retransform, cells were grown and washed as before but not heat-shocked.

Ligations

For average-sized constructs: Vector and inserts were digested overnight and vector was treated with 1uL calf alkaline intestinal phosphatase (CIAP, Roche) in a 35uL volume at 37°C for 15 min. An additional 1uL of CIAP was added and incubated at 55°C for 45 min. 70uL water, 1uL 0.5M EDTA, 2.5uL 20% SDS and 1.5uL Proteinase K were added and incubated at 55°C for 30 min. Sample was extracted in 100uL phenol:chloroform:isoamyl alcohol (25:24:1) and the aqueous layer was gel purified over a 0.8% agarose gel at 135V for 1 hour and extracted using a QiaQuick Gel Extraction kit (Qiagen). Ligation was performed using a 3X molar excess of insert to vector and a total DNA concentration of 10ng/uL total DNA concentration, with 1uL T4 DNA ligase (NEB) at room temperature for 5-30 min.

For large constructs: Final cloning into PL253 involved ligation of a 6.5kB insert into a 19.7kB vector. This ligation was achieved using a 3:1 molar ratio of insert to vector with a 25ng/uL total DNA concentration. Although such a high DNA concentration typically causes end-to-end linear products to predominate in the reaction, in this case because the fragments are so large, the concentrations are appropriate. 25ug of PL253 (19.7kB, containing lox-exon17-*Fmr1* 3'UTR) and 25ug of pCR4-TOPO (containing the 6.5kB Proudfoot-Frt-Neo-Frt-lox-exon17-AcGFP-*Fmr1* 3'UTR insert) were digested overnight with 2uL Bsu36I in a 100uL volume. For pCR4-TOPO, adequate purification of the 6.5kB insert from the 4kB backbone and the 10.5kB uncut vector was achieved by running the reaction over a 0.8% gel for 2 hours and repurifying the upper band over another 0.8% gel for another 3 hours, resulting in a 28% yield. Digested PL253 was treated with CIAP and the CIAP was removed by proteinase K digest, organic extraction and gel purification as above. The vector was recovered using a Qiaex II Gel Extraction kit (Qiagen) designed for large vectors, which when double-eluted with EB resulted in a 10% overall yield. Fragments were ligated using a 3:1 molar ratio of insert to vector, 25ng/uL total DNA in a volume of 20uL, and incubation with 0.5uL concentrated T4 DNA ligase (NEB) for 2 hours at 25°C, followed by addition of another 0.5uL ligase and overnight incubation at 16°C.

14.3kB of *Fmr1* sequence spanning exon 17 was subcloned into PL253 (Frederick National Laboratory Biological Resources Branch) from the BAC RP23-149C7 (obtained from BacPac CHORI, derived from C56BL/6 mice) in the SW106 recombineering strain (Frederick National Laboratory Biological Resources Branch) (see Figure 36). 500nt homology "arms" to each end of the 14.3kB segment were first cloned into PL253. These arms were PCR amplified from the BAC using Accuprime Pfx Supermix (Invitrogen) and the following primers (restriction sites shown in capital letters):

5' *Fmr1* miniarm F (Not1 site)
5'-gccGCGGCCGCgattgaactattctcagcttagaatgtgtc-3'

5' *Fmr1* miniarm R (HindIII site)
5'-gccAAGCTTcaagggcagatcaatatagtgatttcttag-3'

3' *Fmr1* miniarm F (HindIII site)
5'-gccAAGCTTgttgtcctcatcaaaccttcatttcttg-3'

3' *Fmr1* miniarm R (BamH1 site)
5'-gccGGATCCcaaagggttacattatttcaacctgcc-3'

The PCR products and PL253 were digested overnight with the appropriate restriction enzymes (NEB), the vector was CIPped (see protocol below) and all products were gel purified. The fragments were then assembled into PL253 (between the Not1 and BamH1 sites) in a triple ligation using 3X molar excess of miniarms (which are about $1/10^{th}$ the size of the vector) and T4 DNA ligase (NEB). Ligations were transformed into XL10-Gold Ultracompetent cells (Agilent) according to manufacturer's protocol. A plasmid containing both miniarms in correct orientation was chosen by sequencing (Macrogen), maxiprepped (Qiagen HiSpeed Plasmid Maxi Kit), linearized by overnight HindIII digest and gel purified.

Purified BAC RP23-149C7 was transformed into SW106 (see transformation protocol below) with chloramphenicol selection. Purified, linearized PL253 with miniarms was transformed into SW106 cells carrying BAC RP23-149C7 and retrieval of the *Fmr1* sequence by gap repair was achieved by recombineering (see protocol below). Correct clones were selected on carbenicillin and retransformed into SW106 (not carrying the BAC) to obtain pure clones. This step is very important, as cells contain multiple copies

of plasmid during gap repair and not all plasmids will retrieve the *Fmr1* sequence. A correct clone was chosen by restriction digest and fully sequenced (Macrogen).

Targeting of upstream (lone) lox site and arabinose-induced Neo pop-out

100nt PCR primers were designed as depicted in Figure 36. These primers contain 48 or 36nt of homology on either side of a site 439nt upstream of the annotated end of exon 17 (note that an unannotated alternative splice site exists 51nt upstream of the annotated exon boundary), as well as loxP seqeunces, restriction sites and homology to the ends of the Neo cassette in PL452 (Frederick National Laboratory Biological Resources Branch). The sequences of these primers are as follows (*Fmr1* homology is underlined, Neo homology is in capital, restriction sites are in bold, loxP sequence is in plain lowercase): Note that primers must be purified by 2-step HPLC.

F primer
5'-
tgctgtatactttgcctataccttatatattttctattagccaataataacttcgtataatgtatgctatacgaagttatCGACCTG
CAG
CCTGTTGA-3'

R primer
5'agcaaaaatcagtgaggccattcaaattaagttact**gatatcgaattc**ataacttcgtatagcatacattatacgaagttatGT
C
GAGGCTGATCAGCGA-3'

The Neo cassette in PL452 was amplified using these primers and the product was gel purified and transfected into SW106 cells containing PL253 with the retrieved *Fmr1* sequence. (Note that residual plasmid can be digested away using DpnI, but was not done here.) Recombineering resulted in insertion of the lox-neo-lox sequence 439nt upstream of *Fmr1* exon 17. A correct clone was selected by Neo resistance and retransformed, checked by restriction digest and the insert was sequenced through the junctions (Macrogen). Note that as PL253 gets bigger, the correct clones tend to be the more slow-growing ones. The lox-neo-lox cassette was recombined to a single lox site by arabinose-induced lox recombination (SW106 cells contain arabinose-inducible Cre). From an overnight culture of "plain" SW106 cells, 2mL was inoculated into 40mL of LB and grown at 32°C for 2 hrs to OD_{600} of 0.5. 10mL additional LB plus 500uL of 10%

arabinose was added and cells were grown at 32°C for 1 hour to a final OD_{600} of 0.9. 1ng of PL253 containing lox-neo-lox- *Fmr1* was electroporated into the cells. Cells were recovered in 1mL LB at 32°C for 1hr and plated on carbenicillin. Cells were also plated on kanamycin to check for efficiency of pop-out. Correct clones were selected by restriction digest, re-checked on carb and kan plates to ensure they were correct, and sequenced across the lox site (Macrogen). Finally, the correct clone was transformed into SW102, a recombineering strain similar to SW106 that does not contain Cre, and is thus a more stable line to continue with.

Insertion of Proudfoot polyadenylation sequence upstream of Frt-Neo-Frt-lox site

Forward and reverse oligos corresponding to the Proudfoot sequence plus restriction sites were ordered (Fisher, 2-step HPLC purified) and annealed by incubating in a beaker of 90°C water and letting the water cool on the benchtop to room temperature. Oligo was then ligated into PL451 (Frederick National Laboratory Biological Resources Branch) at the HindIII site just upstream of the Frt-Neo-Frt-lox cassette, using 3X molar excess of oligo, in XL10-Gold cells (Agilent). Correct clones were selected by digest and sequenced across junctions (Macrogen). Sequence of the Proudfoot oligo is as follows (added restriction sites in bold):

5'-ccc**aagctt**aataaaagatctttattttcattagatctgtgtgttggttttttgtgtg**catatgaagctt**ggg-3'

Site directed mutagenesis of the Bsu36I site in AcGFP

The Bsu36I site in AcGFP (pAcGFP1-N1, Clontech) was destroyed by a conservative point mutation for cloning purposes using the Stratagene QuikChange Multi Site-Directed Mutagenesis kit. The Bsu36I sequence was changed from CCTGAGG to CCAGAGG using the following PAGE-purified primer (Fisher):

5’-caagagcgccatg**catgagg**gctacatcc-3’

Plasmids were transformed into XL10-Gold cells (Agilent) and a correct clone was obtained by sequencing (Macrogen).

Construction of *Fmr1* exon 17 – AcGFP – fmr1 3'UTR via overlap extension PCR

Design of PCR strategy is depicted below. The TAA stop codon of *Fmr1* exon 17 was removed and a Gly-Pro-Val linker was added. AcGFP (with mutated Bsu36I site) was added in-frame to the linker with a TGA stop codon, followed by the *Fmr1* 3'UTR. PacI and Bsu36I cloning sites were included at the 5' and 3' ends of the final product as indicated in the figure below. Six sets of PCR reactions were performed using Pfx supermix (Invitrogen), followed by gel purifications of each product, as follows:

PCR#1: Primers AF and AR, plasmid PL253- *Fmr1* ("product A" = *Fmr1* exon17 + linker)

PCR#2: Primers BF and BR, plasmid pAcGFP1-N1 ("product B" = linker + AcGFP)

Primers AR and BF create the Gly-Pro-Val linker between exon 17 and AcGFP

PCR#3: Primers AF and BR, products A and B ("product AB" = exon17+AcGFP)

Products A and B overlap (via the linker sequence), so will prime off each other and create product AB in early cycles of PCR#3, which will then be amplified by primers AF and BR

PCR#4: Primers AF and B2R, product AB ("product AB2" = exon17+AcGFP+overlap)

Note – this PCR was necessary because I had not added an overlap "tail" matching the Fmr1 3'UTR sequence to Primer BR originally.

PCR#5: Primers CF and CR, plasmid PL253-fmr1 ("product C" = overlap+ *Fmr1* 3'UTR)

PCR#6: Primers AF and CR, products AB2 and C ("product ABC" = exon17+linker+AcGFP+ *Fmr1* 3'UTR)

Products AB2 and C overlap, so will prime off each other as before and create product ABC in early cycles of PCR#6, which will then be amplified by primers AF and CR.

Products AB and ABC were A-tailed using old-fashioned Taq at 70°C for 20 min, TOPO-TA cloned per manufacturer's instructions (Invitrogen) in TOP10 cells (Invitrogen), and sequenced (Macrogen).

Primers used for overlap extension PCR (AF and AR = forward and reverse respectively, etc):

Gly-Pro-Val linker region is in capitals. PacI and Bsu36I restriction sites in bold. Overlap regions underlined.

Primer AF: 5'-ccc**ttaattaa**agtaacttaatttgaatggcc-3'

Primer AR: 5'-TGACCGGTCCgggtactccattc-3'

Primer BF: 5'-cGGACCGGTCatggtgagcaag-3'

Primer BR: 5'- tcacttgtacagctcatccatgccg -3'

(the 5' end of this primer corresponds to the TGA stop codon of AcGFP)

Primer B2R: 5'-ggaattatgtagcttattcacttgtacagctcatc-3'

Primer CF: 5'-gatgagctgtacaagtgaataagctacataattcc-3'

(Primers B2R and CF are reverse complements of each other, but the primers were never used together in the same reaction. Thus, the entire sequence of each primer generates an overlap region in the products)

Primer CR: 5'- aacaag**cctgagg**acttgagtttgattc -3'

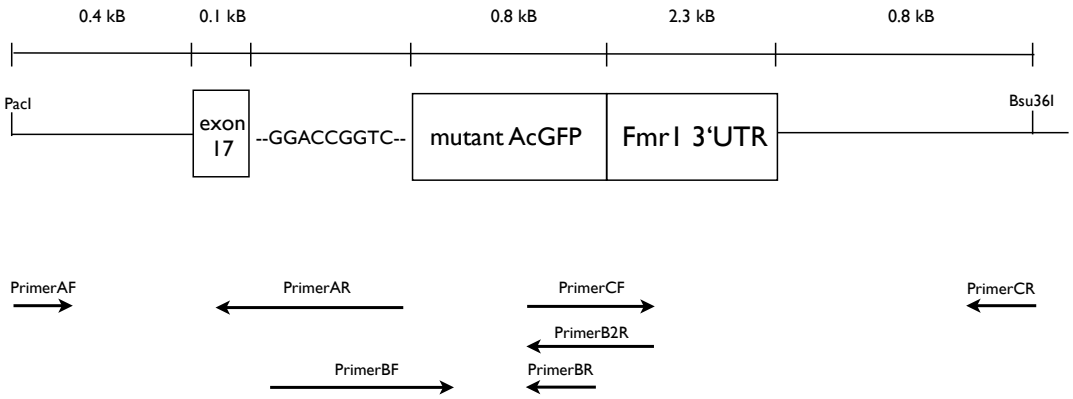

Note: Segments are not drawn to scale, but primers are drawn to show which segments they overlap.

Assembly of final cassette and cloning into PL253

The Bsu36I-Proudfoot-Frt-Neo-Frt-lox cassette was PCR amplified using primers ending in PacI and cloned into pCR4-TOPO (containing *Fmr1*exon17-linker-AcGFP- *Fmr1* 3'UTR cassette as assembled via overlap extension PCR) at the PacI site (see Figure 37). Next, the resulting cassette (Proudfoot-Frt-Neo-Frt-lox- *Fmr1* exon17-linker-AcGFP- *Fmr1* 3'UTR) was cut out by Bsu36I digest and cloned into the Bsu36I site in PL253 (containing lox- *Fmr1* exon17- *Fmr1* 3'UTR) (see further descriptions in Ligations section). Clones were checked by restriction digest and sequencing across junctions.

Construct targeting and breeding of knockin mice

The targeting vector was transfected into male albino C57BL/6 ES cells by the Gene Targeting Resource Center and positive ES cells identified based on Southern blots. 7/200 injected ES cell lines were positive for Neo as assessed by Southern blot. Of these, 1/7 was confirmed correct by further Southern blots (See Figure 39). This ES cell line was injected into C57BL/6 blastocysts and 14 chimeric males were obtained (3 grade A, 3 grade B, 6 grade C and 2 grade D). The best 10 chimeras were bred with female albino C57BL/6 mice. Two chimeric males consistently gave rise all-white litters, indicating the germ cells were fully derived from the injected ES cell, while two other chimeras give litters with some white and some black pups, indicating that only some germ cells were derived from the injected ES cell. In these crosses, all white female progeny were cTAG/+ (see Figure 41). These cTAG/+ females were bred with C57BL/6 males, either wt or expressing Flp or Cre drivers of interest (Mice: EIIa-Cre was a gift from the Roeder lab, Emx1-Cre obtained from Jackson Labs #005628, actin-Flp obtained from Jackson Labs #005703, albino C57BL/6 obtained from Jackson labs #000058). All mice were on the B6 background.

Cre expression in ES cells

ES cells from clone #189 were plated on a feeder layer of mouse embryonic fibroblasts and passaged once by the Gene Targeting Facility, using KDMEM medium (prepared in Gene Targeting facility) on 6-well plates. Cells were then transfected with 1ug pPAC-Cre as follows. Per well, 1ug pPAC-Cre (obtained from Gene Targeting facility) was

mixed with 0.5mL OptiMEM medium (reduced serum plus GlutaMax, Invitrogen). Per well, 20uL Lipofectamine (Invitrogen) was mixed with 0.5mL OptiMEM medium. After 5 min, the two were combined and let sit 20 min at RT. Medium was removed from cells and 1mL plasmid + Lipofectamine mixture was added per well. Cells were incubated 5 hours (cannot go longer or cells will die) and 6mL KDMEM medium was added without removing OptiMEM (cells not adherent under these conditions). (500mL KDMEM prepared by Gene Targeting facility contains 395mL KDMEM, 75mL knockout serum replacement, 10mL L-Glu 100X, 5mL 2-mercaptoethanol 100X, 5mL nucleosides 100X, 5mL nonessential amino acids 100X, and 75uL leukemia inhibitory factor.) Cells were grown KDMEM while still on the feeder layer, changing medium twice per day. 22 hours after transfection, one portion of cells was selected with 1ug/mL puromycin (ideally, should have been 6 hours post transfection). Puromycin was maintained in the medium for 24 hours, and surviving cells were allowed to recover in puromycin-free KDMEM for 2 days. As needed, cells were split into gelatinized flasks by trypsinization and gentle trituration. Once on gelatin instead of the feeder layer, medium was changed to a 50-50 mix of KDMEM and ES Cell medium (500mL ES Cell medium prepared by Gene Targeting facility contains 400mL ES DMEM, 75mL ES FBS, 5mL 2-mercaptoethanol 100X, 5mL nucleosides 100X, 5mL L-Glu 100X, 5mL nonessential amino acids 100X and 50uL leukemia inhibitory factor). Cells were harvested by trypsinization and spun down. Pellets were resuspended in polysome lysis buffer containing RNAsin (ideally, cells should have been washed before lysis to remove RNAse-containing medium. RNA appeared intact on polysome gradients). RNA was prepared from (–)Cre, (+)Cre and (+)Cre/(+)puromycin cells using Trizol LS (Invitrogen) extraction and High Pure RNA isolation kit (Roche) with on-column DNAse treatment. *Fmr1* mRNA positive for AcGFP was detected by hot RT-PCR (see protocol below) using primers in *Fmr1* exon 16 and 3'UTR.

Southern blotting

25ng of PCR-amplified DNA (250-300nt) was combined with 10uL random hexamers (Roche) in a 30uL volume and heated at 95°C for 3 min, then cooled at RT for 3 min. To this, added 10uL 5X buffer (Stratagene Prime-It II kit), 10uL of 6000Ci/mmol P^{32}-dATP

and 1uL Exo-Klenow and incubated at 37°C for 30 min. Reaction was passed twice over G-50 spin columns and specific activity was calculated using Cerenkov counting. To calculate amount of probe needed, used the following formula: (mL of hybridization buffer x 2.5 x 10^6)/CPM. Typical result is 3 million counts per 1uL (specific activity of 10^9). Membranes containing digested DNA (prepared by the Gene Targeting Facility) were combined with 10mL of preheated 65°C QuikHyb buffer (Stratagene) and incubated at 65°C for 1 hr. The calculated volume of probe was combined with 2 volumes salmon sperm DNA and heated at 95°C for 3 minutes, cooled on benchtop, added to 10mL preheated QuikHyb buffer, and put on the membrane. Hybridization was carried out at 65°C for 90 minutes. Longer incubation times, or using more than the calculated amount of probe, resulted in high background. Membrane was then rinsed twice with 25mL 2X SSC and washed 1X at 65°C for 20 min in 50mL of 2X SSC (prewarmed). If Geiger counter was above 0.1X range, another wash in 2X SSC was performed for 30 min. Membranes were exposed to Kodak MR film for 12 hrs-several days. 1L of 2X SSC contained 100mL 20X SSC, 5mL of 20% SDS and 10mL of 10% Na-pyrophosphate.

Hot RT-PCR from ES cells and mouse brain

RNA was prepared from mouse brain or cell lysates by extraction in Trizol LS (Invitrogen) and precipitation as described above (RNA isolation from whole brain). RNA was purified using the High Pure RNA isolation kit (Roche) as described above. cDNA was prepared as above using Superscript III (Invitrogen). PCR was carried out using Accuprime Supermix I (Invitrogen) and 1uL of a 1:10 dilution of P^{32}-dCTP was added in the last two cycles. PCR products were resolved on 6% acrylamide-urea denaturing gels and imaged on Kodak MR film.

Regions amplified:

Fmr1 exon 16 to 3'UTR
Exon 16 primer: 5'- GACGATCATTCCCGAACAGATAATCG-3'
3'UTR primer: 5'- GGACATGAAATGGCACAGCATTTC-3'

Fmr1 exon 11 to exon 17
Exon 11 primer: 5'- CTCAACCTAACAGTACAAAAGTCCAGAGG-3'
Exon 17 primer: 5'- GGGTACTCCATTCACCAGCGG-3'

Fmr1 exon 11 to AcGFP
Exon 11 primer: 5'- CTCAACCTAACAGTACAAAAGTCCAGAGG-3'
AcGFP primer: 5'- GATGCCGGTGAACAGCTCGG-3'

Purification of nuclei from mouse brain

Pelleting under sucrose: Brains from P7 mice were dissected free of white matter, placed with 0.5mL PBS in a 6-well plate over a bed of wet ice, chopped, and UV-crosslinked three times at 400 mJ/cm2 (254 nm UV light) with swirling between each irradiation, using a Stratalinker 2400 (Stratagene). Crosslinked tissue was homogenized in nuclei buffer (0.32M sucrose, 20mM HEPES pH 7.4, 5mM $MgCl_2$, 5mM $CaCl_2$, 0.5 mM dithiothreitol, 1X Complete EDTA-free protease inhibitor cocktail (Roche) and 40 U/ml RNAsin (Promega)) with 10 strokes at 900 rpm in a motor-driven Teflon-pestle 5 ml glass homogenizer (Wheaton). Homogenates were brought to 1% NP-40 or 1% Triton-X from 10% stocks, mixed by inversion and incubated on ice 10 minutes. 2mL of lysate was then loaded over 9mL of 50% sucrose in polysome buffer in 14x3x89 mm polyallomer ultracentrifuge tubes (Beckman 331372) and spun at 25,500 rpm for 2.5 hrs at 4°C in a Beckman SW41 rotor, reserving some input for Western blot. After the spin, tubes were drained and pellets were resuspended in 50uL PBS.

Pelleting in Eppendorf tubes: Brains from P9 mice were dissected free of white matter, chopped and crosslinked as above. Tissue was homogenized as above in polysome lysis buffer (without CHX) and brought to 0.8% NP-40. Lysate was spun at 2000xg for 10 minutes at 4°C. The top 60% of supernatant was removed as a "cytoplasm" sample. The remaining supernatant was discarded and the pellet was very gently resuspended in polysome lysis (containing 0.8% NP-40) buffer by stirring with a P200 tip. The wash was repeated a second time and then the nuclei were resuspended in 200uL lysis buffer (for Western) or PXL (for CLIP, see below).

Separation of membrane-bound and free polysomes from mouse brain

Method 1: Brains from P21 mice were dissected free from white matter and homogenized in 0.32M sucrose, 20mM HEPES pH 7.4, 5mM $MgCl_2$, 0.1M DTT, 1X Complete EDTA-free Protease Inhibitor cocktail (Roche) and 40U/mL RNAsin (Promega), with 10 strokes

at 900rpm in a motor-driven Teflon-pestle 5 ml glass homogenizer (Wheaton). Homogenates were spun at 2000xg at 4°C for 10 minutes. Supernatant was then spun at 10,000xg at 4°C for 10 minutes. Supernatant was then spun at 12,000xg at 4°C for 10 minutes. Final supernatant was spun at 140,000xg at 4°C for 2 hrs in a TLA 120.2 rotor. Pellet was resuspended in the same buffer + 2% NP-40 in 20% of the original volume.

Method 2: Brains from P15 mice were dissected free from white matter and homogenized in 0.8M sucrose, 20mM HEPES pH 7.4, 150mM NaCl, 5mM $MgCl_2$, 0.1M DTT, 1X Complete EDTA-free Protease Inhibitor cocktail (Roche) and 40U/mL RNAsin (Promega), with 10 strokes at 900rpm in a motor-driven Teflon-pestle 5 ml glass homogenizer (Wheaton). Homogenates were spun at 2000xg at 4°C for 10 minutes. Supernatant was then spun at 12,000xg at 4°C for 10 minutes. Supernatant (0.5mL) was then loaded over a discontinuous gradient containing (from bottom): 1.6mL of 2.5M sucrose, 2.5mL of 2.15M sucrose, 5mL of 2.05M sucrose and 3mL of 1.3M sucrose in a 14x3x89 mm polyallomer ultracentrifuge tube (Beckman 331372) and spun at 90,000xg at 4°C for 5 hrs in a Beckman SW41 rotor. 750uL fractions were collected from the top of the gradient by pipette.

Method 3: Brains from P14 mice were dissected free from white matter and homogenized in 1mL polysome buffer + 0.25M sucrose, 0.1M DTT, 1X Complete EDTA-free Protease Inhibitor cocktail (Roche) and 40U/mL RNAsin (Promega), with 6 strokes at 500rpm in a motor-driven Teflon-pestle 5 ml glass homogenizer (Wheaton). Homogenates were spun at 2000xg at 4°C for 10 minutes. Supernatant was then spun at 12,000xg at 4°C for 10 minutes. Supernatant (1mL) was then loaded over a discontinuous gradient containing (from bottom): 1mL of 2.5M sucrose, 5mL of 1.3M sucrose, 4mL of 0.8M sucrose and spun at 140,000xg at 4°C for 2.5 hrs in a Beckman SW41 rotor. 700uL fractions were collected from the top of the gradient by pipette. Samples were ligated to unique linkers and pooled for RNA Seq analysis.

Prepraration of samples for RNA Seq analysis:

Samples were extracted equal volume phenol/chloroform pH4.5, back-extracted in chloroform:isoamyl alcohol and precipitated at -80. Pellets were washed in 70% EtOH and resuspended in water. 2ug RNA was prepared using the Illumina TruSeq protocol using fragmentation instead of Ribo-Minus. Samples were fragmented as follows: 16ul RNA was incubated with 4ul 5x Fragmentation Buffer (Illumina) for 5min at 94C. 2ul Fragmentation Stop Solution (illumina) was added and sample was placed on ice. 2ul 3MNaOAc, 2ul glycogen and 60ul 100%EtOH was added. After precipitation samples were spun at 20000g at 4C for 25min. Samples were washed with 300ul 70%EtOH and resuspended in 11uL water. Preparation of 1st strand cDNA: 11ul fragmented RNA was combined with 1ul random primers and heated at 65C for 5min. 4ul 5x 1st strand buffer, 2ul 100mM DDT, 0.4ul 25mMdNTP mix and 0.5ul RNase Inhibitor were added and incubated at RT for 2min. 1ul SuperScript II (Invitrogen) was then added and reaction was incubated at RT 10min, then at 42C for 50min and 70C for 15min. The standard Illumina TruSeq protocol was then followed starting from 2nd strand cDNA synthesis.

Induction of MECS

Mice were hand carried from the mouse facility a few hours before the experiment and kept in a quiet space. Ear clip pads were dipped in a 2.5M NaCl and placed on the ears. Settings were: Frequency 85 pulses/sec; pulse width 4ms; duration 1 sec, current 25mA. After seizure, if the mouse stopped breathing it was given rescue breaths with a blue rubber Pastuer pipette bulb for approximately 30 seconds until mouse began breathing spontaneously (refreshing air in bulb every 5 squeezes). Mice were then returned to home cages until sacrifice. Time was measured from the induction of the seizure.

FMRP CLIP

Preparation of tissue

Brains were placed in a dish containing a small amount of ice-cold 1X HBSS + 10mM HEPES pH 7.4, chopped with a clean razor blade into ~2mm pieces and UV crosslinked on a bed of ice-slush three times at 400 mJ/cm2 (254 nm UV light) with swirling between each irradiation, using a Stratalinker 2400 (Stratagene). Tissue was then removed from

buffer using curved forceps and homogenized in 1mL PXL (1X PBS [tissue culture grade; no Mg^{2+}, no Ca^{2+}, GIBCO], 0.1% SDS, 0.5% Na-DOC, 0.5% NP-40) plus 0.1M DTT, 1X Complete EDTA-free Protease Inhibitor cocktail (Roche) and 40U/mL RNAsin (Promega), with 10 strokes at 900rpm in a motor-driven Teflon-pestle 5 ml glass homogenizer (Wheaton). For nuclear CLIP, crosslinking was done before purification of nuclei and pellets were resuspended in PXL (see above). Samples were allowed to dissociate in PXL for 10 minutes on ice. Samples were then treated with 50uL RQ1 DNAse (Promega) at 37°C for 5 min, at 1200rpm in thermomixer. Samples were then spun at 32,000xg at 4°C for 20 min in a TLA120.2 rotor. Supernatants were brought to 1mL in PXL and treated with RNase Cocktail, a mixture of RNases A and T1 for more complete digestion (AM2286, Applied Biosystems/Ambion), using a titration of dilutions in the range of 1:20,000 (ie, 10uL of a 1:20,000 serial dilution of RNAse was added to 1mL of sample). Samples were incubated with RNAse at 37°C for 10 minutes and reactions were stopped by putting on ice slush and adding 10uL Superasin (Ambion) plus 4ul RNAsin (Promega) per sample. Samples were then precleared and immunoprecipitated as descibed in the above Immunoprecipitations secion.

Dephosphorylation of RNA, 3' Linker Ligation, and SDS-PAGE Separation of RNABP:RNA Complexes

Immunoprecipitations were treated with calf intestinal phosphatase to remove the 5' phosphate from RNA crosslinked to FMRP (''RNA tags'') so that the RNA could not circularize during ligation, an otherwise predominant competing intramolecular reaction. Beads were resuspended in 0.08 ml of 1X dephosphorylation buffer and 3 units of CIAP (Roche) and incubated in the Thermomixer R at 37°C for 20 min, programmed to shake at 1000rpm for 15 s every 4 min, followed by 2X 1ml washes with PNK buffer (+)EGTA (10mM Tris pH 7.5, 20mM EGTA, 0.5% NP-40) and 3X 1mL washes with PNK buffer (-)EGTA (10mM Tris pH 7.5, 10mM $MgCl_2$, 0.05% NP-40) with one tube change during washing. To ligate a P^{32}-labeled RNA linker to the 3' end of the RNA, the puromycin-blocked linker (L32, 5'-OH-GUGUCAGUCACUUCCAGCGG-3'-puromycin, Dharmacon) was first labeled using T4 phosphonucleotide kinase (PNK, New England Biolabs, NEB). 50 pmol of L32 RNA, 0.015 ml P^{32}-γ -ATP, 1uL RNAsin and 2 ul of T4

PNK in 1X PNK buffer were incubated at 37°C for 30 min, an additional 0.02 ml 1 mM ATP was added and the reaction incubated 5 min. Radiolabeled linker was spun through a G-25 column (Amersham) to remove free ATP. 30 pmol of the labeled 3' RNA linker was added to a 0.08 ml T4 RNA ligase reaction (Fermentas), according to kit instructions, and on-bead ligation reactions were incubated at 16°C for 1 hr in a thermomixer programmed to shake at 1000rpm for 15 sec every 4 min. After 1 hr, 80 pmol of L32 RNA linker WITH 5' phosphate was added to each tube and incubated overnight, followed by 3X washes with PNK buffer. To rephosphorylate the 5' end of the RNA for 5' linker ligation, 80 ul of T4 PNK mix (6 ul of 1 mM ATP, 4 ul T4 PNK enzyme [NEB], 1 ul RNasin in 1X T4 PNK buffer [NEB], total volume 80ul) was added to each tube and incubated for 20 min at 1000rpm shaking for 15 sec every 4 min and washed 3X with PNK buffer. Each tube of beads was resuspended in 40 ul NuPAGE loading buffer (LDS, Invitrogen), containing reducing agent, and incubated at 70°C for 10min at 1000rpm. Supernatants were taken off the beads and run on Novex NuPAGE 10% Bis-Tris gels (Invitrogen) in MOPS running buffer (Invitrogen) for 2 hr at 175V and transferred to Protran nitrocellulose (S&S) using a Novex wet transfer apparatus (Invitrogen). After transfer, the nitrocellulose was quickly rinsed with RNase-free PBS, blotted with Kimwipes, wrapped in plastic wrap and exposed to Biomax MR film (Kodak).

Recovery of Complexes, Protease Digestion, and 5' Linker Ligation

Nitrocellulose membranes were aligned carefully with the exposed film and filter excised with a scalpel from 105-140 kDa (the size range of FMRP crosslinked to RNA of approx. 100 nucleotides). Each band of nitrocellulose membrane was further cut into smaller pieces and proteinase K treated (0.2 ml of a 1:5 dilution of proteinase K (4 mg/ml, Roche) in PK buffer (100 mM Tris-Cl pH 7.5, 50 mM NaCl, 10 mM EDTA)) at 37°C, 1100 rpm for 20 min. Then 0.2 ml of PK plus 7M urea solution was added and incubated for another 20min at 37°C at 1100 rpm. Finally, 0.4 ml of RNA phenol (pH 6.8, Applied Biosystems/Ambion) and 0.13 ml of 49:1 CHCl3:isoamyl alcohol were added and incubated at 37°C, 1100 rpm for additional 20 min. Tubes were spun at 20,000 x g in a desktop microcentrifuge. Glycogen (0.8 ul, Applied Biosystems/Ambion), 50 ul 3M NaOAc pH 5.2, and 1 ml of 1:1 ethanol:isopropanol were added to the aqueous phase in a

fresh tube and RNA was precipitated overnight at -20°C. RNA was pelleted, washed with 75% ethanol, the pellet dried and dissolved in 6 ul RNase-free H_2O. RNA ligation to add the 5' linker (RL5D: 5'-OH-AGGGAGGACGAUGCGGr(N)r(N)r(N)r(N)G3'-OH) was performed with 1 ul 10X T4 RNA ligase buffer (Fermentas), 1 ul BSA (0.2ug/ul), 1 ul ATP (10mM), 0.1 ul T4 RNA ligase (3U, Fermentas), and 20 pmol of RL5D RNA linker in a total volume of 10 ul at 16°C for 5 hrs. To the ligation reaction, 77 ul H_2O, 11 ul 10X RQ1 DNase buffer, 5 ul RQ1 DNase (Promega) and 5 ul RNasin (Promega) were added and incubated at 37°C for 20 min. 0.3 ml H_2O, 0.3 ml RNA phenol (Ambion) and 0.1 ml $CHCl_3$ were added, vortexed, spun and the aqueous layer taken. RNA was precipitated with 50 ul 3M NaOAc pH 5.2, 0.8 ul glycogen (Ambion) and 1 ml 1:1 ethanol:isopropanol overnight at -20°C.

RT-PCR and High-Throughput Sequencing of PCR Products

RNA was pelleted, washed, dried, and resuspended in 8 ul of RNase-free H_2O. The RNA was mixed with 2 ul of primer P32 (3' DNA primer 32, 5'-CTTCACTCACCTCGCAACCG-3', Operon) at 5 pmol/ul, incubated at 65°C for 5 min, chilled, and spun briefly. 3 ul 3mM dNTPs, 1 ul 0.1M DTT, 4 ul 5X SuperScript RT buffer, 1 ul RNasin, and 1 ul SuperScript III (Invitrogen) were added and incubated at 50°C for 30 min, 90°C for 5 min and briefly at 4°C. PCR reactions were performed with 27 ul Accuprime Pfx Supermix (Invitrogen), 1 ul P51 (5' DNA primer 51, 5'-AGGGAGGACGATGCGG-3', Operon) at 5 pmol/ul, 1 ul P32 primer, 5 pmol/ul and 2 ul of the RT reaction, cycled for 20-25 cycles using a program of 95°C for 20 s, 61°C for 30 s, and 68C for 20 s. A 10% denaturing polyacrylamide was poured and the entire PCR reaction was loaded along with 3 ul of Amplisize Molecular Ruler (Biorad). To visualize DNA, the gel was immersed in a 1:10,000-fold dilution of SYBR Gold (Molecular Probes) in TBE for 10 min. Routinely, aliquots of the reaction were removed at various cycle numbers and product excised from the lowest cycle number giving visible product. Acrylamide bands containing DNA of 60-100nts were excised and DNA purified by crushing in diffusion buffer (0.5M ammonium acetate, 10mM Mg acetate, 1mM EDTA, 0.1% SDS), incubating at 50°C for 30 min at 1200rpm, and filtering through Whatman GF/D filters in Nanosep columns (VWR). DNA was recovered from filtrate using

Qiaquick gel purification buffers and columns (Qiagen) and eluted in 30uL TE. An additional PCR reaction was performed using the following fusion primers to permit sequencing on the Illumina platform.

SP5fusion:
5'-AATGATACGGCGACCACC
GACTATGGATACTTAGTCAGGGAGGACGATGCGG-3'

SP3fusion:
5'-CAAGCAGAAGACGGCATACGACCGCTGGAAGTGACTGACAC3'.

PCR amplification was performed using Accuprime Pfx (Invitrogen) and ranged between 6 and 10 cycles. The product was then run on a 2% NuSieve agarose gel and purified using Qiaquick spin columns (QIAGEN). A total of 10-30 ul of DNA (quantified using the Quant-IT kit (Invitrogen)) at 10 nM was submitted for sequencing. The sequencing of CLIP tags was performed using the sequencing primer

SSP1: 5'-CTATGGATACTTAGTCAGGGAGGACGATGCGG-3'.

Data analysis was done using the Galaxy platform (Hillman et al 2012).

Chapter III. Analysis of the mechanism of translational regulation by FMRP

Introduction:

FMRP HITS-CLIP provided the first rigorous, comprehensive view of the set of mRNAs regulated by FMRP. However, a major open question remained – what is the mechanism of translational control that FMRP exerts on these transcripts? Early studies investigating the role of FMRP in translation were based on expression of exogenous FMRP in various reporter systems. For example, preincubation of recombinant FMRP with *in vitro* transcribed reporter mRNAs, followed by translation in either rabbit reticulocyte lysate or live microinjected *Xenopus* oocytes, resulted in FMRP-dependent inhibition of translation (Laggerbauer et al., 2001). Similarly, preincubation of recombinant FMRP with total brain polyA+ mRNA followed by translation in reticulocyte lysate also caused FMRP-dependent translational inhibition (Li et al., 2001). However, results from these studies should be interpreted with caution due to overexpression of FMRP, use of reporter mRNAs, and the requirement for preincubation of FMRP with mRNA prior to translation assay, all factors that create substantial risk of nonphysiologic effects (Kozak, 2006). Efforts to measure FMRP's effect on protein synthesis in more physiologic systems have found that ^{35}S-methionine incorporation was increased in hippocampal slices from *Fmr1* KO mice (Dolen et al., 2007), (Osterweil et al., 2010) and in reticulocyte lysates programmed with brain lysate from *Fmr1* KO mice (Darnell et al., 2011). In perhaps the most physiologically relevant study, brains of live wt and *Fmr1* KO mice were pulsed with radiolabeled leucine, followed by thin sectioning of the brains and exposure to film to measure incorporation of label into newly synthesized proteins *in situ* (Qin et al., 2005). In this assay, *Fmr1* KO mice showed increased protein synthesis in several regions of the brain, most notably in the hippocampus. Overall, these experiments support a model in which FMRP is a negative regulator of translation, although disagreement exists over whether it exerts a semi-global (Osterweil et al., 2010) or specific (Darnell et al., 2011) effect.

Proteomic approaches have the potential to both determine whether FMRP positively or negatively regulates translation and also to identify specific proteins whose levels are changed in the absence of FMRP. Detection of FMRP-dependent differences in steady-

state protein levels by Western blot has been difficult, most likely because Westerns cannot accurately discriminate differences of less than 20%, potentially making small *de novo* changes impossible to detect over steady-state levels. The only case where an FMRP-dependent change in the steady-state level of a protein in total lysate has been reproducibly demonstrated is for Map1B (Lu et al., 2004), (Zhang et al., 2001). However, this result stands out because the assays involved (Western blot and RNAse protection assay in mouse brain) are physiologic and because, in retrospect, they assay one of the top FMRP targets during the window of peak FMRP expression. In addition, Western blots of subcompartments, for example synaptoneurosomes, have identified increases in a number of proteins in the absence of FMRP (Schutt et al., 2009). Unbiased quantitative proteomic screens have met with limited success. In one screen, 23 proteins were identified with differential expression in hippocampal synaptosomes prepared from *Fmr1* KO mouse brain (Klemmer et al., 2011). Encouragingly, of these, 22 had increased expression in the absence of FMRP, consistent with FMRP's role as an inhibitor of translation. Four of the 22 were strong HITS-CLIP targets (*Pclo*, *Syn1*, *Ap2B1* and *Eef2*). In a second screen, 132 proteins with differential expression in cultured primary hippocampal neurons from *Fmr1* KO mice were identified (Liao et al., 2008). Of these, only 39 had increased expression in the KO, and most had only a few CLIP tags. However, this study did detect increased expression of the two top CLIP targets, Apc and Map1B, in *Fmr1* KO neurons. Overall, these studies suggest that FMRP is a negative regulator of translation and give some clue about which proteins are differentially expressed in the absence of FMRP, but give little insight into the mechanism of translational regulation.

Efforts have also been made to characterize FMRP's effect on translation at the mRNA level. Polyribosomes of varying sizes can be separated on sucrose gradients with excellent resolution, such that small differences in ribosome loading are discernable. Two major efforts to characterize FMRP's function using pooled polyribosomes have been made. Careful microarray analysis of both total mRNA and pooled polysomal mRNA from six pairs of wt and *Fmr1* KO mouse brains revealed that not a single gene was significantly increased or decreased in either total or polysomal pools between wt and

KO except, as expected, *Fmr1* (Darnell et al., 2011). However, another study found both increased and decreased mRNA levels in pooled polysomes from lymphoblastoid cells from FXS patients compared to normal controls, some of which were mRNAs that coIPed with FMRP (Brown et al., 2001). These analyses have several limitations, including heterogeneity of cell samples from human patients, lack of a neuron-like phenotype for lymphoblastoid cells, lack of resolution due to pooling of polysomes, possible functional redundancy from FXR1P and/or FXR2P, and limitations in sensitivity and genome coverage of microarrays (at the time, it was not practical to employ more sensitive, low-throughput methods such as Northern blot, RNAse protection assay or QPCR because the identities of FMRP targets were not reliably known). Therefore, from these experiments we cannot firmly conclude whether mRNA association with polysomes is altered in the absence of FMRP, although the microarray results from brain do suggest that any existing effect may be subtle.

Finally, several attempts have been made to determine whether FMRP-associated polysomes are engaged in active translation. Polysomes that are not actively translating should be insensitive to ribosome runoff assays. If initiation is inhibited, ribosomes already engaged in translation will continue translocating and release upon reaching the stop codon, causing the average size of polysomes (as analyzed on sucrose gradients) to gradually diminish and the number of free monosomes to increase. The behavior of FMRP in such a runoff system is predicted to depend on whether FMRP is associated with mRNA on which ribosomes are actively translocating, or is associated with mRNA on which ribosomes are stalled, or is bound to the ribosomes themselves, either translocating or stalled. The behavior of FMRP in runoff assays has been studied using sodium fluoride or sodium azide as inhibitors of initiation, although these drugs act by depleting ATP, which is expected to have pleiotropic effects on other aspects of translation such as preventing amino acid charging of tRNA. In these experiments, FMRP was enriched after runoff in light fractions containing free proteins, free mRNA and monosomes (Feng et al., 1997a), (Wang et al., 2008). This could be interpreted as evidence that FMRP is associated with actively translating polysomes, but it could also be the result of pathologic polysome disassembly due to general poisoning of the cell or it

could reflect a requirement for ATP in FMRP association with polysomes. A more specific method of disengaging translocating ribosomes from mRNAs is use of the drug puromycin, an aminoacyl tRNA analog that causes premature chain termination upon incorporation. Translocating ribosomes that incorporate puromycin fall off of transcripts without completing translation; nontranslocating ribosomes are unaffected by puromycin because incorporation of puromycin into the growing polypeptide is predicated on translocation. Treatment of cells with puromycin thus results in disassembly of actively translating polysomes by a mechanism that specifically acts on translocating ribosomes. Under these conditions, FMRP was observed to migrate in lighter fractions; however, it did not migrate with free proteins at the top of the gradient (Stefani et al., 2004), (Darnell et al., 2011). Rather, FMRP remained in the middle of the gradient, in fractions containing residual polysomes, suggesting that it was associated with transcripts that still contained some ribosomes after puromycin treatment. This suggests that some of the ribosomes on FMRP-associated transcripts are actively translating, while other ribosomes on the same transcripts are stalled.

Results:

Steady state levels of target mRNAs are unaffected by loss of FMRP and FXR2P

As a first step in investigating the mechanism of translational control by FMRP, we looked for changes in total steady state mRNA levels of FMRP targets. As a polysome-associated protein, FMRP could inhibit translation by directing turnover of target mRNAs. Examples of mRNA degradation linked to translation include sequestration of Ago-bound mRNAs in P-bodies (Djuranovic et al., 2011) and nonsense-mediated decay triggered by the presence of exon junction complexes in 3'UTRs where they are not displaced during the pioneer round of translation (Giorgi et al., 2007). Although our earlier microarray analysis did not detect changes in the steady-state polysome pool in the absence of FMRP, subsequent identification of FMRP targets by CLIP allows productive interrogation of candidate mRNAs by QPCR, which is considerably more sensitive. To reduce possible functional compensation by FMRP's paralogs, *Fxr2*$^{+/-}$ mice were compared to *Fmr1*/*Fxr2* DKO mice (*Fxr2*$^{+/-}$ mice were chosen to use as a control instead of wt mice in order to increase the number of usable litters, and of the available

heterozygous genotypes were judged least likely to have phenotypes similar to *Fmr1* KO mice). To further increase our chances of establishing statistical significance for subtle alterations, ten littermate pairs were used and samples were handled blind to genotype. Total RNA was prepared from cortex in the second postnatal week. To establish the best possible normalization controls, a panel of 16 housekeeping genes from diverse metabolic pathways was screened against the full set of 20 samples and the GeNorm program was used to rank the control mRNAs according to expression stability. The GeNorm program is designed to overcome the circular problem of how to chose stably expressed internal controls without a previously established baseline against which to normalize (Vandesompele et al., 2002). In an ideal scenario (ie one in which samples are identical), the ratio of two internal control genes will not change from sample to sample. In real life, this ratio will change, and the more variable the ratio is, the less stable one or both of the control genes are. However, it cannot be known from just two control genes whether variation is inherent in the samples (ie one sample is more concentrated that the other) or whether one or both of the control genes is/are differentially expressed between the samples. The GeNorm program addresses this problem by starting with a large set of potential control genes and comparing each control gene to all other control genes in pairwise fashion, assigning a stability measure, M, based on the average pairwise variation of each gene with all other genes. The worst performing control gene (ie with the highest M value) is then removed from the set and the analysis is repeated, ultimately ranking all control genes according to their relative stabilities. Furthermore, it is recognized that use of more than one internal control will improve normalization accuracy. In order to determine the optimal point at which inclusion of additional control genes only minimally improves accuracy (or even decreases accuracy, if poorly performing controls with high M value are included), the program calculates normalization factors based on stepwise inclusion of additional control genes and then assesses the impact on normalization accuracy from the inclusion of each additional gene. To do this, it calculates the pairwise variation, $V_{n/n+1}$, between the normalization factors for n control genes and n+1 control genes. If $V_{n/n+1}$ is large compared to $V_{n+1/n+2}$, it means that inclusion of the $(n+1)^{th}$ control gene will significantly improve normalization accuracy. Based on Genorm analysis, the three most stable control genes, *Hprt1*, *TBP*

and *B2M*, were used to normalize the data. Four additional control mRNAs not included in calculation of the normalization factor were also examined, and –RT controls were performed for all genes. Analysis of the seven nontargets plus nine strong FMRP target mRNAs showed no significant changes in steady state mRNA levels upon loss of FMRP and FXR2P expression (**Figure 1).**

Steady state polysome profiles of target mRNAs are unaffected in *Fmr1* KO or I304N brain

We next looked at steady state polysome distributions of target mRNAs, to investigate FMRP's effect on translational status. In order to perceive possible small shifts in gradient distribution that would be missed by pooling polysomes, individual fractions were analyzed. Brains from littermate pairs of wt and *Fmr1* KO or wt and I304N knockin mice in the third postnatal week were homogenized in a cycloheximide-containing buffer, which stabilizes polysomes. Lysates were fractionated over 20-50% sucrose gradients and RNA was extracted from each fraction, reverse transcribed, and analyzed by QPCR. It was found that column-based RNA purification suffered from high levels of technical variation, even when using columns designed to recover picogram-quantity amounts of RNA, so RNA was purified using liquid phase extraction. Considerable effort was made to determine the most accurate way to normalize the data. The fractions could not be normalized to total RNA, because rRNA levels vary enormously across polysome gradients. The fractions also could not be normalized to the profile of a control mRNA, because housekeeping genes are not typically under translational control and thus nearly all the QPCR signal is consolidated in two or three fractions (ie most molecules of that mRNA have a similar number of ribosomes). Thus, fractions not overlapping with this "peak" would be normalized to values close to zero, which is not very meaningful or accurate. An effort was made to use spiked-in luciferase mRNA for a normalization control, adding 8pg of *Luc* mRNA to each fraction after addition of Trizol LS. While this method should work in principle, in practice we found that technical duplicates (ie, a single gradient with each fraction split into two) normalized in this manner were less identical than those simply prepared starting with an equal volume of each fraction and carried through with careful volumetric pipetting. In

the end, it was found that liquid-phase extraction of equal volumes of samples gave highly reproducible results without further normalization. QPCR measurements were made for each of 16 gradient fractions, for 9 control genes and 9 target genes, with each fraction plotted as a percentage of the sum of the gradient fractions for a given gene (**Figure 2**). It was also confirmed that each primer pair generated a single product of expected size on a gel (**Figure 3).** In agreement with previous microarray analysis of pooled polysomes (Darnell 2011), there were no significant changes in the steady state polysome profiles of target mRNAs in the absence of FMRP.

Runoff of polysomes with puromycin in live cells shows that FMRP is associated with mRNAs containing both active and stalled ribosomes

Although presence of mRNA in heavy polysome fractions is commonly considered a direct measure of translational output, these fractions can also contain transcripts on which ribosomes are engaged but not translocating. For example, binding of the miRNA let-7a to the *lin-41* 3'UTR repressed expression of reporter mRNAs without affecting migration of the mRNA on sucrose gradients (Nottrott et al., 2006). As discussed above, one method of distinguishing actively translating polysomes from stalled polysomes is to remove translocating ribosomes from mRNA using puromycin. Treatment of neuroblastoma (N2A) cells with puromycin revealed that while FMRP-associated polysomes were partially sensitive to puromycin, these transcripts remained associated with 3 or 4 ribosomes after runoff, even after treatment with a high concentration of puromycin (1mM) (Stefani et al., 2004). The fact that these ribosomes remain associated with mRNA after puromycin treatment suggests that they are nontranslocating, as puromycin can only be incorporated by actively translating ribosomes. Since FMRP remained in heavier fractions after puromycin treatment than other RBPs such as polyA binding protein (PABP) and Hu (Darnell et al., 2011), this suggests that polysomes associated with FMRP are less sensitive to puromycin than the general polysome population.

Gradient fractions containing FMRP after puromycin runoff should also contain FMRP target transcripts. Furthermore, if these transcripts are less sensitive to puromycin

because FMRP causes ribosomes to stall, then removal of FMRP from its target transcripts might allow stalled ribosomes to resume translocation, rendering them sensitive to puromycin. To test this, puromycin runoff was performed in N2A cells in which expression of FMRP, FXR1P and FXR2P was simultaneously knocked down. Cells were treated with pools of four siRNAs for each protein, for five hours on each of two consecutive days. On the third day, cells were treated with puromycin for 1 hour and then arrested with cycloheximide. All three FXRPs were successfully knocked down by approximately 90%. Lysates were loaded over 20-50% sucrose gradients and analyzed by Western and QPCR as before. Interestingly, the triple knockdown increased the sensitivity of target transcripts to puromycin, without affecting puromycin sensitivity of nontarget transcripts (**Figure 4**). This suggests that ribosome stalling is a reversible phenomenon regulated by FMRP (and/or its paralogs) that is limited to a particular set of mRNAs.

FMRP target transcripts are resistant to puromycin in an *in vitro* translation system programmed with endogenous brain polysomes

The results from N2A cells suggest that FMRP stalls ribosomal translocation on target mRNAs. However, since N2A cells do not express many of the FMRP target transcripts and the physiology of cultured cells is not reflective of that of neurons in brain, their usefulness for investigating FMRP's role in brain is limited. In particular, development of a functional assay for FMRP in mouse brain, the same system in which FMRP's targets were identified by HITS-CLIP (Darnell et al., 2011), would allow direct comparison of results from binding and functional assays. However, freshly prepared mouse brain lysate does not support translation. In order to examine FMRP's effects on its endogenous mRNA targets while preserving normal FMRP:RNA stoichiometry, Jennifer Darnell developed the IVT-EBP assay (*in vitro* translation of endogenous brain polysomes). In this assay, freshly homogenized postnuclear mouse brain lysate is mixed with amino acids, ATP and rabbit reticulocyte lysate (in which globin and other reticulocyte mRNAs have been destroyed by micrococcal nuclease). Incubation of the mixture with puromycin resulted in ribosome runoff evident by 2 minutes and complete by 20 minutes, as measured by A_{254} trace of ribosome distribution and ^{35}S-methionine

incorporation into new protein (Darnell et al., 2011). Increasing the incubation to 45 minutes or increasing the concentration of puromycin by 10-fold did not induce additional loss of ribosomes from mRNA. If puromycin's effect was blocked by inclusion of cycloheximide in the reaction, polysomes remained intact, indicating that the decrease in A_{254} signal corresponds to ribosome runoff and not degradation of mRNA during the incubation. Finally, blockade of initiation using hippuristanol, an inhibitor of the helicase eIF4A, had no significant effect on incorporation of ^{35}S-methionine during elongation in the absence of puromycin, indicating that new initiation is limited in this system and therefore suggesting that observed runoff primarily involves ribosomes that initiated translation *in vivo*. Importantly, distributions of FMRP and other RBPs after puromycin runoff in the IVT-EBP system appeared extremely similar to their distributions after puromycin runoff in N2A cells: in both systems, FMRP was retained in heavier sucrose fractions after runoff than other polysome-associated RBPs, and in both systems FMRP and other RBPs migrated at the top of the gradient after EDTA treatment. Collectively, these results suggest that the IVT-EBP system offers a valid approach to studying ribosomal translocation on endogenous brain polysomes.

We next investigated the effect of FMRP loss-of-function in the IVT-EBP system on the sensitivity of target transcripts to puromycin. Lysates from wt/*Fmr1* KO and wt/I304N littermate pairs in the third postnatal week were incubated with puromycin in the IVT-EBP system and then separated over 20-50% gradients. The gradient distribution of FMRP was assayed by Western blot before and after runoff, confirming that FMRP remained in relatively heavy fractions after puromycin treatment (**Figure 5**). Fractions were collected and analyzed by QPCR as before, and the gradient distributions of nine target and nine nontarget mRNAs were assayed. In both *Fmr1* KO and I304N lysates, target mRNAs were more sensitive to puromycin than in wt lysates (**Figure 6**). This suggests that FMRP inhibits ribosomal translocation on endogenous brain transcripts, and suggests that it is specifically the polysome-binding activity of FMRP (which is abrogated in the I304N mouse) that is responsible for this effect. Nontarget transcripts did not exhibit significant increases in puromycin sensitivity in the absence of polysome association by FMRP, further strengthening the argument that physical association of

FMRP with transcripts (as assayed by CLIP) is the key factor that determines the differential puromycin sensitivity.

Because the IVT-EBP system experiences little translational initiation, it primarily assays runoff of ribosomes previously engaged on transcripts *in vivo*. We were interested to know whether FMRP's inhibition of ribosomal translocation could be acutely relieved, to show that observed effects are due directly to FMRP loss-of-function, rather than to possible secondary consequences of long-term loss of FMRP function in animal models (for example, FMRP targets the elongation factor eEF2, which would be predicted to chronically inhibit global elongation). Treatment of polysomes with kcRNA, an aptamer for FMRP identified in SELEX experiments, has been shown to effectively and specifically remove FMRP and its paralogs FXR1P and FXR2P from polysomes without affecting polysome integrity (Darnell et al., 2005a), (Darnell et al., 2009). Wt brain lysate from the third postnatal week was treated with 1uM kcRNA or $kcRNA_{C50G}$ (a point mutant that does not bind to FMRP) immediately prior to addition of the other components of the IVT-EBP system. Reactions were terminated with cycloheximide, fractionated over 20-50% sucrose gradients and analyzed by QPCR as before, for the same set of 9 targets and 9 nontargets. As expected, kcRNA released FMRP from polysomes in the IVT-EBP system, while treatment with $kcRNA_{C50G}$ did not affect migration of FMRP on sucrose gradients compared to puromycin treatment alone (**Figure 5**). We found that acute removal of FXRPs from polysomes relieved ribosome stalling, increasing sensitivity of target but not nontarget transcripts to puromycin (**Figure 7**). In fact, there was a significantly greater effect on the target mRNAs compared to runoff in *Fmr1* KO or I304N brain (**Figure 9** and related text), which may be due to the fact that kcRNA removes both FMRP and its paralogs from polysomes.

One important control concerns the fact that the stoichiometry between FMRP and associated mRNAs is unknown. In theory, if enough molecules of FMRP associated with individual transcripts, loss of FMRP alone could cause transcripts to migrate at lower densities on sucrose gradients. FMRP's molecular weight (75kD) is roughly $1/50^{th}$ that of a eukaryotic ribosome (4000kD). Loss of FMRP during puromycin runoff causes

mRNA migration shifts consistent with loss of approximately 4-8 ribosomes. Although migration on a sucrose gradient is not strictly proportional to molecular weight, it can be estimated that loss of 200-400 molecules of FMRP from a transcript in theory could produce such a shift in its gradient migration. To test whether the observed migration shift of target mRNAs to lower gradient densities in presence of kcRNA during puromycin runoff is associated with loss of translocating ribosomes or is due solely to loss of FXRPs, removal of FXRPs by kcRNA was delayed until after puromycin runoff was complete. To ensure that elongation was completely halted before addition of kcRNA, reactions were placed on ice slush and treated with both cycloheximide and anisomycin, inhibitors of elongation that target the translocation and peptidyl bond formation steps, respectively. Under these conditions, kcRNA removed approximately 80% of FMRP from polysomes (**Figure 8**). Reassuringly, removal of FXRPs from polysomes after the runoff reaction was stopped had almost no effect on the gradient migration of target transcripts (**Figure 8**). This suggests that the FMRP-dependent shift of target mRNAs to lighter gradient fractions during puromycin runoff is indeed due to increased loss of translocating ribosomes and does not simply reflect loss of FMRP mass from polysomes.

The specificity of the above findings for transcripts targeted by FMRP suggested there might be a correlation between the magnitude of the FMRP-dependent puromycin shift and the degree of FMRP binding as assayed by CLIP. In order to make statistical comparisons between the two experiments, the IVT-EBP kcRNA dataset was expanded to 22 targets and 17 nontargets (**Figure 7**). Because some mRNAs with the highest numbers of tags have long coding sequence lengths, a number of target mRNAs with shorter coding sequence lengths were purposefully selected, as well as several nontargets with long coding sequence lengths (**Table 1**). Nontargets were also well expressed in neurons, according to a published database of neuron-specific gene expression in mice of similar age to those used in our experiments (**Table 1**, Cahoy 2008). In order to quantify the increase in ribosome runoff upon removal of FMRP from polysomes, transcript abundance in each fraction was weighted for the number of ribosomes per transcript in that fraction (**Figure 9A**). To do this, the linearity of the sucrose gradients was first

established by measurement of the sucrose concentration in each fraction of a blank gradient using a sucrose refractometer. Next, the number of ribosomes per transcript was counted for the first nine fractions of a cycloheximide-treated gradient based on peaks in the UV_{254} profile. The number of ribosomes per transcript in fractions 10-16 was then extrapolated using a best-fit curve. Weighting transcript abundance according to ribosome loading in this way transforms each QPCR data point into a measure of translational potential. The sum of the ribosome-weighted values for each fraction of the gradient thus represents the total translational potential of a transcript, in this case reflective of the number of ribosomes retained on the transcript after puromycin runoff. The difference in this final value after puromycin runoff in the presence versus absence of FMRP is a metric we call the retained ribosome score (RRS). The RRS is thus a measure of how much FMRP-dependent ribosome stalling occurs on target transcripts.

The RRS was significantly higher for targets compared to nontargets in all three loss-of-function models used in the puromycin runoff assay (**Figure 9B**). The difference was particularly significant for the expanded kcRNA dataset of 22 targets and 17 nontargets ($p=9.7x10^{-8}$) (**Figure 9D**). RRS was not correlated with transcript abundance or steady-state ribosome loading. There was a correlation of RRS with coding sequence length, mainly due to an effect of the targets (R^2=0.17 for nontargets, 0.56 for targets and 0.41 overall) (**Figure 9E**), consistent with the idea that since longer transcripts tend to be associated with more ribosomes, more ribosomes are potentially available for stalling. Importantly, however, RRS was still significantly increased for 7 targets of moderate coding sequence length (1000-2000nt) compared to a matched set of 6 nontargets within the same CDS length window (**Figure 9F**). RRS also correlated well with FMRP target specificity as assayed by FMRP polysome CLIP, both in terms of chi-square score (R^2=0.53) and tags per gene (R^2=0.39) (**Figure 9C** and data not shown), providing further evidence that the magnitude of ribosome stalling depends on the extent of FMRP interaction with specific targets.

Inspection of the kcRNA runoff results shows that even nontarget mRNAs contain some residual ribosomes after runoff is complete (with peaks in fractions 5-8), though these

residual ribosomes do not become sensitive to puromycin in the absence of FMRP. While we do not understand why these residual ribosomes are present, the number of residual ribosomes reflects the original number of ribosomes loaded on transcripts in the steady state, and such an effect has previously been observed by others (Maroney et al., 2006). Removal of residual ribosomes by inclusion of 30mM EDTA during puromycin runoff caused mRNAs to migrate in lighter fractions, usually fractions 4-5 (**Figure 10**), consistent with puromycin-resistant complexes containing ribosomes. For a few genes, EDTA treatment revealed that a large portion of mRNA was not associated with ribosomes in steady state, for example *Bsn*, *Adcy1* and *Pabpc1*, suggesting additional mechanisms of translational control based on inhibition of initiation or sequestration of mRNAs from translational machinery. Overall, most transcripts migrated in somewhat heavier fractions after EDTA treatment than had been expected based on the canonical view that transcripts shift to the lightest gradient fractions (eg, fraction 2) after EDTA treatment (Matthews et al., 2007). However, these original findings were based on analysis of housekeeping mRNAs that have short coding sequences and are likely under little regulatory control by associated RBPs (Fagan et al., 1991), both factors that would be predicted to result in migration in lighter fractions. In agreement with this prediction, we did find that the mRNA of the short housekeeping gene *Hprt1* migrated in fraction 2 after EDTA treatment.

Complexes retained in heavy fractions after runoff contain ribosomes and FMRP

The facts that FMRP-associated transcripts are partially sensitive to puromycin and that puromycin-resistant complexes can be further shifted by EDTA suggest that these transcripts are in polysomal complexes. However, more direct evidence that the FMRP migrating in dense fractions after puromycin treatment is associated with polysomes is desirable. There are examples of large RNPs that cosediment with polysomes on sucrose gradients but are not actually polysomes (for example see (Thermann and Hentze, 2007)). Immunoprecipitation experiments do suggest that FMRP is buried in some sort of complex, as it is largely inaccessible to antibodies under native conditions. Immunoprecipitation of FMRP from mouse brain is limited unless lysate is treated in ways that disrupt RNPs, such as with RNAse, EDTA, or kcRNA (**Figure 11**). These

results are consistent with disruption of FMRP-polysome interactions, but could also be consistent with disruption of other kinds of RNPs. To directly visualize complexes present in fractions containing FMRP and puromycin-resistant transcripts, puromycin runoff of brain polysomes was performed in the IVT-EBP system and lysates were separated over sucrose gradients. Fraction 9 (which contains FMRP after runoff) from both puromycin-treated and cycloheximide-treated gradients was examined by electron microscopy using negative staining with uranyl acetate. Both samples were richly populated with structures of approximately 100nm in diameter containing multiple globules of a size consistent with that of eukaryotic ribosomes (**Figure 12**). Importantly, these structures appear extremely similar to previously published electron micrographs of polysomes (for example see (de Petris, 1970)), suggesting that they are indeed polysomes. Markedly fewer polysomes were visible by EM after puromycin runoff, consistent with disassembly of most polysomes during runoff. To assess whether polysomes that survive runoff are compact RNPs, an additional sample was treated with micrococcal nuclease after puromycin runoff to cleave any RNA not protected by RBPs. Micrococcal nuclease treatment caused no apparent differences in the appearance or size of the residual polysomes compared to puromycin runoff alone, suggesting that polysomes remaining after puromycin runoff do not contain freely accessible RNA and consistent with a model of tightly stacked stalled ribosomes (see discussion). No other large structures such as granules were obvious in any of the preparations. Polysomes were further characterized by immuno-electron microscopy (IEM). Because previous evidence suggested that it might be difficult to achieve antibody binding to FMRP on intact polysomes (**Figure 11**), we piloted IEM conditions using EGFP-tagged ribosomal protein L10a. Polysomes were prepared from cerebella of *Pcp2*-promoter driven EGFP-tagged rpL0a BAC transgenic mice, which express EGFP-tagged ribosomes in Purkinje cells (Heiman et al., 2008). Fractions were fixed with 4% paraformaldehyde and 0.08% glutaraldehyde to preserve polysome structure during immunolabeling and probed with an EGFP antibody coupled to 6nm gold particles. Although images were less distinct due to antibody incubation and limitations of fixation procedures, they appeared similar in composition to those previously seen. We observed antibody binding to a minority of the polysomes (roughly 1%), consistent with the fact that EGFP-rpL10a is expressed in a

subpopulation of neurons (**Figure 13**). Although most polysomes were unlabeled, multiple gold particles were often observed on those that were labeled, consistent with multiple EGFP-tagged ribosomes existing on polysomes from Purkinje cells. Together, these results support the morphologic evidence that the observed structures are polysomes, although lack of an EGFP-negative control in this pilot study precludes definitive conclusions based on the immunolabeling. We next attempted IEM of polysomal FMRP, using EGFP-tagged FMRP expressed in 293T cells in hopes of presenting a more accessible antigen. Polysomes were compared from lysates containing either N-terminally or C-terminally tagged FMRP constructs and it was found that better signal was obtained with the N-terminal tag. Direct probing for FMRP using the antibody 17722, which recognizes an epitope in the C-terminal, also failed to produce labeling. Together these results are consistent with the C-terminal of FMRP being less accessible *in vivo* than the N-terminal. 293T cells transfected with N-terminally tagged EGFP-FMRP or EGFP alone (which is not expected to associate with polysomes) for 2 days were treated with puromycin for 1 hour and then arrested with cycloheximide as before. As a control, cells expressing each construct were treated with cycloheximide alone. Lysates from the four conditions were separated over 20-50% sucrose gradients and fraction 10 was fixed in 4% paraformaldehyde and 0.1% glutaraldehde and processed for IEM using an EGFP antibody coupled to 12nm gold. 500 polysomes were counted from each condition and the number of gold particles per polysome was noted. A greater percentage of polysomes were positive for EGFP labeling after puromycin runoff compared to the cycloheximide control, indicating enrichment for FMRP-containing complexes after runoff of actively translating polysomes (**Figure 16**). Overall, 13.4% of polysomes from cells expressing EGFP-FMRP were labeled after puromycin runoff, compared with 7.2% of polysomes from cells treated with cycloheximide and 0.02% of polysomes from cells expressing EGFP alone. In sum, these results show that fractions containing target transcripts resistant to puromycin also contain structures with the morphologic appearance of polysomes that include both ribosomes and FMRP. Together, these results support the assertion that target transcripts are associated with both FMRP and stalled ribosomes.

Discussion:

Recent identification of hundreds of FMRP-associated mRNAs by HITS-CLIP (Darnell et al., 2011) provided a critical clue about FMRP regulatory function – that FMRP associates with the entire coding sequence of target mRNAs. Historically, attempts to elucidate FMRP's function have produced a jumble of results, with descriptions of FMRP directing miRNA-mediated translational repression (Muddashetty et al., 2011), (Edbauer et al., 2010), FMRP regulating mRNA stability via 3'UTR interactions (Zalfa et al., 2007), (Schutt et al., 2009), FMRP inhibiting translation initiation via interaction with the eIF4E-binding protein Cyfip1 (Napoli et al., 2008), FMRP potentiating translation by binding the novel SoSLIP RNA motif (Bechara et al., 2009), and even a report of a FMRP binding site functioning as a splicing enhancer (Didiot et al., 2008). While in general, consensus seemed to be that FMRP was a negative regulator of translation, *in vivo* evidence of such was limited and somewhat inconsistent (see Introduction). In retrospect, much of the difficulty in ascertaining the mechanistic function of FMRP appears to stem from the fact that loss of FMRP does not cause obvious, easy-to-detect changes in the translational status or protein levels of its targets, as well as from frequent reliance on overexpressed recombinant proteins (which can have nonphysiologic RNA association properties) (Laggerbauer et al., 2001), (Coffee et al., 2012), (Gross et al., 2011) and reporter transcripts (which are not FMRP targets and are often designed to assay FMRP association with 3'UTRs rather than coding sequence) (Wang et al., 2004), (Edbauer et al., 2010). Here, we used the finding from the unbiased, rigorous HITS-CLIP assay that FMRP associates with the coding sequence of particular mRNAs to guide the design of a functional assay for FMRP's role in translation. Through use of puromycin-induced ribosome runoff assays in multiple genetic, molecular and biochemical FMRP loss-of-function models, we demonstrate that FMRP inhibits ribosome translocation on a specific set of mRNAs shown to physically associate *in vivo* with FMRP by HITS-CLIP.

FMRP stalls ribosomes on target transcripts

Early translational runoff assays found that disassembly of translating polysomes was associated with FMRP migration at lighter densities on sucrose gradients (Stefani et al.,

2004), (Feng et al., 1997a), (Wang et al., 2008). These experiments were interpreted as evidence that FMRP was associated with actively translating polysomes that were disrupted during runoff. However, various other findings suggested that FMRP inhibited translation, apparently inconsistent with a role on actively translating polysomes (Laggerbauer et al., 2001), (Li et al., 2001), (Qin et al., 2005), (Lu et al., 2004), (Zhang et al., 2001). In particular, loss of FMRP was associated with increased incorporation of ^{35}S-methionine in hippocampal slices and *in vitro* translation systems (Darnell et al., 2011), (Osterweil et al., 2010), consistent with negative regulation of protein synthesis by FMRP. Together, these results created an apparent paradox as to how FMRP could be associated with actively translating polysomes and yet inhibit protein synthesis.

Resolution of this paradox was set in motion by the realization that FMRP-associated transcripts are only partially sensitive to translational runoff. Examination of sucrose gradients after puromycin runoff in cells showed that FMRP migrated in fractions containing polysomes that still retained some ribosomes after runoff (Stefani et al., 2004), (Darnell et al., 2011). These results are consistent with a model in which FMRP associates with polysomes on which some ribosomes are sensitive to puromycin and some ribosomes are not. Since only translocating ribosomes are sensitive to puromycin, this suggests that FMRP-associated mRNAs contain some translocating and some stalled (nontranslocating) ribosomes. However, it does not necessarily follow that FMRP *causes* reduced sensitivity to puromycin. To address whether FMRP directly causes polysomes to be less sensitive to puromycin, it must be demonstrated that acute loss of FMRP results in increased puromycin sensitivity and that this effect is limited to FMRP target transcripts. In other words, loss of FMRP should result in resumption of ribosome translocation on a set of specific FMRP-associated mRNAs.

To investigate whether FMRP directly causes ribosome stalling, puromycin runoff assays were first performed in N2A cells in which expression of the FXRPs was knocked down. In this system, loss of FXRP expression resulted in increased runoff of ribosomes from target mRNAs but did not affect runoff of nontarget mRNAs, consistent with inhibition of ribosome translocation on specific mRNAs *in vivo* by FXRPs. In order to extend this

result to mouse brain, the system in which FMRP-associated mRNAs were identified by HITS-CLIP and the system most relevant to FXS pathology, Jennifer Darnell developed the IVT-EBP system, in which endogenous brain polysomes are used to program a puromycin runoff assay performed in reticulocyte lysate. Although the IVT-EBP assay is an *in vitro* system, because it is based on freshly prepared mouse brain lysate it maintains several advantages reminiscent of *in vivo* assays: endogenous levels and stoichiometries of all RBPs and mRNAs are maintained, posttranslational modifications of FMRP or other RBPs are established *in vivo*, and initiation of translation and FMRP association with mRNAs occurs *in vivo*. In agreement with previous results in N2A cells, polysomes from *Fmr1* KO brains exhibited quantifiably increased puromycin sensitivity compared to polysomes from wt brains, and the increased puromycin sensitivity was limited to FMRP target transcripts. Importantly, this effect was due specifically to the RNA-binding function of FMRP: the I304N point mutation that abolishes FMRP polysome association and recapitulates major aspects of FXS in mice (Zang et al., 2009) also resulted in increased puromycin sensitivity of the same set of target transcripts but not nontarget transcripts. Finally, FMRP-dependent ribosome stalling was found to be an acutely reversible effect, since removal of FXRPs from polysomes by kcRNA treatment at the beginning of the puromycin runoff assay recapitulated the findings from runoff assays using *Fmr1* KO and I304N brains. Acute reversibility of FMRP-dependent ribosome stalling is an important point, since it demonstrates that the increased sensitivity to puromycin during runoff is directly due to loss of FMRP and is not a secondary effect of long-term loss of function of FMRP (for example, via downregulation of targets with roles in translation, such as the elongation factor eEF2). Notably, the kcRNA-dependent effects on target mRNAs were quantifiably greater than those observed using genetic models, presumably because kcRNA treatment also removes the FXRPs, which likely provide some functional redundancy to FMRP (Spencer et al., 2006), (Darnell et al., 2009). Together, these results constitute a coherent set of assays in four models that reproducibly demonstrate increased puromycin sensitivity of ribosomes on target but not nontarget mRNAs upon FMRP loss of function. Since puromycin specifically affects translocating ribosomes, these results are consistent with a model in which FMRP represses translation by stalling ribosomes during elongation.

Results from puromycin runoff assays were quantified by weighting measurements of transcript abundance to reflect ribosome loading in each gradient fraction. This approach transformed measurements of mRNA distributions into measurements of protein producing capacity, since polysomes contain varying numbers of ribosomes but all polysomes contain a single molecule of mRNA. Transforming the data in this way more accurately reflects the effect of FMRP on protein production; since polysome fractionation is nonlinear with respect to polysome size, small shifts in mRNA distribution in dense fractions represent a much greater change in total ribosome loading than do small shifts in mRNA distribution in light fractions. We developed a metric called the Retained Ribosome Score (RRS) that defines the magnitude of FMRP's effect on ribosome stalling as the difference in total ribosome loading of transcripts after puromycin runoff in the presence versus absence of FMRP. Thus, a positive RRS indicates that more ribosomes are stalled in the presence FMRP than in the absence of FMRP. An RRS of zero indicates that FMRP has no effect on ribosome stalling.

RRS was significantly increased for target mRNAs compared to nontargets for all three platforms assayed in the IVT-EBP system (wt/*Fmr1* KO, wt/I304N and kcRNA/ $kcRNA_{C50G}$), with the greatest increases seen for the kcRNA platform, in which both FMRP and its paralogs were removed from polysomes. There was a correlation of RRS with coding sequence length of target transcripts (RRS was only weakly correlated with coding sequence length of nontargets). This finding is consistent with the facts that FMRP associates with the entire length of the coding sequence of target transcripts and that long transcripts tend to be more heavily loaded with ribosomes (and thus may have more stalled ribosomes). Importantly, we controlled for coding sequence length by intentionally assaying both short targets and long nontargets. Within a restricted set of CDS-matched targets and nontargets, RRS was still significantly increased for the targets. RRS also correlated well with HITS-CLIP ranking of target mRNAs, linking physical association of FMRP with specific mRNAs to increased ribosome stalling on the same transcripts. Overall, although the RRS findings are highly significant, there were some outliers. Adcy1 and Bassoon are top FMRP targets as assayed by CLIP, and yet had low

RRS scores. Interestingly, comparison of the EDTA and cycloheximide control gradients showed that most *Adcy1* and *Bassoon* mRNA was not associated with ribosomes in the steady state. In the case of Bassoon, there was a subset of ribosome-loaded transcripts that did exhibit increased puromycin sensitivity in the absence of FMRP. The finding that these mRNAs are largely translationally silent is consistent with a literature describing translational repression of specific mRNAs under certain conditions, for example during transport to synapses (Wang et al., 2010), and explains the low RRS scores of these strong targets. Another outlier, Atp1a3, was originally predicted to be a strong target based on its high number of CLIP tags, yet exhibited a low RRS in the IVT-EBP assay. In retrospect, *Atp1a3* mRNA is extremely abundant and therefore may not in fact be highly FMRP-associated. A third set of outliers (*Dlg4*, *Pctk1*, and *Gnb1*) had almost no residual ribosomes left after runoff even when FMRP was present. The fact that these mRNAs experienced more complete runoff than other genes may be related to the fact that they were somewhat more lightly loaded with ribosomes in steady state. However, we do not fully understand why stalled ribosomes were not detectable for these mRNAs. Finally, there was a small FMRP-dependent effect on nontargets. In most cases this effect was minimal and may reflect a minor degree of nonspecific reassociation of FMRP with nontarget transcripts *in vitro*. In a few cases (*Vldlr* and *Npepps*), nonspecific effects were larger even though these mRNAs have very few FMRP CLIP tags. Since these mRNAs were assayed in the kcRNA platform but not the FMRP-specific loss-of-function platforms, it is possible that they could be targets of FXR1P or FXR2P but not FMRP.

The evidence from puromycin runoff assays supporting a model of ribosome stalling by FMRP is augmented by results from ^{35}S-methionine incorporation assays performed by Jennifer Darnell (Darnell et al., 2011). In these experiments, mRNAs from mouse brain lysate in the IVT-EBP system were allowed to elongate in the absence of puromycin and incorporation of ^{35}S-methionine into growing peptide chains was monitored by gel separation and phosphorimaging. ^{35}S-methionine was incorporated into proteins of all molecular weights and removal of FMRP from polysomes by kcRNA treatment had no effect on global ^{35}S-methionine incorporation. However, immunoprecipitation of Lingo1

or CamKIIa polypeptides using N-terminal antibodies showed increased ^{35}S-methionine incorporation into these proteins when FMRP was removed from polysomes. In contrast, immunoprecipitation of Pabpc1, whose mRNA is not associated with FMRP, did not show increased ^{35}S-methionine incorporation when FMRP was removed from polysomes. These results are consistent with the target specificity demonstrated in the puromycin runoff and HITS-CLIP assays and support the assertion that FMRP inhibits protein synthesis.

Physical properties of FMRP-stalled transcripts

Electron microscopy was used to visualize RNPs present in fractions containing FMRP and residual polysomes after puromycin runoff. The morphology and size of observed RNPs before and after puromycin runoff closely resembled previously published electron micrographs of polysomes (de Petris, 1970), a conclusion also supported by the findings that the majority of purported polysomes were dismantled by puromycin treatment and that immunolabeling of EGFP-tagged ribosomes was observed. Importantly, EGFP-FMRP immunolabeling was detected on a subset of polysomes and this subset was enriched after puromycin runoff. This finding provides evidence that FMRP physically associates with the polysomes remaining in dense gradient fractions after puromycin treatment, a conclusion that cannot be drawn simply from comigration on gradients.

Treatment with micrococcal nuclease after runoff did not noticeably alter the morphology of polysomes remaining in dense fractions. Micrococcal nuclease preferentially cleaves single stranded RNA, so treatment with this enzyme will digest unprotected mRNA while leaving ribosomes and mRNA segments protected by ribosomes intact. The finding that micrococcal nuclease treatment did not dissociate polysomes remaining in heavy fractions after puromycin runoff suggests that ribosomes on these transcripts are closely packed such that the nuclease cannot cleave in between them. Biochemical experiments conducted by Jennifer Darnell support this conclusion (Darnell et al., 2011). In these experiments, dense fractions from gradients after puromycin runoff were treated with micrococcal nuclease and surviving polysomes were pelleted under a sucrose cushion. This treatment freed nearly all polyA binding protein, as expected for a protein associated

with 3'UTRs. However, this treatment freed very little FMRP, consistent with a model in which most FMRP is associated with regions protected by packed ribosomes. Notably, a small amount of FMRP was released by micrococcal nuclease treatment, consistent with HITS-CLIP evidence of some FMRP binding in 3'UTRs. Remarkably, even after exposure of nuclease concentrations of 20U/uL a significant fraction of FMRP remained in dense fractions. Overall, these results suggest that FMRP is associated with transcripts on which multiple, closely packed ribosomes are present.

Figure 1. Measurement of steady state mRNA levels from *Fmr1*$^{+/+}$, *Fxr2*$^{+/-}$ and *Fmr1*$^{-/-}$, *Fxr2*$^{-/-}$ littermate pairs.

mRNA levels of 16 genes were measured total mouse brain extract prepared from 20 animals (10 littermate pairs) by QPCR; the data were then averaged by genotype. Normalization was carried out using GeNorm analysis as described in the text. No significant differences were observed for any mRNAs.

Effect of loss of FXR expression on mRNA levels in brain

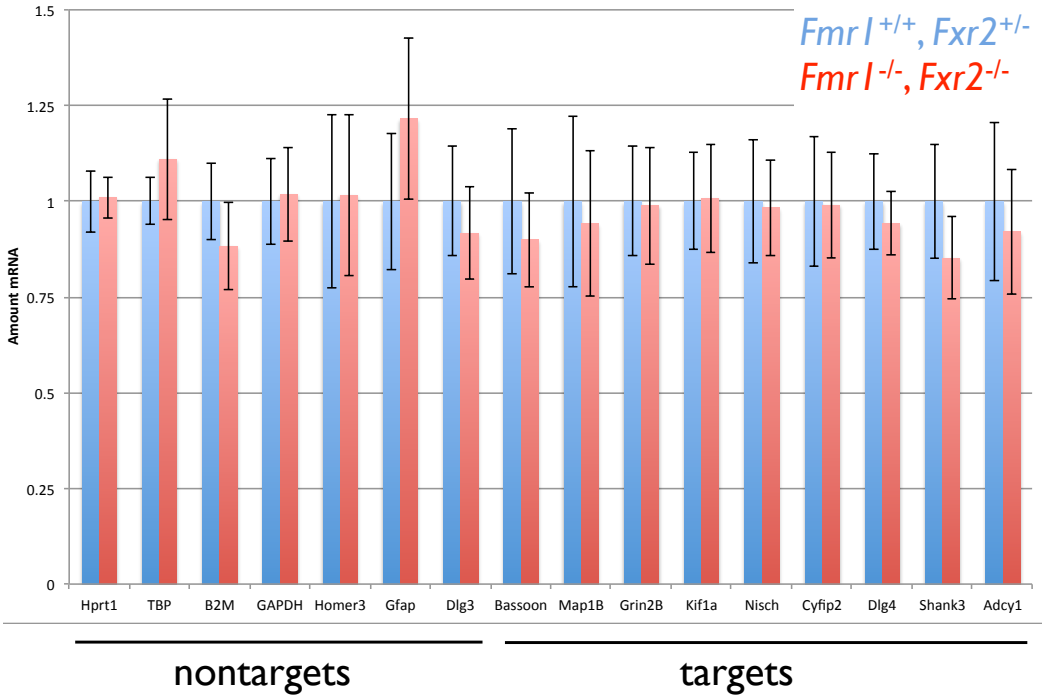

Figure 2. FMRP loss-of-function does not affect mRNA steady-state polysome distribution.

Polysome profiles of target and nontarget mRNAs from wt (black), *Fmr1* KO (red) and I304N (orange) mouse brains are shown, measured by QPCR. Brain lysates were treated with cycloheximide to stabilize polysomes. Both FMRP target and nontarget mRNAs are shown (following pages). FMRP loss-of-function did not affect the distribution of target or nontarget mRNAs on sucrose gradients. Error bars represent technical triplicates of QPCR measurements.

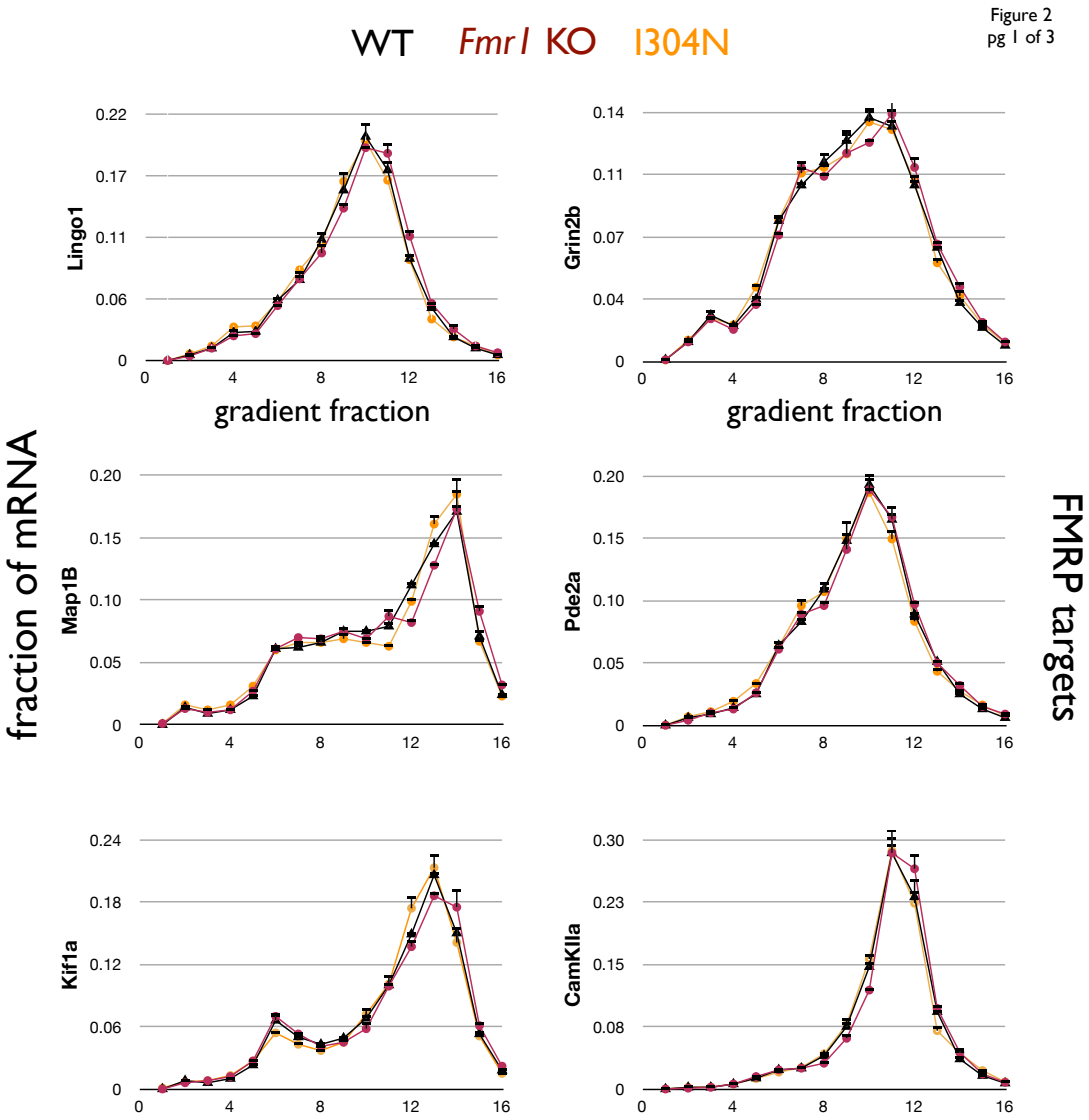
WT
Fmr1 KO
I304N
fraction of mRNA
FMRP targets
Lingo1
Grin2b
Map1B
Pde2a
Kif1a
CamKIIa
gradient fraction
gradient fraction

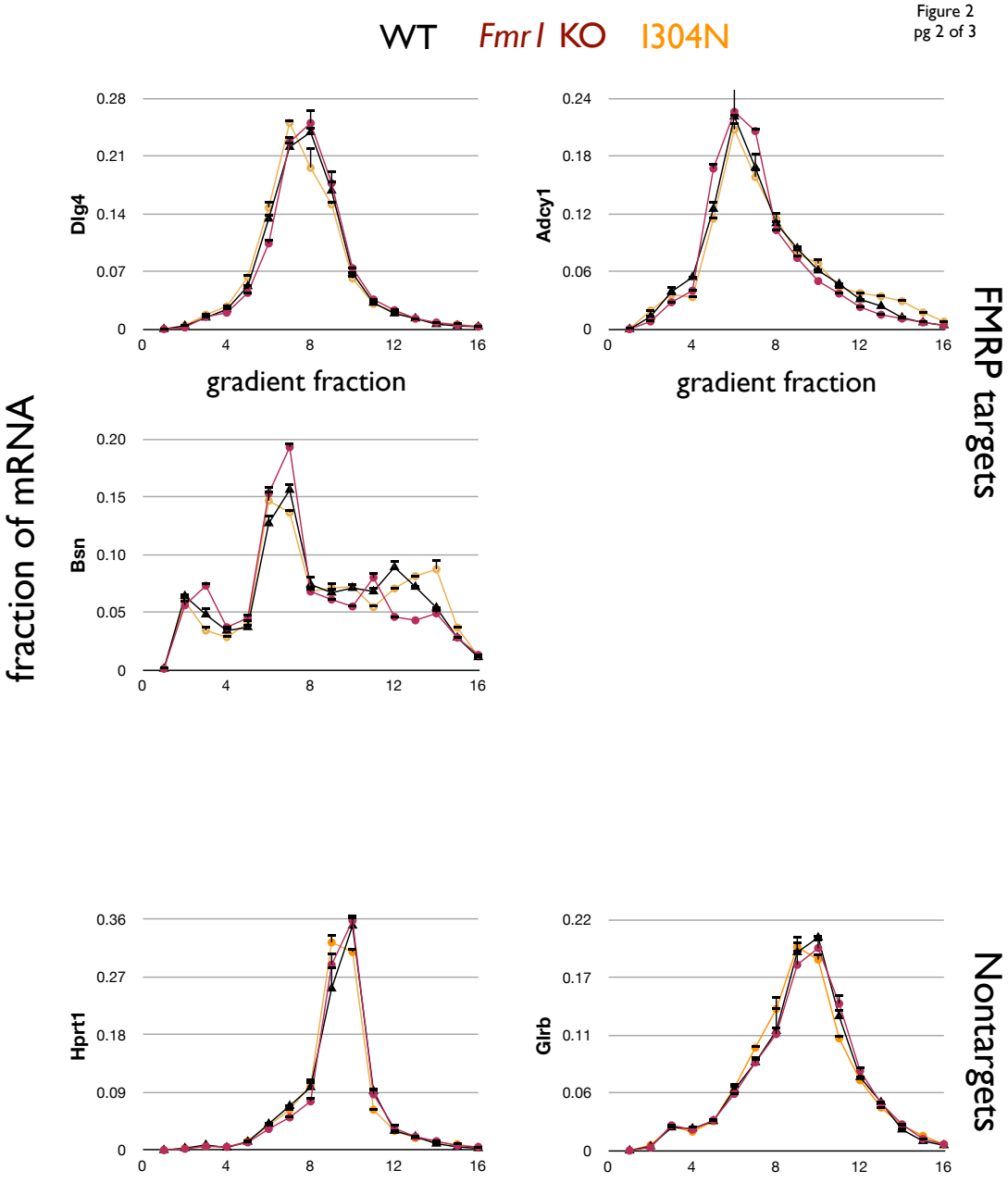
WT
Fmr1 KO
I304N
fraction of mRNA
gradient fraction
gradient fraction
Dlg4
Adcy1
Bsn
Hprt1
Glrb
FMRP targets
Nontargets

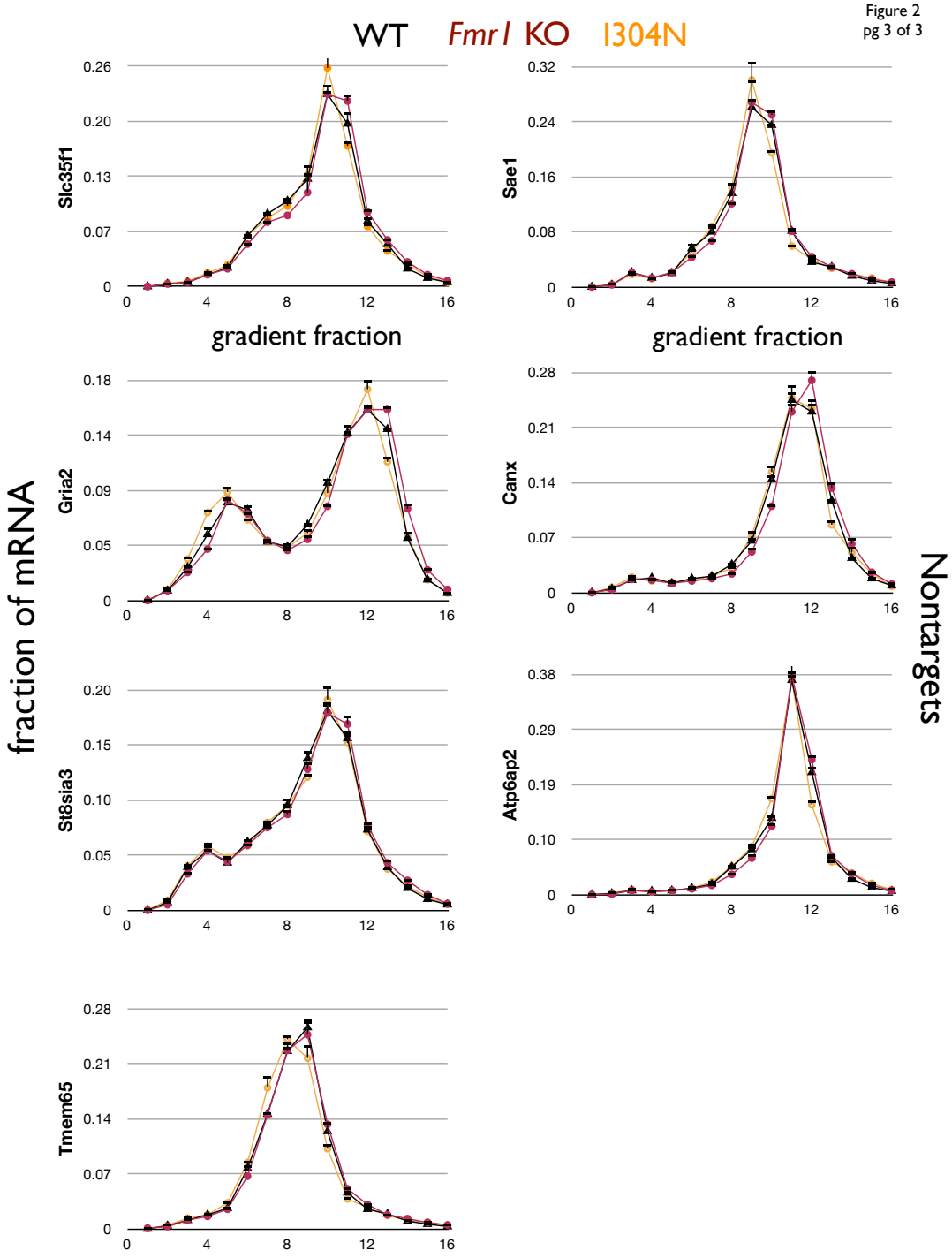
WT
Fmr1 KO
I304N
fraction of mRNA
gradient fraction
gradient fraction
Nontargets
Slc35f1
Sae1
Gria2
Canx
St8sia3
Atp6ap2
Tmem65

Figure 3. RT-PCR reactions performed with the QPCR primers used to analyze mRNA distributions on polysome gradients.

cDNA was prepared from pooled brain polysomes. All QPCR primer pairs produced a single product of expected size (indicated in parentheses after gene symbols). Products were separated by agarose gel.

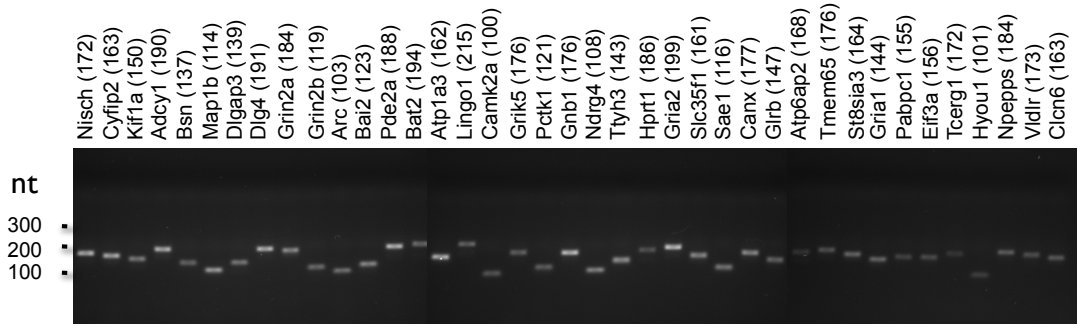
Nisch (172)
Cyfip2 (163)
Kif1a (150)
Adcy1 (190)
Bsn (137)
Map1b (114)
Dlgap3 (139)
Dlg4 (191)
Grin2a (184)
Grin2b (119)
Arc (103)
Bai2 (123)
Pde2a (188)
Bat2 (194)
Atp1a3 (162)
Lingo1 (215)
Camk2a (100)
Grik5 (176)
Pctk1 (121)
Gnb1 (176)
Ndrg4 (108)
Ttyh3 (143)
Hprt1 (186)
Gria2 (199)
Slc35f1 (161)
Sae1 (116)
Canx (177)
Glrb (147)
Atp6ap2 (168)
Tmem65 (176)
St8sia3 (164)
Gria1 (144)
Pabpc1 (155)
Eif3a (156)
Tcerg1 (172)
Hyou1 (101)
Npepps (184)
Vldlr (173)
Clcn6 (163)
nt
300
200
100

Figure 4. Puromycin runoff of polysomes in N2A cells after triple knockdown of FXRs.

Following knockdown of FMRP, FXR1P and FXR2P, N2A cells were treated with puromycin to induce ribosome runoff. Remaining polysomes were stabilized with cycloheximide after 1 hour of puromycin treatment and cells were lysed and subjected to sucrose gradient fractionation.

A) UV_{254} traces of sucrose gradients showing polysome runoff with puromycin treatment. Slightly more polysome runoff was observed after knockdown of FXRPs.

B) Western blot analysis shows all three FXRPs were successfully knocked down.

C) Runoff of individual mRNAs was measured by QPCR. Triple knockdown of FXRPs resulted in increased ribosome runoff of target mRNAs *Map1B* and *Huwe1* (as evidenced by a shift to lighter gradient fractions) but did not affect runoff of a nontarget mRNA (*Hprt1*).

A

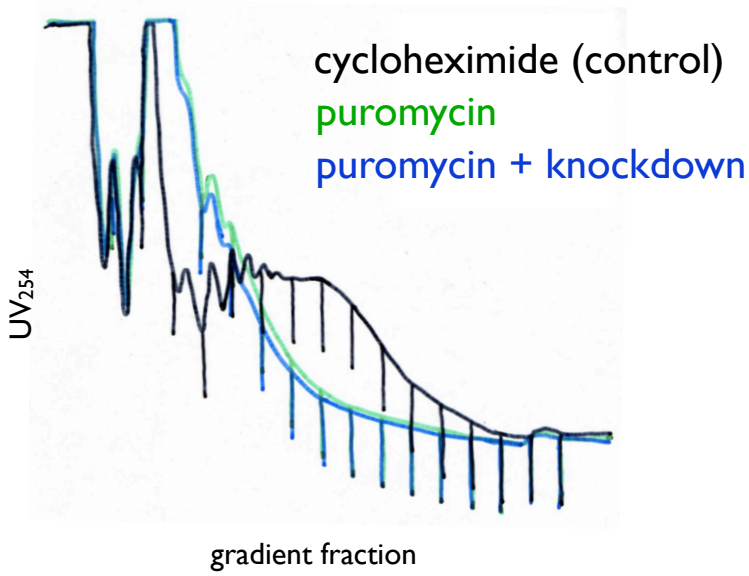
cycloheximide (control)
puromycin
puromycin + knockdown
UV254
gradient fraction

B

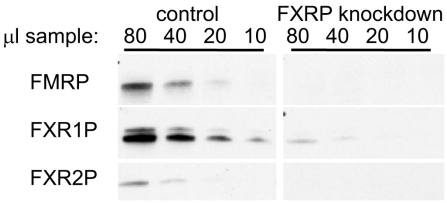
control
FXRP knockdown
µl sample:
80 40 20 10
80 40 20 10
FMRP
FXR1P
FXR2P

C

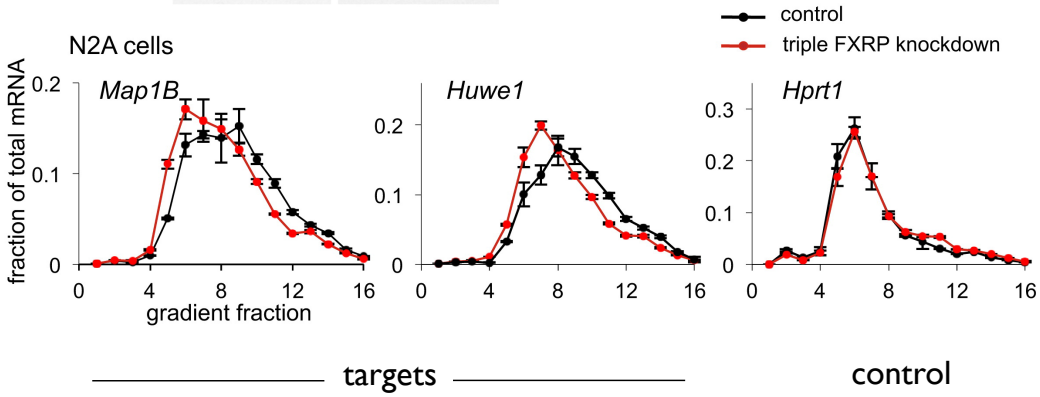
N2A cells
control
triple FXRP knockdown
fraction of total mRNA
Map1B
Huwe1
Hprt1
gradient fraction
targets
control

Figure 5. Distribution of FMRP on sucrose gradients in steady state and after runoff.

Brain polysomes were separated on sucrose gradients after puromycin runoff in the IVT-EBP system and fractions were analyzed by Western blot. FMRP was associated with heavy polysomes in the steady state (cycloheximide treated; CHX) and was associated with the heaviest remaining polysomes after puromycin runoff in the IVT-EBP system (puro). Treatment with kcRNA during puromycin runoff removed FMRP from polysomes, allowing it to migrate with free proteins in light fractions. The inactive mutant $kcRNA_{C50G}$ did not affect FMRP distribution on polysomes during runoff.

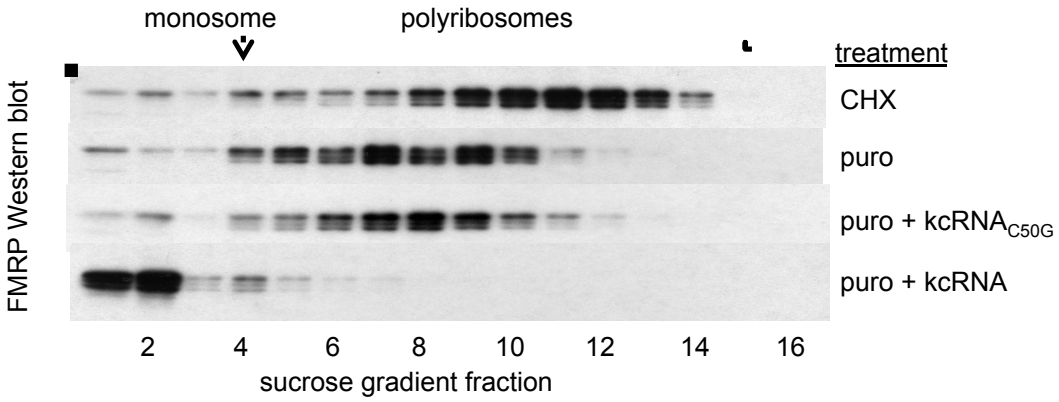
monosome
polyribosomes
treatment
CHX
puro
puro + kcRNA$_{C50G}$
puro + kcRNA
FMRP Western blot
2
4
6
8
10
12
14
16
sucrose gradient fraction

Figure 6. Ribosome stalling on FMRP target transcripts was relieved in two genetic models of FMRP loss-of-function.

Brain lysates from littermate pairs of wt/*Fmr1* KO (black/red) or wt/I304N (black/orange) mice were subjected to ribosome runoff using puromycin in the IVT-EBP system. Reactions were separated over sucrose gradients and the mRNA levels of individual genes were measured by QPCR for each fraction. A cycloheximide control (light blue) indicates original steady-state distributions of transcripts. FMRP loss-of-function in both models was associated with increased ribosome runoff of target transcripts, as evidenced by migration of target transcripts in lighter gradient fractions. FMRP loss-of-function did not alter runoff of nontarget transcripts. Error bars represent technical triplicates of QPCR measurements.

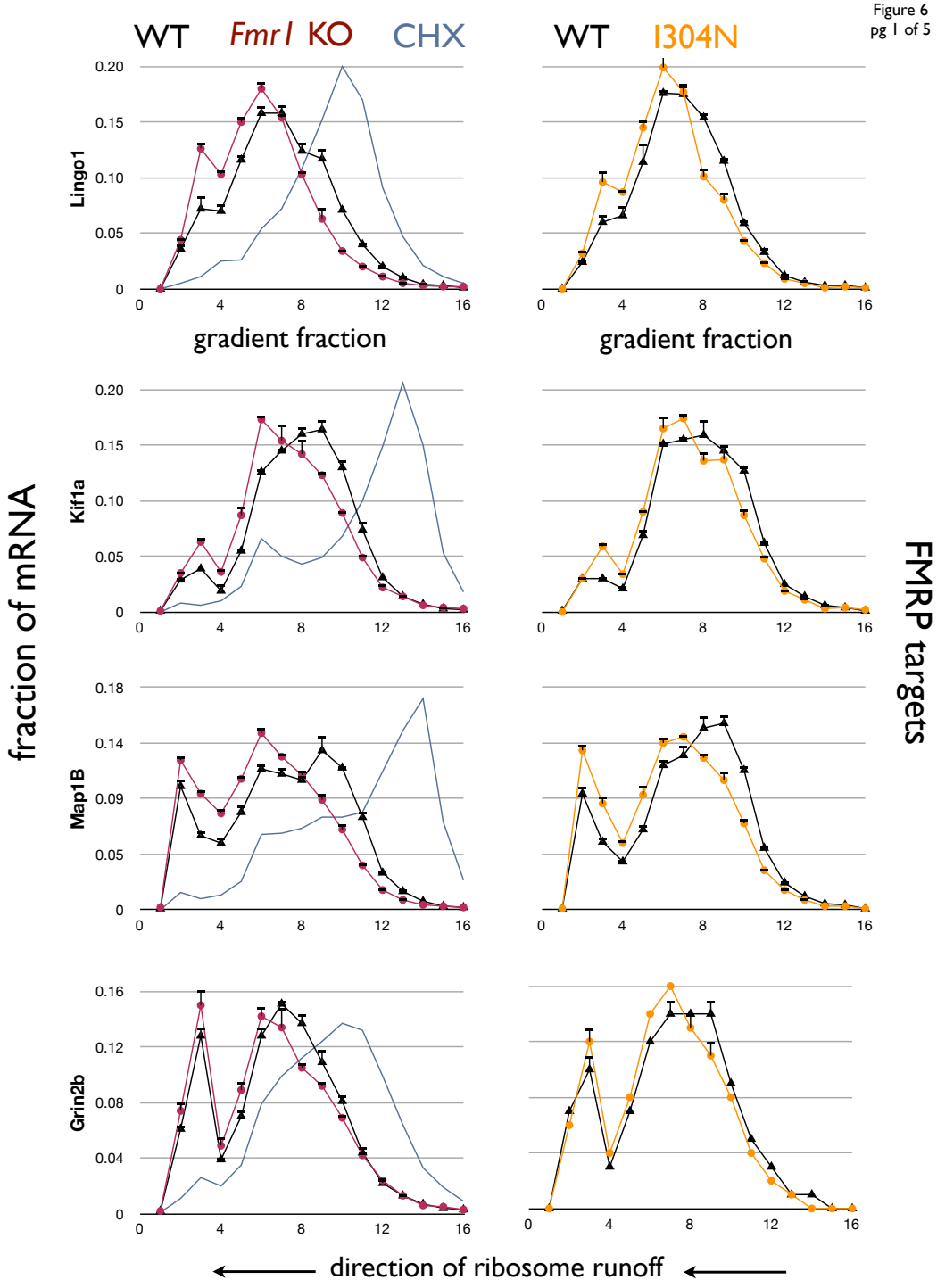
WT
Fmr1 KO
CHX
WT
I304N
Lingo1
Kif1a
Map1B
Grin2b
gradient fraction
gradient fraction
fraction of mRNA
FMRP targets
direction of ribosome runoff

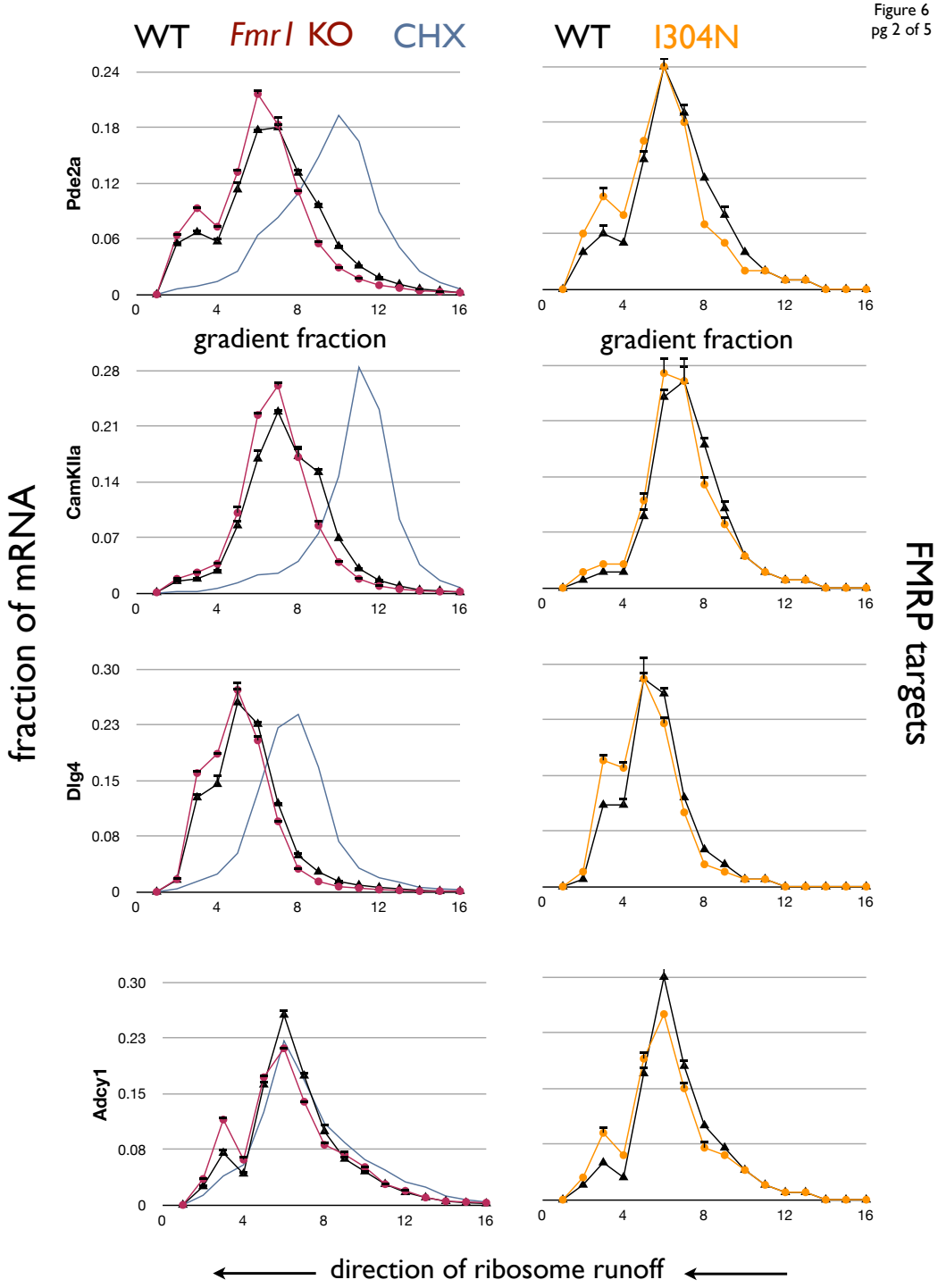
WT
Fmr1 KO
CHX
WT
I304N
fraction of mRNA
FMRP targets
Pde2a
CamKIIa
Dlg4
Adcy1
gradient fraction
gradient fraction
direction of ribosome runoff

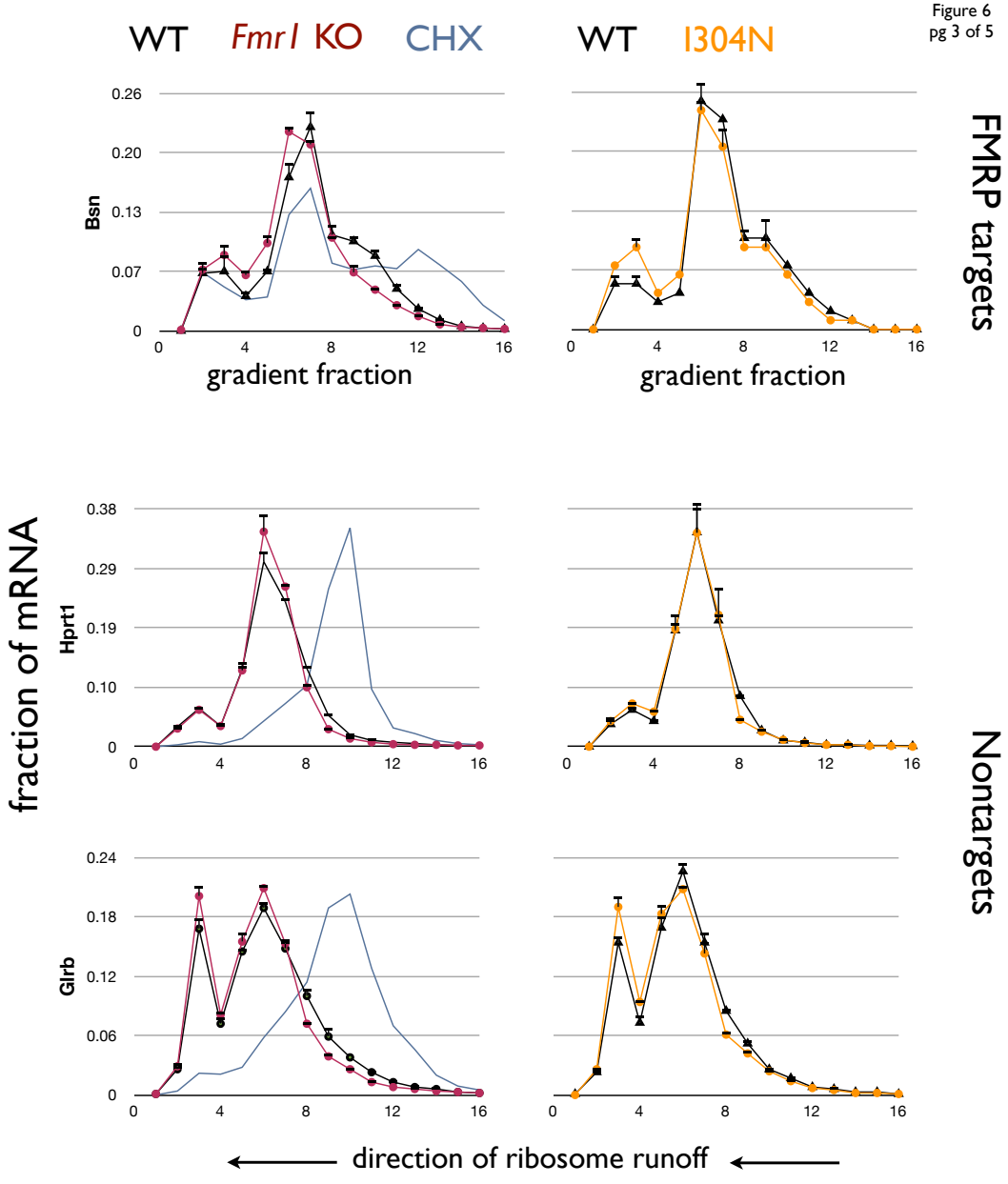
WT
Fmr1 KO
CHX
WT
I304N
FMRP targets
Nontargets
fraction of mRNA
Bsn
Hprt1
Glrb
0.26
0.20
0.13
0.07
0
0.38
0.29
0.19
0.10
0.24
0.18
0.12
0.06
0
4
8
12
16
gradient fraction
direction of ribosome runoff

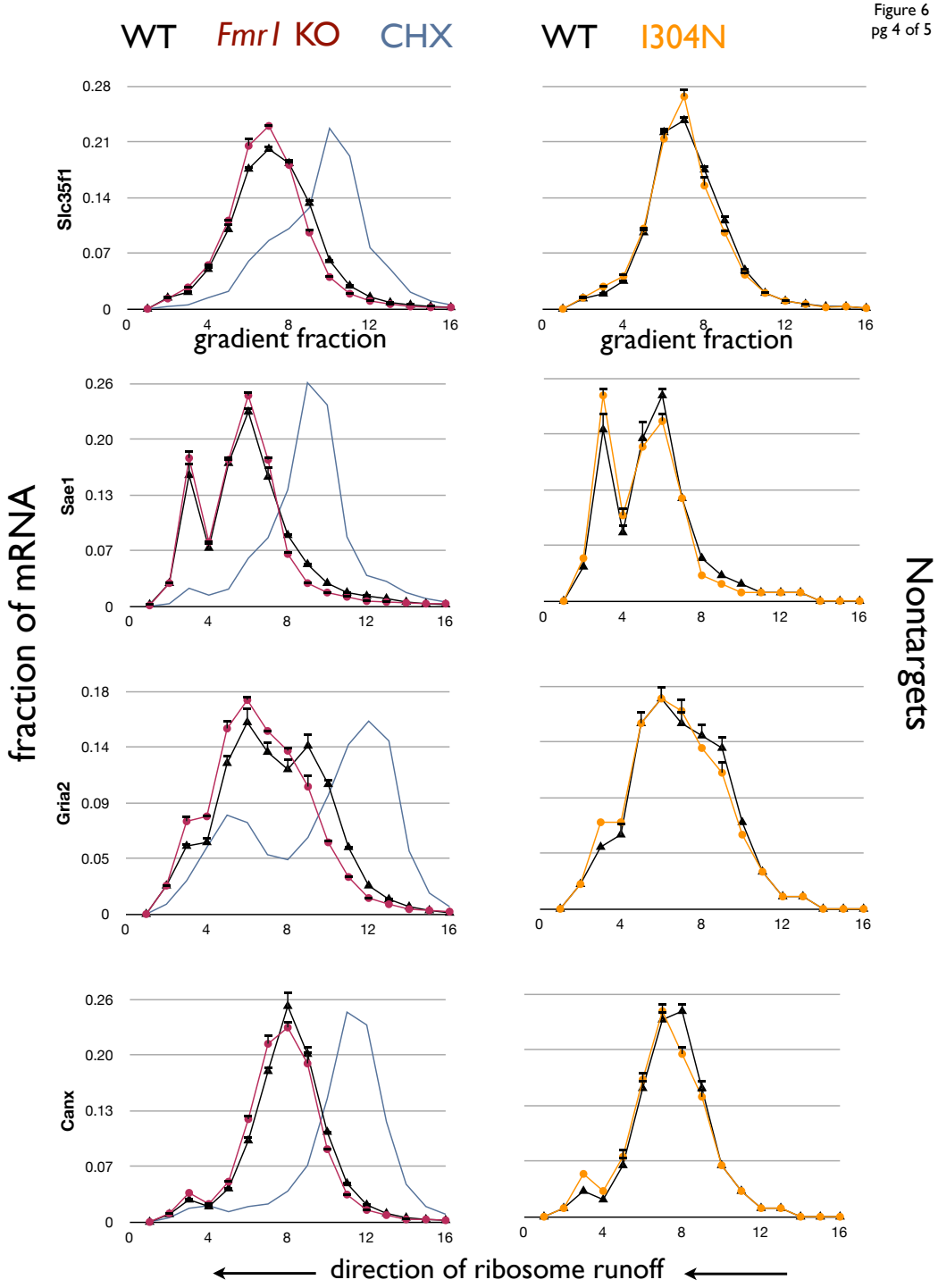
WT
Fmr1 KO
CHX
WT
I304N
Slc35f1
Sae1
Gria2
Canx
0.28
0.21
0.14
0.07
0
0.26
0.20
0.13
0.18
0.09
0.05
0 4 8 12 16
gradient fraction
fraction of mRNA
Nontargets
direction of ribosome runoff

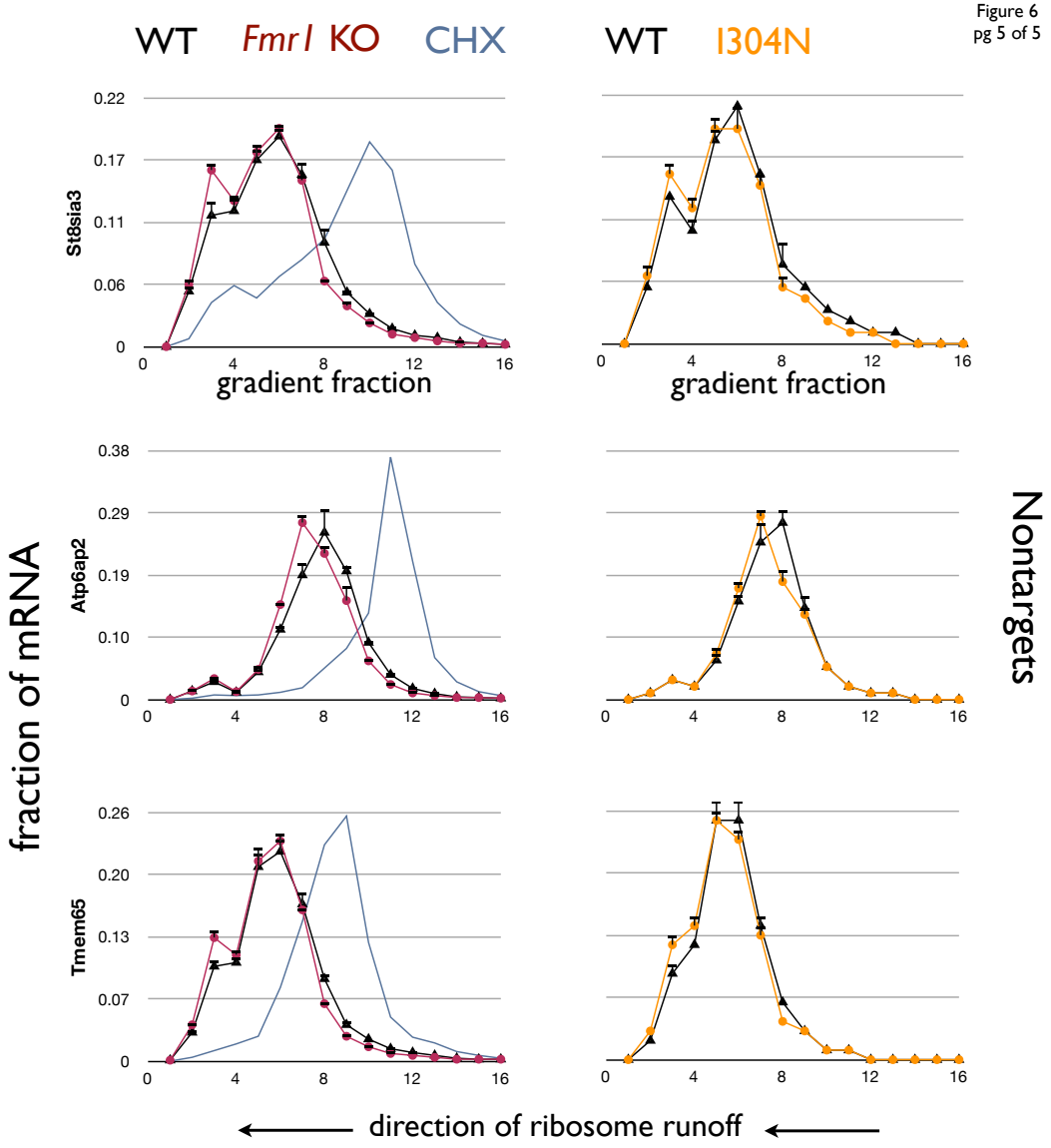
WT
Fmr1 KO
CHX
WT
I304N
St8sia3
Atp6ap2
Tmem65
0.22
0.17
0.11
0.06
0
0.38
0.29
0.19
0.10
0.26
0.20
0.13
0.07
0
4
8
12
16
gradient fraction
fraction of mRNA
Nontargets
direction of ribosome runoff

Figure 7. Ribosome stalling on FMRP target transcripts was relieved by acute FXRP loss-of-function.

Brain lysates from wt mice were treated with kcRNA or inactive mutant $kcRNA_{C50G}$ to acutely remove FXRPs from polysomes during ribosome runoff using puromycin in the IVT-EBP system. Reactions were separated over sucrose gradients and the mRNA levels of individual genes were measured by QPCR for each fraction. A cycloheximide control (light blue) indicates original steady-state distributions of transcripts. Acute FXRP loss-of-function was associated with increased ribosome runoff of FMRP target transcripts, as evidenced by migration of target transcripts in lighter gradient fractions. FXRP loss-of-function did not alter runoff of nontarget transcripts. In the right-hand column, QPCR signal was weighted to reflect ribosome loading of transcripts, as described in the text. This representation more realistically reflects the protein-producing capacity of polysomes, since mRNAs in heavy fractions are associated with more ribosomes than mRNAs in light fractions. Error bars represent technical triplicates of QPCR measurements.

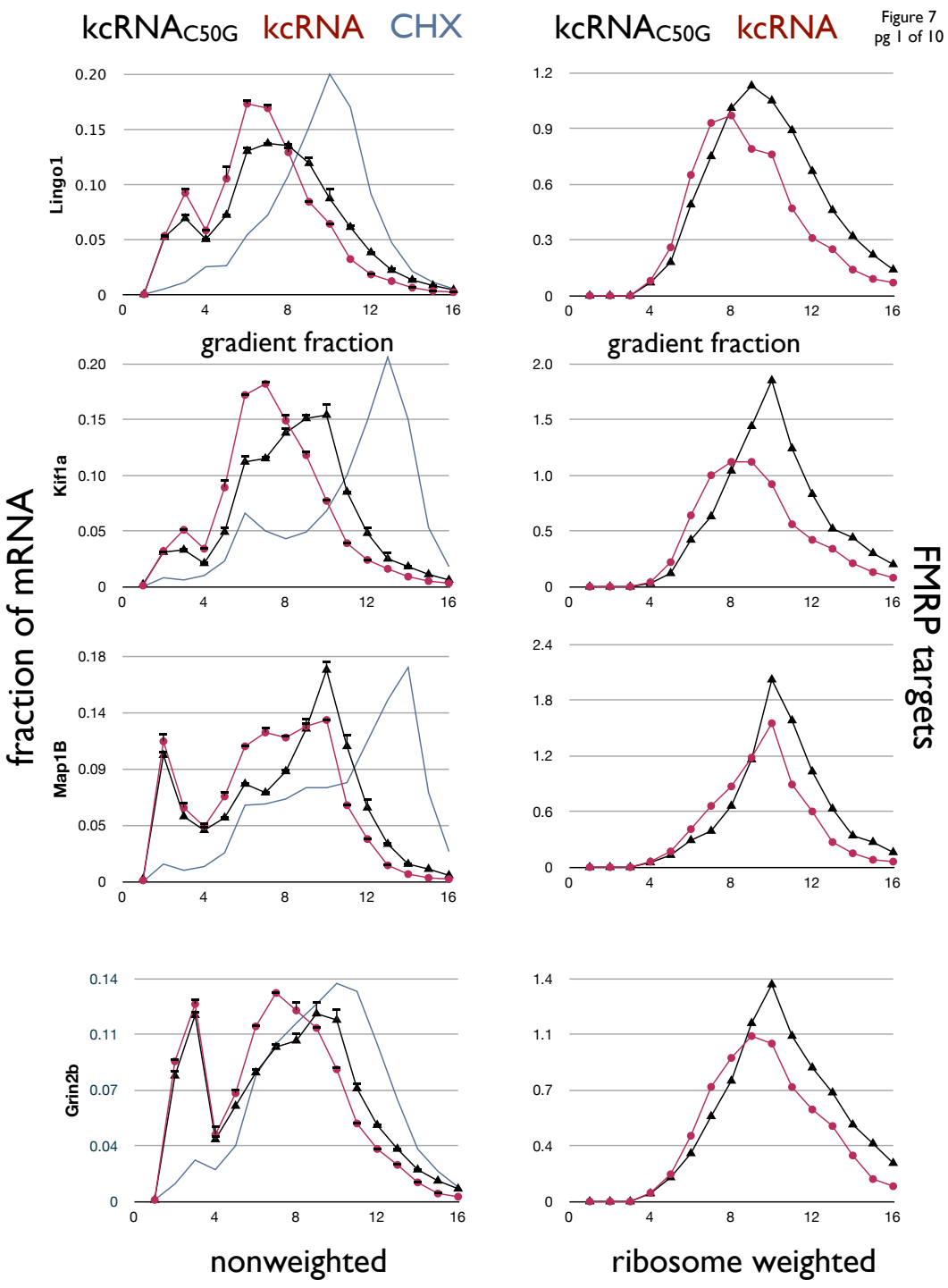
kcRNAC50G
kcRNA
CHX
kcRNAC50G
kcRNA
fraction of mRNA
FMRP targets
Lingo1
Kif1a
Map1B
Grin2b
gradient fraction
gradient fraction
nonweighted
ribosome weighted

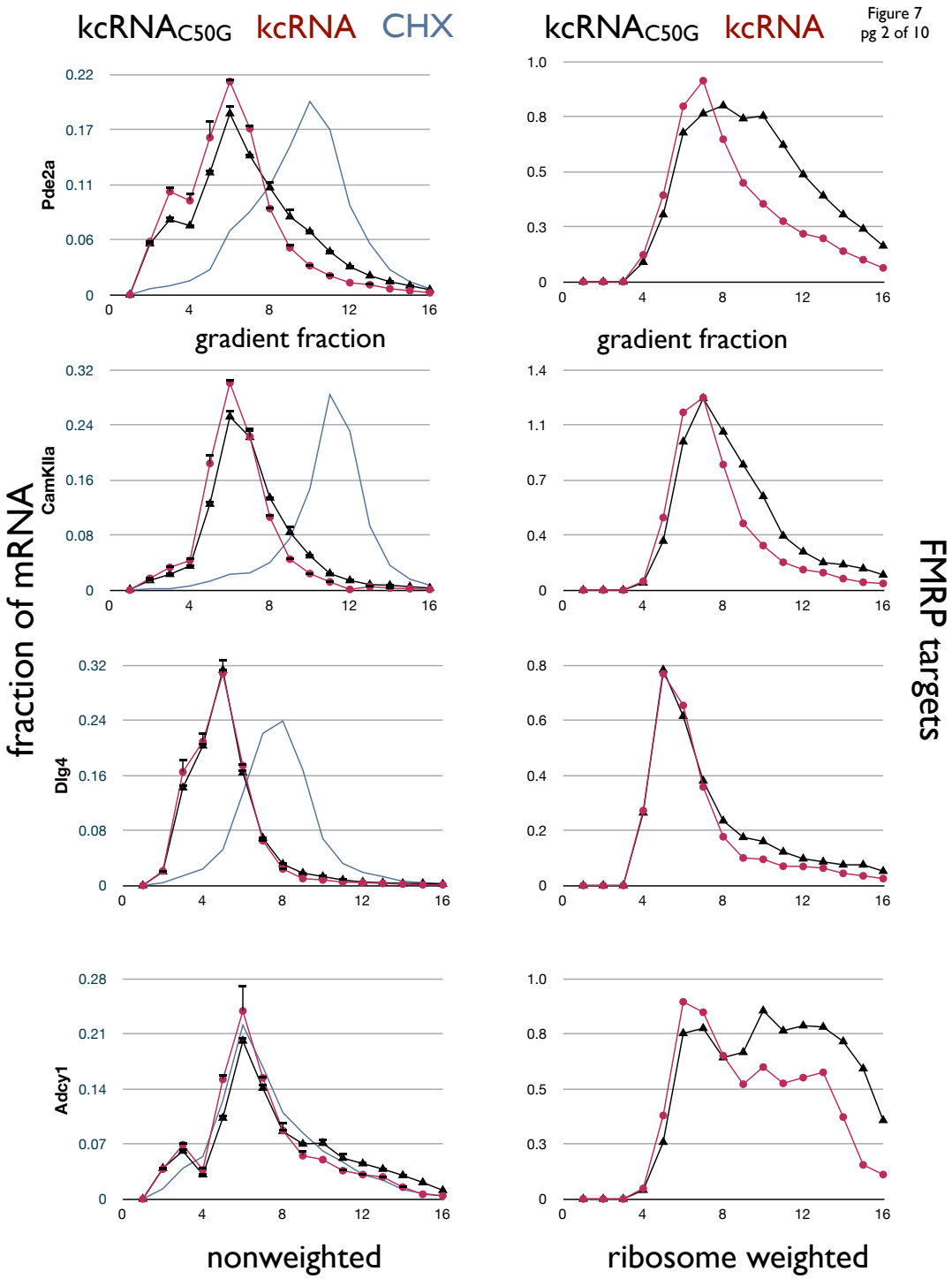
kcRNAC50G
kcRNA
CHX
kcRNAC50G
kcRNA
fraction of mRNA
FMRP targets
Pde2a
CamKIIa
Dlg4
Adcy1
gradient fraction
gradient fraction
nonweighted
ribosome weighted

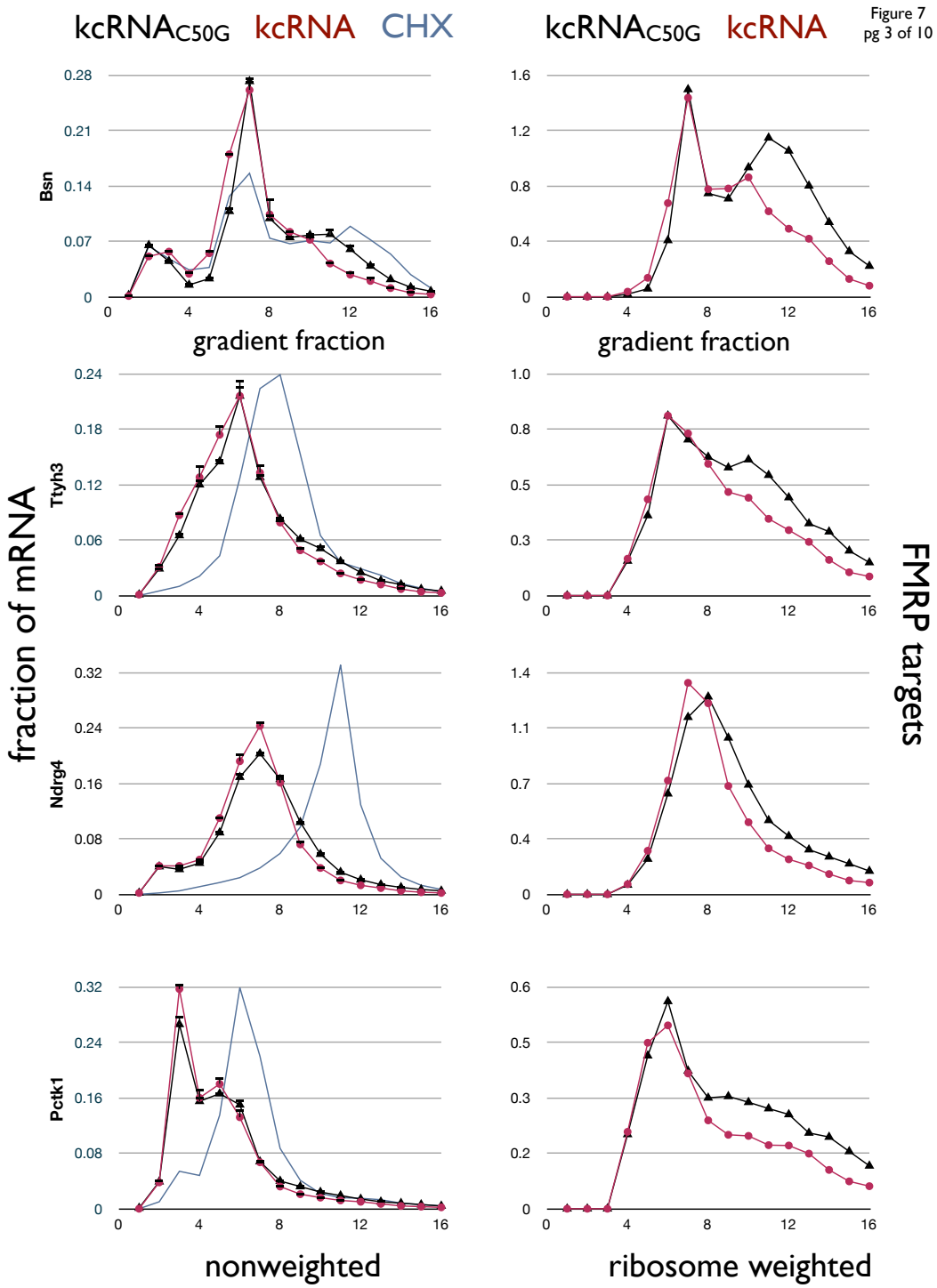
kcRNAC50G kcRNA CHX
kcRNAC50G kcRNA
fraction of mRNA
FMRP targets
Bsn
Ttyh3
Ndrg4
Pctk1
gradient fraction
gradient fraction
nonweighted
ribosome weighted

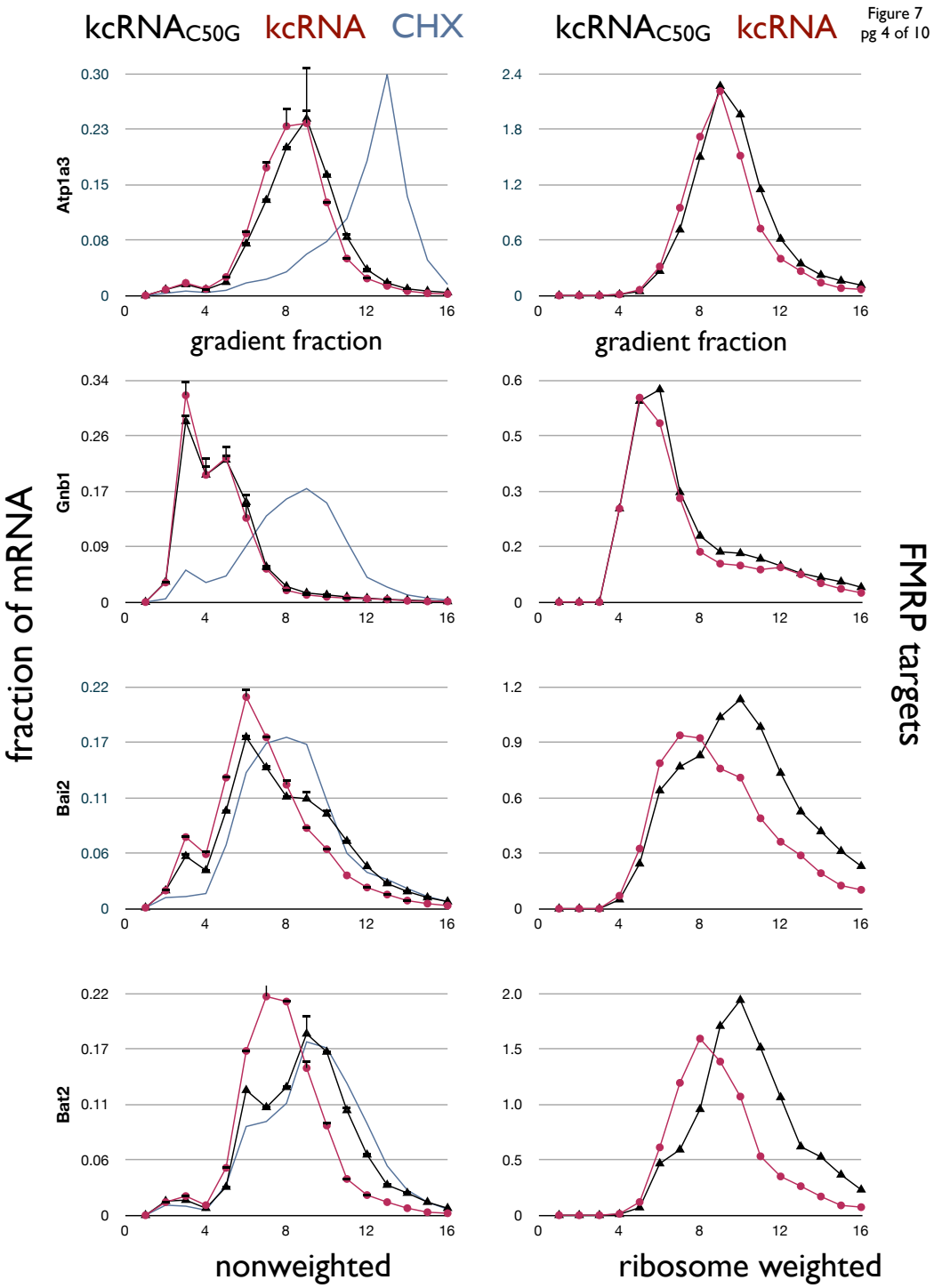
kcRNAC50G
kcRNA
CHX
kcRNAC50G
kcRNA
fraction of mRNA
FMRP targets
Atp1a3
Gnb1
Bai2
Bat2
gradient fraction
gradient fraction
nonweighted
ribosome weighted

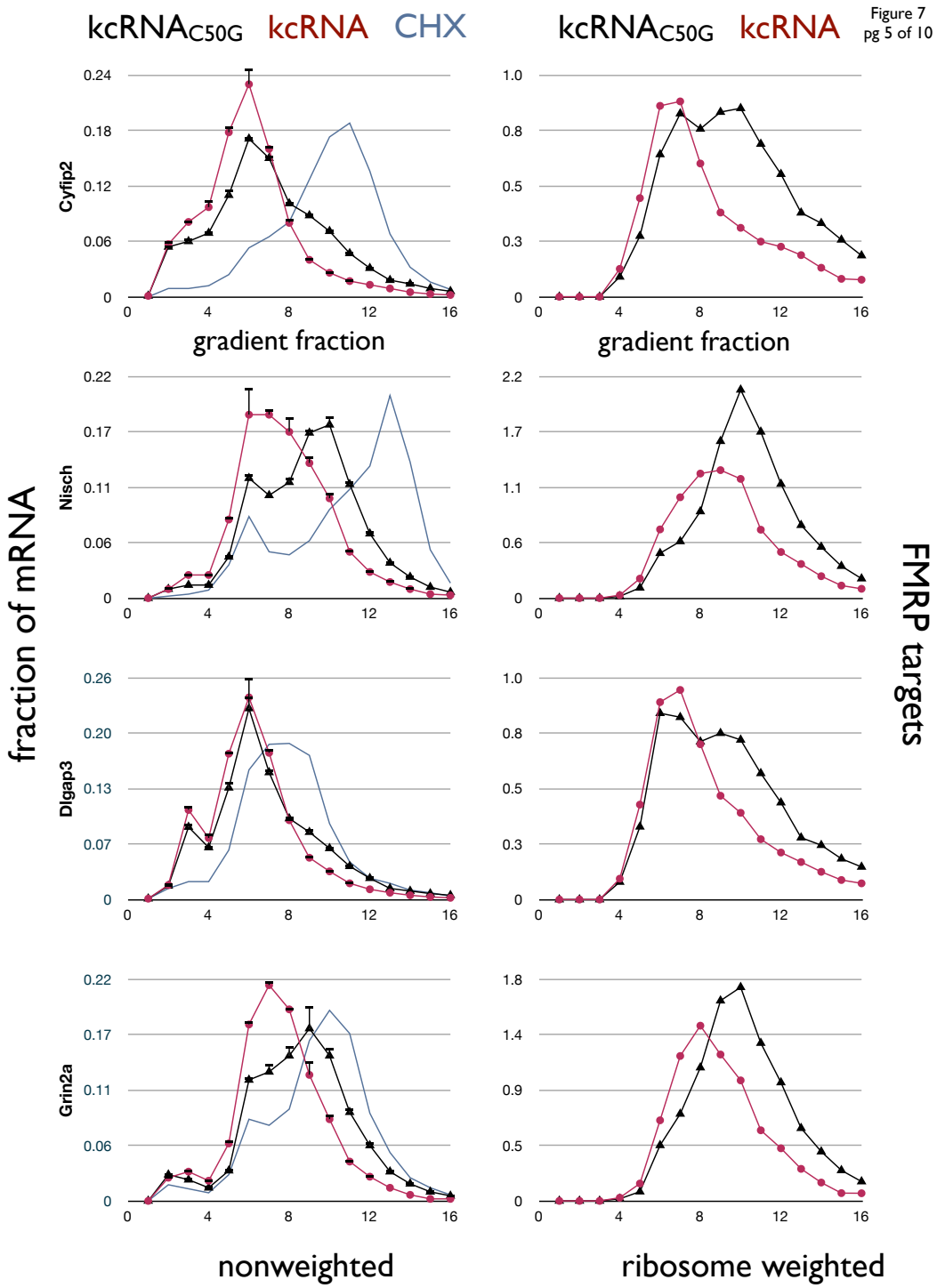
kcRNAC50G kcRNA CHX
kcRNAC50G kcRNA
fraction of mRNA
FMRP targets
Cyfip2
Nisch
Dlgap3
Grin2a
gradient fraction
gradient fraction
nonweighted
ribosome weighted

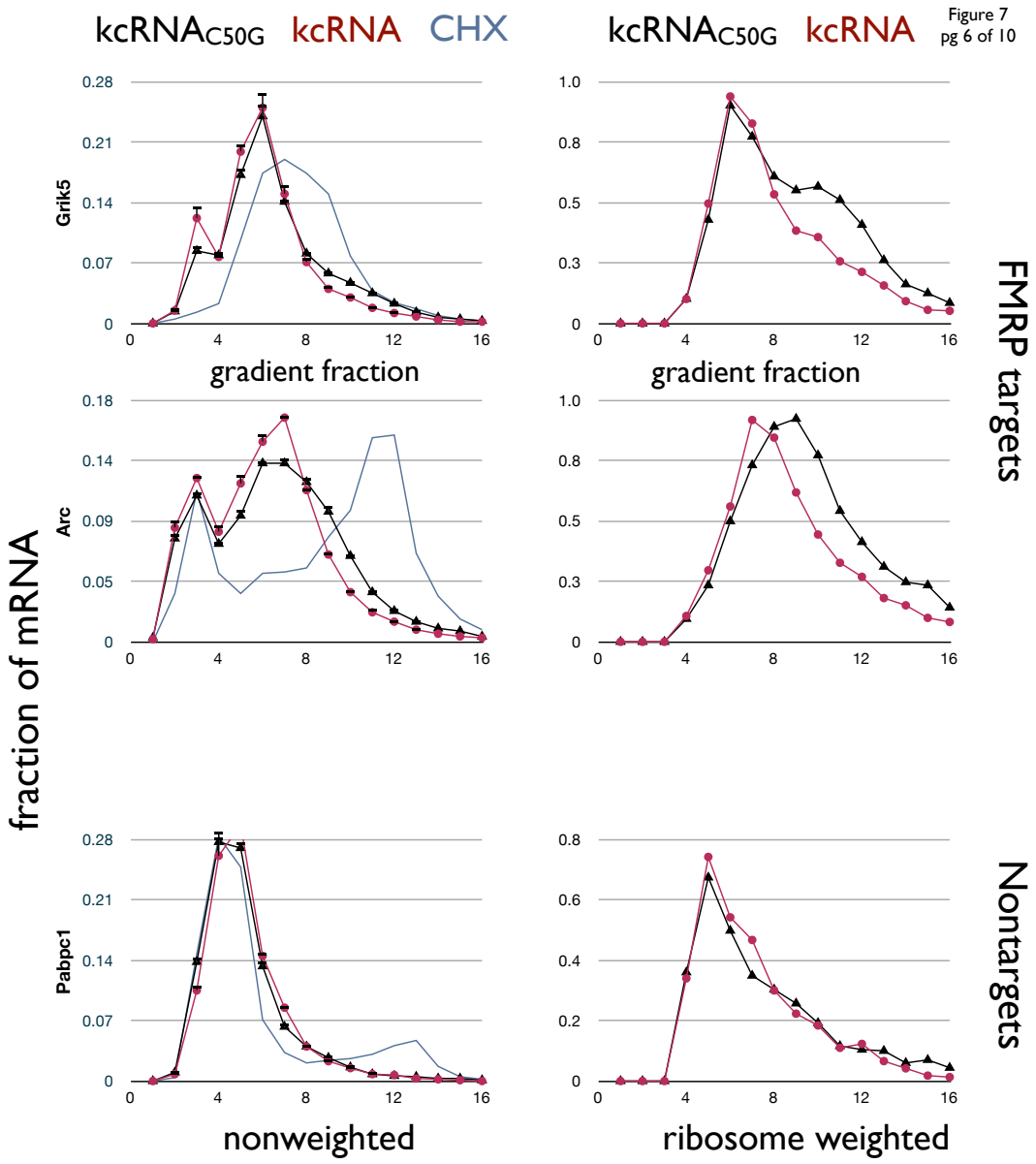
kcRNAC50G
kcRNA
CHX
kcRNAC50G
kcRNA
fraction of mRNA
FMRP targets
Nontargets
Grik5
Arc
Pabpc1
gradient fraction
gradient fraction
nonweighted
ribosome weighted

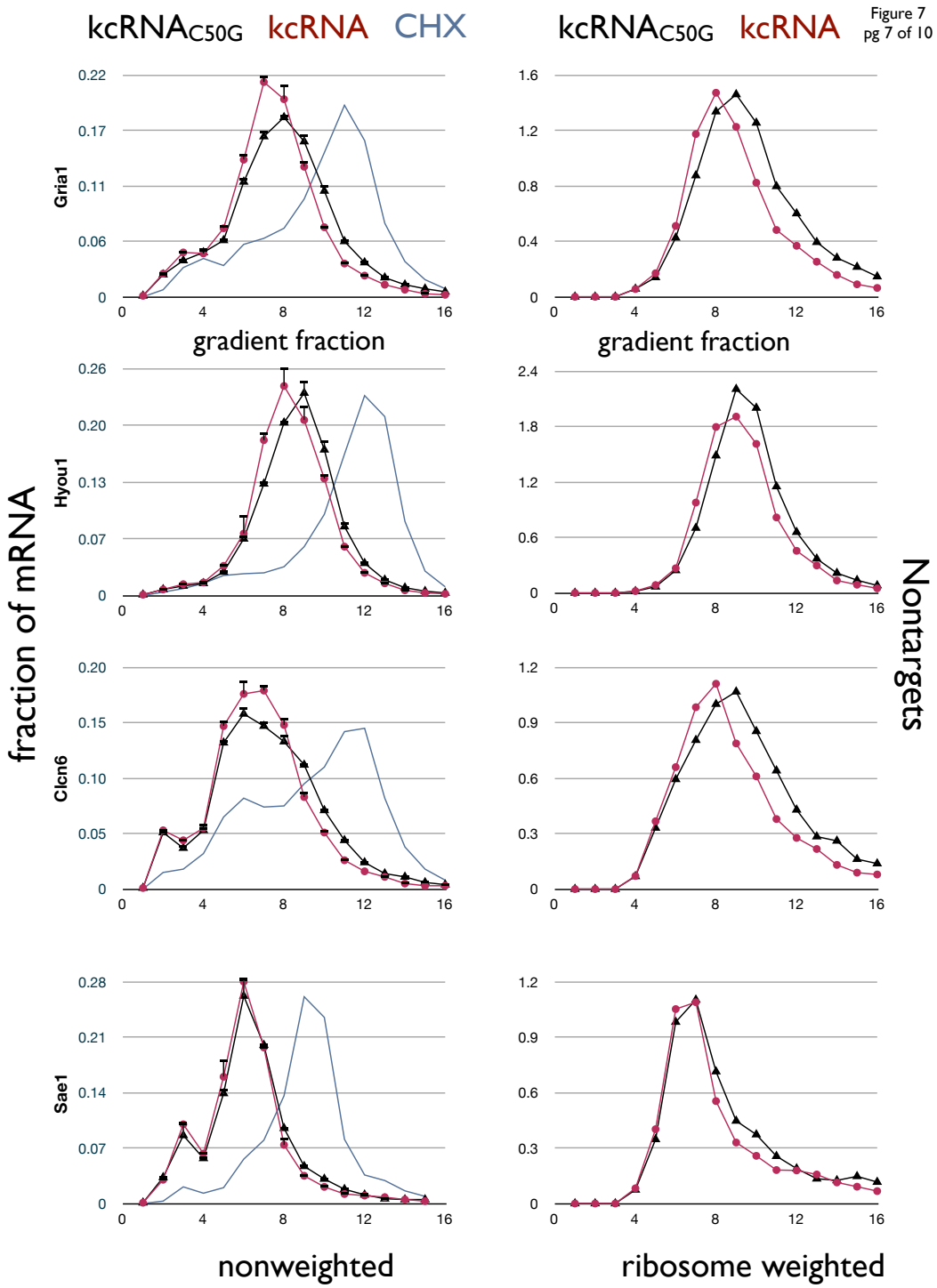
kcRNAC50G
kcRNA
CHX
kcRNAC50G
kcRNA
fraction of mRNA
Nontargets
Gria1
Hyou1
Clcn6
Sae1
gradient fraction
gradient fraction
nonweighted
ribosome weighted

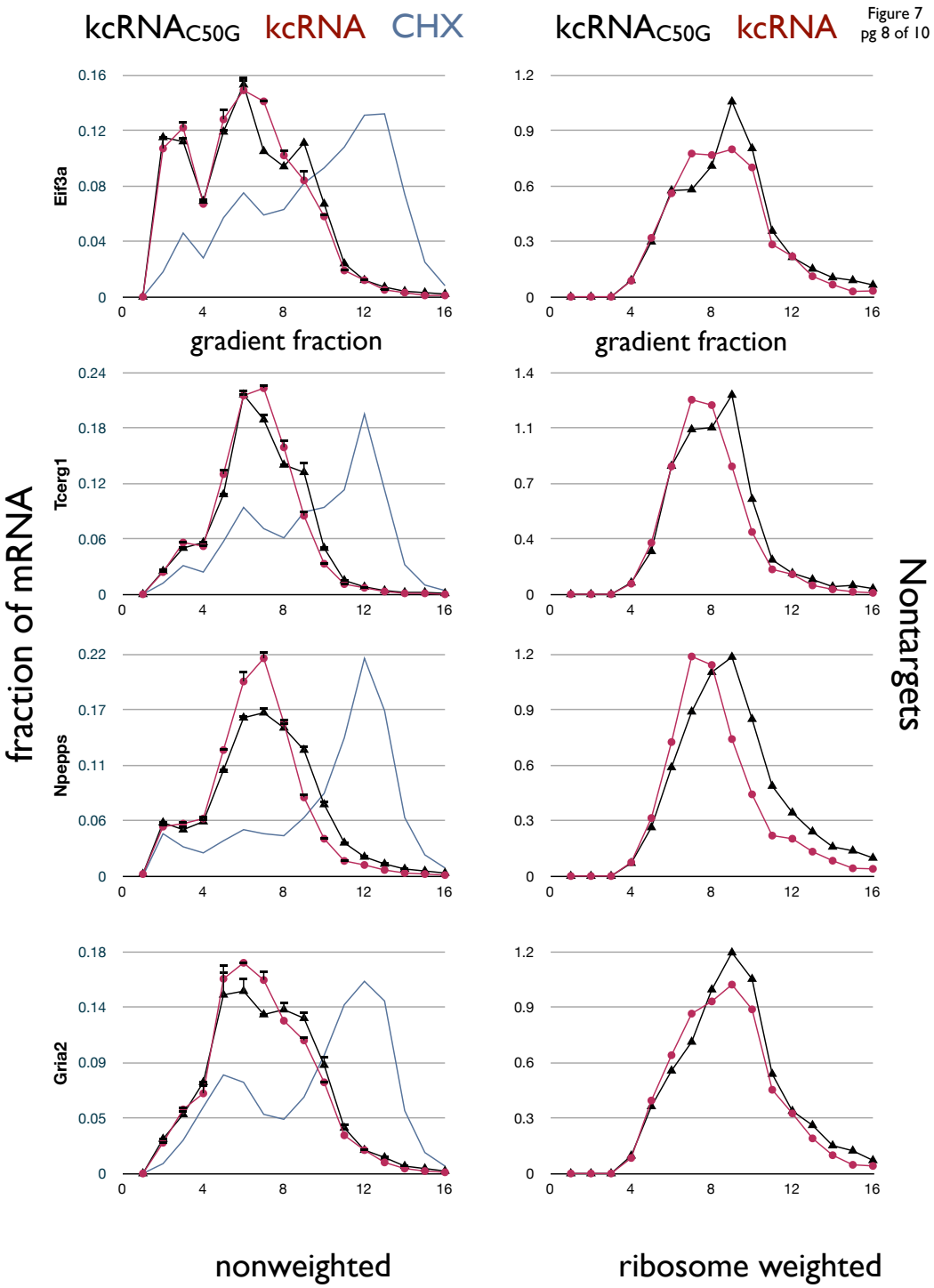
kcRNAC50G
kcRNA
CHX
kcRNAC50G
kcRNA
fraction of mRNA
Nontargets
Eif3a
Tcerg1
Npepps
Gria2
gradient fraction
gradient fraction
nonweighted
ribosome weighted

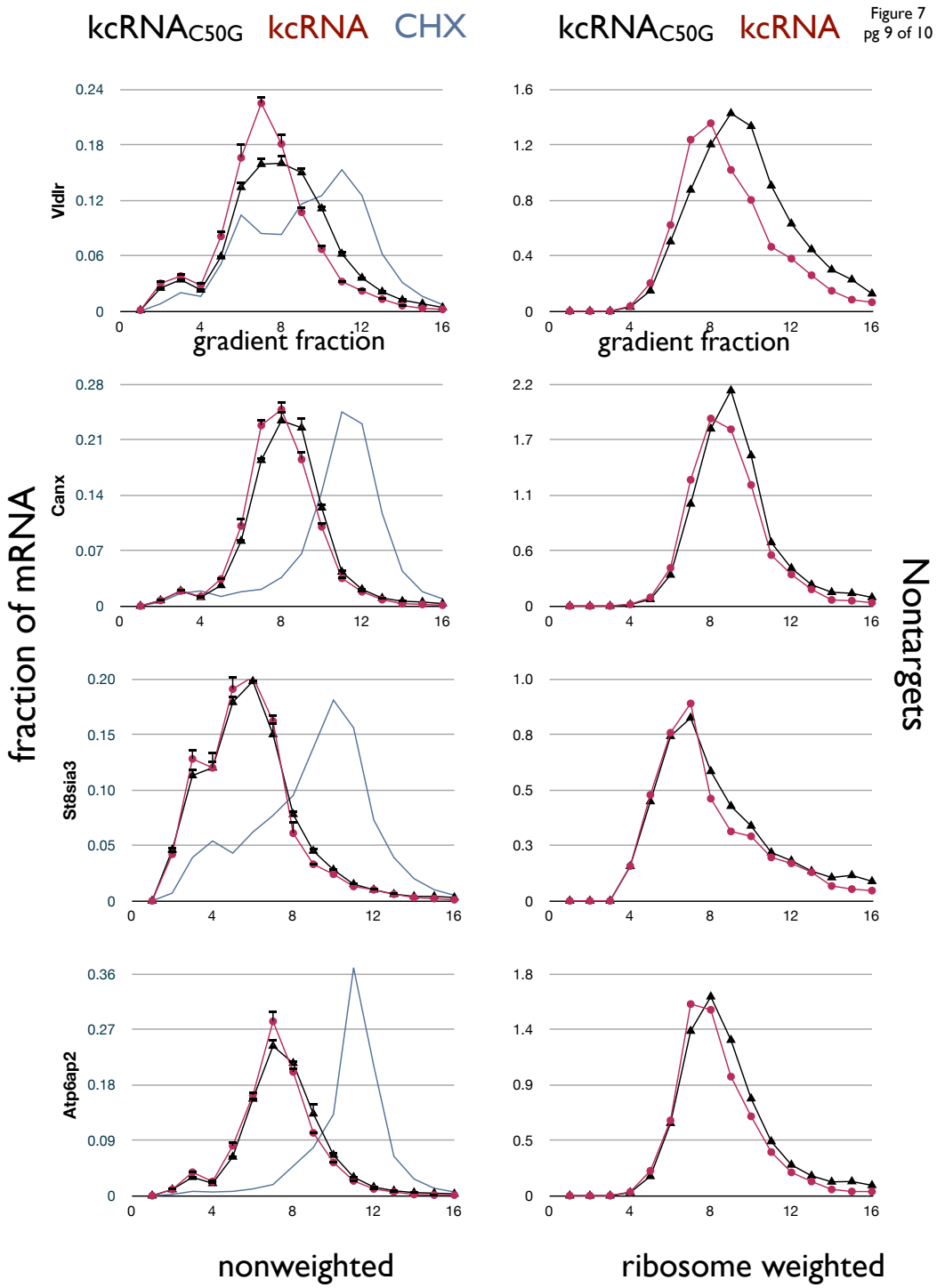
kcRNAC50G
kcRNA
CHX
kcRNAC50G
kcRNA
fraction of mRNA
Nontargets
Vldlr
Canx
St8sia3
Atp6ap2
gradient fraction
gradient fraction
nonweighted
ribosome weighted

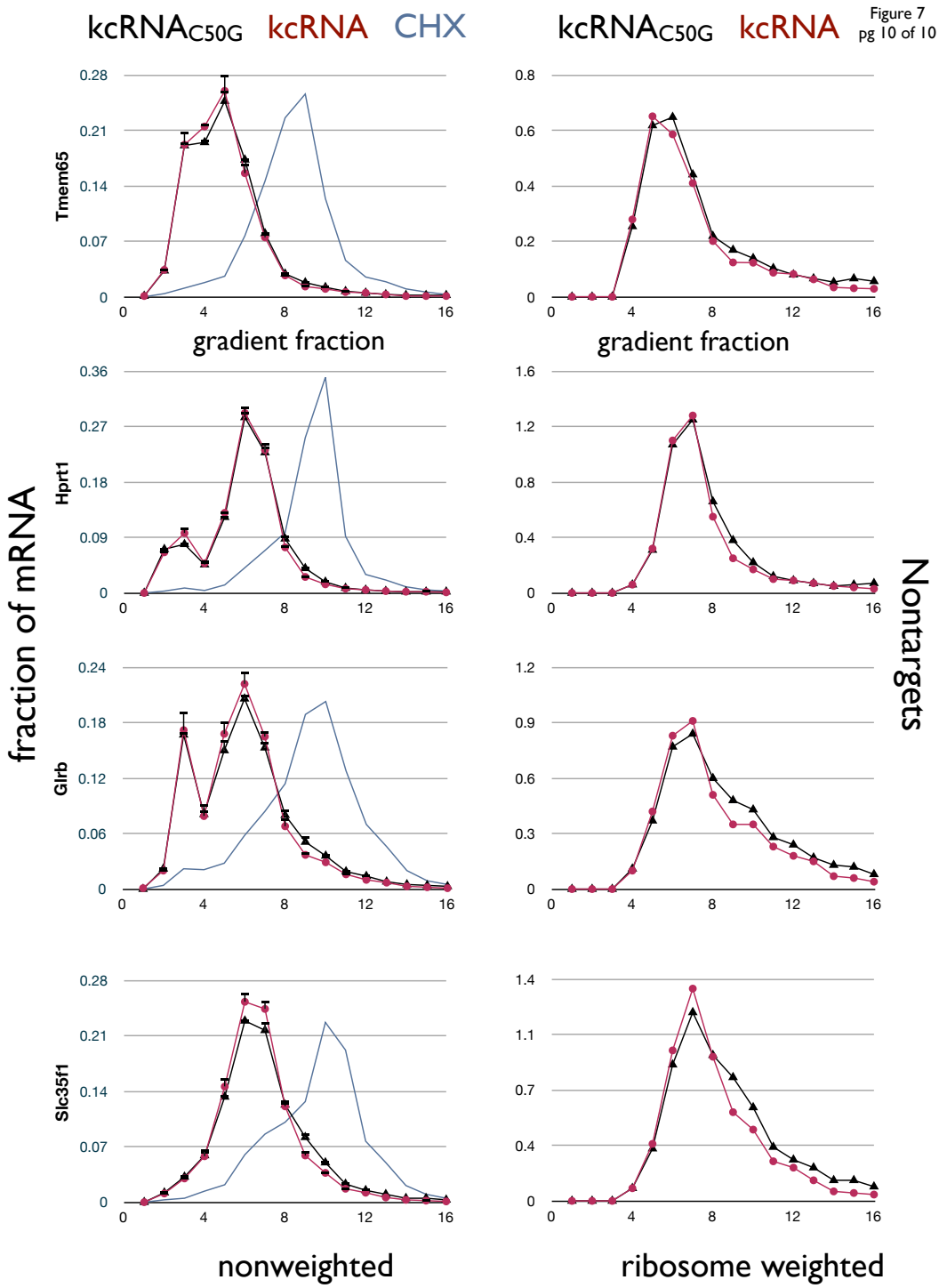
kcRNAC50G kcRNA CHX
kcRNAC50G kcRNA
fraction of mRNA
Nontargets
Tmem65
Hprt1
Glrb
Slc35f1
gradient fraction
gradient fraction
nonweighted
ribosome weighted

Table 1: 39 FMRP target mRNAs assayed in the IVT-EBP system.

Number of CLIP tags per gene for whole brain and polysome CLIP experiments is shown, along with coding sequence length (CDS Length), neuronal mRNA abundance (Cahoy 2008), Retained Ribosome score (RRS) and Ribosome Loading score (a measure of the total number of ribosomes associated with transcripts on polyribosome gradients before run-off, calculated by summation of the ribosome-weighted QPCR values for all 16 fractions of a CHX-treated gradient).

Gene	Common Name	Tags: Whole Brain	Tags: Poly-some	CDs Length	mRNA Abund	RRS	Ribosome Loading
TARGETS							
Mtap1b	Map1b	5959	797	7395	1038	178	15.7
Kif1a	Kinesin 1A	3256	565	5094	240	224	16.2
Bsn	Bassoon	2067	568	11829	3738	176	10
Adcy1	Adenylate cyclase 1	1630	414	3357	3795	175	6.8
Cyfip2	Cytoplasmic FMRP-interacting protein 2	1225	355	3762	3029	211	12.5
Nisch	Nischarin	970	261	4782	6435	263	15.7
Pde2a	Phosphodiesterase 2a	925	192	2808	6392	167	11.5
Camk2a	Ca/Calmodulin dep. kinase IIa	662	143	1437	1624	112	14.7
Dlg4	PSD-95	587	157	2175	NA	39	7.5
Pctk1	PCTAIRE protein kinase 1	587	95	1491	2711	75	5.4
Bat2	HLA-B associated transcript 2	538	187	6477	1360	259	11.1
Bai2	Brain-specific angiogenesis inhibitor 2	531	213	4650	NA	183	8.8
Grin2b	NMDAR subunit 2B	422	143	4449	903	134	11.2
Lingo1	Lingo1	355	101	1845	1879	161	11.4
Grik5	Kainate receptor 5, KA5	298	111	2940	679	102	7.4
Dlgap3	SAPAP3	269	86	2934	267	126	7.9
Atp1a3	ATPase, Na+/K+ transporting, alpha 3	246	161	3162	5499	91	17.8
Gnb1	G protein, beta polypeptide 1	221	83	1023	3804	29	8.9
Grin2a	NMDAR subunit 2A	205	86	4395	35	220	11.3

Gene	Common Name	Tags: Whole Brain	Tags: Polys	CDs Length	mRNA Abund	RRS	Ribosome Loading
NON-TARGETS							
Eif3a	Eukaryotic initiation factor 3a	104	11	4035	2674	49	12.5
Ndrg4	NDRG family member 4	79	62	1020	12009	94	13.4
Ttyh3	Tweety homolog 3	58	41	1575	2831	92	8
Npepps	Aminopeptidase puromycin sensitive	55	11	2763	1861	107	13.8
Pabpc1	PABP	53	11	1911	3161	0	4.9
Gria1	AMPAR subunit GluR1	51	29	2724	1710	113	12.3
Gria2	AMPAR subunit GluR2	40	17	2652	3090	47	12.4
St8sia3	ST8 a-N-Ac-neuraminide a-2,8-sialyltransf. 3	31	8	1143	926	35	10.3
Glrb	Glycine receptor, beta	30	8	1491	2573	46	10.8
Tcerg1	Transcription elongation regulator 1	28	5	3303	1344	47	12
Canx	Calnexin	16	14	1776	3584	68	14.7
Vldlr	Very low density lipoprotein receptor	14	0	2622	NA	148	12.2
Clcn6	Chloride channel 6	12	1	2613	1478	88	11.7
Arc	Arg3.1/Arc	11	9	1191	903	114	10.8
Sae1	SUMO1 activating enzyme subunit 1	10	2	1053	1759	45	10.2
Hyou1	Hypoxia up-regulated 1	9	3	3000	1272	83	17
Atp6ap2	ATPase, H+ transp., lysosomal acc. prot. 2	9	1	1053	10196	64	14.5
Hprt1	Hypoxanthine phosphoribosyltrans.1	4	5	657	4553	29	10.7
Slc35f1	Solute carrier family 35, member F1	3	6	1227	2092	56	11.6
Tmem65	Transmembrane protein 65	2	4	705	1264	21	8.8

Figure 8. Removal of FMRP from polysomes after completion of puromycin runoff had no effect on mRNA migration on sucrose gradients.

Wt brain lysate was subjected to ribosome runoff using puromycin in the IVT-EBP system and treatment with kcRNA or $kcRNA_{C50G}$ was delayed until after runoff was complete.

A) Removal of FXRPs from polysomes by kcRNA treatment after completion of runoff did not affect migration of target mRNAs (for comparison to the effect of kcRNA addition during runoff, see Figure 7). This indicates that the FMRP-dependent migration shift of target mRNAs on sucrose gradients is due to loss of ribosomes and not to loss of FMRP.

B) Western blot of FMRP from heavy polysome fractions. kcRNA treatment is usually performed at 30°C. To ensure that kcRNA treatment at 4°C was also effective at removing FMRP from polysomes, the amount of FMRP remaining in heavy polysomes was compared after kcRNA treatment at the two temperatures. kcRNA was largely effective at 4°C (removing ~80% of FMRP from polysomes).

A

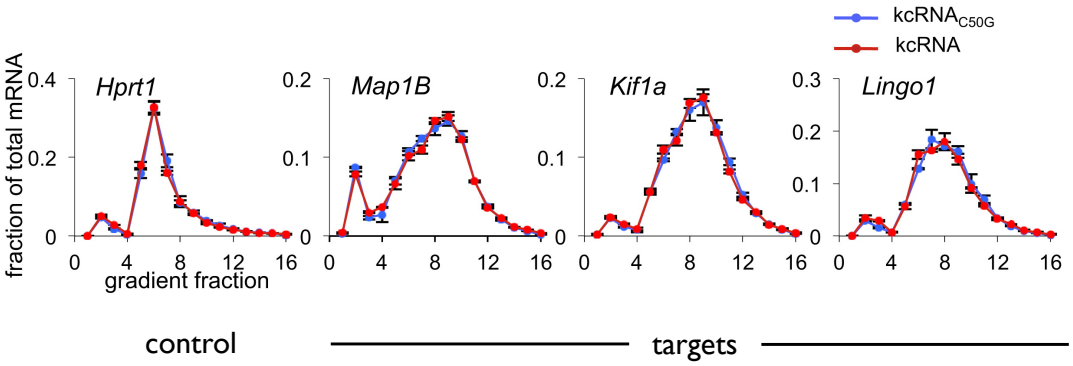
kcRNA$_{C50G}$
kcRNA
fraction of total mRNA
Hprt1
Map1B
Kif1a
Lingo1
gradient fraction
control
targets

B

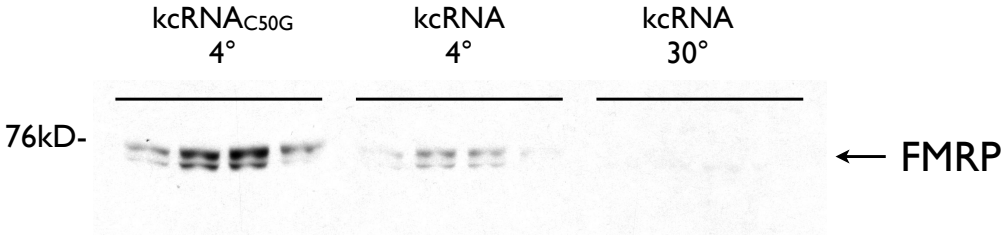
kcRNA$_{C50G}$ 4°
kcRNA 4°
kcRNA 30°
76kD-
FMRP

Figure 9. Quantitation of FMRP-mediated ribosome stalling

A) Characterization of sucrose gradients used in retained ribosome score (RRS) calculations. Top: the percent sucrose (w/w) measured in each gradient fraction using a refractometer was linear with fraction number ($R^2 = 0.99$). Fractions 1 and 2 correspond to lysate. Bottom: determination of the approximate number of ribosomes (open circles) in sucrose gradient fractions by extrapolation from those that can be directly counted (black circles), using linear regression analysis ($R^2 = 0.999$), based on the linearity determined in the top panel. Figures reflecting the number of ribosomes per transcript in each fraction were used to weight mRNA measurements from QPCR analysis of gradient fractions (as in Figure 7, right-hand column).

B) Bar graphs plotting RRS scores in three different FMRP loss of function models (I304N, *Fmr1* KO, kcRNA) for nine target (gold) and nine nontarget (red) transcripts. Significant differences were evident between targets and nontargets in all three systems, as well as a significantly greater effect of kcRNA than either genetic FMRP loss of function model. Error bars depict the standard error of the mean (SEM).

C) FMRP binding to target mRNAs (chi-square score of polysome CLIP targets, see Darnell 2011) compared with ribosome retention scores from puromycin runoff assays in the IVT-EBP system showed a significant correlation for 39 tested transcripts. Target transcripts (shaded gold) showed high chi-square values and RRS scores relative to nontargets (shaded red), with some outliers.

D) Twenty FMRP targets and 16 nontargets showed a significant difference in RRS (RRS_{Avg}(target) = 148.1 +/- 14.6; RRS_{Avg}(nontarget) = 58.3 +/- 8.9; $p = 9.7 \times 10^{-6}$). This analysis includes every mRNA tested except *Arc* and *Gria1*.

E) RRS was highly correlated with coding sequence (CDS) length for FMRP targets (excluding an outlier, *Bsn*; CDS 11,829 nts), consistent with FMRP stalling ribosomes across the length of the CDS of its target transcripts.

F) Six FMRP targets and seven nontargets matched for length (in the 1000-2000nt window) showed a significant difference in RRS (RRS_{Avg}(target) = 93.7 +/- 17.6; RRS_{Avg}(nontarget) = 44.8 +/- 8.6; p = 0.040).

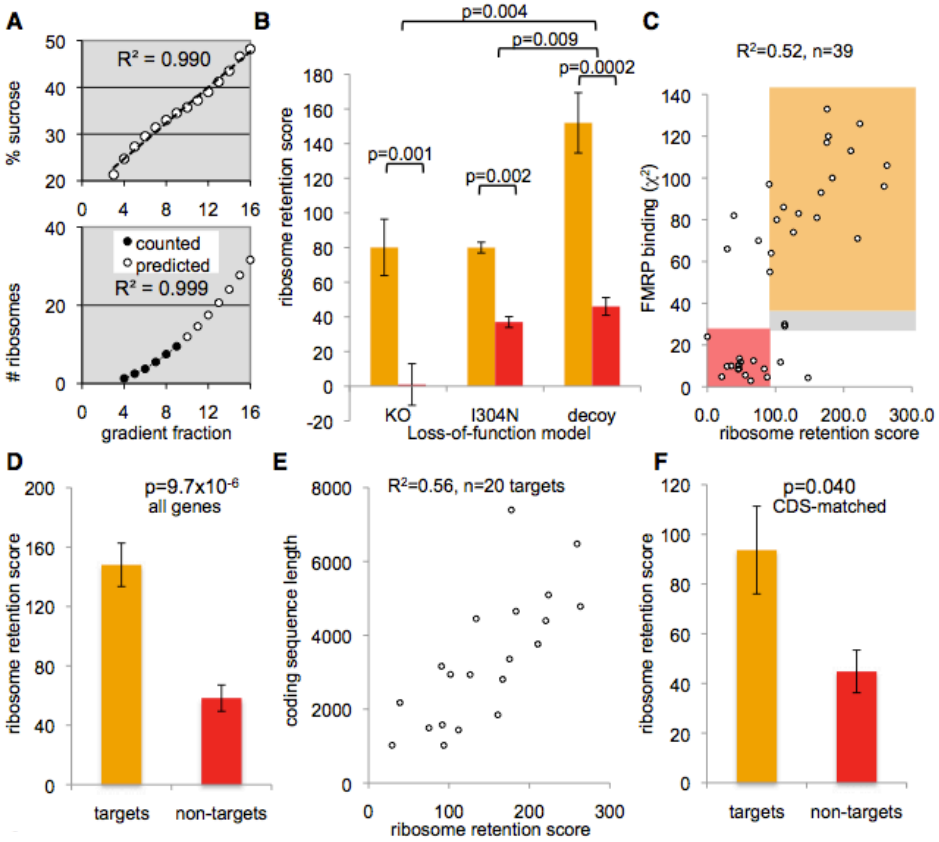
A
% sucrose
R² = 0.990
# ribosomes
counted
predicted
R² = 0.999
gradient fraction
B
p=0.004
p=0.009
p=0.0002
p=0.001
p=0.002
ribosome retention score
KO
I304N
decoy
Loss-of-function model
C
R²=0.52, n=39
FMRP binding (χ²)
ribosome retention score
D
p=9.7x10⁻⁶
all genes
ribosome retention score
targets
non-targets
E
R²=0.56, n=20 targets
coding sequence length
ribosome retention score
F
p=0.040
CDS-matched
ribosome retention score
targets
non-targets

Figure 10. EDTA profiles of FMRP target and nontarget transcripts after puromycin runoff.

Ribosome runoff of brain polysomes using puromycin in the IVT-EBP system was conducted in the presence of kcRNA (red) or kcRNA plus 30mM EDTA (green). Samples were separated over sucrose gradients and QPCR was used to measure the levels of the indicated mRNAs in each fraction. Individual mRNAs and their "ribosome loading" scores are indicated on each graph. Ribosome loading is a measure of the total number of ribosomes associated with transcripts on polyribosome gradients before runoff. Graphs are arranged in order of descending ribosome loading, and illustrate the dependence of the number of residual ribosomes (the difference between the red and green traces) on the number of ribosomes initially associated with each transcript. EDTA treatment caused mRNAs to migrate in lighter gradient fractions, consistent with removal of residual ribosomes. Note that while only FMRP target mRNAs were further shifted by FMRP loss-of-function during runoff (Figure 7), residual ribosomes from both target and nontarget mRNAs were removed by EDTA treatment.

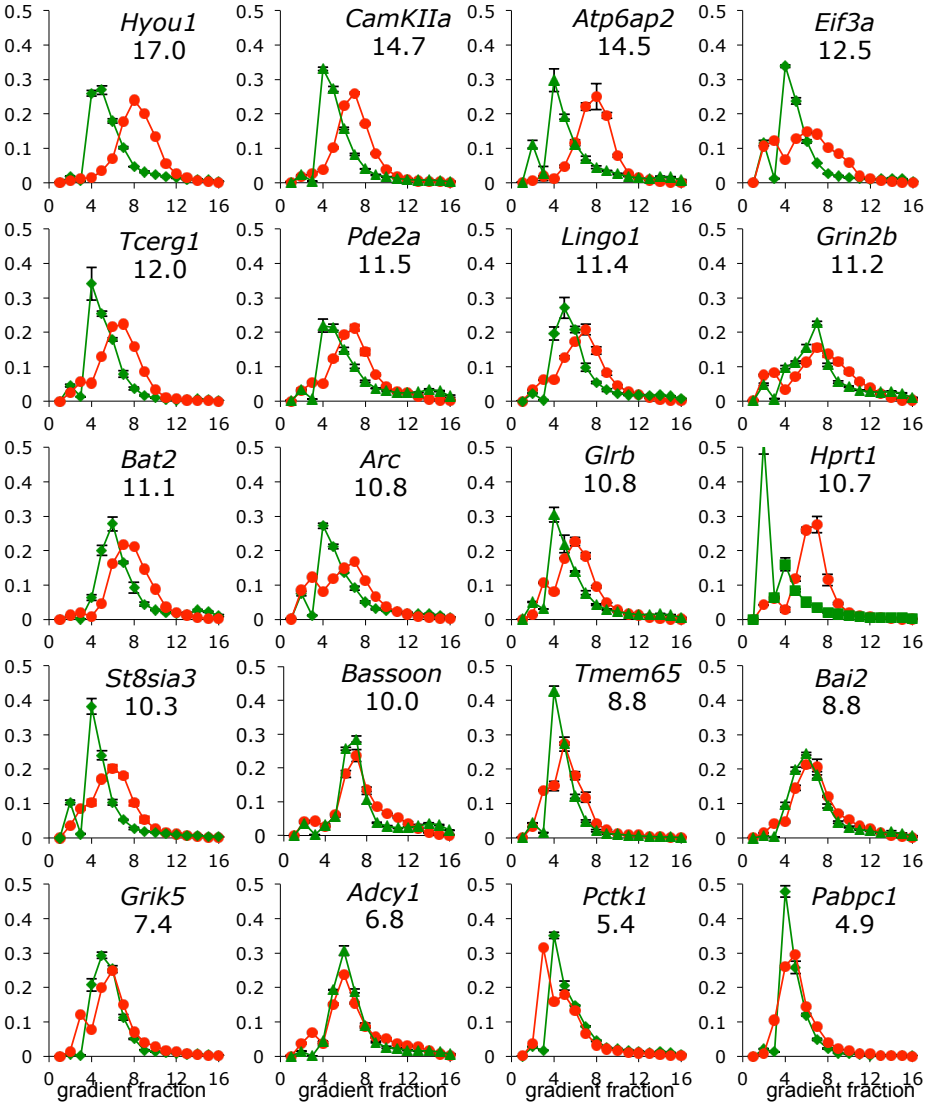
Hyou1
17.0
CamKIIa
14.7
Atp6ap2
14.5
Eif3a
12.5
Tcerg1
12.0
Pde2a
11.5
Lingo1
11.4
Grin2b
11.2
Bat2
11.1
Arc
10.8
Glrb
10.8
Hprt1
10.7
St8sia3
10.3
Bassoon
10.0
Tmem65
8.8
Bai2
8.8
Grik5
7.4
Adcy1
6.8
Pctk1
5.4
Pabpc1
4.9
0.5
0.4
0.3
0.2
0.1
0
0 4 8 12 16
gradient fraction

Figure 11. Immunoprecipitation of FMRP from mouse brain.

FMRP was immunoprecipitated from mouse brain using the FMRP monoclonal antibody 7G1. Treatment with 200nM kcRNA, RNAse A/T1 cocktail or 30mM EDTA markedly improved pulldown of FMRP compared to untreated lysate. The Western blot was probed with FMRP monoclonal antibody 2F5. These results suggest that FMRP's epitopes are masked *in vivo* by association with an RNA-containing complex, and that removal of FMRP from this complex facilitates immunoprecipitation.

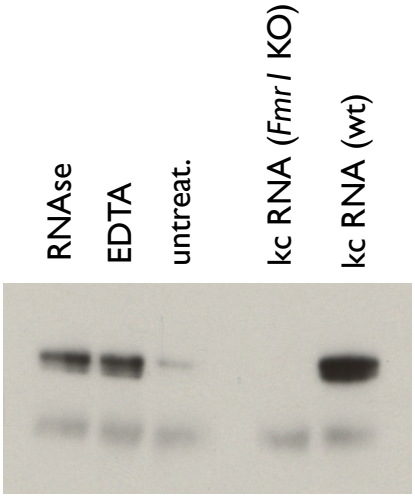

FMRP IP from brain

Figure 12. Electron micrographs of polyribosomes from mouse brain.
Polysomes purified on sucrose gradients were examined using uranyl acetate negative staining.

Top row: Steady-state polyribosomes treated with cycloheximide.

Middle row: Some intact polyribosomes remained in heavy fractions after puromycin runoff (puro), suggesting that they contain ribosomes not sensitive to puromycin.

Bottom row: Some polyribosomes remained in heavy fractions even after both puromycin runoff and micrococcal nuclease (MN) treatment, suggesting that remaining ribosomes are tightly packed in vivo, protecting underlying mRNA from nuclease digestion. Two different magnifications are shown.

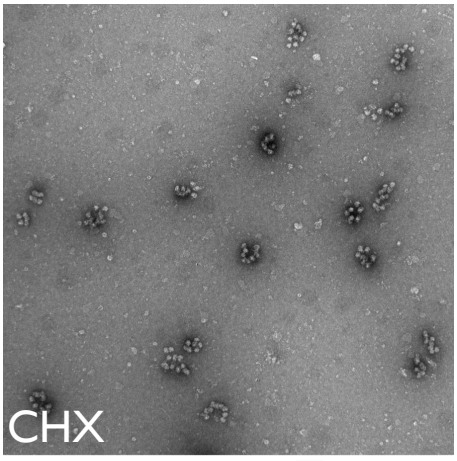
CHX
100 nm
Direct Mag: 20000x

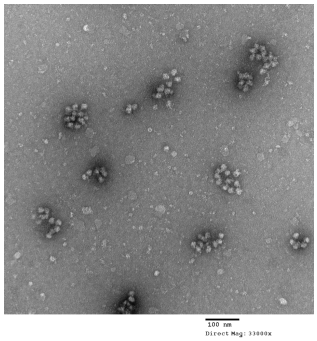
100 nm
Direct Mag: 33000x

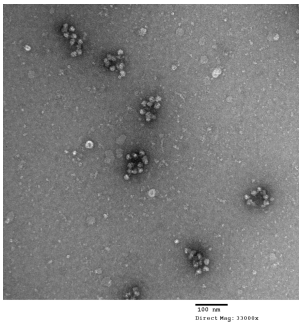
100 nm
Direct Mag: 33000x

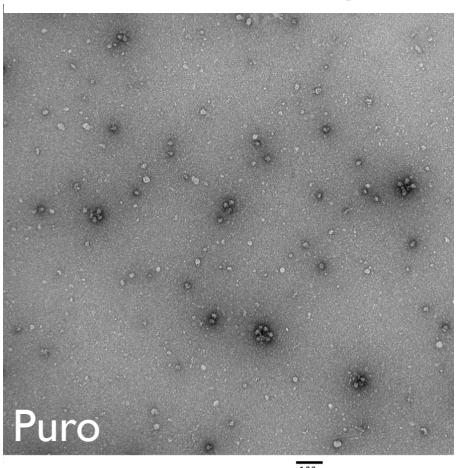
Puro
100 nm
Direct Mag: 20000x

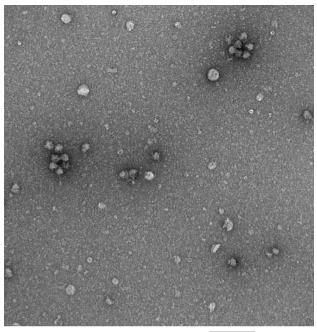
100 nm
Direct Mag: 33000x

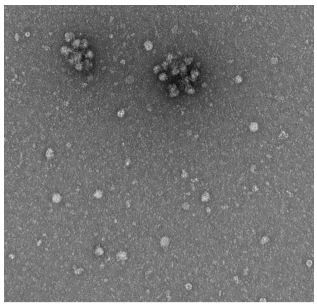
100 nm
Direct Mag: 33000x

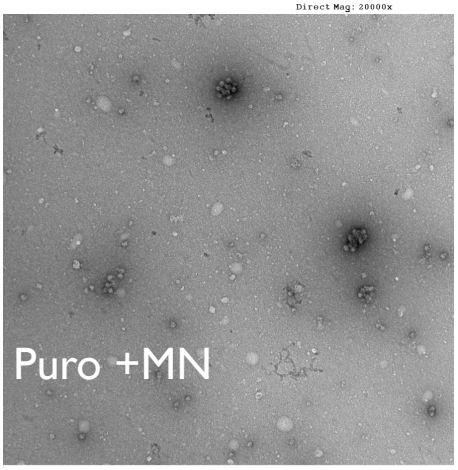
Puro +MN
100 nm
Direct Mag: 20000x

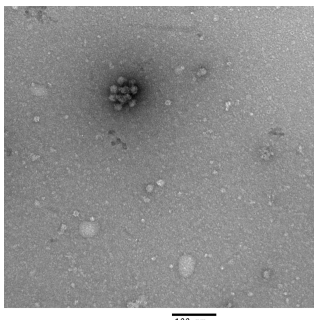
100 nm
Direct Mag: 33000x

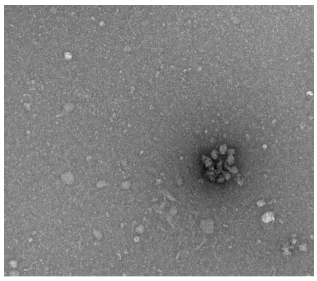
100 nm
Direct Mag: 33000x

Figure 13. Immunoelectron micrographs of polyribosomes containing EGFP-tagged ribosomal protein L10a.

Sucrose gradients were prepared from cerebellum of the Purkinje cell-specific *Pcp2*-promoter driven EGFP-tagged rpL10a BAC transgenic mice (Heiman et al 2008), and polyribosome fractions were processed for IEM using an EGFP antibody and a secondary antibody labeled with 6nM gold. Specific staining on clustered structures is indicated (white arrows); nearby unlabeled polysomes are also shown. Only ~1% of polysomes showed labeling, consistent with the use of whole cerebellum for analysis, yet most that were labeled had multiple labels, consistent with polysomes from Purkinje cells carrying multiple EGFP-tagged ribosomes.

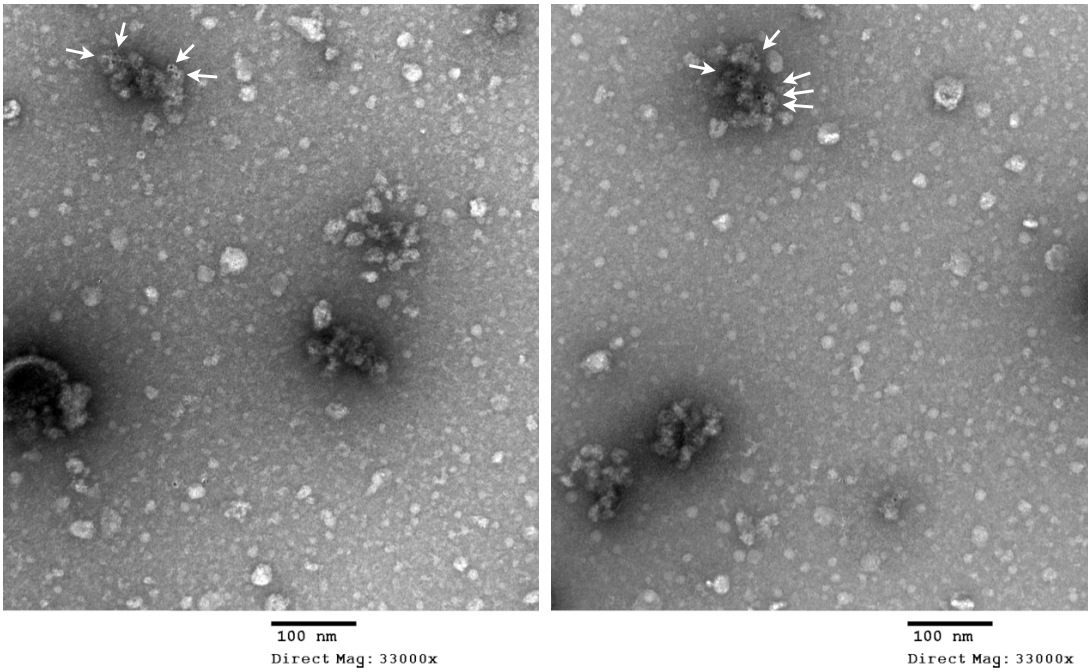
100 nm
Direct Mag: 33000x
100 nm
Direct Mag: 33000x

Figure 14. Immunoelectron micrographs of EGFP-FMRP associated with stalled polyribosomal complexes after puromycin run-off *in vivo* in transfected 293T cells.

A) Constructs expressing N-terminally tagged EGFP-FMRP or EGFP alone were transiently transfected into 293T cells. Cells were treated with puromycin for 1 hour to induce ribosome runoff and then treated with cycloheximide (CHX) to stabilize remaining polysomes. As a control, some cells were treated only with CHX. A Western blot for EGFP shows each protein was expressed at sufficient levels and was of expected size.

B) Cell lysates were then fractionated over sucrose gradients, and fractions from EGFP-FMRP transfected cells were analyzed by Western blot. EGFP-FMRP associated with normal distribution on polysomes, compared with the endogenous form of FMRP (which migrates at 75kD). Puromycin runoff caused both EGFP-FMRP and endogenous FMRP to shift to somewhat lighter gradient fractions, but in both cases FMRP remained associated with polysomes. A sample of sucrose gradient fraction #10 was processed for immunoelectron microscopy (IEM) using an EGFP antibody and a secondary antibody labeled with 12nM gold (see images on following page).

C) Quantification of IEM data (from the following page). 7.2% of polyribosomes were labeled in the presence of EGFP-FMRP in steady state (CHX), while 13.5% of residual polyribosomes were labeled in the presence of EGFP-FMRP after ribosome runoff (puro), indicating an enrichment of stalled polysomes carrying FMRP after runoff of translating polysomes. Only 0.02% of polyribosomes from EGFP-expressing cells were associated with gold, indicating specificity of the labeling. 500 polysomes were counted for each treatment.

D) (Following page) EGFP-FMRP was detected on polysomes by IEM in both steady state (CHX; top panel) and following puromycin runoff (puro; bottom panel). Gold particles are indicated by white arrows.

A

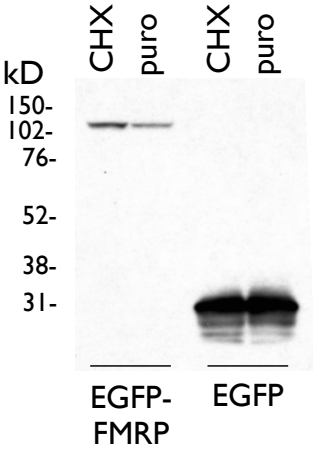

B

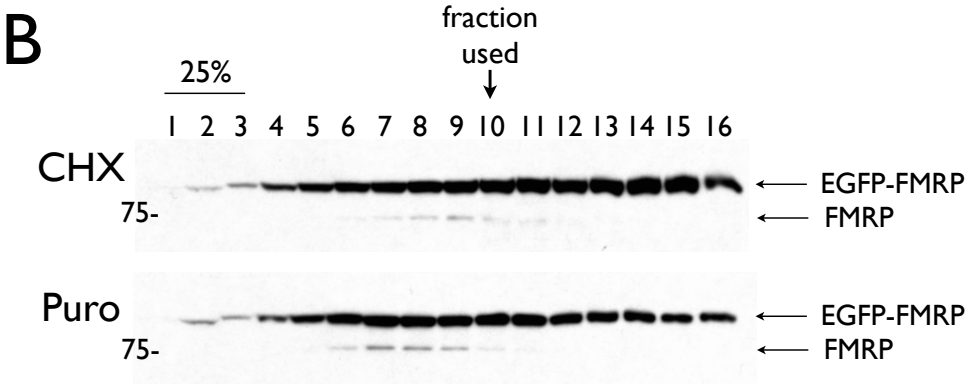

C

Golds per polysome:

		1	2	3+
CHX	EGFP-FMRP	20	8	8
	EGFP	0	0	0
Puro	EGFP-FMRP	32	21	14
	EGFP	1	0	0

n=500

D

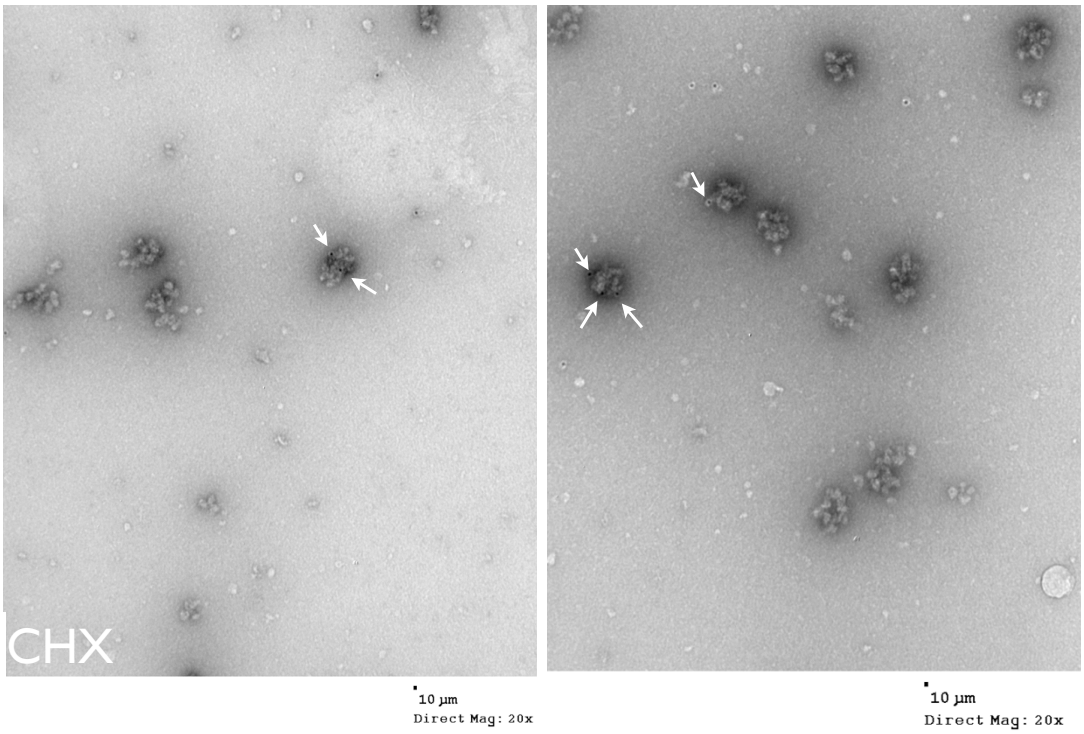
CHX
10 µm
Direct Mag: 20x
10 µm
Direct Mag: 20x
Puro
10 µm
Direct Mag: 20x
10 µm
Direct Mag: 20x

Chapter IV. Efforts to identify origin of FMRP target specificity

Introduction:

Data from the previous chapters suggest that FMRP is associated with a specific subset of mRNAs. There is little correlation between number of FMRP polysome CLIP tags per gene and transcript abundance on polysomes as measured by exon array, indicating that FMRP selectively binds a subset of translated mRNAs (Darnell et al., 2011). Although such a result could arise if the polysomal mRNA pool included abundant glial-specific mRNAs to which FMRP does not bind, there is also no correlation between number of tags per gene in FMRP polysome CLIP and abundance of neuronal mRNAs, supporting the view that FMRP selectively interacts with particular transcripts. However, the polysome CLIP data also show that that FMRP associates with target mRNAs relatively evenly along the full length coding sequence without evident sites of specific binding, leading one to wonder how specific association with target mRNAs arises. CLIP experiments on other RBPs such as Nova, Argonaute and Fox2 have revealed discrete "peaks" or clusters of tags, indicating specific binding of proteins at these sites (Chi et al., 2009), (Licatalosi et al., 2008), (Yeo et al., 2009). In the case of Nova and Fox2, binding sites identified by CLIP contain sequence motifs that, in combination with other data, can be used to greatly increase the confidence of binding site identification (Zhang et al., 2010). In this light, the broad distribution of tags observed in FMRP polysome CLIP is somewhat unusual. Interestingly, the FMRP tag distribution profile appears similar to that observed in ribosome profiling experiments (Ingolia et al., 2011). Together with the finding that FMRP induces ribosome stalling, these observations support the hypothesis that FMRP may associate directly with ribosomes, and that the coding sequence tags observed in CLIP may arise due to transient contacts between FMRP and the mRNA as FMRP travels along with the ribosome during elongation.

In such an FMRP-ribosome association model, specificity for the mRNA could arise prior to the onset of elongation. One might imagine several scenarios in which this could occur. For example, FMRP could directly bind mRNA at specific sites in 5'UTRs and then be packaged into the ribosome as the preinitiation complex matures. Tags from this

sort of interaction would be represented in the polysome CLIP data, since mature mRNAs loaded with multiple ribosomes still receive newly initiating ribosomes. However, if direct FMRP binding to mRNA occurs only briefly before FMRP is picked up by the scanning 60S preinitiation complex, then there might be only a few tags generated from direct mRNA binding compared to those that reflect 60S scanning. FMRP could also interact with the preinitiation complex via binding to 3'UTRs. This type of looped-polysome model has precedent; for example, the protein CBEP binds cytoplasmic polyadenylation elements in 3'UTRs and inhibits translation via interaction with Maskin, an eIF4E binding protein (Stebbins-Boaz et al., 1999).

Initial specific contact with the mRNA could also be mediated through another protein or a small RNA. If selectivity were mediated via a protein-protein interaction, CLIP tags might not be generated because FMRP would be less likely to be positioned within bond length of the mRNA. While FMRP has been reported to interact with a number of proteins (Bardoni et al., 1999), (Bardoni et al., 2003), (Schenck et al., 2001), (Davidovic et al., 2006), the only proteins that are solidly established as interacting partners are its paralogs FXR1P and FXR2P (Zhang et al., 1995), (Siomi et al., 1996), (Tamanini et al., 1999). Furthermore, a point mutation in the KH2 domain causes FXS phenotypes in mouse and human and completely abrogates the polysome association of FMRP (Zang et al., 2009), (Darnell et al., 2005b), (De Boulle et al., 1993), indicating the primacy of FMRP-RNA interaction in FMRP function. Nonetheless, it remains a possibility that FMRP could be initially recruited to specific mRNAs via a protein-protein interaction, and is thereafter associated with ribosomes or mRNA in a KH2 domain-dependent manner. In the case of mediation via a small RNA, a model has been proposed in which FMRP inhibits translation via the small RNA BC1 (Zalfa et al., 2003), (Zalfa et al., 2005), (Napoli et al., 2008). Wang et al found BC1 bound to eIF4A and PABP and proposed a mechanism of nonspecific control whereby BC1 could inhibit translation of most/all mRNAs during initiation by inhibiting assembly of eIF4F (Wang et al., 2005). However, Zalfa et al proposed that BC1 mediates association between FMRP and its targets via binding directly to the 3'UTRs of particular mRNAs (Zalfa et al., 2003), (Zalfa et al., 2005). Later, this same group proposed a new model in which BC1

mediates interaction between FMRP and a newly discovered 4EBP, Cyfip1, instead of binding mRNA directly (Napoli et al., 2008). In this model, FMRP is predicted to repress initiation by promoting Cyfip1 binding to eIF4E, although Cyfip1 and eIF4E remain associated in the *Fmr1* KO. However, while this group claimed that FMRP bound BC1 under conditions of 750mM salt in an electromobility shift assay (Zalfa et al., 2003), others could only recapitulate the binding under conditions of 100mM salt and found it was completely abrogated by nonspecific competitor RNA, indicating the purported binding underlying the entire mechanism was weak and nonspecific (Iacoangeli et al., 2008). Furthermore, the assumption that translation is stalled at initation was based on a moderate reduction in polysome association of target mRNAs in the presence of FMRP and the fact that FMRP was observed only in initiation complexes and not on polysomes (Zalfa et al., 2003). We and others find that the vast majority of FMRP is in fact on polysomes under similar buffer conditions (Stefani et al., 2004), (Khandjian et al., 2004), (Davidovic et al., 2005). This calls into question the findings of shifted polysome association of target mRNAs, further weakening the premise of the BC1 model. However, even though a role for BC1 in FMRP function seems doubtful, it is still conceivable that FMRP could select its targets using small RNAs as guides.

Another possibility is that a subset of ribosomal subunits carry FMRP prior to mRNA docking, and somehow these ribosomes engage a particular set of transcripts due to some unrecognized feature shared by the target mRNAs. One possibility is simply that FMRP is loaded onto ribosomes locally, perhaps in response to neuronal activity, and any transcripts in the vicinity of FMRP-carrying ribosomes become targets. Alternatively, target transcripts could somehow actively recruit an FMRP-carrying subclass of ribosomes during translation initiation, for example via a specialized initiation factor. Interestingly, it was recently shown that mutation of ribosomal protein L38 resulted in decreased translation of a specific set of Hox genes in the mouse embryo without a change in global protein synthesis (Kondrashov et al., 2011). Rpl38 sits near an evolutionarily recent, conformationally dynamic expansion segment of rRNA, and the authors suggest that Rpl38 binding near this region could alter ribosome conformation and thus somehow affect the ability of ribosomes to initiate on particular mRNAs.

Finally, we must consider the possibility that the coding sequence tags do not arise from FMRP moving along transcripts during elongation, but rather reflect association of stationary FMRP at random intervals along the coding sequence. Since CLIP data represent population averages, the fact that mapped tags appear to coat the coding sequence does not mean that FMRP must coat the coding sequence of individual transcripts. However, the fact that treatment of polysomes with micrococcal nuclease releases very little FMRP suggests that the majority of FMRP must associate with mRNAs in some sort of RNAse-protected protein complex large enough to pellet with ribosomes (Darnell et al., 2011). In theory, FMRP could extensively multimerize along transcripts to produce this effect. However, data presented in this thesis show that removing the FXRs from polysomes by kcRNA treatment after puromycin runoff did not change the gradient migration of FMRP target transcripts, suggesting that multimerization extensive enough to protect a fragment that cosediments with ribosomes is unlikely. Nonetheless, this does not rule out the possibility that FMRP could exist on polysomes as part of some other large, nonribosomal multiprotein complex. This scenario would still require some kind of mechanism to generate specificity for target mRNAs. One theoretical possibility is that FMRP could associate with a transcription factor (thus generating specificity for a subset of transcripts) and then be deposited along premRNAs during transcription. An example of an RBP that is deposited in the nucleus but still associates with polysomes is Hrp36, which associates with premRNAs during transcription and is then exported to cytoplasm, where it associates with polysomes along the length of the mRNA coding sequence (Visa et al., 1996). Or, FMRP could associate with all transcripts in a particular location; for example, FMRP associated with the endoplasmic reticulum could in theory make contact with mRNAs as they are docked at translocons. Importantly, models in which FMRP associates directly with coding sequence could still be consistent with a stalling effect on ribosomes.

Results:

FMRP HITS-CLIP in total mouse brain and purified brain nuclei

The above scenarios suggest various ways in which FMRP could specifically associate with a subset of mRNAs. We hypothesized that specific FMRP binding sites could exist on RNA species not abundant or not included in the pool used for polysome CLIP; for example, pre-mRNAs, noncoding RNAs or transcripts undergoing a pioneer round of initiation. To look for possible FMRP associations with RNAs other than mature mRNAs, a renewed attempt was made to perform FMRP HITS-CLIP in whole cell lysate. Whole brains from a P14 WT and *Fmr1* KO littermate pair were chopped and immediately crosslinked before homogenization. Homogenates were processed according to the standard CLIP protocol (see Methods) using the polyclonal antibody 17722. CLIP tag DNA was recovered from the wt sample after 26 cycles of PCR, while no signal was observed in the KO sample until 32 cycles (**Figure 15**). Illumina sequencing of the wt products resulted in 497,050 unique mappable tags. 1740 mRNAs were identified that had at least 50 exonic CLIP tags (**Table 2***)*. Importantly, target specificity was still observed: of 16286 mRNAs with measurable neuronal expression values (Cahoy et al., 2008), no correlation was found with number of exonic CLIP tags per gene ($R^2 = 0.03$) (**Figure 16).**

Of the 497,050 unique tags, 84.6% mapped to exonic sequences (either coding sequence or UTRs) (**Figure 17**). Only 5.6% mapped to introns, and of these, most corresponded either to ncRNA sequences within introns (eg rRNA or tRNA genes) or to misannotated exons (eg, *Ank2* and *Ank3* each have a short isoform with an apparent misannotation of the first exon). The remaining intronic tags were sparsely distributed with no discernable pattern in distribution. The number of exonic tags per gene observed in whole brain CLIP correlated highly with that observed in the polysome CLIP experiments ($R^2 = 0.87$) (**Figure 16**). In addition, tag distributions on exonic sequence appeared similar to that previously documented for polysome CLIP (**Figure 18** and (Darnell et al., 2011)). Together, these observations suggest that the majority of FMRP:RNA interactions involve mature mRNA.

Under our lab's standard tag mapping pipeline, CLIP tags are not mapped if they match more than one genomic locus. However, many ncRNAs exist in multiple copies in the genome; for example, rRNA genes are present in hundreds of copies on multiple chromosomes. In order to more carefully analyze whether FMRP significantly interacts with ncRNA, the whole brain CLIP data was remapped using the alignment program Bowtie, using parameters under which any given tag was allowed to map to up to 100 locations in the genome. Although some ncRNAs exist in more than 100 copies, this ceiling was selected due to limits in computational power. To reduce noise, single tags not overlapping with another tag were discarded. When the data were reanalyzed in this manner, the percentage of deep intergenic tags in clusters of 2+ rose from 3.7% to 29.3% (**Figure 17**). Of the deep intergenic tag clusters, 32% were in unannotated regions, while 64.6% were repetitive or low complexity regions such as LINEs, SINEs, LTRs, simple repeats, or satellite DNA. The remaining 3.4% of clusters mapped to ncRNAs of potential interest, such as rRNA (222 clusters), tRNA (175 clusters), snRNA (166 clusters), scRNA (120 clusters), srpRNA (7 clusters), or other ncRNAs (19 clusters). In general, the number of tags in individual clusters was low, with a maximum of about 200 tags per cluster and most clusters containing fewer than 100 tags (with the exception of rRNAs, which had high tag numbers in agreement with the extremely high representation of rRNAs on polysomes). Two non-rRNA clusters stood out as having relatively high numbers of tags. The first, with 216 tags, mapped to Y RNA, a ncRNA of poorly characterized function that exists as an RNP with the Ro autoantigen and may play a role in degradation of misfolded RNAs (Fuchs et al., 2006). Human Y RNAs are highly abundant, within an order of magnitude of 5S rRNA abundance (Christov et al., 2006). The second example, with clusters of 118, 118 and 138 tags on three different chromosomes, mapped to 7SK RNA, another highly abundant ncRNA with a role in transcription (Diribarne and Bensaude, 2009). Tellingly, nearly all HITS-CLIP studies performed in our lab show high numbers of tags at both of these loci, including HITS-CLIP experiments for Nova, Hu, Ago, brPTB, Mbn13 and Fus. The fact that several RBPs of disparate functions have tags on highly abundant ncRNAs suggests that these tags may represent nonspecific "sampling" protein:RNA interaction events. Overall, at

this time we cannot show that FMRP interacts with ncRNAs in a functionally significant manner.

Although FMRP has a predominantly cytoplasmic localization in steady state, it contains both an NLS and an NES and can be observed in the nucleus if the NES is inactivated by point mutation (Fridell et al., 1996) or deleted by truncation construct (Eberhart et al., 1996). This suggests that FMRP could bind pre-mRNAs and remain associated with them during translation. Although few intronic tags were observed in the whole brain CLIP dataset, this does not rule out the possibility that FMRP has discrete binding sites on pre-mRNAs, either in introns or in exons, since half-lives of pre-mRNAs are on the order of minutes (Rabani et al., 2011) while half lives of most mRNAs are on the order of hours (Sharova et al., 2009). To investigate whether the specificity of FMRP for its mRNA targets arises at the pre-mRNA level, we enriched the pre-mRNA population by performing CLIP on purified brain nuclei.

In a first attempt, brains from mice in the first postnatal week were crosslinked and homogenized in low salt buffer containing 0.32M sucrose. After homogenization, lysate was brought to either 1% NP-40 or 1% Triton-X100 to solubilize the outer nuclear envelope, which is continuous with the polysome-containing rough ER, without lysing the nuclei. Lysates were then spun over a column of 1.8M sucrose to pellet the nuclei and strip off any remaining rough ER fragments. Nuclei appeared as a small, clear flat pellet. Crosslinking reduced the size of the nuclear pellet by approximately half, indicating that this process lysed some nuclei. Western blot analysis of resuspended pellets and total lysate showed that FMRP was present in both fractions, while the neuronal nuclear marker NeuN (Fox3) was highly enriched in the nuclear pellet and the cytosolic marker GAPDH was entirely absent from the pellet (**Figure 19**). Importantly, the integral membrane ER protein calnexin was also entirely absent from the nuclear pellet, indicating successful removal of ER membranes from nuclei. Resuspended pellets were DNAse treated and processed according to the standard CLIP protocol using the 17722 FMRP antibody. The wash series after IP was amended to include a second high salt and omit the low salt washes, in an attempt to reduce clumping of beads (thought to

be due to hydrophilic interactions between DNA and Dynabeads). Unfortunately, although FMRP was efficiently depleted in the IP, no FMRP-specific signal was seen after separating products by urea-PAGE, indicating a high level of background in the IPs (**Figure 20**). Several attempts to reduce background in *Fmr1* KO samples were unsuccessful, including increasing the time of a preclearing step, increasing stringency of washes, and on-bead DNAse treatment after IP.

Because other members of the lab had successfully performed CLIP on nuclei prepared by simple low speed pelleting, we decided to try this approach. Although nuclei prepared according to this method are not are pure as those fractionated through sucrose, a high level of enrichment for pre-mRNAs compared to whole lysate should still be achieved. Nuclear lysate was prepared in a similar manner as above, homogenizing in the same buffer and dissolving ER membranes in 0.8% NP-40. Lysates were spun at 2000xg for 10 minutes and pellets were gently washed twice in the homogenization buffer by stirring with a pipette tip. Bradford assays indicated the final pellet contained about 8% of total cellular protein. Western analysis showed that GAPDH was present only in the cytosolic fraction, while histones, hnRNP C1/C2 and NeuN were present only in the nuclear fraction (**Figure 21**). Again, calnexin was only present in the cytosolic fraction, indicating dissolution of ER membranes. As expected, both the cytoplasmic and nuclear fractions contained ribosomes. FMRP was also present in both fractions, with approximately 11% of total cellular FMRP in the nuclear fraction (in agreement with previous observations by Jen Darnell in our lab). In a pilot CLIP experiment, the 17722 antibody unexpectedly recognized a nonspecific band of the same molecular weight as FMRP which was not seen in whole brain or polysome CLIP experiments (**Figure 22**). However, a different FMRP antibody, 27455, specifically recognized FMRP in nuclear lysates (**Figure 22**). Comparison of FMRP pulldown by 17722 and 27455 found that 27455 also IPed FMRP much more strongly. Therefore, nuclear FMRP CLIP was repeated using the 27455 antibody (**Figure 23**). Encouragingly, separation of PCR products revealed that the nonspecific signal from the *Fmr1* KO control was lighter than the wt sample and had a more banded (rather than smeared) distribution. Since this type of banded signal is often the result of linker-linker ligation reactions that can predominate

in the absence of CLIP tags, products from this sample were TOPO cloned and sequenced. Of the 17 sequences obtained, 7 were indeed primer artifacts and 4 mapped to repetitive regions. Although the remaining 5 tags did map to genic regions, it is expected that IPs performed in the absence of antigen will be more susceptible to nonspecific antibody interactions. The wt sample was then submitted for Illumina sequencing.

102,698 unique mappable tags were sequenced in the nuclear CLIP experiment. More intronic tags were observed in nuclear CLIP (17.9% of total tags) than in whole brain CLIP (5.6% of total tags) (**Figure 24**). Nonetheless, overall tag distributions on individual transcripts were highly similar to those observed for whole brain CLIP (**Figure 25)** and the number of exonic tags per gene observed in nuclear CLIP was well correlated with that observed in whole brain CLIP (R^2=0.68) **(Figure 26).** Of the 18,430 intronic tags, 63.5% did not overlap with any other tag and were discarded to reduce noise. Of the remaining 6735 tags, 27% mapped to repetitive/low complexity regions and were not examined further. 2.5% mapped to rRNA, while 1.6% mapped to other ncRNAs, mainly snRNAs. 7.1% mapped to large misannotated exons in Ank2 and Ank3; these were also discarded. Of the clusters not in the above categories, 55% mapped to introns in genes with Entrez ID numbers. The 3734 intronic tags mapped to 1023 genes, and 524 were in clusters containing at least 5 tags (80 clusters, with the top cluster containing 20 tags). The number of intronic tags per gene did not correlate with mRNA abundance in neurons from mice of similar age (R^2=0.004, Cahoy 2008) or to the number of exonic tags per gene as measured in the same experiment (R^2=0.0005) (**Figure 26**). The clusters did not appear to be distributed in any discernable pattern. Since it did not appear that FMRP associated with intronic sequence in any consistent manner, the increased number of intronic tags in the nuclear CLIP experiment may reflect higher nonspecific background in the IP resulting from enrichment of pre-mRNAs in nuclear lysate, and most exonic tags sequenced in this experiment may reflect presence of perinuclear polysomes.

FMRP HITS-CLIP after seizure:

Thus far, we have only looked for specific binding sites for FMRP in the steady state. However, gene expression in neurons can be highly dynamic in non-resting states, with rapid changes in transcription and translation underwriting changes in learning and memory. There is a broad assumption that FMRP is likely to respond to synaptic activity, but evidence directly linking synaptic activity to differential translation of target mRNAs in an FMRP-dependent manner is limited. The best examples may be a report that mGluR activity results in increased translation of two major FMRP targets, Map1B and CamKIIa, in wt hippocampal slices, while synthesis of these proteins is constitutively elevated in *Fmr1* KO slices, consistent with chronic overtranslation of target mRNAs in the absence of FMRP (Hou et al., 2006), and a similar recent report for Arc (Niere et al., 2012). In addition, a number of studies have suggested that FMRP levels and/or phosphorylation state may respond to synaptic activity induced by a variety of stimuli, including pharmacological activation of mGluR and NMDA receptors, whisker stimulation, or exposure to light (Narayanan et al., 2007), (Zhao et al., 2011), (Weiler et al., 1997), (Nalavadi et al., 2012), (Lee et al., 2011), (Todd et al., 2003), (Gabel et al., 2004). We hypothesized that if FMRP binds specific sites on target mRNAs after transcription or in early stages of translation, CLIP tags mapping to these sites might be enriched after a synchronized transcriptional burst, for example on early immediate genes (IEGs) that are induced by seizure, because this situation would temporarily enrich the pre-mRNA populations of these genes. In addition, such an experiment would offer the first glimpse of how FMRP association with target mRNAs might be affected by changes in synaptic activity, and whether FMRP plays a role in regulating gene expression in response to synaptic activity.

Brief seizure activity induced by a single maximal electroconvulsive shock (MECS) is an established model for induction of immediate early genes (IEGs) (Cole et al., 1990), (Lyford et al., 1995), (Wallace et al., 1998). Mice exposed to a current via ear-clip electrodes experience a short tonic-clonic seizure that results in rapid transcriptional upregulation of a number of genes including Arc, c-Fos, zif268/Egr1 and c-Jun. Many of these IEGs are transcription factors, which initiate cascades of further gene expression.

Others, such as Arc, have direct roles at the synapse important for synaptic plasticity. Collectively, expression of IEGs is a central element in the dynamic response of neurons to stimuli. Importantly, many of the IEGs identified using seizure models have subsequently been shown to be similarly upregulated in response to more natural stimuli, such as spatial learning (Marrone et al., 2008). In particular, two IEGs with low numbers of FMRP CLIP tags in the steady state drew our attention as possible important targets.

The first, Arc, stood out among other IEGs in early studies because its mRNA is transported to dendrites after induction (Wallace et al., 1998). Arc plays a critical role in consolidation of memory, as *Arc* KO mice exhibit deficits in long term memory yet have normal short term memory (Plath et al., 2006). *Arc* KO mice also have defects in long-term synaptic plasticity (both LTP and LTD) at Schaffer collateral – CA1 synapses in the hippocampus, suggesting that abnormal plasticity at these synapses underlie the defects in memory consolidation. Arc is also essential for the expression of mGluR-LTD, a form of plasticity abnormally enhanced in *Fmr1* KO mice (Waung et al., 2008), (Park et al., 2008). While activation of mGluRs normally causes a rapid increase in Arc protein levels, the *Fmr1* KO was shown to have constitutively upregulated Arc levels that were not further increased upon stimulation (Niere et al., 2012). Interestingly, Arc expression is tightly controlled at both the mRNA and protein levels. *Arc* mRNA contains an intron within its 3'UTR, rendering it susceptible to exon junction complex-mediated decay after the pioneer round of transcription (Giorgi et al., 2007). Additionally, Arc protein is ubiquitinylated by the activity-regulated ubiquitin ligase Ube3a (Greer et al., 2010). Both of these mechanisms limit Arc levels after an initial short burst of expression. If Arc were a target of FMRP (which is difficult to assess under steady state conditions, when *Arc* mRNA levels are very low), release of FMRP-mediated translational inhibition could facilitate the rapid Arc translation observed at synapses after mGluR activition. Limiting derepression of FMRP to a short window could then confine translation of Arc to a short burst.

Another IEG, Homer1a, is of interest because it physically interacts with group I mGluRs (Brakeman et al., 1997). Homer proteins interact with one another through C-terminal

coiled-coil domains and are abundant PSD scaffolding proteins, interacting with Shanks and various receptors (Hayashi et al., 2009). Homer1a is the only isoform that is upregulated by synaptic activity, and it is the only isoform lacking coiled-coil domains (Xiao et al., 1998). Since mGluRs that bind Homer1a do not participate in scaffolding with long Homer isoforms, Homer1a was predicted to have a dominant negative effect on mGluR activity (Xiao et al., 1998). This was demonstrated by expression of either Homer1a or a point mutant of Homer1a incapable of binding mGluRs in neurons stimulated with DHPG. Expression of Homer1a disrupted mGluR-mediated inhibition of EPSCs, while expression of the point mutant did not (Kammermeier and Worley, 2007). Interestingly, Homer1a-mGluR interaction was increased in the *Fmr1* KO mouse, which suggests that Homer1a might be upregulated by FMRP loss-of-function (Ronesi et al., 2012).

To characterize FMRP association with target mRNAs after synaptic activity and look for potential specific binding sites that might be present under these conditions, we performed HITS-CLIP in mice subject to MECS compared to resting mice. Briefly, mice were exposed to a 25mA current for 1s via ear clips and allowed to recover in their home cages for different periods of time before sacrifice. To minimize stimulation due to transport from the animal facility, all mice were carried by hand to the lab and rested in a quiet space for at least several hours prior to the experiment. To confirm that the MECS protocol was successful, RNA was prepared from cortices and hippocampi from resting and MECS mice and *Arc* mRNA levels were analyzed by QPCR. As expected, *Arc* levels were increased several fold by 30 minutes in both brain regions (**Table 3**). Mice in the third postnatal week were stimulated by MECS and sacrificed 5 min, 15 min or 30 min after seizure, with resting controls. This shorter timepoints were chosen to maximize the chances of catching mRNAs immediately after transcription or during the pioneer round of translation, while the longer timepoint reflects a point of more substantial *Arc* upregulation, as observed by QPCR and reported in the literature (Guzowski et al., 1999), (Lyford et al., 1995). Cortices plus hippocampi were rapidly dissected under ice-cold buffer, chopped and crosslinked. Tissues were then homogenized and processed for CLIP using the standard whole brain protocol (**Figure 27**). Although good results were

obtained for all four samples, only the resting and 15 minute samples were submitted for Illumina sequencing, as a cost-saving measure given the status as a pilot experiment.

Similar numbers of total unique tags were mapped for resting and MECS samples (1,105,165 tags for resting and 820,939 tags for MECS). The tag ratio (resting/MECS) was calculated for each gene, normalized to the total number of tags sequenced in each sample to control for differences in sequencing depth. Of 4949 mRNAs with a total of at least 50 tags between the two samples, 117 had at least a 50% increase in tag ratio (indicating more tags in the MECS sample), while only 18 had more than a 50% decrease in tag ratio (**Table 4**). The maximal tag ratio observed in this set of mRNAs was 7.2. Although we did not perform RNA Seq due to cost considerations for a pilot experiment, it is likely that at some level, increases or decreases in the number of FMRP CLIP tags reflect changes in mRNA abundance due to transcriptional regulation. In keeping with this possibility, GO analysis of the 117 mRNAs with increased tags after MECS showed enrichment for categories including PolII transcription (biologic process), transcription factor complex (cellular component) and DNA binding (molecular function), as well as an enrichment for proteins containing leucine zipper domains (UniProt sequence feature) (**Table 5**). Overall, this is consistent with upregulation of transcription factors (especially leucine zipper transcription factors, such as c-Fos and c-Jun) in response to MECS and is consistent with the literature on IEGs. We observed at least a 2X increase in tags on three canonical IEGs: c-Fos, zif268/Egr1 and c-Jun, while Arc had a 1.5X increase in tags (**Table 4**). Two possible models suggest themselves in this situation. Given the extensive literature on IEGs, it is safe to assume that at least some of these genes are transcriptionally upregulated after MECS. In one model, FMRP could reduce its association with these mRNAs, in order to facilitate their increased expression (ie, if a 2X increase in FMRP CLIP tags was observed but the mRNA in question increased 10X in abundance, what appeared to be increased FMRP association could in reality be the opposite). In an alternative model, FMRP could exert a counterbalance at the translational level on the expression of IEGs at the transcriptional level. In order to examine whether any mRNAs had decreased tags after MECS, the threshold for total tags between the two samples was lowered to 25. Of the 6791 mRNAs in this set, 102 had

more than a 50% decrease in tag ratio. GO analysis of these mRNAs showed enrichment in categories including monovalent cation transport (biologic process) and alkali metal ion binding (molecular function) (**Table 5**). A logical supposition would be that neurons might respond to high levels of synaptic activity by decreasing expression of genes involved in membrane excitability, which would be consistent with decreased numbers of FMRP CLIP tags on these transcripts.

The number of exonic tags per gene was extremely similar between the resting and MECS conditions (R^2=0.99) and tag distributions were also extremely similar, both overall and on individual transcripts (**Figures 28 and 29**). In particular, transcripts with increased numbers of tags after MECS did not show obvious changes in the distribution of the tags, suggesting that newly transcribed mRNAs were rapidly engaged in translation (**Figure 29**). We had guessed that Homer1a might have an increased number of FMRP tags after MECS, based on its status as an IEG with a dominant negative effect over mGluR scaffolding interactions with long Homer isoforms. In fact, we found no difference in the number or distribution of Homer1a tags after MECS. However, due to the markedly improved sequencing depth obtained in this experiment, we were able to observe a number tags mapping immediately downstream of the annotated ends of the 3'UTRs for both short and long Homer1 isoforms, suggesting unannotated 3'UTR extensions exist. Binding of an RBP to unannotated extensions of 3'UTRs has been previously described, (Licatalosi et al., 2008) and suggests that HITS-CLIP maps can inform gene annotation under certain circumstances. However, the lack of change in FMRP:Homer1a association 15 minutes after MECS does not rule out the possibility that FMRP may dynamically regulate Homer1a. Fluorescent in situ hybridization studies using riboprobes to 5' and 3' ends of the 50kB Homer1a gene have shown that although Homer1a transcription begins within minutes of MECS stimulus, transcription does not finish until nearly 30 minutes later (Vazdarjanova et al., 2002), (Bottai et al., 2002). Therefore, translation of newly transcribed Homer1a would not be expected to be observable at the 15 minute timepoint used in this pilot study.

Analysis of FMRP target mRNA distribution on cytosolic versus ER-associated polyribosomes

As discussed earlier in this chapter, specificity of FMRP for target mRNAs could in theory arise not due to specific binding sites on mRNAs but due to FMRP association with all mRNAs in some common location. For example, FMRP could associate with translocons on ER membranes and make contact with ER-associated mRNAs during translation. Interest in this possible mechanism was piqued by a report that ER-associated polysomes are less sensitive to puromycin than free polysomes (Unsworth et al., 2010). In theory, FMRP recruitment of polysomes to ER membranes could explain the observed reduction in puromycin sensitivity of targets discussed in the previous chapter. Although the canonical model dictates that ER-associated transcripts primarily encode secreted proteins or integral membrane proteins, there are reports of a number of ER-associated mRNAs encoding soluble proteins, which could be translated on the surface of the ER (Lerner et al., 2003), (Diehn et al., 2006), (Kraut-Cohen and Gerst, 2010). Thus, it could be plausible for mRNAs targeted by FMRP to associate with ER membranes even if they encode soluble proteins.

We purified free polysomes and membrane-associated polysomes from mouse brain and analyzed mRNAs associated with each fraction in order to assess the potential correlation between membrane association of polysomes and FMRP association with transcripts. Several methods of purification were tried. In the first attempt, brain from the third postnatal week was homogenized in low salt buffer containing 320mM sucrose using a Potter-Elvehjem homogenizer. Microsomes were pelleted from post-mitochondrial supernatants at 140,000xg for 2 hours. Western blot analysis for the ER integral membrane marker calnexin and the cytosolic marker GAPDH revealed that while this method successfully pelleted microsomes, the pellet was contaminated by substantial amounts of cytosolic protein (**Figure 30**). In a second attempt, lysate prepared similarly to above was layered between a 2.5M sucrose cushion and overlying 2.05M and 1.3M layers of sucrose. After spinning at 90,000xg for 5 hours, free polysomes remained below the 2.05M sucrose layer, while a portion of microsomes floated into the 1.3M sucrose layer as expected. However, Western blots showed much calnexin remained

stuck below the 2.05M sucrose layer, indicating substantial microsome contamination of free polysomes (**Figure 30**). In a third attempt, brain was homogenized in physiologic buffer containing 250mM sucrose. Post-mitochondrial supernatant was loaded over a discontinuous gradient consisting of 0.8M and 1.3M sucrose layers over a 2.5M sucrose cushion. After spinning at 140,000xg for 2.5hrs, free polysomes migrated in the 1.3M sucrose layer, while microsomes (which are less dense) were contained within the 0.8M sucrose layer and cytosol floated above the 0.8M sucrose layer (**Figure 31**). 150uL from fractions 3-9 was pooled as an "ER-associated" fraction, while 150uL from fractions 11-15 was pooled as a "free polysomes" fraction. The two pooled fractions were brought to equal volumes and Westerns were repeated to quantify the relative amount of FMRP in each pool. Although in the FMRP blot of the full gradient it appeared that FMRP was associated primarily with free polysome fractions, re-analysis of pooled fractions showed that FMRP was present in both pools in roughly equal amounts. Separate linkers were ligated to RNA from each pool and the two pools were sequenced in the same run by Illumina RNA-Seq.

24,905,839 mappable unique tags were sequenced from the ER-associated fraction, while 23,098,197 were sequenced from the free polysome fraction. RPKM (reads per kilobase of exon model per million mapped reads) was calculated for each gene, so that the ER-associated and free polysome fractions could be directly compared despite different sequencing depths. Results were filtered to eliminate very low abundance mRNAs with total RPKM values (the sum of RPKM in both pools) of less than 10. The fractional distribution of each mRNA in ER-associated and free polysome pools was calculated by dividing the RPKM value for each pool by the sum of the RPKMs for both pools. The maximal enrichment observed in the ER-associated fraction in this filtered set was 96% (for neurensin-1, a neuron-specific vesicular transmembrane protein (Kadota et al., 1997), indicating that it is possible to achieve near-complete separation of mRNAs into the ER-associated fraction (**Figure 32**). The maximal enrichment observed in the free polysome fraction was 85%. Assuming there are some mRNAs that are strictly cytosolic, this suggests there was about 15% crosscontamination from the free polysome fraction into the ER-associated fraction, consistent with free polysomes having to pass through the

ER-associated layer during the purification. Overall, most mRNAs had split distributions in both fractions: out of 8356 genes with total RPKM scores of at least 10, only 2126 were at least 70% enriched in one fraction (**Figure 32**). The ER-associated and free polysome pools were further characterized by gene ontology (GO) analysis. Out of 1644 mRNA enriched at least 70% in the ER-associated fraction, 856 coded for integral membrane proteins (**Table 6**). 106 were secreted proteins and 367 had a characterized signal peptide. Furthermore, the categories of N-linked glycosylation and disulfide bond formation, both protein maturation events associated with the ER, had 494 genes and 249 genes, respectively. Of the 481 mRNAs enriched at least 70% in the free polysome fraction, the most enriched categories were nucleoside binding (molecular function), cytosol (cellular compartment) and cellular carbohydrate catabolic process (biologic process), indicating a general role for these mRNAs in basic metabolic processes, in particular glycolysis (**Table 6**). Interestingly, 213 mRNAs from the free polysome fraction encoded acetylated proteins, a modification that can occur cotranslationally on N-terminal peptides and actively directs translation to the cytosolic compartment (Forte et al., 2011). Finally, we found the subset of mRNAs enriched at least 70% in the ER-associated fraction contained 71% of the mRNAs coding for ribosomal proteins (35 out of 49 genes with RPKM of at least 10), although only 20% of all mRNAs are ER-associated to this degree. Although ribosomal proteins do not exist within the ER, this result is consistent with the finding discussed above that proteins required in the nucleus (in this case, for ribosome biogenesis) may be translated nearby, eg on ER membranes.

Importantly, we found no correlation between the fraction of a transcript associated with the ER and the number of exonic CLIP tags on that transcript in whole brain CLIP (R^2=0.002) (**Figure 33**). There was also no correlation between the fraction of a transcript associated with the ER and the ribosome retention score (RRS) of the 39 mRNAs whose polysome profiles were assayed by QPCR after puromycin runoff (R^2=0.05) (**Figure 33**). Finally, outlier control genes (*Vldlr* and *Npepps*) from puromycin runoff assays were not preferentially ER-associated (68% and 32% ER association, respectively). Together, these analyses suggest that the FMRP-dependent reduction in

puromycin sensitivity observed in Chapter 2 is not caused by target mRNA association with ER membranes.

Although we hypothesized that FMRP tags in nuclear CLIP derive mainly from polysomes associated with perinuclear ER, there was no correlation between the fraction of a transcript associated with the ER and the number of exonic CLIP tags on that transcript in nuclear CLIP (R^2=0.001) (**Figure 33**). However, the method used to purify ER membranes by necessity cannot include detergent, so it is expected that ER membranes closest to the nucleus would be removed during nuclear pelleting. Since the nuclear envelope is a recognized subdomain of the ER with a distinct set of associated proteins (Voeltz et al., 2002), it would not be surprising if it also contained a distinct complement of mRNAs. Therefore, we would not necessarily expect nuclear CLIP results to be correlated with ER association measurements.

Discussion:

Data from previous chapters show that FMRP interacts with a specific set of mRNAs. Broadly, FMRP regulates many mRNAs involved with specialized aspects of neuronal function such as glutamateric signaling and small GTPase regulation, and in general is not a strong regulator of housekeeping genes. However, the question of how FMRP's specificity for certain mRNAs arises is currently one of the major unanswered questions in the field. HITS-CLIP studies performed on purified polysomes showed that FMRP interacts with the entire coding sequence of target mRNAs, in addition to a lesser degree of association with 5' and 3' UTRs (Darnell et al., 2011). Together with puromycin runoff assays showing decreased ribosome runoff from target transcripts in the presence of FMRP, a model was formulated in which FMRP stalls ribosomes during elongation. The data suggest, but do not show, that FMRP might associate directly with ribosomes, making transient contacts with the length of the mRNA coding sequence as ribosomes progress. However, certain aspects of the data are not explained by this model, in particular how FMRP associates with 3'UTRs, which are not in contact with the ribosome (Ingolia et al., 2011). Together with the fact that the ribosome stalling model does not explain the origin of FMRP's specificity for its targets, this suggests that there

are elements of FMRP function that we do not understand, some of which are perhaps unobservable in polysome HITS-CLIP, in which only mature, translating mRNAs are assayed. In an attempt to more fully understand FMRP's function and understand how target specificity arises, pilot HITS-CLIP studies were performed on whole cell lysate and purified nuclear lysate, in order to examine possible FMRP interactions with earlier stages in the lifecycle of mRNAs, such as pre-mRNAs and mature mRNAs undergoing a pioneer round of translation, as well as examine possible FMRP interactions with ncRNAs.

Results from the pilot whole brain CLIP experiment were highly correlated with those from earlier polysome CLIP studies, both in terms of the number CLIP tags per gene and the tag distributions. Importantly, the same degree of target specificity was also maintained, with no correlation between abundance of neuronal mRNAs and number of CLIP tags per gene. Very few intronic tags were observed, and we did not find convincing evidence of specific FMRP association with non-ribosomal ncRNAs. Together, these results suggest that the majority of functional FMRP:RNA interactions are indeed with translating polysomes. However, these results do not rule out the possibility that functionally important but transient FMRP interactions with mRNAs or pre-mRNAs might still occur, since transient interactions are more difficult to observe. Interestingly, FMRP is predicted to have a nuclear function, based on functional characterization of NLS and NES sequences (Willemsen et al., 1996), (Eberhart et al., 1996), (Fridell et al., 1996), (Kim et al., 2009). Immunogold electron microscopy experiments have detected FMRP in neuronal nuclei but not glial nuclei (FMRP is not expressed in glia) (Feng et al., 1997b) (Bakker et al., 2000). Although these reports are not entirely convincing due to sparse labeling and lack of *Fmr1* KO controls, if only a small fraction of FMRP exists in the nucleus in steady state, it might very well be difficult to observe. To explore the possibility that target specificity might arise during FMRP association with pre-mRNAs, which are typically very short-lived compared to mature mRNAs, a pilot FMRP HITS-CLIP study was performed on nuclear lysates from mouse brain. We hypothesized that CLIP tags arising from potential FMRP:pre-mRNA interactions would be likely to have a different distribution than tags arising from FMRP

interactions with mature mRNAs; for example, pre-mRNA tags might be present in introns or be enriched in UTRs. While we did observe more intronic tags in the nuclear CLIP experiment than in the whole brain CLIP experiment, there did not appear to be a relationship between the number of intronic tags and the number of exonic tags for a given gene, as might be expected if binding to intronic sequences gave rise to association with exonic sequences. Furthermore, intronic tags were not distributed in any noticeable pattern (eg, always in the first intron, etc). Therefore, it seems most likely that intronic tags represent nonspecific background due to high enrichment of intronic sequences in nuclear lysate.

Although the number of exonic tags per gene observed in nuclear CLIP was fairly well correlated with that observed in whole brain CLIP, several mRNAs were highly enriched for exonic tags in the nuclear CLIP experiment. Interestingly, most of these genes coded for cytoskeletal proteins, including ankyrins 2 and 3, spectrins a2, b2 and b3, AHNAK, macf1 and dystonin. The simplest explanation for why these mRNAs were enriched for tags in nuclear CLIP compared to whole brain CLIP would be that these mRNAs are enriched around the nucleus. The encoded proteins could be used locally, either inside the nuclei as part of the nuclear matrix, or as part of the cytoskeleton anchoring the nucleus within the cell. Since the targets enriched in this experiment are extremely large (on the order of hundreds of kD), they are expected to have limited diffusion capability and thus local translation is likely an efficient cellular strategy. Interestingly, proteomic studies have indeed identified spectrins, dystonin and AHNAK as components of the nuclear matrix or the nuclear envelope (Albrethsen et al., 2009), (Ocampo et al., 2005), (Kallappagoudar et al., 2010), (Young and Kothary, 2005), (Young et al., 2006), (Young and Kothary, 2008). The nuclear pore can accommodate molecules up to 39nm in diameter (Pante and Kann, 2002), which is large enough to export ribosomes and should easily accommodate proteins of this size. We also observed a strong enrichment in tags per gene for Akap6, which is a 254kD protein that anchors PKA to the nuclear membrane (Dodge-Kafka et al., 2008), further supporting the possibility that certain large proteins with nuclear roles may be locally translated near the nucleus. FMRP therefore appears to

regulate local translation in the perinuclear compartment in addition to its much-studied role in local translation in neurites.

An alternative possible origin for target specificity would be if FMRP associated with mRNAs with a common localization. For example, it has been shown that ER-associated mRNAs exhibit reduced puromycin sensitivity in runoff assays (Unsworth et al., 2010). If FMRP actively recruited transcripts to the ER, this could potentially account for the observed reduction in puromycin sensitivity in the absence of FMRP. Previous ER purifications from cells have found that ER-association is a broadly represented characteristic of many transcripts, including many that do not code for secreted or integral membrane proteins (Lerner et al., 2003), (Diehn et al., 2006). Together, these findings suggested it was at least conceivable that ER-association might be a general characteristic of FMRP target mRNAs, and that this might explain both the reduced sensitivity of target mRNAs to puromycin in runoff assays and how FMRP comes to be associated with a particular set mRNAs. To address this possibility, we purified populations of ER-associated and free polysomes from mouse brain and characterized them by high throughput sequencing. Western blot and GO analyses confirmed that our purification was successful, with very high enrichment for known ER-associated and cytoplasmic proteins and mRNAs in respective pools. Interestingly, we did not observe a bimodal separation of ER-associated and free mRNAs, as might be predicted if presence of a signal peptide were the sole arbitrator of ER localization. Rather, we found that the majority of mRNAs were represented in both pools, a finding consistent with a recent purification of membrane-associated versus free polysomes from 11 human cell lines, in which 40% of UniGene clusters were not enriched one fraction versus the other (using a cutoff of 74% enrichment) (Diehn et al., 2006). While no purification is ever absolute, there are *bona fide* biological reasons why a given mRNA might associate with both ER and free polysome pools. For example, alternative splice isoforms may differentially associate with the ER (Li et al., 2003). In addition, since mRNAs begin translation in the cytosol and canonically do not become membrane-associated until after membrane-targeting peptide sequences have been translated, the free polysome fraction should contain some mRNAs ultimately destined for ER association. Finally, it has been shown

in vitro that post-termination ribosomes can remain associated with the ER and initiate a new round of translation with mRNAs encoding soluble proteins (Seiser and Nicchitta, 2000), (Potter and Nicchitta, 2000). Importantly, we observed no correlation between the fraction of a transcript associated with the ER and the number of exonic CLIP tags on that transcript or the RRS score for that transcript, suggesting that mRNAs regulated by FMRP are not enriched on ER membranes. Unexpectedly, we did find a strong enrichment for mRNAs encoding ribosomal proteins in the ER pool, an example of mRNAs encoding cytosolic proteins associating with ER membranes. Local translation of mRNAs encoding ribosomal proteins on ER membranes would ensure production of ribosomal proteins near the nucleus, where they must be imported for ribosome biogenesis. Together with our previous finding that FMRP targeting of mRNAs encoding cytoskeletal proteins was enriched in the perinuclear compartment, these results hint that the ER might have a role in directing local translation of mRNAs whose protein products do not enter the canonical ER-Golgi pathway.

A second major outstanding question in the field concerns how FMRP function is linked to neuronal activity. Synaptic plasticity defects are among the best-characterized FXS phenotypes (Bear et al., 2004), (Volk et al., 2007), and FMRP regulates many genes involved with the expression of synaptic plasticity (Darnell et al., 2011). We hypothesized that FMRP:RNA associations might be altered in response to synaptic activity; for example, FMRP might increase or decrease its association with particular mRNAs in response to neuronal signaling. To explore the role of neuronal activity in FMRP function, HITS-CLIP was performed after induction of a single tonic-clonic seizure by MECS, a well-characterized paradigm that was instrumental in early study of IEGs (Yamagata et al., 1994b), (Yamagata et al., 1994a), (Lyford et al., 1995), (Wallace et al., 1998). We found that the number of FMRP CLIP tags increased on a number of mRNAs after MECS, including several canonical IEGs such as c-Fos, c-Jun, zif268/Egr1 and Arc. Interestingly, many of the mRNAs with the greatest increase in tags have functions with potential tie-ins to known FMRP biology. For example, gene with the greatest increase in FMRP tags after MECS, Ddx3, is a DEAD box RNA helicase which, at physiologic levels, appears to facilitate translation of mRNAs with long and/or

structured 5'UTRs, although it can inhibit translation when overexpressed (Tarn and Chang, 2009). In another example, three genes with at least 2X increase in tags have potential links to autism. One of these, Dhcr7, encodes a dihydrocholesterol reductase (catalyses final step in cholesterol synthesis), deficiency of which causes Smith-Lemli-Opitz syndrome, which is associated with autistic-like symptoms (Tierney et al., 2000), (Tierney et al., 2001). Two others, Uty and Jarid1d, are histone demethylases. Several histone demethylases were recently linked to autism in a whole-exome sequencing study (Iossifov et al., 2012), and a child with autism was found to have a missense mutation in *Jarid1c* (Adegbola et al., 2008). Two ubiquitin ligases, Ube2q2 (Melner et al., 2006) and Rnf180 (Ogawa et al., 2008), also had more than 2X increase in tags. The ubiquitin system has emerged as an important player in synaptic plasticity, underlying the importance of protein expression levels in neuronal function (for review see (Hegde, 2010). Finally, we observed a 4X increase in FMRP tags for a newly characterized IEG, Npas4. Unlike other activity-dependent transcription factors, Npas4 is only upregulated in response to calcium signaling, not neurotrophin or PKA signaling (Lin et al., 2008). Npas4 plays an important role in the balance of network excitability, upregulating expression of genes involved in the formation and/or maintenance of inhibitory synapses in response to excitatory stimulation of neurons in culture. Npas4 is upregulated in the visual cortex by exposure of dark-reared animals to light (Lin et al., 2008) and in hippocampal area CA3 by learning paradigms such as contextual fear conditioning (Ramamoorthi et al., 2011). In an elegant study, acute deletion of *Npas4* in CA3 by injection of virally expressed Cre-recombinase into the *Npas4* cKO mouse impaired contextual learning, while reintroduction of *Npas4* to CA3 in the global KO by similar strategy rescued the defect (Ramamoorthi et al., 2011). Overall, this pilot study points to a potential role for FMRP in the active modulation of translational bursts from acutely expressed genes important for neuronal function.

It should be noted that regulation of genes important for neuronal function and plasticity does not necessarily imply that FMRP mainly functions at synapses. While it is clear that some FMRP is indeed localized postsynaptically and does appear to locally regulate translation at these sites (Antar et al., 2005), (Muddashetty et al., 2007), the fact is that

most FMRP is somatic. Models of FMRP function often propose that somatic FMRP associates with translationally repressed mRNP particles and is trafficked out to dendrites in this state (Antar et al., 2005), (Dictenberg et al., 2008). There is good evidence that some FMRP targets such as Arc are indeed translationally repressed during dendritic transport (Steward et al., 1998b), so it is reasonable to suppose that FMRP might be cotransported in these cases, although FMRP appears not to be required for transport (Steward et al., 1998a). However, the facts that the vast majority of FMRP is somatic and at least 90% of FMRP is on heavy polysomes indicate that most somatic FMRP must be engaged on polysomes. This is consistent with our finding that FMRP is associated with the coding sequence of perinuclear polysomes and with our finding that the mRNAs of many FMRP targets (for example those encoding receptors, Bassoon and Piccolo) are associated with the ER, and suggests that FMRP could locally regulate translation of certain mRNAs in one cellular compartment (eg synapses) and of other mRNAs in another compartment (eg perinuclear sites). Alternatively, FMRP could play a role in neuron-wide regulation of translation. In addition to various forms of Hebbian plasticity that increase or decrease the strength of individual synapses in response to local signaling, neurons must undergo cell-wide adjustment of excitability to maintain synaptic strengths within a physiologically appropriate dynamic range, a form of homeostatic plasticity called synaptic scaling (Turrigiano, 2008). FMRP could contribute to synaptic scaling through somatic regulation of mRNAs important for neuronal excitability. Hints at such processes have begun to be reported in the literature. For example, synaptic scaling induced by concurrent blockade of action potentials and NMDAR activity in hippocampal slices was impaired in the *Fmr1* KO (Soden and Chen, 2010). In another example, the synaptic reweighting that occurs during sleep after a period of wakefulness was defective in *dfmr1* KO flies (Bushey et al., 2011). These findings suggest that FMRP plays a broader role in neuronal plasticity than previously appreciated, and, together with results from the MECS CLIP pilot study, suggest that regulation of translation by FMRP is a dynamic process that actively responds to changes in neuronal signaling and gene expression.

Figure 15. FMRP HITS-CLIP from whole mouse brain.

A) Autoradiogram of labeled RNA:protein complexes immunoprecipitated after limited RNAse digest. Gel was transferred to nitrocellulose and membrane was cut at regions indicated by brackets.

B) RNAs purified from nitrocellulose were reverse transcribed, amplified by PCR and further purified by urea-PAGE. DNAs of correct size are visualized as a smear between 100-150nt. DNA was recovered from the gel cut at bracketed regions. No signal was observed in *Fmr1* KO or (-)RT lanes.

C) Agarose gel showing final CLIP products. Gel was cut at regions indicated by dots and DNA was sent for high throughput sequencing.

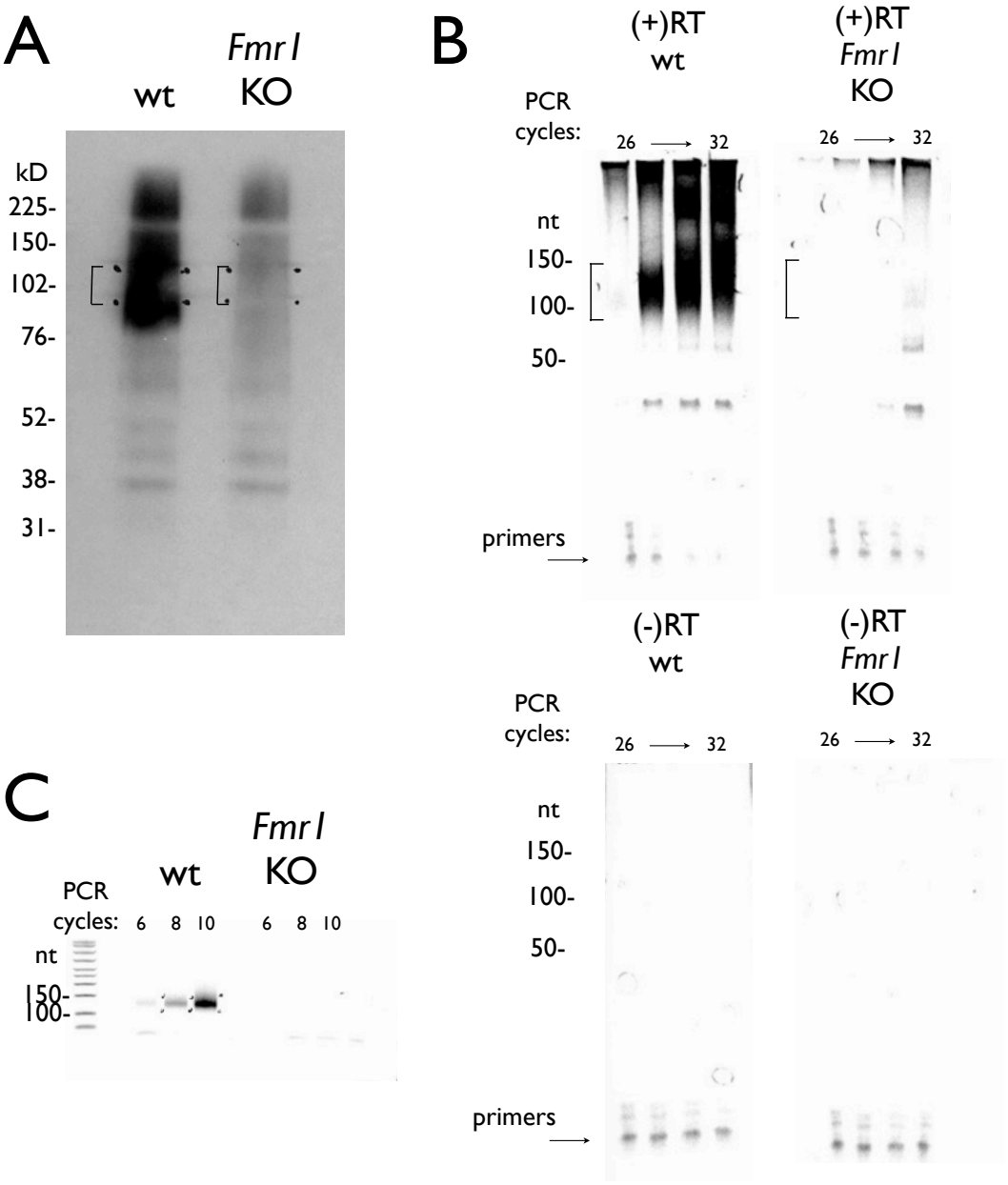
A
wt
Fmr1 KO
kD
225-
150-
102-
76-
52-
38-
31-
B
(+)RT
wt
(+)RT
Fmr1 KO
PCR cycles:
26 → 32
26 → 32
nt
150-
100-
50-
primers
(-)RT
wt
(-)RT
Fmr1 KO
PCR cycles:
26 → 32
26 → 32
nt
150-
100-
50-
primers
C
wt
Fmr1 KO
PCR cycles:
6 8 10
6 8 10
nt
150-
100-

Table 2: Top 50 FMRP targets identified by whole brain HITS-CLIP.

The number of exonic tags per gene is shown.

Gene Name	Exonic Tags
Apc	5959
Mtap1b	5083
Kif1a	3256
Kif5a	3158
Mtap1a	2886
Huwe1	2368
Ank2	2162
Bsn	2067
Dync1h1	1903
Kif1b	1858
Spnb2	1852
Pclo	1790
Macf1	1741
2610507B11Rik	1673
Adcy1	1630
Hivep2	1592
Ttc3	1574
Ank3	1528
Spnb3	1497
Mycbp2	1481
Herc2	1378
Nf1	1363
Usp9x	1356
Dst	1353
Ubr4	1240

Gene Name	Exonic Tags
Cyfip2	1225
Mtap2	1196
Akap6	1176
Usp34	1169
Birc6	1142
Wdfy3	1142
Centg1	1110
Spna2	1075
Lphn1	1060
Wnk1	1046
Itpr1	1044
Nbea	1038
Kif5c	1035
Grit	1033
Nisch	970
Dennd5a	953
Shank1	933
Dmxl2	928
Pde2a	925
Unc13c	913
Myo5a	897
Nckap1	893
Clasp2	864
Herc1	861
Fry	852

Figure 16. Correlation of whole brain FMRP CLIP data with polysome FMRP CLIP data and with neuronal mRNA abundance.

A) The number of exonic CLIP tags per gene was highly correlated between whole brain FMRP CLIP and polysome FMRP CLIP experiments (Darnell 2011). The top 5000 targets were included in the analysis.

B) The number of exonic CLIP tags per gene from the whole brain CLIP experiment was not correlated to abundance of neuronal mRNAs (Cahoy 2008). All mRNAs with measurable expression levels were included in the analysis.

A

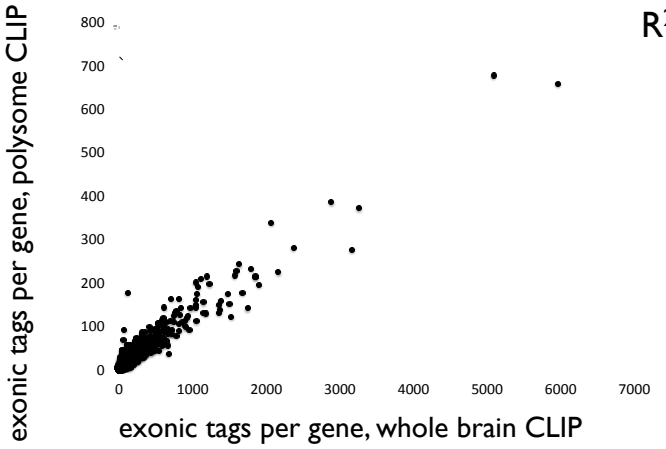

R^2=0.87

B

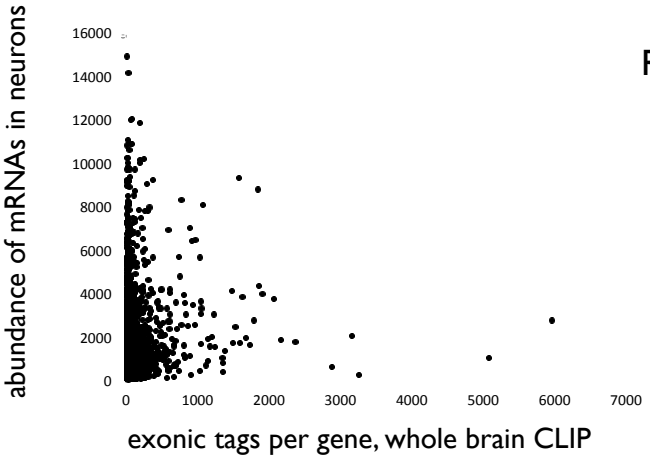

R^2=0.03

Figure 17. Genomic distributions of FMRP CLIP tags.

A) Whole brain CLIP, all tags.

B) Exclusion of single, nonoverlapping tags from whole brain CLIP slightly reduced intronic and intergenic signal.

C) For comparison, distribution of FMRP polysome CLIP tags (Darnell 2011, all tags). Polysome CLIP had proportionally more intergenic tags than whole brain CLIP because sample was dissociated more harshly during resuspension of the polysome pellet (boiled in 2% SDS), exposing more rRNA.

D) Whole brain CLIP, allowing up to 100 alignments for each tag to facilitate mapping of sequences derived from ncRNAs. Single, nonoverlapping tags were excluded.

E) Breakdown of tags aligning to noncoding regions from (D).

A

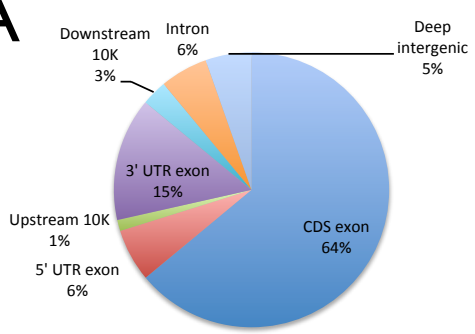
Downstream 10K 3%
Intron 6%
Deep intergenic 5%
3' UTR exon 15%
Upstream 10K 1%
5' UTR exon 6%
CDS exon 64%

B

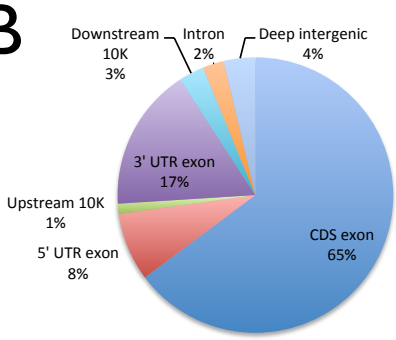
Downstream 10K 3%
Intron 2%
Deep intergenic 4%
3' UTR exon 17%
Upstream 10K 1%
5' UTR exon 8%
CDS exon 65%

C

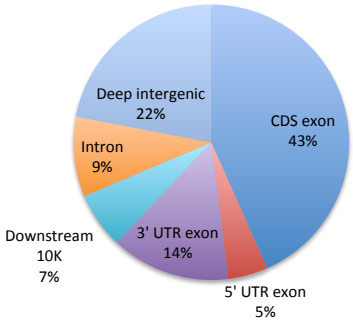
Deep intergenic 22%
CDS exon 43%
Intron 9%
Downstream 10K 7%
3' UTR exon 14%
5' UTR exon 5%

D

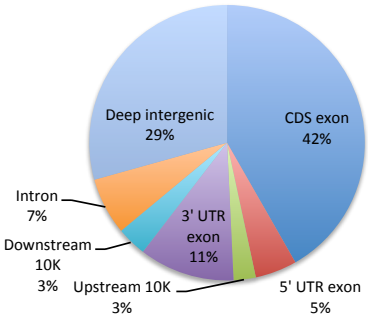
Deep intergenic 29%
CDS exon 42%
Intron 7%
Downstream 10K 3%
3' UTR exon 11%
Upstream 10K 3%
5' UTR exon 5%

E

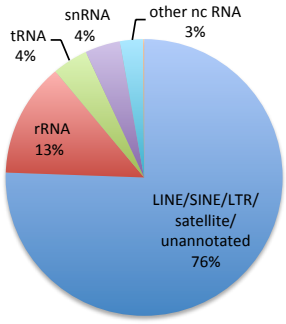
snRNA 4%
other nc RNA 3%
tRNA 4%
rRNA 13%
LINE/SINE/LTR/ satellite/ unannotated 76%

Figure 18. FMRP CLIP tag distributions on mature mRNA transcripts.
Representative transcripts have high tag numbers and a single major isoform.

Top panel: Cumulative tag distribution. Tags mapping to the 5‘UTR are plotted in red, those mapping to coding region are plotted in blue, and those mapping to the 3‘UTR are plotted in green.

Bottom panel: Relative distribution of CLIP tags. In general, FMRP CLIP tags are distributed evenly along the coding sequence, with fewer tags observed in UTRs.

Figure 18
pg 1 of 8

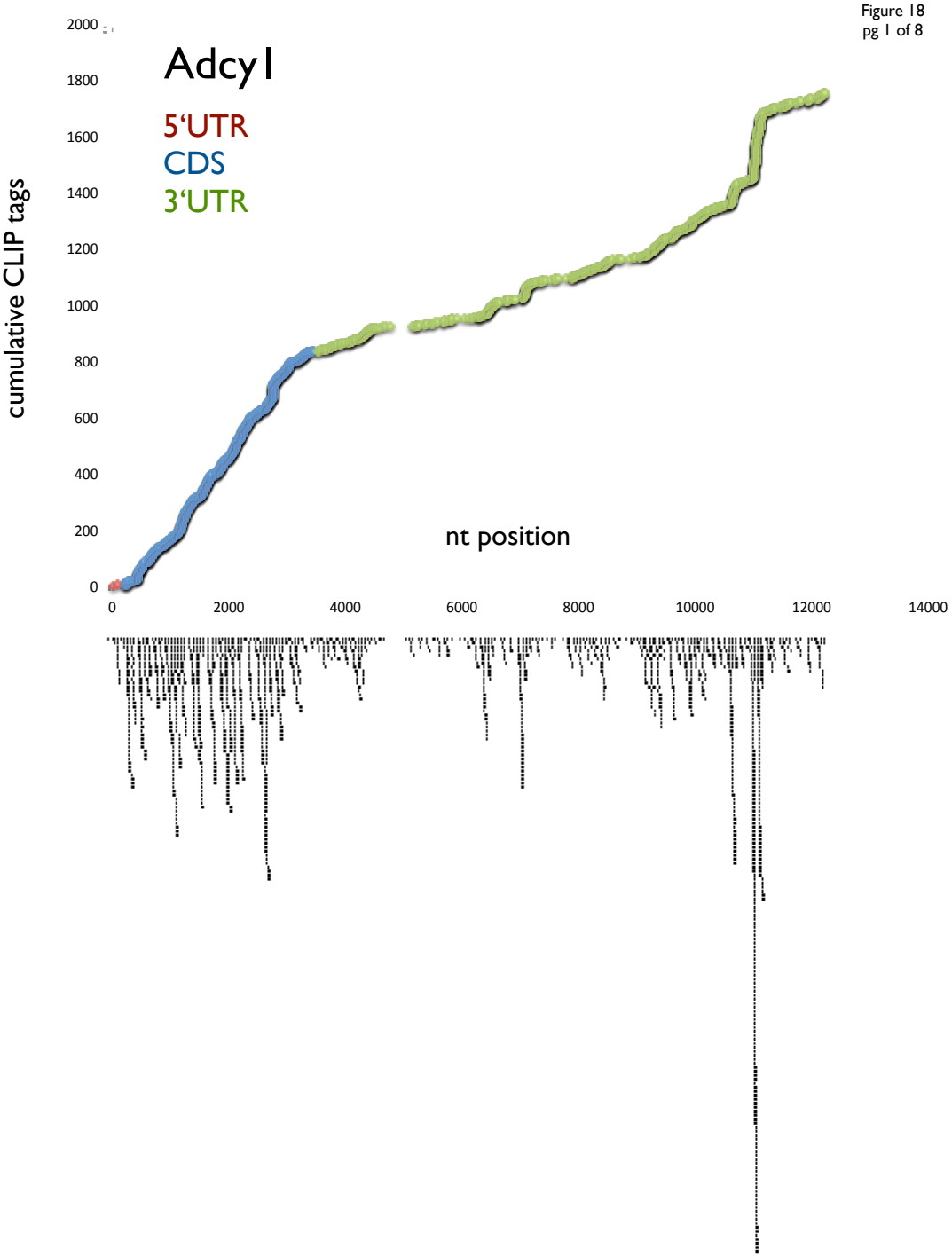

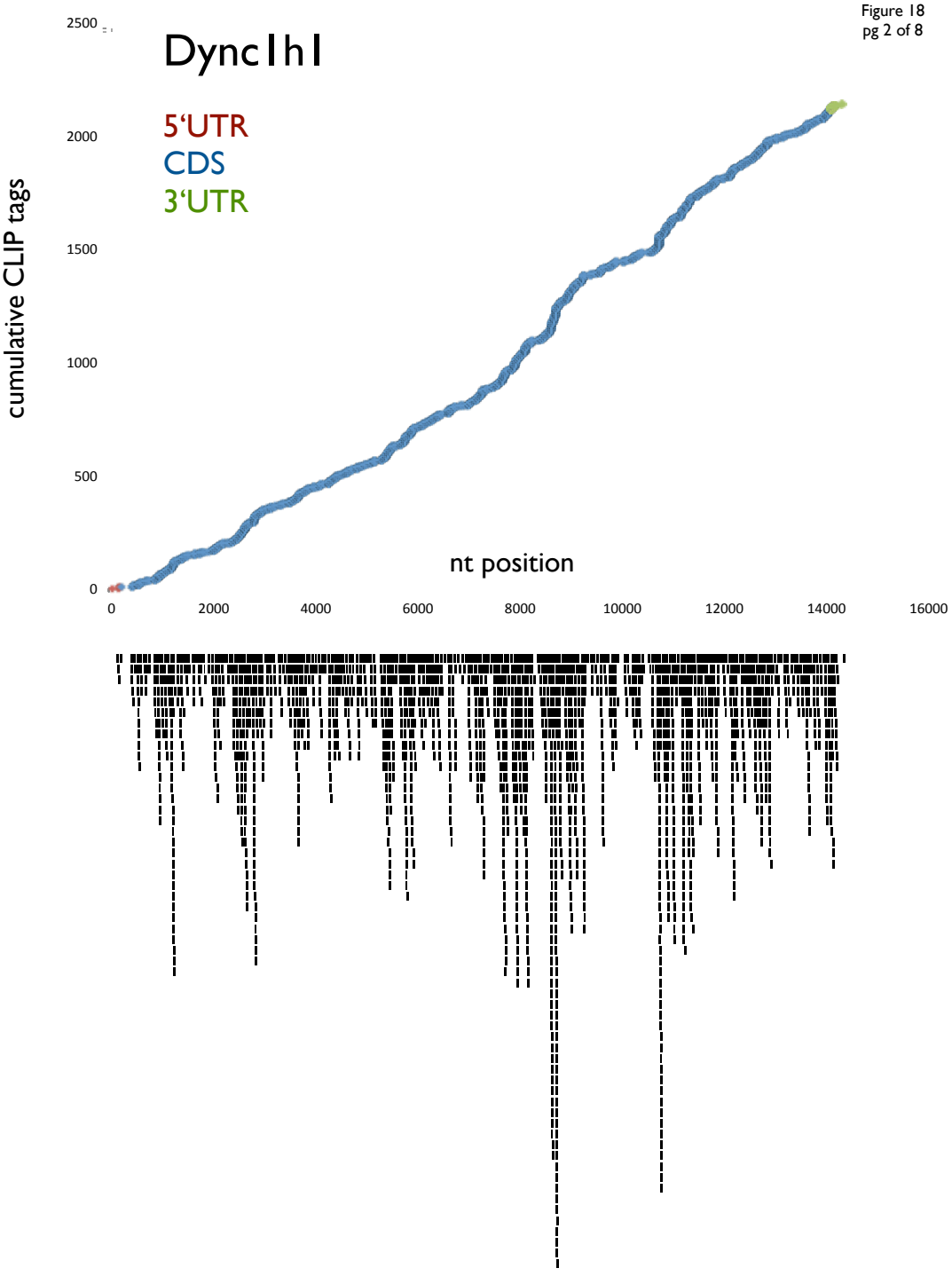
Dync1h1
5'UTR
CDS
3'UTR
cumulative CLIP tags
2500
2000
1500
1000
500
0
nt position
0
2000
4000
6000
8000
10000
12000
14000
16000

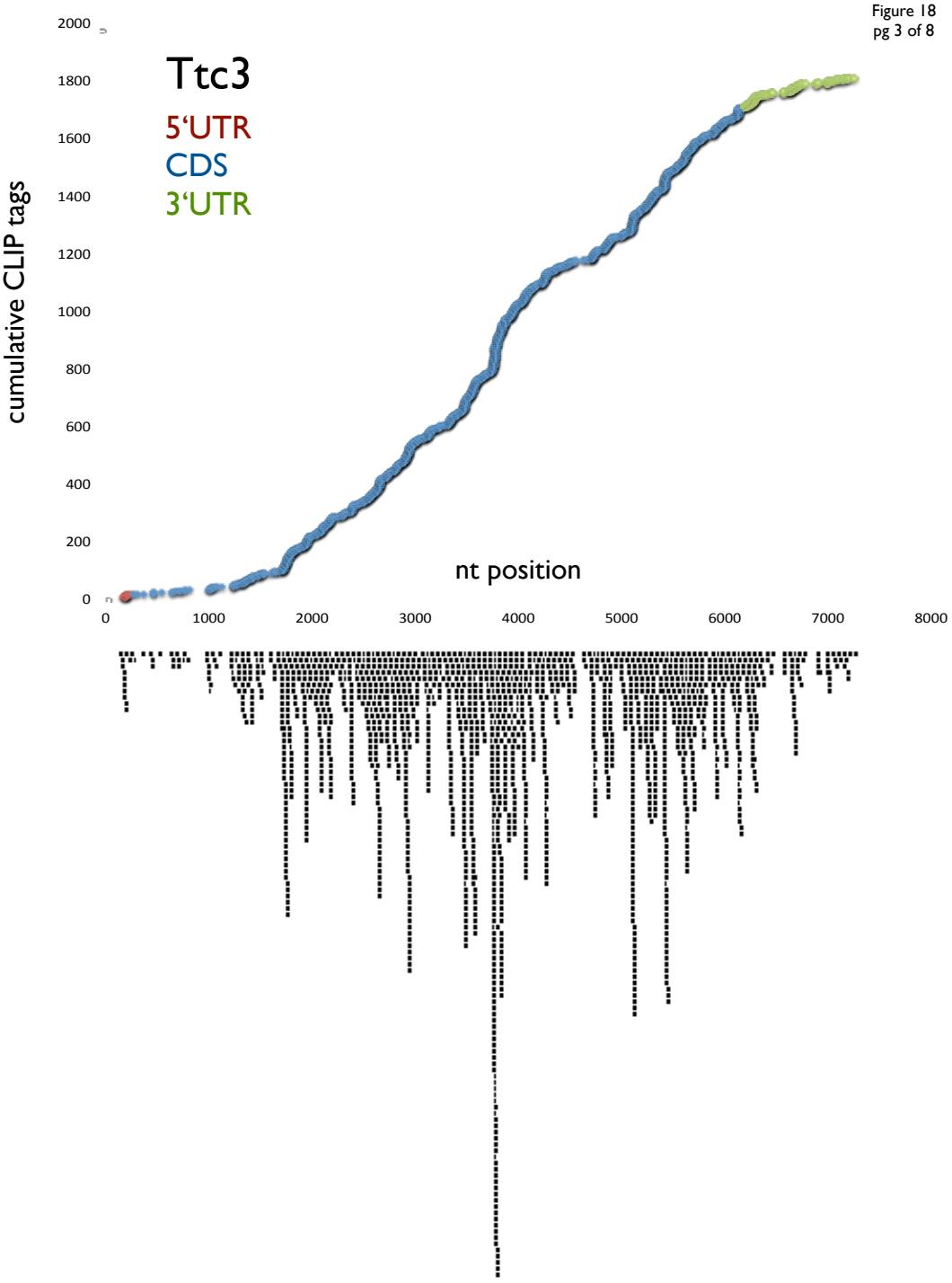
Ttc3
5'UTR
CDS
3'UTR
cumulative CLIP tags
nt position
0
200
400
600
800
1000
1200
1400
1600
1800
2000
0
1000
2000
3000
4000
5000
6000
7000
8000

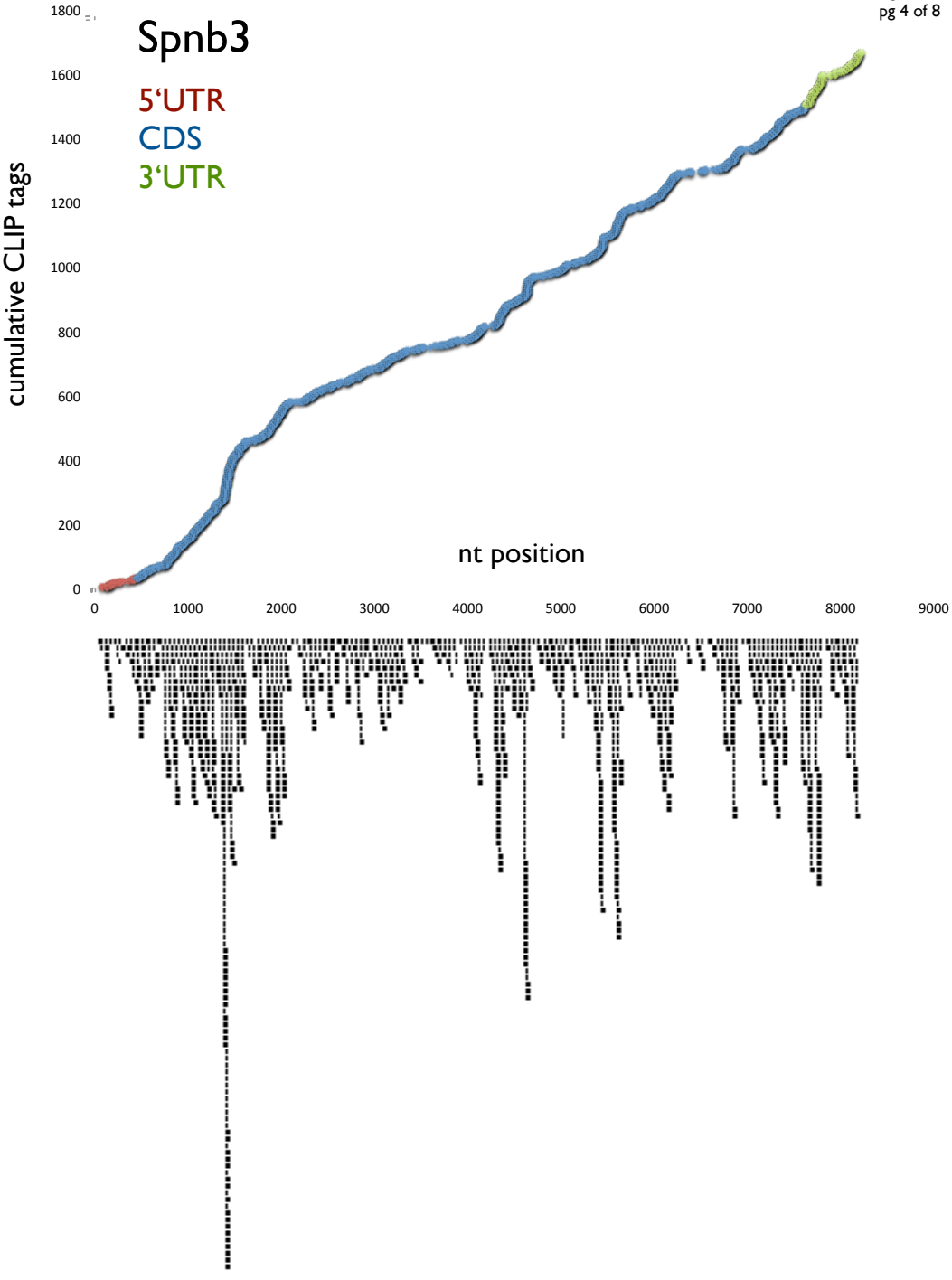
Spnb3
5'UTR
CDS
3'UTR
cumulative CLIP tags
nt position
0
200
400
600
800
1000
1200
1400
1600
1800
0
1000
2000
3000
4000
5000
6000
7000
8000
9000

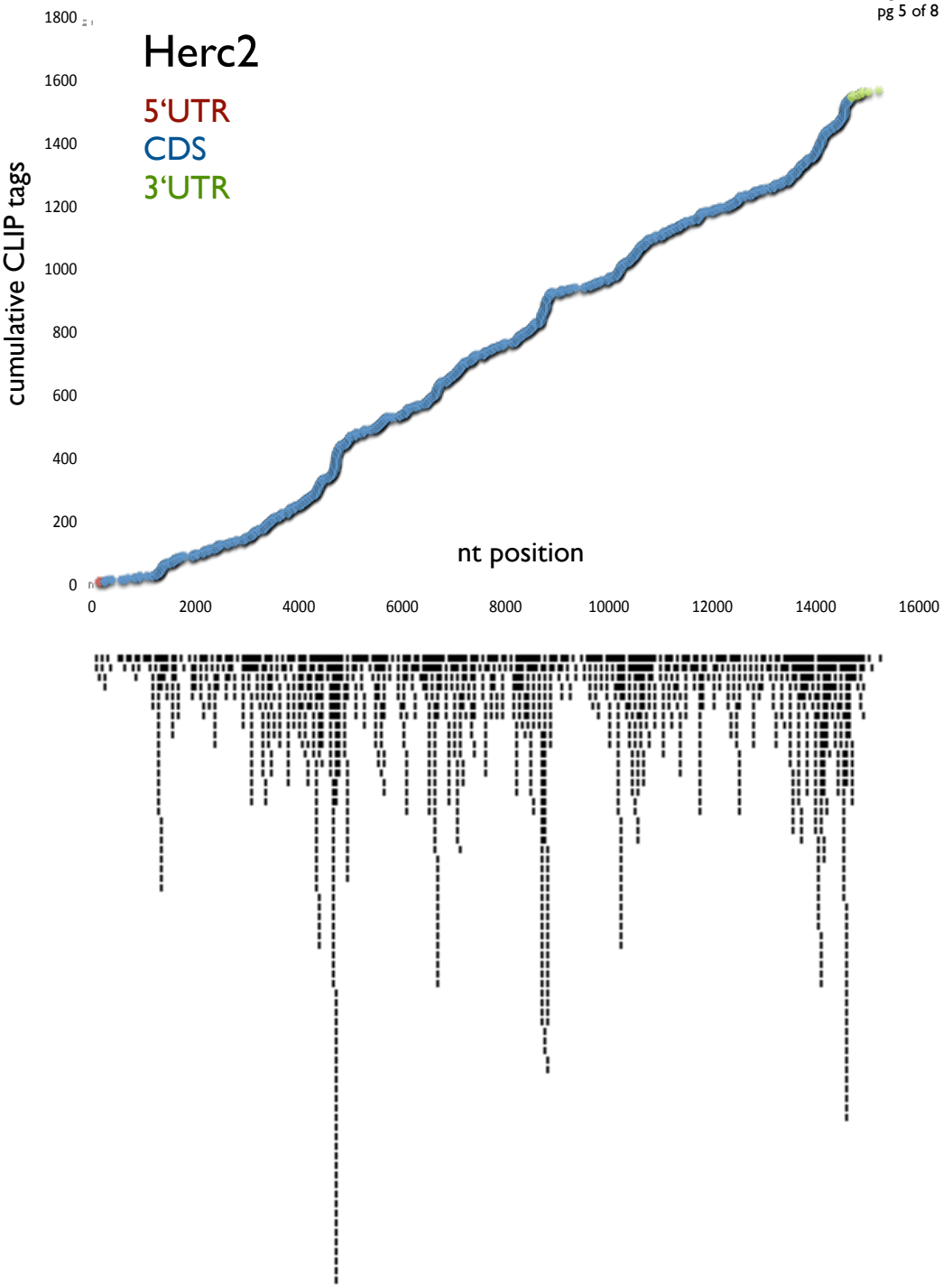
Herc2
5'UTR
CDS
3'UTR
cumulative CLIP tags
nt position
0
200
400
600
800
1000
1200
1400
1600
1800
0
2000
4000
6000
8000
10000
12000
14000
16000

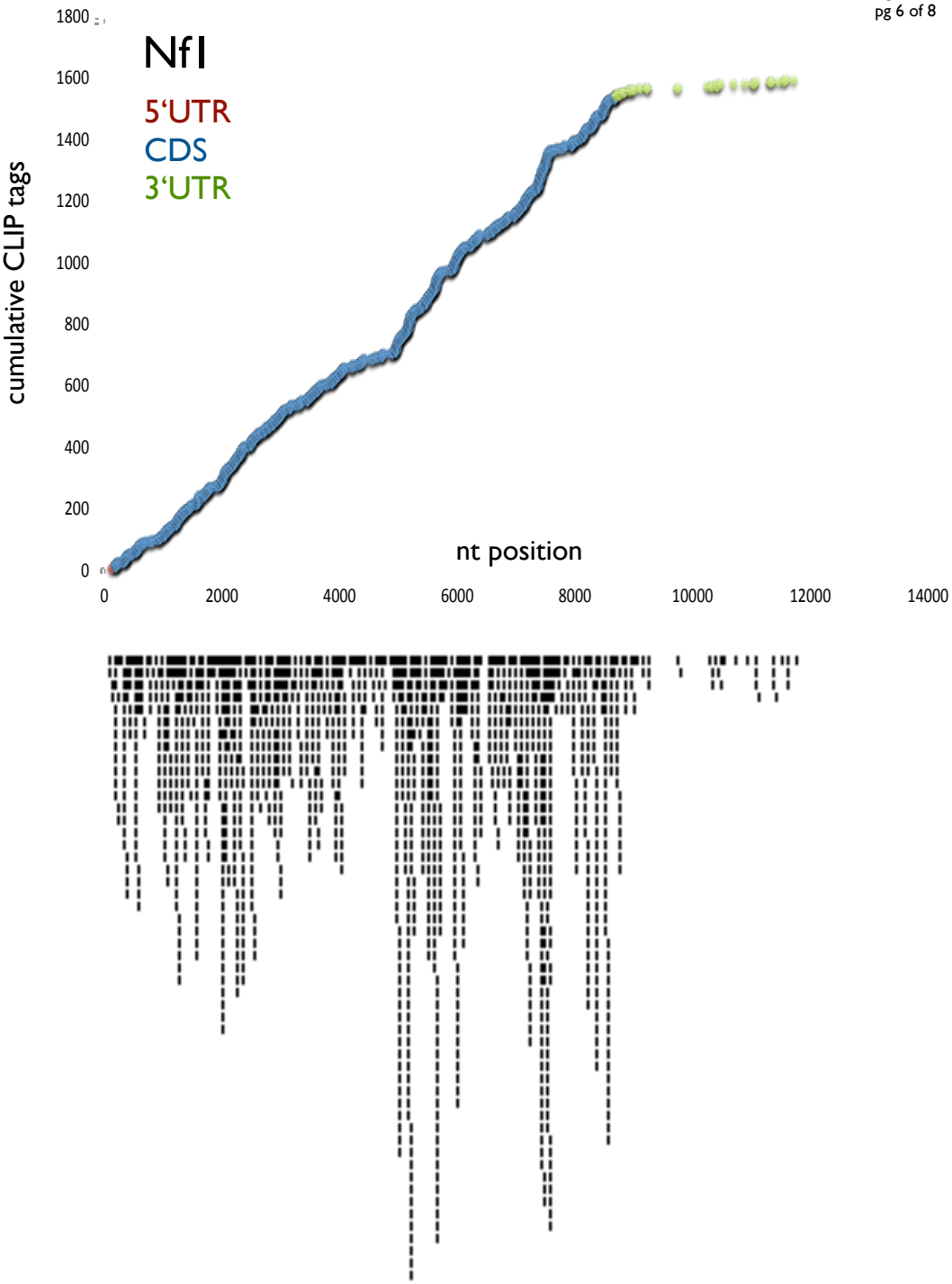
Nf1
5'UTR
CDS
3'UTR
cumulative CLIP tags
nt position
0
200
400
600
800
1000
1200
1400
1600
1800
0
2000
4000
6000
8000
10000
12000
14000

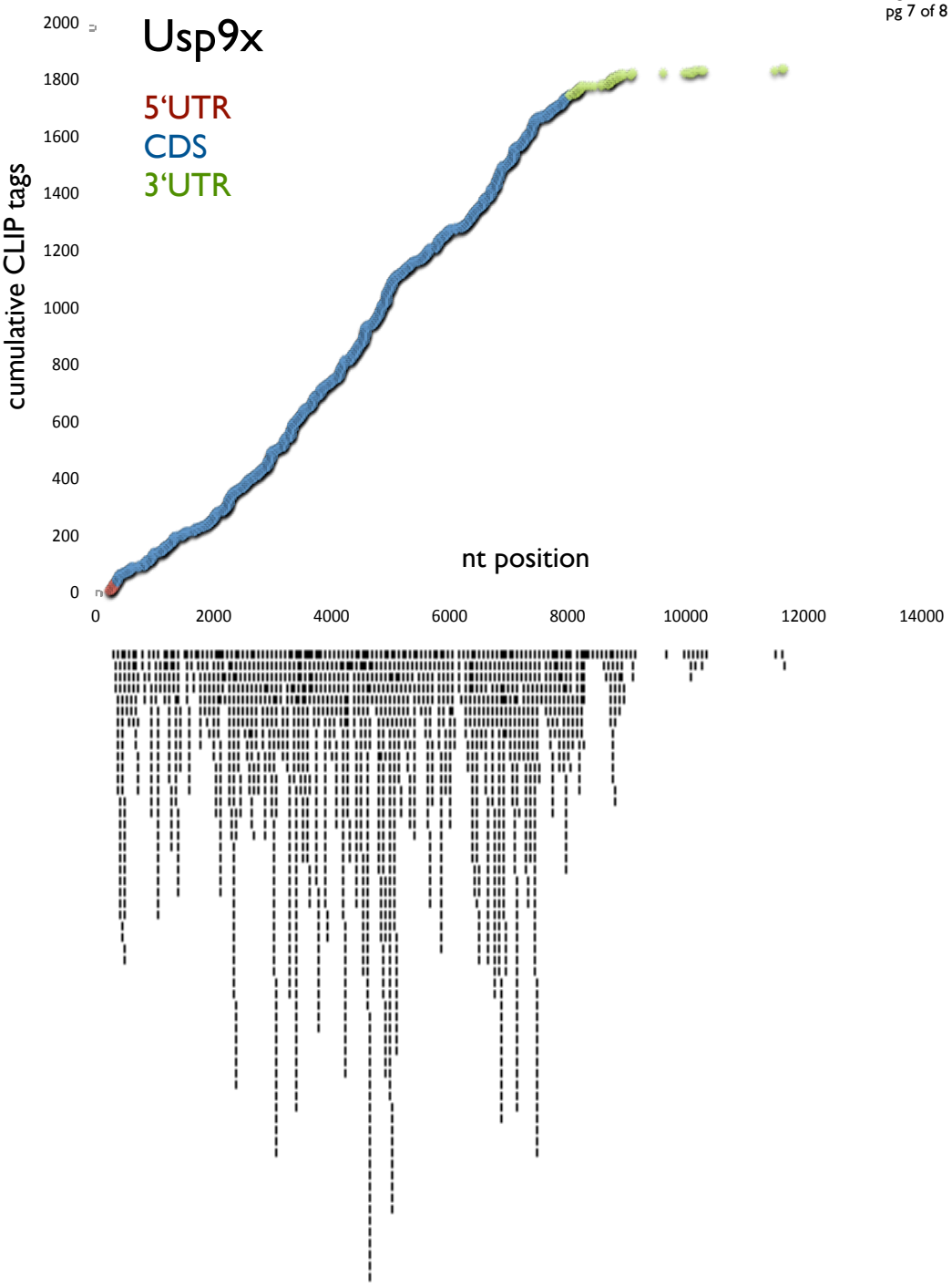
Usp9x
5'UTR
CDS
3'UTR
cumulative CLIP tags
2000
1800
1600
1400
1200
1000
800
600
400
200
0
nt position
0
2000
4000
6000
8000
10000
12000
14000

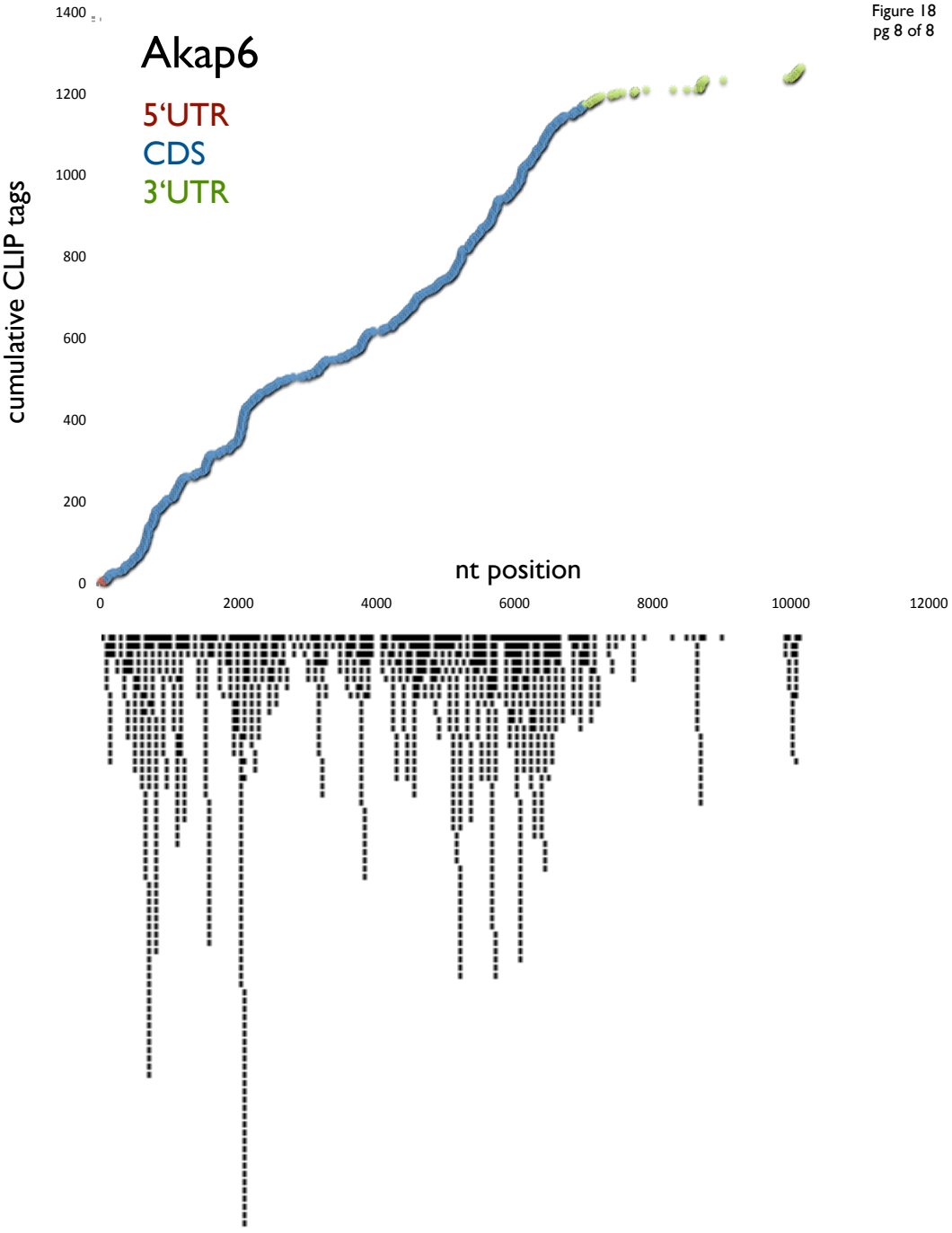
Akap6
5'UTR
CDS
3'UTR
cumulative CLIP tags
nt position
0
200
400
600
800
1000
1200
1400
0
2000
4000
6000
8000
10000
12000

Figure 19. Purification of cellular nuclei from mouse brain by sedimentation through sucrose.

Nuclei were isolated from detergent-treated brain extracts by centrifugation over a column of 50% w/w sucrose. Total lysate (T) and the nuclear fraction (N) were analyzed by Western blot, loading equal milligram amounts of protein from each fraction. GAPDH is a marker of the cytosolic fraction, NeUN (Fox3) is a marker of neuronal nuclei, and calnexin is an integral membrane protein that is a marker of the endoplasmic reticulum. No calnexin copurified with the nuclear fraction, indicating that ER membranes were largely dissolved or stripped during purification. FMRP was present in both cytoplasmic and nuclear fractions.

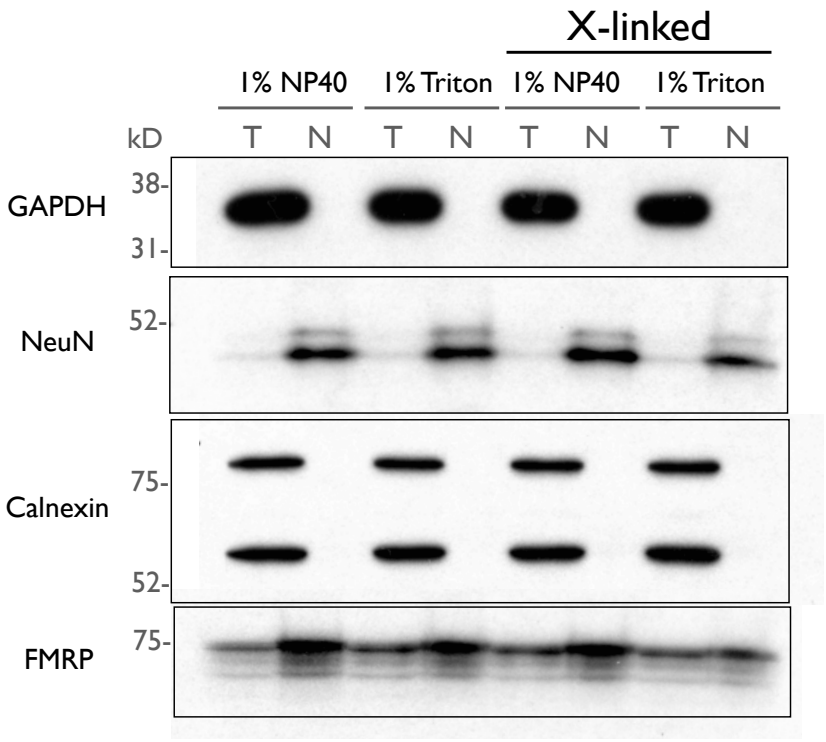
X-linked
1% NP40
1% Triton
1% NP40
1% Triton
kD
T
N
T
N
T
N
T
N
GAPDH
38-
31-
NeuN
52-
Calnexin
75-
52-
FMRP
75-

Figure 20. FMRP CLIP of brain nuclei pelleted under sucrose.

A) Autoradiogram of labeled RNA:protein complexes immunoprecipitated after a titrated RNAse digest (RNAse dilution indicated over each lane). Gel was transferred to nitrocellulose and membrane was cut at regions indicated by dots.

B) Western blot showing successful depletion of FMRP from extracts after the CLIP immunoprecipitation step.

C) RNAs purified from nitrocellulose were reverse transcribed, amplified by PCR and further purified by urea-PAGE. DNAs of correct size are visualized as a smear between 100-150nt. However, in this experiment the signal was not specific to the wt lanes. Although the water control indicated some level of reagent contamination, the *Fmr1* KO lanes also contained additional background signal that gained in intensity with increasing PCR cycles, suggesting that the contaminating DNA contains linker sequences recognized by the PCR primers and indicating that the IP may contain RNAs crosslinked to proteins other than FMRP.

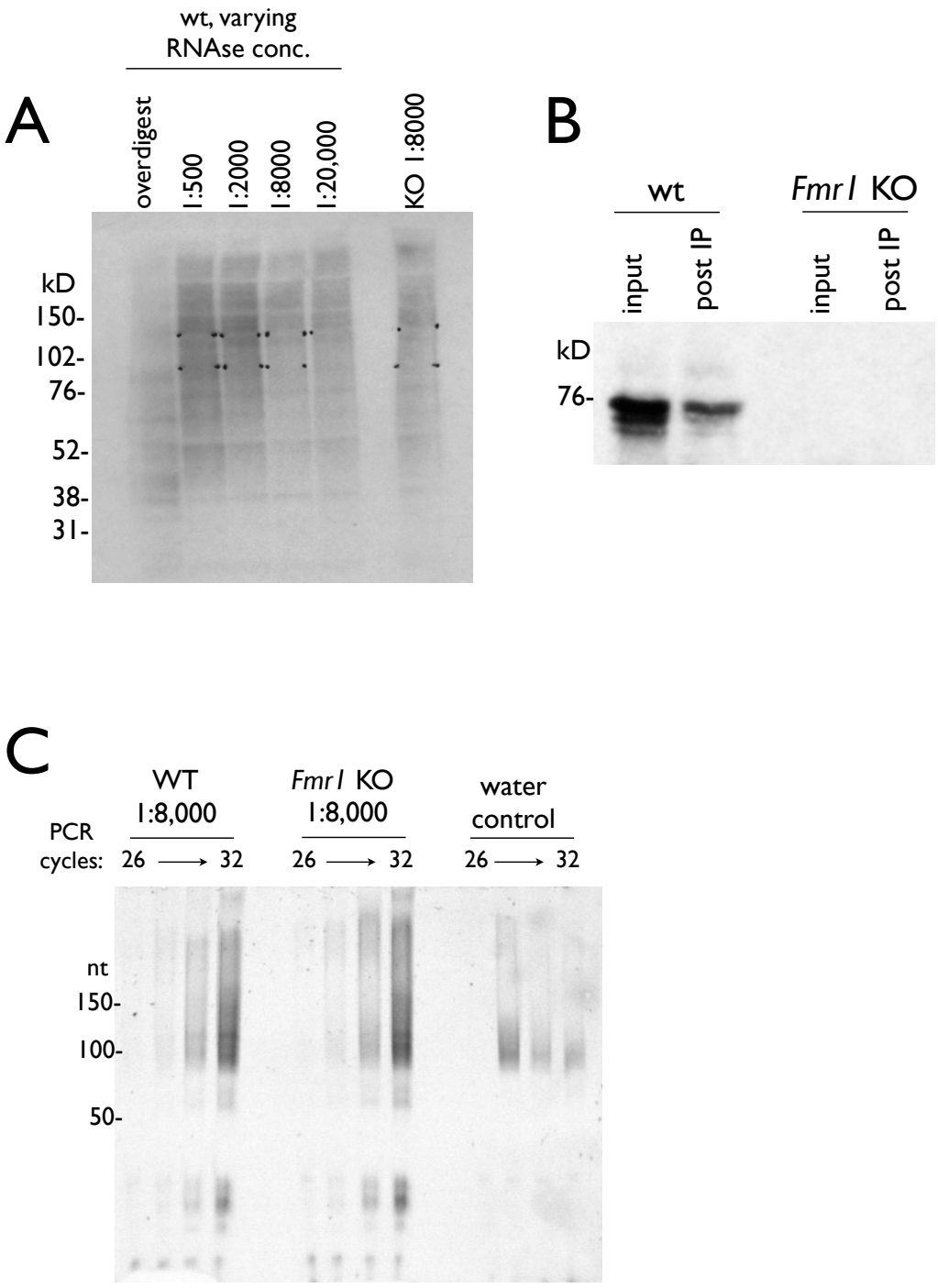
A
wt, varying
RNAse conc.
overdigest
1:500
1:2000
1:8000
1:20,000
KO 1:8000
kD
150-
102-
76-
52-
38-
31-
B
wt
Fmr1 KO
input
post IP
input
post IP
kD
76-
C
WT
1:8,000
Fmr1 KO
1:8,000
water
control
PCR
cycles:
26 → 32
26 → 32
26 → 32
nt
150-
100-
50-

Figure 21. Purification of cellular nuclei from mouse brain by pelleting extracts at 2000xg.

Nuclei were isolated from brain extracts treated with 0.8% NP-40 by centrifugation at 2000xg, with two gentle washes. Total extract (T), the cytoplasmic fraction (C) and the nuclear fraction (N) were analyzed by Western blot, loading 6uL of each fraction (by Bradford, the nuclear fraction was 5X less concentrated than the other fractions). Gapdh is a marker of the cytosolic fraction; hpRNP C1/C2, NeUN (Fox3) and histones are markers of the nuclear fraction; calnexin is an integral membrane protein that is a marker of the endoplasmic reticulum. No calnexin purified in the nuclear fraction, indicating that the majority of ER membranes were removed from nuclei by the detergent treatment. FMRP was present in both cytoplasmic and nuclear fractions.

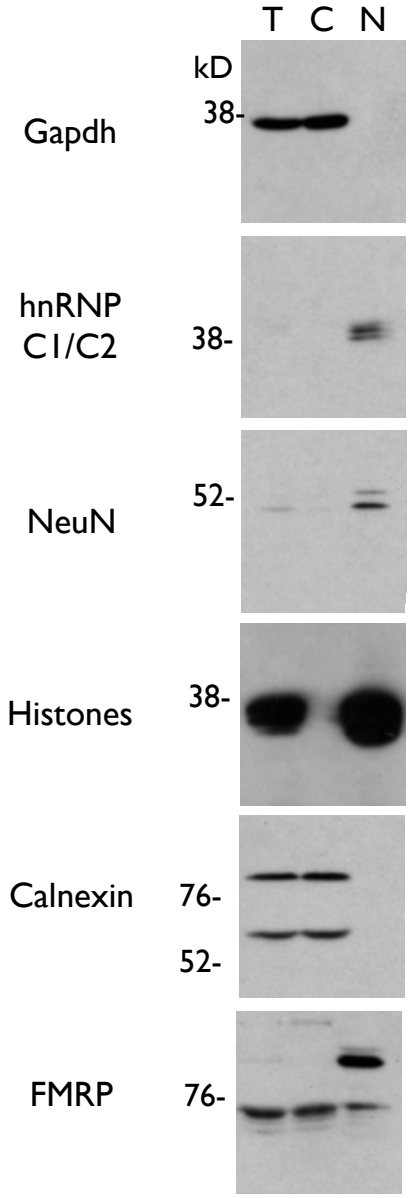
T C N
kD
38-
Gapdh
hnRNP
C1/C2
38-
52-
NeuN
38-
Histones
76-
52-
Calnexin
76-
FMRP

Figure 22. Comparison of two different antibodies in immunoprecipitation of FMRP from mouse brain nuclear extracts.

A) Western blot of inputs (I) and post-IP supernatants (P) from immunoprecipitations of FMRP with antibody 17722, blotted with the same antibody. A nonspecific band of the same size as FMRP was observed in nuclear extracts from *Fmr1* KO mice (this band was not observed in *Fmr1* KO samples from whole brain extracts).

B) Western blot of nuclear extracts from wt and *Fmr1* KO mouse brain using FMRP antibody 27455. No nonspecific bands were observed.

C) Western blots showing input, post-IP supernatants and IP eluates from immunoprecipitations using antibodies 27455 or 17722, blotted with 17722. The 27455 antibody immunoprecipitated much more FMRP than an equivalent amount of the 17722 antibody.

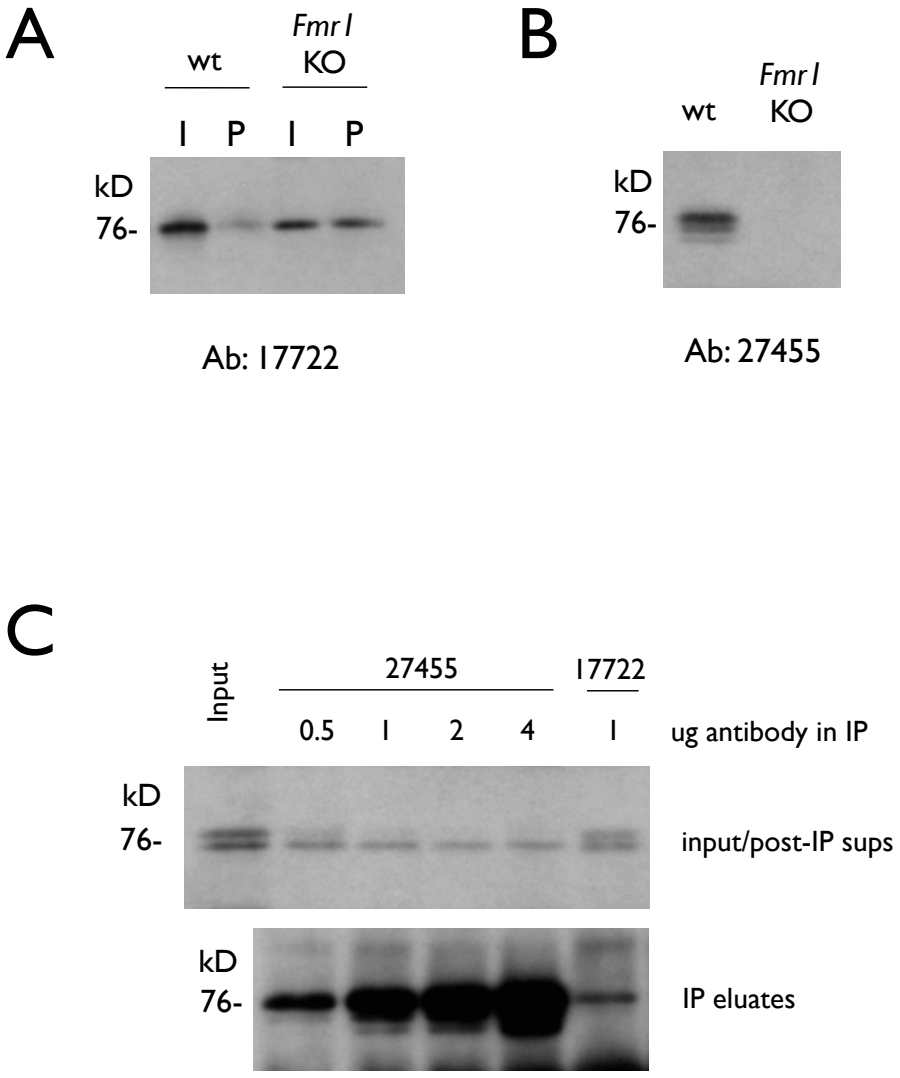
A
wt
Fmr1 KO
I P I P
kD
76-
Ab: 17722
B
wt
Fmr1 KO
kD
76-
Ab: 27455
C
Input
27455
17722
0.5 1 2 4 1
ug antibody in IP
kD
76-
input/post-IP sups
kD
76-
IP eluates

Figure 23. FMRP CLIP of brain nuclei pelleted at 2000xg using antibody 27455.

A) Autoradiogram of labeled RNA:protein complexes immunoprecipitated after a titrated RNAse digest (RNAse dilution indicated over each lane). More signal in the bracketed region was observed in wt lanes than in RNAse overdigest, no-crosslink or *Fmr1* KO control lanes. The gel was transferred to nitrocellulose and membrane was cut at regions indicated by brackets.

B) RNAs purified from nitrocellulose were reverse transcribed, amplified by PCR and further purified by urea-PAGE . DNAs of correct size are between 100-150nt. DNA was recovered from the gel cut at bracketed regions.

C) Agarose gel showing final CLIP products. Gel was cut at bracketed regions and DNA was sent for high throughput sequencing.

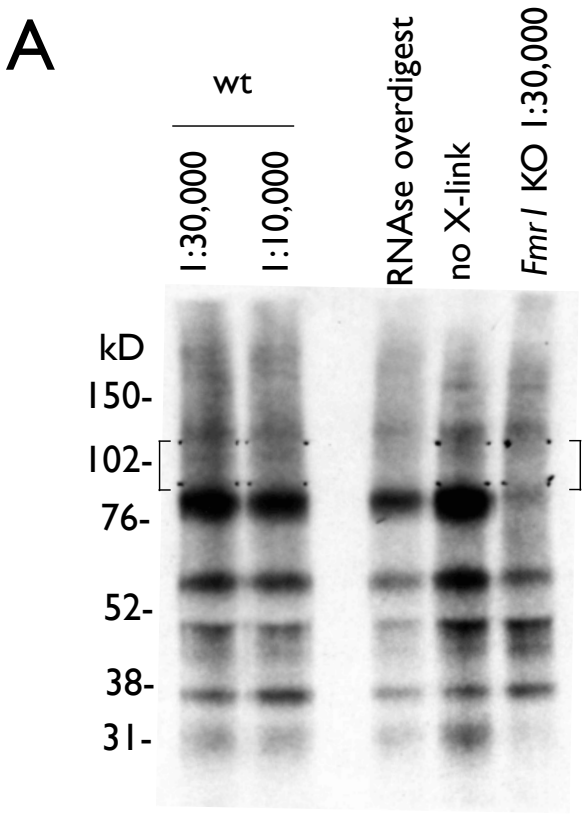
A
wt
1:30,000
1:10,000
RNAse overdigest
no X-link
Fmr1 KO 1:30,000
kD
150-
102-
76-
52-
38-
31-

B

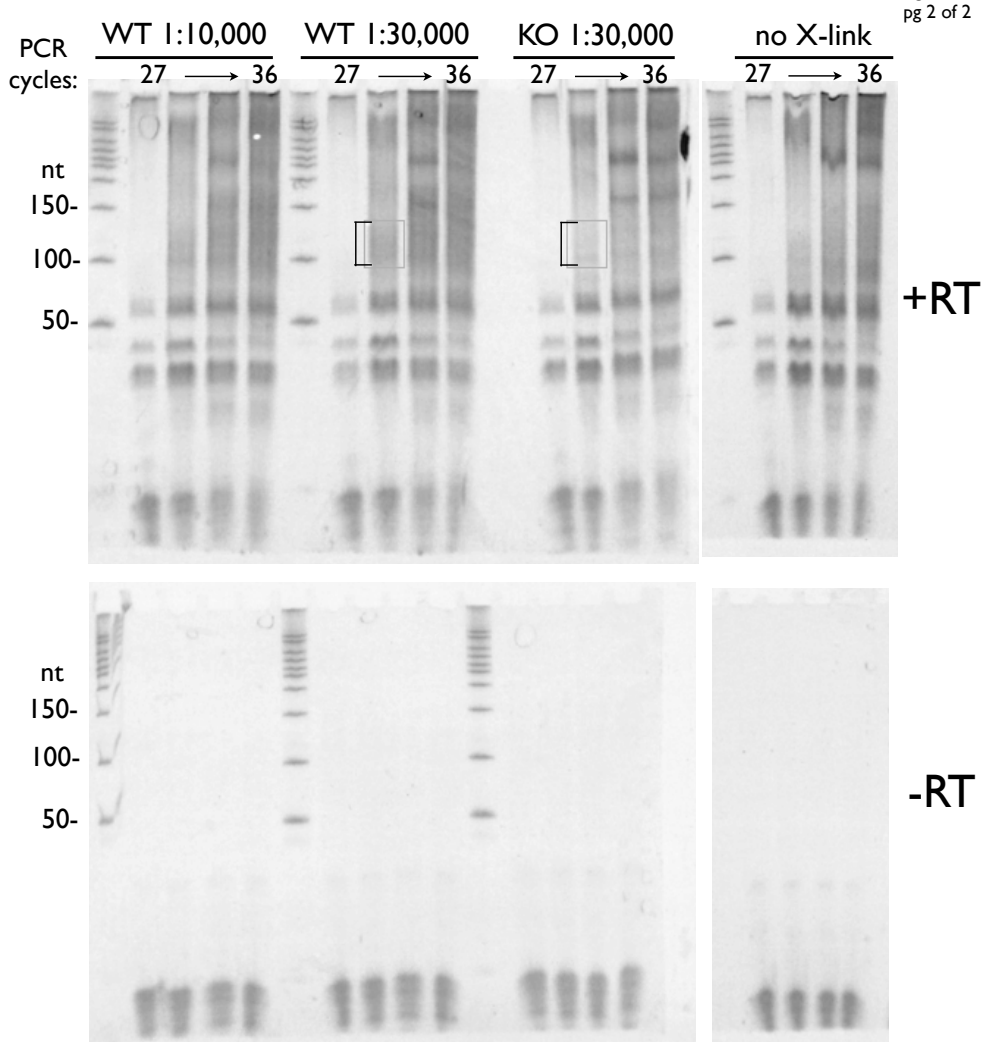
WT 1:10,000
WT 1:30,000
KO 1:30,000
no X-link
PCR cycles:
27 → 36
nt
150-
100-
50-
+RT
-RT

C

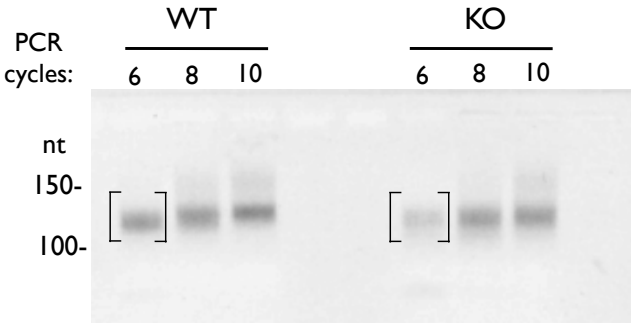
WT
KO
PCR cycles:
6 8 10
nt
150-
100-

Figure 24. Genomic distributions of FMRP nuclear CLIP tags.

A) All tags.

B) Exclusion of single, nonoverlapping tags reduced intronic and intergenic signal.

C) Breakdown of tags aligning to intronic sequences.

A

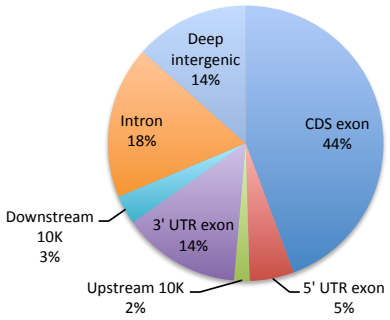
Deep intergenic 14%
CDS exon 44%
Intron 18%
Downstream 10K 3%
3' UTR exon 14%
Upstream 10K 2%
5' UTR exon 5%

B

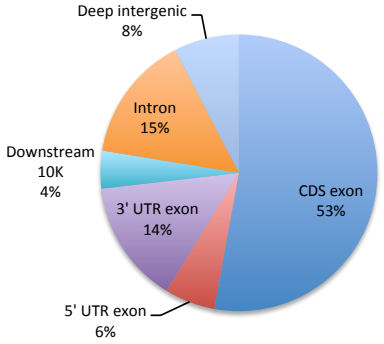
Deep intergenic 8%
Intron 15%
Downstream 10K 4%
CDS exon 53%
3' UTR exon 14%
5' UTR exon 6%

C

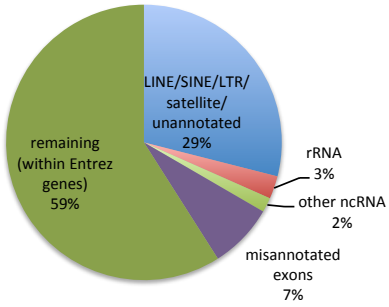
LINE/SINE/LTR/ satellite/ unannotated 29%
rRNA 3%
other ncRNA 2%
misannotated exons 7%
remaining (within Entrez genes) 59%

Figure 25. Comparison of FMRP CLIP tag distributions from CLIP experiments performed on whole brain, brain polysomes, and brain nuclei.

Tags are plotted as RPKM (Reads Per Kilobase of exon model per Million mapped reads) in order to visually compare results from experiments with different sequencing depths. Read depth is indicated for each track on the Y-axis. Four examples of genes are shown. On this page: *Map1B* in upper panel, *Huwe1* in lower panel. On next page: *Apc* in upper panel, *Bassoon* in lower panel. The tag tracks are represented in the following order (top to bottom within panels): nuclear CLIP, whole brain CLIP, polysome CLIP.

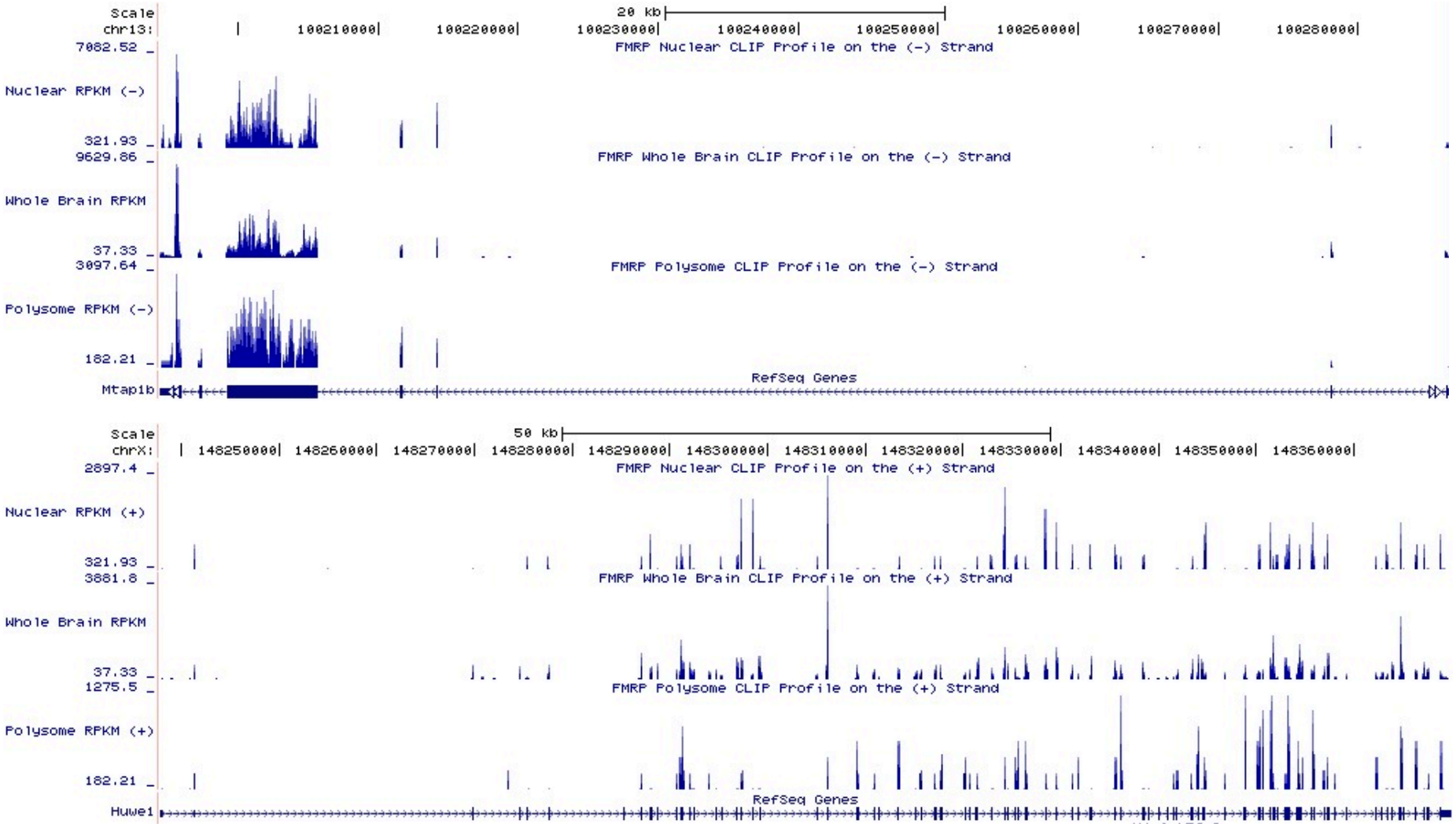
Scale
chr13:
20 kb
100210000
100220000
100230000
100240000
100250000
100260000
100270000
100280000
7082.52
FMRP Nuclear CLIP Profile on the (-) Strand
Nuclear RPKM (-)
321.93
9629.86
FMRP Whole Brain CLIP Profile on the (-) Strand
Whole Brain RPKM
37.33
3097.64
FMRP Polysome CLIP Profile on the (-) Strand
Polysome RPKM (-)
182.21
RefSeq Genes
Mtap1b
Scale
chrX:
50 kb
148250000
148260000
148270000
148280000
148290000
148300000
148310000
148320000
148330000
148340000
148350000
148360000
2897.4
FMRP Nuclear CLIP Profile on the (+) Strand
Nuclear RPKM (+)
321.93
3881.8
FMRP Whole Brain CLIP Profile on the (+) Strand
Whole Brain RPKM
37.33
1275.5
FMRP Polysome CLIP Profile on the (+) Strand
Polysome RPKM (+)
182.21
RefSeq Genes
Huwe1


6
Nuclear R
9
Whole Bra
2
Polysome
Nuclear R
2
Whole Bra
1
Polysome

Figure 26. Analysis of nuclear FMRP CLIP data.

A) The number of exonic CLIP tags per gene was fairly well correlated between nuclear FMRP CLIP and whole brain FMRP CLIP experiments. The top 5000 targets were included in the analysis.

B) The number of exonic CLIP tags per gene from the whole brain CLIP experiment was not correlated to abundance of neuronal mRNAs (Cahoy 2008). All mRNAs with measurable expression levels and at least two overlapping intronic CLIP tags were included in the analysis.

C) The number of intronic tags per gene was not correlated with the number of exonic tags per gene. All 1023 genes with at least 2 overlapping intronic tags were included in the analysis.

A

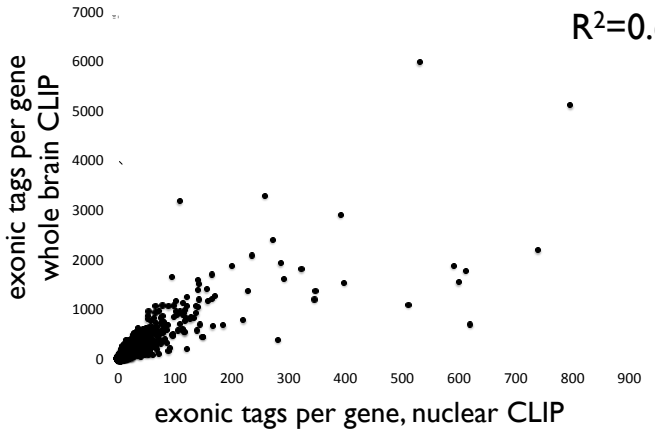
R2=0.68
exonic tags per gene whole brain CLIP
exonic tags per gene, nuclear CLIP
0
1000
2000
3000
4000
5000
6000
7000
0
100
200
300
400
500
600
700
800
900

B

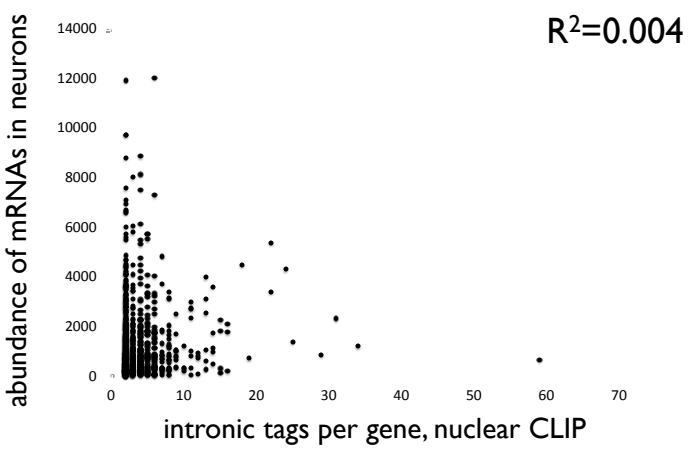
R2=0.004
abundance of mRNAs in neurons
intronic tags per gene, nuclear CLIP
0
2000
4000
6000
8000
10000
12000
14000
0
10
20
30
40
50
60
70

C

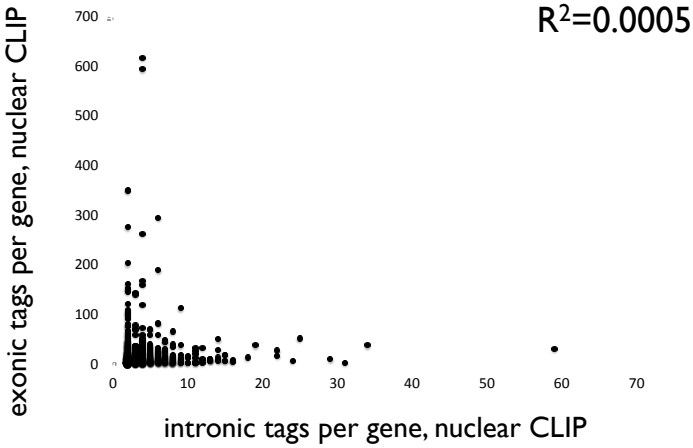
R2=0.0005
exonic tags per gene, nuclear CLIP
intronic tags per gene, nuclear CLIP
0
100
200
300
400
500
600
700
0
10
20
30
40
50
60
70

Table 3: Fold *Arc* mRNA induction in mouse brain after seizure, compared to resting animals.

Single tonic-clonic seizures were induced by the MECS protocol as described in text. At the indicated times after induction of seizure, mice were sacrificed and RNA was isolated from brain lysates (from hippocampus or cortex, as indicated). *Arc* mRNA levels were measured by QPCR. In Experiment 1, only hippocampus was assayed. In Experiment 2, both hippocampus and cortex were assayed. Values were normalized to *Arc* levels in resting animals. Three animals were used per timepoint and for resting controls.

Minutes Post-Seizure	Fold *Arc* Induction		
	Expt1 Hp	Expt2 Hp	Expt2 Cx
5	3.4		
10	5.4		
30	8.8	10	2.6
90		7.5	1

Table 4: mRNAs with increased whole brain FMRP CLIP tags after seizure.

Single tonic-clonic seizures were induced by the MECS protocol as described in text. Mice were sacrificed 15 minutes after the induction of seizure, in addition to resting controls. FMRP HITS-CLIP was performed on total brain. All mRNAs with at least a 50% increase in FMRP CLIP tags (normalized to the total number of tags sequenced per condition) are listed. The number of tags per gene after seizure and the fold increase in tags compared to the resting control are shown.

Gene Name	Tags after MECS	Fold Increase in Tags
Ddx3y	43	7.24
Fos	49	6.60
Uty	92	5.38
Jarid1d	69	4.42
Npas4	85	3.95
Mirnlet7i	63	3.14
Sall3	41	2.51
Ube2q2	39	2.50
Mirn153	67	2.37
Fmo1	37	2.37
Rnf180	43	2.32
Mirn30a	120	2.31
Mirn708	110	2.24
Notch3	31	2.20
Mrpl3	31	2.20
Egr1	93	2.12
Mirn26a-2	138	2.11
Dhcr7	31	2.09
Jun	34	2.08
Htatsf1	34	1.99
Tlr4	31	1.99
Mirn9-3	192	1.96
Scg3	46	1.94
Mirn181a-2	46	1.94
Dusp6	33	1.93
Gnl2	31	1.90
Tubb3	43	1.87
Mirn9-2	54	1.86
Mtss1	47	1.86
Mtf2	29	1.86
Creb1	40	1.86
Setdb2	33	1.85
Atad5	33	1.85
C130039O16Rik	37	1.84
Mdh2	38	1.83
Lta4h	31	1.81
Trim25	36	1.79
Tmem135	37	1.78
Api5	33	1.78

Gene Name	Tags after MECS	Fold Increase in Tags
Tpcn1	54	1.77
Klhdc8a	35	1.75
Ppp2r3c	31	1.74
Isyna1	31	1.74
Phf17	36	1.73
Kat2b	59	1.73
Tmco3	41	1.72
Pcdh15	32	1.72
1810013L24Rik	32	1.72
BC017647	37	1.72
Snx1	33	1.71
Mirn340	29	1.70
Nrbp2	34	1.70
2310061I04Rik	34	1.70
Amot	44	1.69
Scg5	30	1.68
4930504E06Rik	30	1.68
Edem1	45	1.68
Pcbp1	41	1.67
Ldb1	36	1.67
Stk24	31	1.67
Shroom4	31	1.67
Tex15	47	1.67
Nudt4	89	1.66
Fem1c	85	1.66
Nr4a1	70	1.65
Zfp426	44	1.65
Wars	28	1.64
Tcfe3	28	1.64
Nbn	28	1.64
Arhgap18	28	1.64
A930017M01Rik	45	1.64
Me2	51	1.63
Rock1	177	1.63
Mirn30d	63	1.63
Nrg1	29	1.63
1110067D22Rik	35	1.62
Frmpd4	957	1.62
Dock8	49	1.61

Gene Name	Tags after MECS	Fold Increase in Tags
Gab1	69	1.60
41154	44	1.60
Gpx1	32	1.60
Mirn30e	112	1.59
Cops3	33	1.59
AF529169	33	1.59
Myt1	27	1.58
Ppp1r7	34	1.58
Casp8ap2	130	1.58
Mtmr10	104	1.57
Cpne5	35	1.57
0610007P08Rik	85	1.57
Nup88	43	1.56
Zfx	58	1.56
Uba3	58	1.56
Cops5	29	1.56
Arc	29	1.56
Smek1	131	1.55
Dscaml1	87	1.54
Zmat4	32	1.54
Zfp385a	32	1.54
Maml1	32	1.54
Myh14	41	1.53
Rnf103	75	1.53
Ntng1	50	1.53
Tiparp	92	1.53
Aldh3a2	34	1.53
Tjp2	77	1.52
Ric8b	43	1.52
Cyc1	35	1.52
Hrb	142	1.52
Tmeff1	36	1.51
Rp2h	27	1.51
Fn1	73	1.51
Tfg	46	1.51
Pik3c3	46	1.51
Mfsd4	29	1.50
Cggbp1	29	1.50
Ik	39	1.50

Table 5: GO analyses of mRNAs with increases or decreases in FMRP CLIP tags after seizure.

mRNAs with at least a 50% increase or 50% decrease in CLIP tags (and meeting minimum thresholds for total tags – see text) were used for analysis. Terms with $p<0.01$ are shown. The GO categories for biologic process, cellular compartment and molecular function are shown, as well as UniProt sequence features.

Increased FMRP CLIP tags after MECS			
Category	**Term**	**Count**	**PValue**
UP_SEQ_FEATURE	domain:Leucine-zipper	5	0.005
UP_SEQ_FEATURE	DNA-binding region:Basic motif	5	0.008
GOTERM_BP_FAT	GO:0045944~positive regulation of transcription from RNA polymerase II promoter	9	0.004
GOTERM_BP_FAT	GO:0055114~oxidation reduction	9	0.004
GOTERM_BP_FAT	GO:0010557~positive regulation of macromolecule biosynthetic process	10	0.008
GOTERM_BP_FAT	GO:0031328~positive regulation of cellular biosynthetic process	10	0.010
GOTERM_BP_FAT	GO:0045893~positive regulation of transcription, DNA-dependent	9	0.010
GOTERM_BP_FAT	GO:0051173~positive regulation of nitrogen compound metabolic process	10	0.010
GOTERM_CC_FAT	GO:0005667~transcription factor complex	6	0.008
GOTERM_MF_FAT	GO:0003677~DNA binding	22	0.009

Decreased FMRP CLIP tags after MECS			
Category	**Term**	**Count**	**PValue**
GOTERM_BP_FAT	GO:0015672~monovalent inorganic cation transport	8	0.002
GOTERM_BP_FAT	GO:0055085~transmembrane transport	8	0.007
GOTERM_BP_FAT	GO:0006812~cation transport	9	0.008
GOTERM_MF_FAT	GO:0031420~alkali metal ion binding	6	0.010

Figure 27. FMRP HITS-CLIP from whole mouse brain after seizure.

Mice were subjected to a single tonic clonic seizure using MECS as described in text. Brains were harvested 15 minutes after induction of the seizure. Resting animals were used for controls.

A) Autoradiogram of labeled RNA:protein complexes immunoprecipitated after limited RNAse digest. Gel was transferred to nitrocellulose and membrane was cut at regions indicated by brackets.

B) RNAs purified from nitrocellulose were reverse transcribed, amplified by PCR and further purified by urea-PAGE. DNAs of correct size are visualized as a smear between 100-150nt. DNA was recovered from the gel cut at bracketed regions.

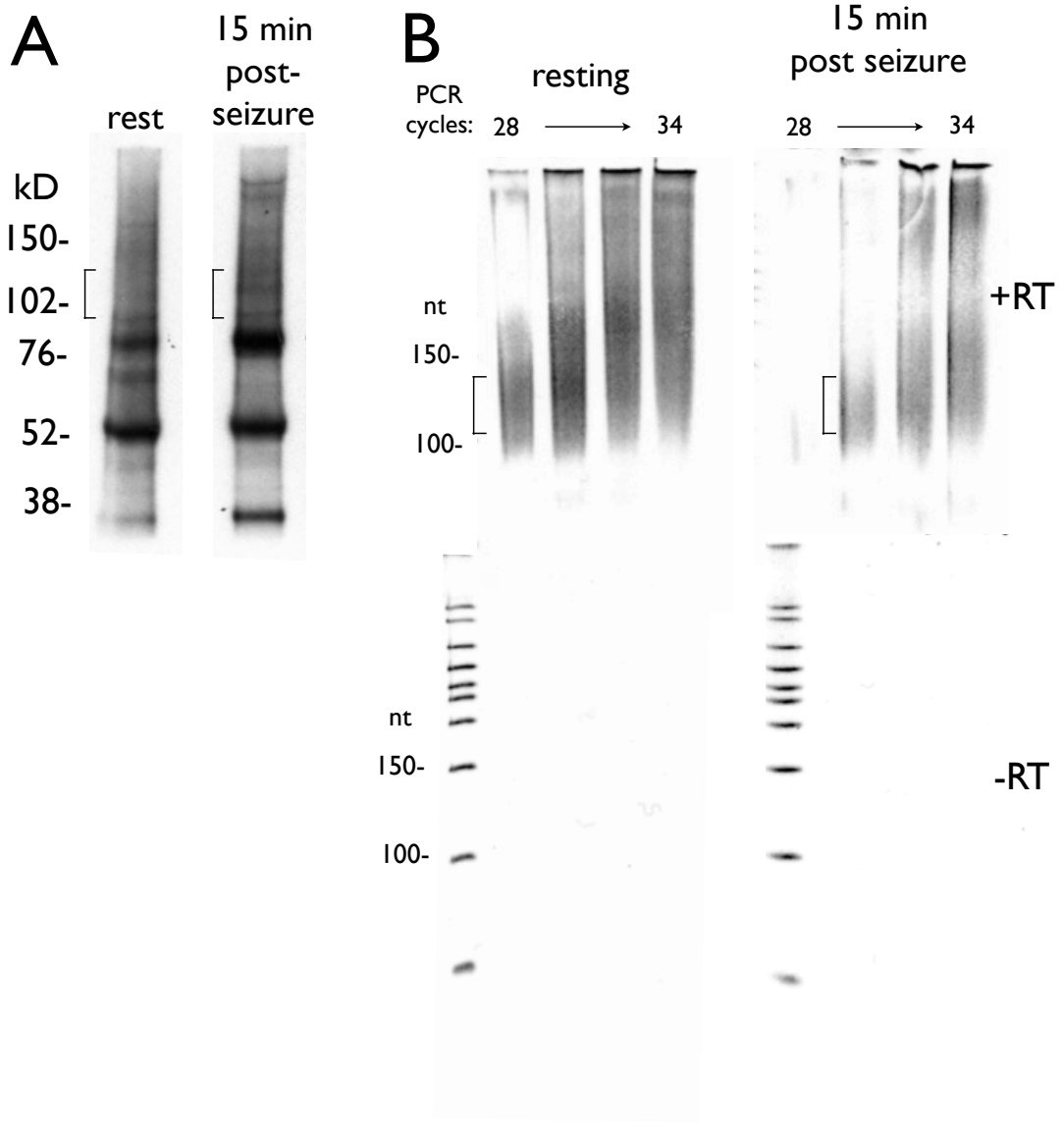
A
rest
15 min
post-
seizure
kD
150-
102-
76-
52-
38-
B
resting
15 min
post seizure
PCR
cycles:
28
34
28
34
nt
150-
100-
+RT
nt
150-
100-
-RT

Figure 28. Analysis of FMRP HITS-CLIP from mouse brain after seizure compared to resting mice.

A) The number of exonic tags per gene was highly correlated between seizure and resting samples. 2966 genes with at least 50 tags post-seizure were included for analysis.

B) The overall genomic distribution of CLIP tags was unchanged by seizure.

A

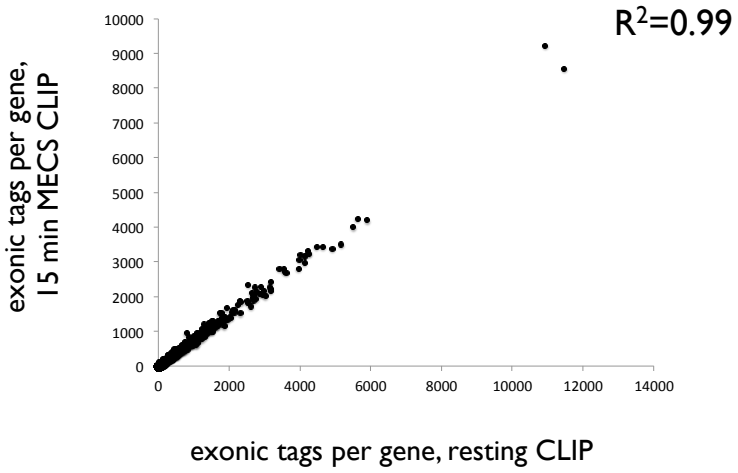

B

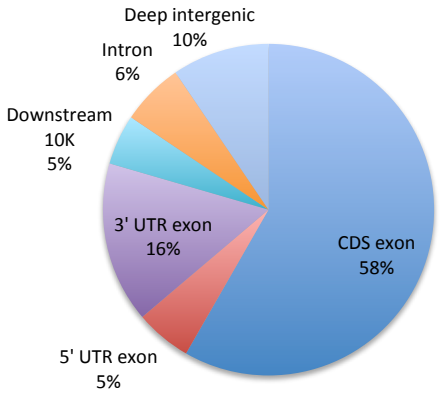

Resting

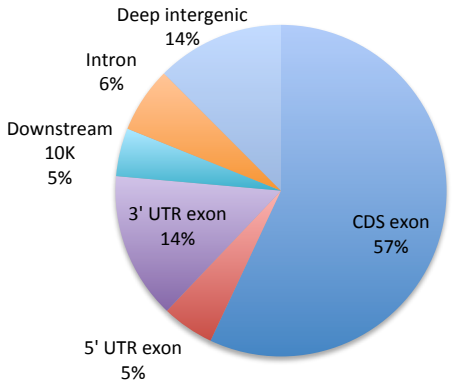

15 min post-seizure

Figure 29. Comparison of FMRP CLIP tag distributions in resting mice and mice subjected to seizure by MECS.

CLIP tags are represented as small rectangles above the RefSeq gene map. Two tag tracks are plotted; the name of each is above the track (resting versus 15 minutes post-seizure). The lengths of the tags are all similar; note that the scale of the middle panel is decreased to accommodate the longer sequence of *Jarid1*. The genes shown here (from top to bottom on this page: *Egr1*, *Jarid1d* and *Fos*; from top to bottom on next page: *Npas4* and *Homer1* (3' end only)) all have increased numbers of FMRP CLIP tags after seizure. However, tag distributions appear unchanged. On the following page, the 3' end of *Homer1* is shown to illustrate that FMRP CLIP tags map to regions downstream of both 3'UTRs, suggesting that these 3'UTRs may have unannotated extensions.

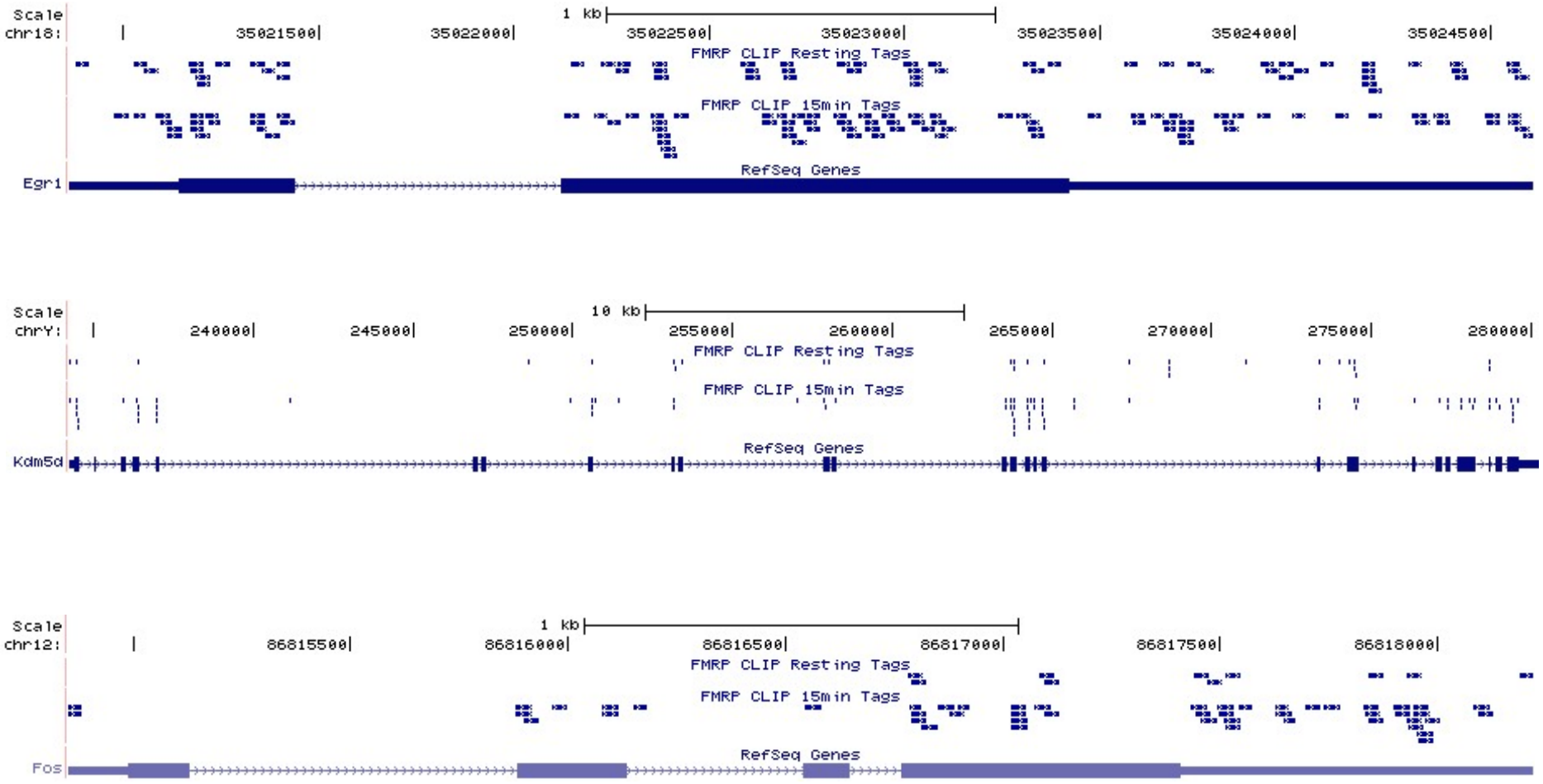
Scale
chr18:
1 kb
35021500
35022000
35022500
35023000
35023500
35024000
35024500
FMRP CLIP Resting Tags
FMRP CLIP 15min Tags
RefSeq Genes
Egr1
Scale
chrY:
10 kb
240000
245000
250000
255000
260000
265000
270000
275000
280000
FMRP CLIP Resting Tags
FMRP CLIP 15min Tags
RefSeq Genes
Kdm5d
Scale
chr12:
1 kb
86815500
86816000
86816500
86817000
86817500
86818000
FMRP CLIP Resting Tags
FMRP CLIP 15min Tags
RefSeq Genes
Fos

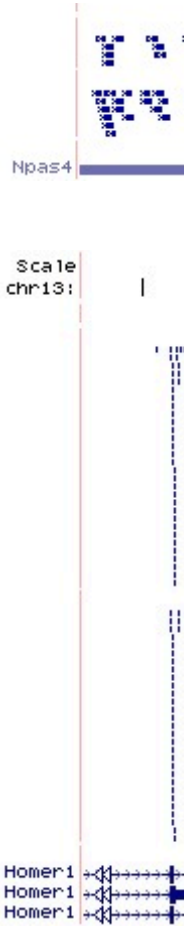
Npas4
Scale
chr13:
Homer1
Homer1
Homer1

Figure 30. Purification of free (cytosolic) and membrane-associated polyribosomes from mouse brain, pilot methods.

Calnexin was used as a marker of ER membranes and Gapdh was used as a cytosolic marker.

A) Pelleting of microsomes from postmitochondrial supernatant. Western blots of pellet and supernatant show substantial contamination of the microsome pellet with cytosolic protein.

B) Isopycnic floatation of microsomes from 2.15M sucrose into 1.3M sucrose (extract was layered under the 2.0M sucrose layer). Western blot of gradient fractions showed that while some microsomes floated to the 1.3M layer, a large portion of microsomes remained stuck in the 2.15M layer.

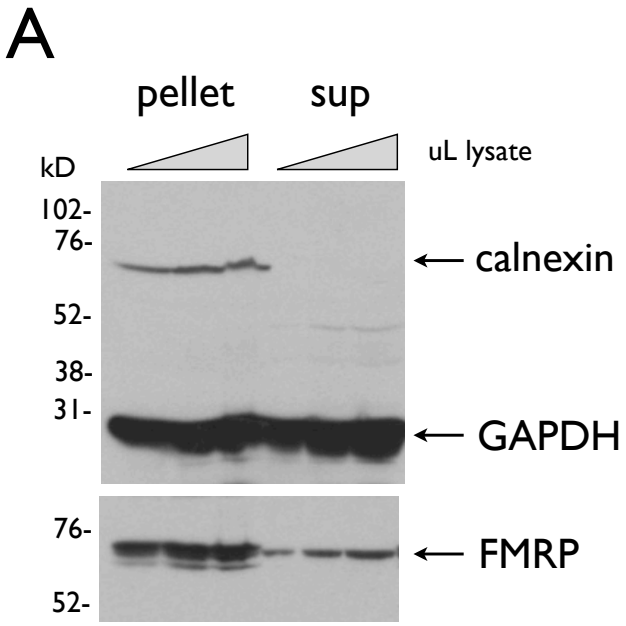
A
pellet
sup
uL lysate
kD
102-
76-
52-
38-
31-
calnexin
GAPDH
76-
52-
FMRP

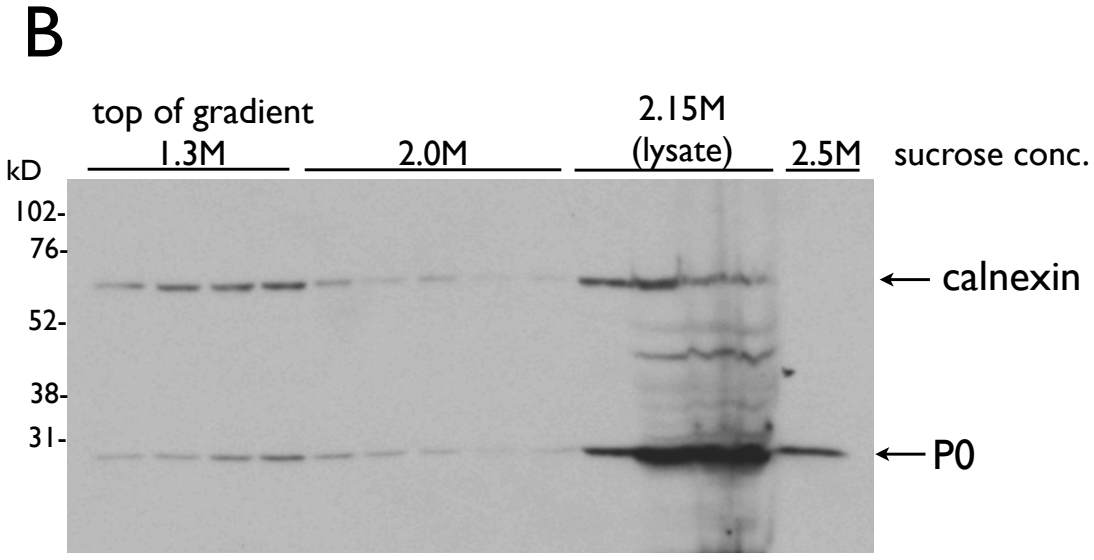
B
top of gradient
1.3M
2.0M
2.15M
(lysate)
2.5M
sucrose conc.
kD
102-
76-
52-
38-
31-
calnexin
P0

Figure 31. Purification of free (cytosolic) and membrane-associated polyribosomes from mouse brain, final method.

Calnexin was used as a marker of ER membranes; GAPDH was used as a cytosolic marker.

A) Separation of free polysomes and microsome-associated polysomes on a discontinuous sucrose gradient (extract was layered on the top of the gradient). Western blots of gradient fractions showed good separation of cytosol, microsomes and free polysomes. Polysomes were present in both microsome and free polysome fractions, as indicated by presence of ribosomal protein P0.

B) Pooled, volume-normalized microsome-associated and free polysome fractions were reprobed by Western blot to more accurately quantify FMRP and calnexin association with each fraction. Approximately equal amounts of FMRP were present in each pool.

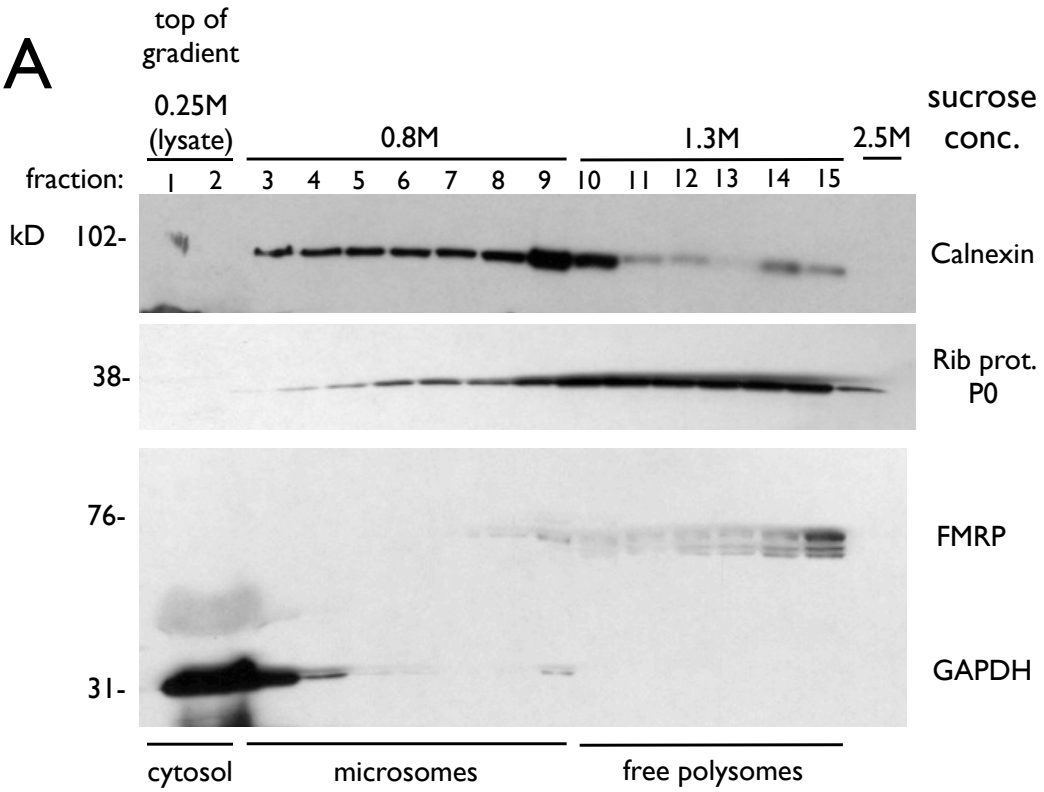
A
top of gradient
0.25M (lysate)
0.8M
1.3M
2.5M
sucrose conc.
fraction:
1 2 3 4 5 6 7 8 9 10 11 12 13 14 15
kD
102-
Calnexin
38-
Rib prot. P0
76-
FMRP
31-
GAPDH
cytosol
microsomes
free polysomes

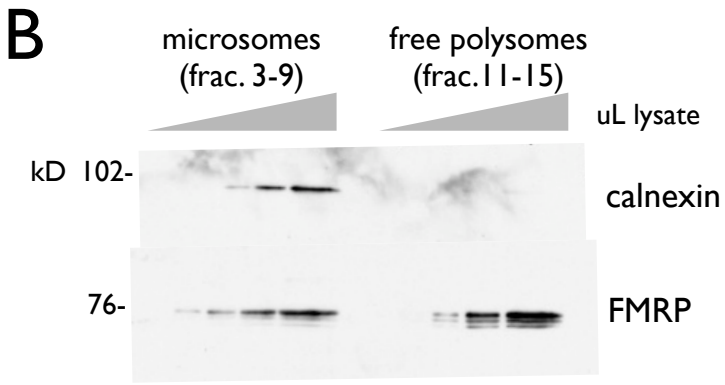
B
microsomes (frac. 3-9)
free polysomes (frac.11-15)
uL lysate
kD
102-
calnexin
76-
FMRP

Figure 32. Fractions of individual mRNAs associated with membranes.

mRNAs from membrane-associated and cytosolic fractions (see previous figure) were analyzed by RNA Seq and the relative fraction of each mRNA in the membrane-associated pool was calculated. The values for all 8355 mRNAs with total (free + membrane associated) RPKM values of at least 10 are plotted. Most mRNAs were present in both membrane-associated and cytosolic fractions.

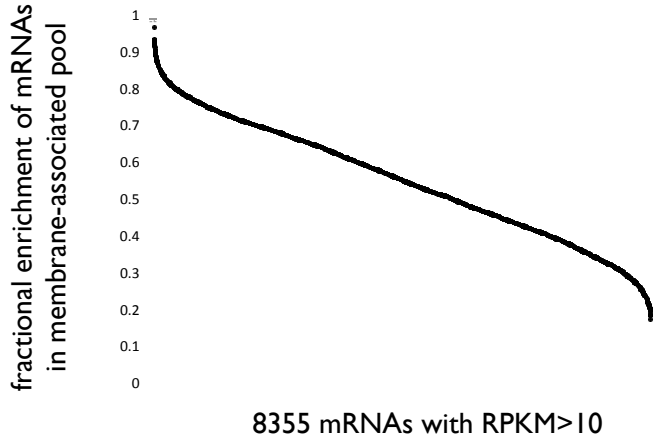
fractional enrichment of mRNAs in membrane-associated pool
1
0.9
0.8
0.7
0.6
0.5
0.4
0.3
0.2
0.1
0
8355 mRNAs with RPKM>10

Table 6: GO analyses of mRNAs enriched in membrane and cytosolic fractions isolated from mouse brain.

All mRNAs enriched at least 70% in either fraction were analyzed. The top terms from each category are shown. The GO categories for biologic process, cellular compartment and molecular function are shown, as well as UniProt keywords.

Membrane-associated mRNAs			
Category	**Term**	**Count**	**PValue**
GOTERM_MF_FAT	GO:0022803~passive transmembrane transporter activity	65	1.5E-13
GOTERM_MF_FAT	GO:0015267~channel activity	65	1.5E-13
GOTERM_MF_FAT	GO:0022838~substrate specific channel activity	63	9.8E-13
GOTERM_MF_FAT	GO:0046873~metal ion transmembrane transporter activity	56	2.2E-12
GOTERM_MF_FAT	GO:0005216~ion channel activity	62	2.5E-12
GOTERM_MF_FAT	GO:0015293~symporter activity	30	3.3E-10
GOTERM_MF_FAT	GO:0022836~gated channel activity	51	3.8E-09
GOTERM_MF_FAT	GO:0031420~alkali metal ion binding	39	9.0E-09
GOTERM_CC_FAT	GO:0031224~intrinsic to membrane	856	3.6E-153
GOTERM_CC_FAT	GO:0016021~integral to membrane	829	1.2E-152
GOTERM_CC_FAT	GO:0005576~extracellular region	128	8.7E-14
GOTERM_CC_FAT	GO:0005783~endoplasmic reticulum	182	9.1E-13
GOTERM_CC_FAT	GO:0044421~extracellular region part	63	4.1E-09
GOTERM_CC_FAT	GO:0005615~extracellular space	43	2.8E-06
GOTERM_CC_FAT	GO:0005887~integral to plasma membrane	56	3.0E-06
GOTERM_CC_FAT	GO:0031226~intrinsic to plasma membrane	58	3.8E-06
GOTERM_BP_FAT	GO:0006811~ion transport	122	2.8E-20
GOTERM_BP_FAT	GO:0030001~metal ion transport	80	7.4E-15
GOTERM_BP_FAT	GO:0006812~cation transport	89	8.5E-14
GOTERM_BP_FAT	GO:0048878~chemical homeostasis	68	3.3E-10
GOTERM_BP_FAT	GO:0043413~biopolymer glycosylation	26	2.4E-09
GOTERM_BP_FAT	GO:0070085~glycosylation	26	2.4E-09
GOTERM_BP_FAT	GO:0006486~protein amino acid glycosylation	26	2.4E-09
GOTERM_BP_FAT	GO:0009100~glycoprotein metabolic process	36	2.8E-09
SP_PIR_KEYWORDS	transmembrane	820	1.9E-218
SP_PIR_KEYWORDS	membrane	915	1.4E-143
SP_PIR_KEYWORDS	glycoprotein	507	2.9E-135
SP_PIR_KEYWORDS	signal peptide	367	8.5E-89
SP_PIR_KEYWORDS	disulfide bond	249	3.4E-54
SP_PIR_KEYWORDS	endoplasmic reticulum	161	1.7E-22
SP_PIR_KEYWORDS	Signal-anchor	82	9.2E-22
SP_PIR_KEYWORDS	ion transport	104	2.6E-19
SP_PIR_KEYWORDS	Secreted	106	9.9E-19
SP_PIR_KEYWORDS	receptor	108	2.0E-15

Cytosolic mRNAs			
Category	Term	Count	PValue
GOTERM_MF_FAT	GO:0001882~nucleoside binding	100	7.00E-10
GOTERM_MF_FAT	GO:0000166~nucleotide binding	135	8.00E-10
GOTERM_MF_FAT	GO:0030554~adenyl nucleotide binding	99	9.80E-10
GOTERM_MF_FAT	GO:0001883~purine nucleoside binding	99	1.30E-09
GOTERM_MF_FAT	GO:0005524~ATP binding	94	2.10E-09
GOTERM_MF_FAT	GO:0032559~adenyl ribonucleotide binding	94	4.20E-09
GOTERM_MF_FAT	GO:0017076~purine nucleotide binding	115	7.10E-09
GOTERM_MF_FAT	GO:0032553~ribonucleotide binding	110	2.90E-08
GOTERM_CC_FAT	GO:0005829~cytosol	49	1.40E-07
GOTERM_CC_FAT	GO:0030684~preribosome	6	8.20E-05
GOTERM_CC_FAT	GO:0031980~mitochondrial lumen	21	1.00E-04
GOTERM_CC_FAT	GO:0005759~mitochondrial matrix	21	1.00E-04
GOTERM_CC_FAT	GO:0031974~membrane-enclosed lumen	73	2.10E-04
GOTERM_CC_FAT	GO:0043233~organelle lumen	71	2.20E-04
GOTERM_CC_FAT	GO:0070013~intracellular organelle lumen	70	3.50E-04
GOTERM_CC_FAT	GO:0030529~ribonucleoprotein complex	36	6.60E-04
GOTERM_BP_FAT	GO:0044275~cellular carbohydrate catabolic process	22	4.70E-17
GOTERM_BP_FAT	GO:0006007~glucose catabolic process	20	7.80E-16
GOTERM_BP_FAT	GO:0046365~monosaccharide catabolic process	20	7.80E-16
GOTERM_BP_FAT	GO:0019320~hexose catabolic process	20	7.80E-16
GOTERM_BP_FAT	GO:0016052~carbohydrate catabolic process	22	1.20E-15
GOTERM_BP_FAT	GO:0046164~alcohol catabolic process	21	2.40E-15
GOTERM_BP_FAT	GO:0006096~glycolysis	17	5.10E-14
GOTERM_BP_FAT	GO:0006006~glucose metabolic process	26	4.40E-12
SP_PIR_KEYWORDS	phosphoprotein	313	6.70E-17
SP_PIR_KEYWORDS	acetylation	213	1.60E-31
SP_PIR_KEYWORDS	cytoplasm	168	6.20E-10
SP_PIR_KEYWORDS	nucleus	147	8.50E-03
SP_PIR_KEYWORDS	nucleotide-binding	104	1.10E-10
SP_PIR_KEYWORDS	atp-binding	86	4.00E-11
SP_PIR_KEYWORDS	hydrolase	54	2.70E-02
SP_PIR_KEYWORDS	transferase	54	9.50E-02
SP_PIR_KEYWORDS	mitochondrion	47	2.10E-02
SP_PIR_KEYWORDS	transit peptide	40	9.00E-05

Figure 33. mRNA association with membranes is not correlated with FMRP association or retained ribosome score (RRS).

A) The fractional enrichment of mRNAs in the membrane-associated pool was not correlated with the number of exonic tags per gene in nuclear FMRP CLIP. 444 mRNAs with at least 25 exonic tags in nuclear FMRP CLIP were included in the analysis.

B) The fractional enrichment of mRNAs in the membrane-associated pool was not correlated with the number of exonic tags per gene in whole brain FMRP CLIP. 1625 mRNAs with at least 50 exonic tags in whole brain FMRP CLIP were included in the analysis.

C) The fractional enrichment of mRNAs in the membrane-associated pool was not correlated with the retained ribosome score. The 39 mRNAs for which RRS was measured were included in the analysis.

A

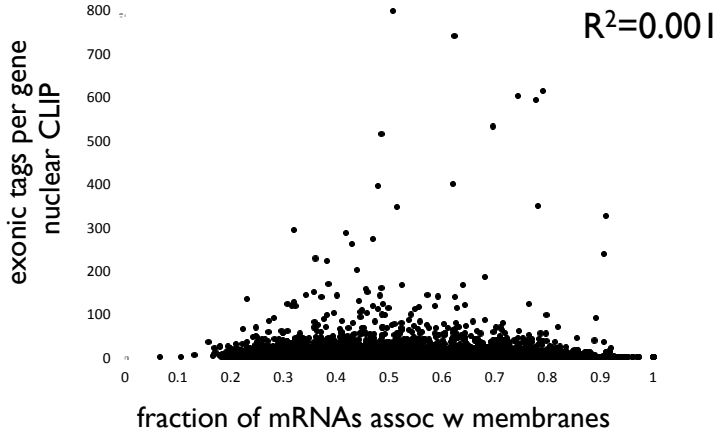
R2=0.001
exonic tags per gene
nuclear CLIP
800
700
600
500
400
300
200
100
0
0
0.1
0.2
0.3
0.4
0.5
0.6
0.7
0.8
0.9
1
fraction of mRNAs assoc w membranes

B

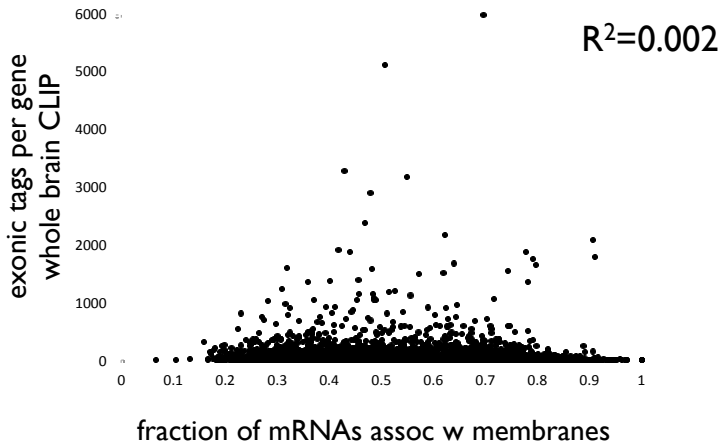
R2=0.002
exonic tags per gene
whole brain CLIP
6000
5000
4000
3000
2000
1000
0
0
0.1
0.2
0.3
0.4
0.5
0.6
0.7
0.8
0.9
1
fraction of mRNAs assoc w membranes

C

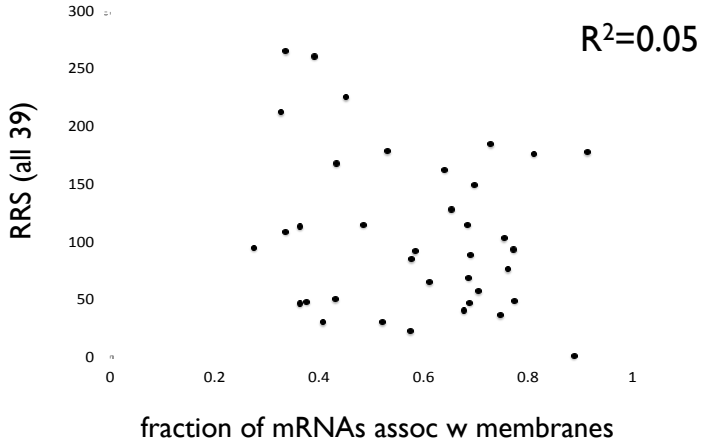
R2=0.05
RRS (all 39)
300
250
200
150
100
50
0
0
0.2
0.4
0.6
0.8
1
fraction of mRNAs assoc w membranes

Chapter V. Design and construction of a new mouse model, the FMRP cTAG mouse

Introduction:

HITS-CLIP results define a set of approximately 1000 mRNAs regulated by FMRP. However, these results are based on immunoprecipitation of transcripts from total brain, reflecting a mixture of mRNAs from all cells expressing FMRP. The brain contains an incredible diversity of neurons, and a more nuanced picture of which mRNAs are regulated by FMRP in individual neuron types is lacking. It is likely that many of the mRNAs targeted by FMRP exhibit restricted expression patterns. For example, PSD-95 and Syngap1 are both strong targets that associate with one another and mediate NMDA receptor signaling (Kim et al., 1998). However, detailed *in situ* analysis revealed that expression of Syngap1 is much more restricted than that of PSD-95, both temporally and spatially (Porter et al., 2005). More generally, the heterogeneity of translational profiles from different neuronal cell types has been demonstrated using immunoprecipitation of GFP-tagged ribosomes (Doyle et al., 2008). Results showed that translatomes from different classes of neurons are highly diverse, and that highly specialized cell types, such as Purkinje neurons, have translational profiles with relatively low similarity to other cell types. Importantly, many mRNAs that were of low abundance in whole cell lysate were enriched in rare cell types, emphasizing the point that analysis at the level of individual cell types is critical for understanding the ramifications of gene expression in local context. Furthermore, the authors found that a large fraction of translational diversity was driven by expression of cell-surface proteins such as receptors and ion channels, transcription factors, and calcium-binding proteins, a set that overlaps the population of mRNAs regulated by FMRP. Additional observations underscoring the importance of cell type-specific molecular analysis include preliminary data from cell-specific HITS-CLIP results in motor neurons for the splicing factor Nova (see below), as well as results from cell type-specific miRNA profiling experiments that reveal distinct complements of miRNAs in different populations of neurons (He et al., 2012). Cell type-specific molecular targeting has also been used to label discrete populations of dorsal root ganglia neurons, allowing complex anatomies of axonal endings to be visually resolved and mapped (Li et al., 2011), and to acutely inhibit activity of individual populations of neurons in conscious mice (Ray et al., 2011). Collectively, these studies show that

analysis at the level of individual cell types can uncover biology unobservable in whole-tissue studies due to heterogeneity of gene expression and diversity of neuronal physiology.

We are most interested in the FMRP targets that significantly contribute to FXS phenotypes. Not all mRNAs regulated by FMRP can be expected to make equal contributions to the pathology of the syndrome. Regulatory effects of FMRP have to compete with other drivers of protein dynamics, including other mechanisms of translational control as well as transcriptional control and protein turnover. Furthermore, targets must be dose-dependent enough in local context for the net outcome to matter to the cell. It is likely that exact dosage of certain proteins is indeed critical for neuronal function. For example, Shank3, a strong FMRP target closely linked to autism, is degraded via ubiquintylation when not in complex with Homer proteins, suggesting that the amount of existing Shank3 is titrated to fit local scaffolding needs (Bangash et al., 2011). The reduction in Shank3 levels was associated with defects in synaptic plasticity and social interaction in mice, demonstrating functional consequences of degradation. In a second example, a screen for protein-level changes at PSDs during activity identified ten proteins whose local abundance was decreased during synaptic activity (Ehlers, 2003). Three of these, Shank, GKAP and AKAP79, were ubiquitinylated, suggesting local degradation of scaffolding proteins might be a general driver of changes in overall PSD composition during activity. In support of this finding, Bingol et al also observed increased ubiquitinylation of synaptic substrates during activity, and found that this was associated with proteasomal movement into dendritic spines (Bingol and Schuman, 2006). Overall, these results support the assertion that dose-dependence of many proteins is critical to neuronal function, and thus translational regulatory actions of FMRP are predicted to be of significant importance. However, we must be able to define which expression changes are most relevant to FXS phenotypes.

To do this, we must link phenotypes to the regulation of particular mRNAs with the highest possible degree of resolution. The barrel cortex has been a useful system for characterization of very specific developmental defects in *Fmr1* KO mice. For example,

development of the thalamocortical synapse that mediates input to the barrel is delayed in *Fmr1* KO mice, resulting in an increased number of silent synapses persisting through the first postnatal week and a commensurately extended window of LTP at these synapses (Harlow et al., 2010). *Fmr1* KO mice also exhibit a significant delay in the next stage of barrel cortex development, formation of the major ascending projection from layer 4 onto layer 3 (Bureau et al., 2008). As for defects seen during thalamocortical synapse development, defects in development of the L4:L3 synapse are transient: they are evident during the second postnatal week but normalized by the third postnatal week. Together, these papers show that FMRP function is of particular importance during discrete critical periods at specific synapses, and future work will likely further elucidate such roles. However, it has not yet been shown that cell-autonomous loss of FMRP in layer 4 neurons results in the observed phenotypes. Use of the conditional *Fmr1* KO to establish that loss of FMRP in specific cells results in particular phenotypes will be crucial to efforts to identify functionally important FMRP:RNA interactions.

Two such uses of the conditional *Fmr1* KO have been published. The most recent investigated the role of FMRP in adult neurogenesis in the dentate gyrus. The authors found that loss of FMRP in adult neural stem cells (aNSCs) resulted in multiple abnormal phenotypes in stem cell progenitors, including defects in proliferation, differentiation and dendritic arbor complexity (Guo et al., 2011). Importantly, these phenotypes were associated with behavioral consequences and were correctable by conditional expression of FMRP in aNSCs in *Fmr1* KO mice. Although this would be an obviously attractive system for the study of cell-autonomous mRNA regulation by FMRP, HITS-CLIP is not sufficiently sensitive at this time to support analysis of such a small population of cells. An appealing alternative system is offered by the first published use of the conditional *Fmr1* KO mouse, in which it was found that loss of FMRP in Purkinje neurons resulted in defects in eyeblink conditioning, a form of classical conditioning that reflects the ability of an animal to learn to anticipate a puff of air to the eye when it is preceded by playing of a tone (Koekkoek et al., 2005). Defects in eyeblink conditioning were also observed in FXS patients, underscoring the relevance of this phenotype to human disease (Koekkoek et al., 2005). Knockout of FMRP in Purkinje neurons also resulted in

increased mGluR-LTD at Purkinje cell – parallel fiber synapses, a form of LTD that is depended on protein synthesis (Karachot et al., 2001) and for which the molecular underpinnings are fairly well understood (Kano et al., 2008), and elongation of dendritic spines at these synapses. Together, these phenotypes are extremely relevant to FXS biology and promise to be informative with respect to FMRP function.

Recent experiments in our lab offer proof in principle that cell type-specific HITS-CLIP is a productive approach generating novel results not discernable by general HITS-CLIP. HITS-CLIP performed on AcGFP-Nova driven from the motor neuron-specific choline O-acetyltransferase (Chat) promoter, using AcGFP as an IPable tag, successfully identified a set of motor neuron-enriched transcripts regulated by Nova (Y. Yuan, unpublished). However, the design of this experiment has one potentially significant drawback, which is that protein expressed from a BAC is likely to be overexpressed and may not exhibit normal expression patterns compared to wt protein. In the case of FMRP, this may constitute a serious problem. Overexpression of FMRP has been shown to result in aberrant phenotypes, including hypoactivity, increased anxiety and reduced mGluR-LTD in mice and defects in flying, rough eyes, underelaboration of neuromuscular junction synapses and increased death in flies ((Peier and Nelson, 2002), (Hou et al., 2006), (Zhang et al., 2001)). More subtly, activation of group I mGluRs in hippocampal slices results in a burst of *Fmr1* translation that raises FMRP levels by 40% (Hou et al., 2006). This increase is transient (lasting approximately 5 minutes), due to ubiquitinylation and degradation of FMRP shortly after the translational burst. Together, these actions produce a rapid, sharp increase and decrease of FMRP levels in response to synaptic activity. There have also been reports of FMRP levels increasing in response to activity *in vivo*. In one study, dark-reared rats were acutely exposed to light, resulting in a transient increase in FMRP in visual cortex after 15 minutes (Gabel et al., 2004). In another study, whisker stimulation resulted in increased FMRP levels in barrel cortex, although over a longer timescale (4 hours) (Todd et al., 2003). Together, these results suggest that FMRP levels are tightly regulated in response to synaptic activity, indicating that maintenance of wildtype expression levels for tagged constructs may be of paramount importance.

Results:

Construct design and targeting

We engineered a new mouse model, the conditionally tagged AcGFP-FMRP ("cTAG") mouse, to allow cell type-specific HITS-CLIP of AcGFP-FMRP expressed at endogenous levels while also maintaining normal wt FMRP expression in cells not expressing AcGFP-FMRP. Based on the reports discussed above that FMRP levels are acutely regulated in response to activity and overexpression of FMRP results in aberrant phenotypes, we opted to create a knock-in mouse in order to maintain normal expression levels and patterns of FMRP. We also wished to maintain normal wt FMRP expression in neurons not expressing AcGFP-FMRP, so that synaptic inputs from these cells onto neurons expressing the tagged allele would be normal. To meet these criteria, we designed a bifunctional construct in which either wt FMRP or AcGFP-FMRP can be expressed from the same allele, based on floxing the endogenous terminal exon of *Fmr1* (exon 17) and adding an alternative, downstream AcGFP-tagged terminal exon (**Figure 34**). In the presence of Cre, the endogenous terminal exon, including the entire 3'UTR, is excised, and the downstream, tagged terminal exon (which also includes the entire 3'UTR) is used. In the absence of Cre, the endogenous terminal exon is used, resulting in wt expression of FMRP.

AcGFP was selected for use as an IPable tag because protein tags can generally be IPed with higher efficiency than peptide tags such as HA (personal communication, Mike Rout). AcGFP is a monomeric alternative to EGFP, avoiding potential problems arising from nonphysiologic dimerization of AcGFP-FMRP via the tag. Sucrose gradient analysis was performed on 293T cells transfected with AcGFP-FMRP, to confirm that tagging FMRP with AcGFP does not alter its polysome association (**Figure 35**). A conservative point mutation was made in AcGFP to destroy a Bsu36I site for cloning purposes. Finally, AcGFP was cloned in-frame with *Fmr1* exon 17, replacing the *Fmr1* stop codon with the same Gly-Pro-Val swivel as used in pFMRP-AcGFP in Figure 35, using overlap extension PCR (Nelson and Fitch, 2011).

The cTAG targeting vector was constructed using a hybrid approach of recombineering plus standard cloning. Recombineering offers an efficient method of cloning based on homologous recombination in *E. coli* that does not require use of restriction endonucleases or DNA ligases (Copeland et al., 2001). We used a modified version of the BAC host strain DH10B called SW106, in which the lambda phage Red system is integrated into the host genome. The Red system encodes three proteins, Exo, Beta and Gam, under a temperature-sensitive promoter. Exo is a 5'-to-3' exonuclease that creates overhangs on linear dsDNA targeting cassettes. Beta then binds these ssDNA overhangs and promotes recombination with homologous regions in host plasmids, assisted by Gam, which inhibits the endogenous recombinase recBCD. Expression of the Red proteins is undetectable at 32°C, yet reaches high levels after 15 minutes at 42°C. Together with inhibition of endogenous recombinase activity by Gam, this results in a system in which the potential for homologous recombination is restricted to a discrete induction window, limiting unwanted recombination events. Overall, this system offers highly efficient rates of recombination with as little as 50nt of homology. 14.3kB of sequence of *Fmr1* was subcloned into PL253 from the BAC RP23-149C7 (which is derived from C56BL/6 mice) in the SW106 recombineering strain, taking advantage of the gap repair activity inherent in this system. Briefly, 500nt "arms" homologous to either end of the *Fmr1* fragment were cloned into PL253, which was then cut between the arms, resulting in a linearized plasmid with one homology arm on each end. This vector was electroporated into SW106 cells carrying the RP23-149C7 BAC and induction of the Red genes resulted in efficient retrieval of the 14.3kB sequence by recombination of the PL253 arms with homologous regions of the BAC (in 10 out of 12 miniprepped clones) (**Figure 36**). A correct clone was purified by re-transformation and sequenced.

Next, targeting of the upstream "lone" lox site was achieved by PCR amplification of a neomycin cassette from PL452 using primers containing the 34nt loxP sequence and short 5' sequences homologous to the flanking regions of the targeting locus (**Figure 36**). The PCR product was transfected into SW106 cells containing PL253 with the retrieved *Fmr1* sequence. Induction of the Red genes resulted in insertion of the lox-neo-lox

sequence 439nt upstream of *Fmr1* exon 17, in 14 out of 14 miniprepped clones. The lox-neo-lox cassette was then reduced to a single lox site by arabinose induction of Cre.

The remainder of the insert (see below) was assembled in pCR4-TOPO and then subcloned into PL253 using a native unique restriction site, Bsu36I, that exists 0.8kB downstream of the *Fmr1* 3'UTR (**Figure 37**). This insert could not be targeted by recombineering due to extensive homology between the two copies of exon 17. Use of this native site allowed homology to be uninterrupted downstream of AcGFP, so that the downstream copy of the *Fmr1* 3'UTR, which is 2.4kB, contributed to the total 5.9kB length of the 3' homology arm used for embryonic stem cell (ES cell) targeting. This limited the total nonhomologous length of the targeting construct to 7kB, and limited total plasmid size (including left and right homology arms of 7.9kB and 5.9 kB, respectively) to 26.2kB. If we had not used this strategy, the nonhomologous region would have been 9.4kB and we would have also needed to increase the length of the homology arms, resulting in a final plasmid size of approximately 34kB, which would have been much more difficult to handle.

The insert assembled in pCR4-TOPO consisted of a Proudfoot minimal polyadenylation sequence (Levitt et al., 1989), an Frt-Neo-Frt-lox cassette and the AcGFP-tagged version of *Fmr1* exon 17 generated by overlap extension PCR (**Figure 37**). We positioned the Proudfoot polyA sequence downstream of the native polyA site as a backstop to prevent transcriptional read-through and ensure that splicing to the downstream, tagged exon would not occur in the absence of Cre. The Frt-Neo-Frt-lox cassette allows selection in ES cells and also introduces the second lox site. Overall, elements (including the upstream lox site described earlier) were placed well away from annotated exons and conserved regions. This is important to avoid placing elements in unannotated extensions of 3'UTRs and to avoid interference with potential splicing factor binding sites. Final cloning into PL253 involved ligation of a 6.5kB insert into a 19.7kB vector. This ligation was achieved after significant optimization of conditions using a 3:1 molar ratio of insert to vector with a 25ng/uL total DNA concentration and overnight incubation of the ligase. Although such a high DNA concentration typically causes ligation to result only in end-

to-end linear products, in this case because the fragments were so large, their molar concentrations were appropriate. Ultimately, one correct ligation product was obtained out of 28 miniprepped clones. The cloning junctions were sequenced and three different restriction digests generating 7-10 bands each were performed, confirming that the construct was correct (**Figure 38**).

The construct was targeted in male albino C57BL/6 ES cells by the Genome Targeting Resource Center and one correct clone was identified out of 200 based on Southern blots. The Southern blotting strategy is described in **Figure 39a-e**. Probes were less than 300nt in length and had specific activities on the order of 10^9. The primary Southern screen identified seven out of 200 clones containing the Neo selection cassette (**Figure 39a**). These seven clones were then further tested by Southern blotting to confirm presence of the lone lox and AcGFP elements (**Figure 39b,c**). Three of seven clones contained both these elements. However, two of the three (#70 and #89) also contained bands that appeared as if the clones were mixed with wt cells. Upon repurification, these clones did not appear correct. This left clone #189 as the only clone containing all three elements (lone lox site, FNF cassette and AcGFP-tagged exon). To check for internal duplications or rearrangements, the clones were subjected to further Southern blotting using internal probes (**Figure 39d,e**). Clone #189 again appeared correct in both blots.

To test for correct Cre-dependent recombination, ES cells from clone #189 were transfected with pPAC-Cre to induce expression of AcGFP-FMRP. A portion of the transfected cells were selected with puromycin to enrich for cells expressing Cre, since the Gene Targeting facility typically observes transfection rates for ES cells on the order of 1%. RNA was prepared from –Cre, +Cre and +Cre/+puro cells and reverse transcribed products were PCR amplified using primers in exon 16 and the 3'UTR. This resulted in a 0.6kB or 1.3kB product depending on whether or not AcGFP was included in the mRNA. The 1.3kB product was expected to be rare due to low Cre transfection rates. To facilitate detection of rare products, ^{32}P-dCTP was added to the last two cycles of the PCR reaction and products were visualized by urea-PAGE. A high molecular weight

band consistent with the expected size for AcGFP inclusion was observed in the +Cre samples, with expected enrichment in the puromycin-selected sample (**Figure 40**).

ES cells from clone #189 were then injected into C57BL/6 blastocysts with successful production of 12 chimeric males (3 grade A, 3 grade B, 6 grade C and 2 grade D). Use of albino C57BL/6 ES cells allowed chimeras to be graded on coat color even though both the ES cells and the blastocyst were of the same genetic background (thus eliminating the need for backcrossing). The ten best chimeras were mated to female albino C57BL/6 mice (Jackson Labs #000058). Because *Fmr1* is on the X chromosome, every white, female pup should carry a copy of the cTAG allele **(Figure 41**). Two of the chimeras repeatedly produced all-white litters, indicating that the cTAG allele was fully germline in these animals and providing a reliable source of cTAG het pups. Presence of the cTAG allele was confirmed by genotyping. The Neo selection cassette was removed by crossing the cTAG+/- females to males expressing Flp recombinase under an actin promoter (Jackson Labs #005703).

Characterization of cTAG mice

To confirm correct expression of AcGFP-FMRP, a germline cTAG male chimera was crossed with a female expressing Cre driven by the adenovirus EIIa promoter, which is expressed early in development (before implantation to the uterine wall) and in a wide variety of tissues including brain. This cross resulted in Cre+, cTAG/+ mice that expressed both tagged and untagged versions of FMRP, allowing direct comparison of the two. As a control, a germline chimera was also bred to a female albino C57BL/6 mouse, resulting in Cre-, cTAG/+ mice. Brain lysates from each were fractionated over 20-50% sucrose gradients and blotted with an antibody against FMRP that recognizes both wt FMRP and AcGFP-FMRP. Both forms of FMRP were of anticipated molecular weights and were present in roughly equal ratios in +Cre mice (**Figure 42**). No AcGFP-FMRP was observed in –Cre lysate. Although expression of AcGFP-FMRP did not appear to result in a commensurate decrease in expression of wt FMRP compared to the –Cre mouse, the +Cre mouse used in this experiment was six days younger than the –Cre mouse, and thus expressed higher levels of FMRP overall. Importantly, wt FMRP and

AcGFP-FMRP were identically distributed on polysome gradients (**Figure 43**). No AcGFP-FMRP was observed on polysomes from –Cre lysate (a more stringent test of expression, since polysome-associated proteins can often be detected on gradient purifications even when undetectable in total lysates), even when the film was overexposed. RNA was prepared from these lysates as before and reverse transcribed products were PCR amplified as before using primers in exon 16 and the 3'UTR and with the addition of ^{32}P-dCTP in the final two cycles. Two products of expected sizes (0.6kB and 1.3kB) were observed in the +Cre samples, expressed at more equivalent levels than was observed for Cre-transfected ES cells (**Figure 42**). Although the 1.3kB product was somewhat less strongly detected, this was expected due to mosaic expression of EIIa-Cre and less efficient amplification of larger PCR products.

To further characterize expression of the cTAG allele, protein lysates and RNA were prepared from a panel of 16 mice varying in *Fmr1* genotype, Cre expression, and retention of the Neo selection cassette (**Table 7, Figure 44**). Importantly, Western blot analysis showed that mice homozygous for the cTAG allele expressed normal levels of wt FMRP in the absence of Cre, showing that the cTAG allele is truly bifunctional. In mice expressing Cre, AcGFP-FMRP was detected at levels commensurate with the strength and expression pattern of the Cre driver (note that our male EIIa Cre mouse expressed extremely low levels of Cre, unlike its female counterpart and consistent with this line exhibiting mosaicism). AcGFP-FMRP bands reacted with both the 17722 FMRP antibody and two different GFP antibodies. Unexpectedly, removal of the Neo selection cassette resulted in a low level of leaky AcGFP-FMRP expression in the absence of Cre. Although we are unsure why this occurs, one possibility is that removal of the Neo cassette might change the nucleosome context of the associated lox site, which could in theory promote some level of Cre-independent recombination. To more carefully quantify relative levels of wt *Fmr1* and *AcGFP-Fmr1*, QPCR primers were designed to amplify the region between exon 16 and either the 3' end of exon 17 (to quantify total *Fmr1* mRNA from both wt and cTAG alleles) or the 5' end of AcGFP (to quantify mRNA from the cTAG allele alone). Two sets of primers were designed for each region, to ensure consistency of results. Amplicons were all within range of

efficient QPCR amplification (130-192nt). Primer efficiencies were measured using serial dilutions and all had near-perfect efficiencies of 1.97-2.01. Melt curves and –RT controls were also performed. QPCR analysis showed that *AcGFP-Fmr1* was expressed in a dose-dependant manner: 26% of total *Fmr1* mRNA in a cTAG/+ mouse under the EIIa Cre driver, 45% in a cTAG/+ mouse under the panneuronal Emx1 Cre driver, and 59% in a cTAG/Y mouse under the Emx1 driver. *AcGFP-Fmr1* mRNA constituted 6%-7% of total *Fmr1* mRNA in –Cre, -Neo cTAG/Y mice, indicating a moderate level of leaky Cre-independent AcGFP-FMRP expression upon removal of the Neo cassette. In future experiments, AcGFP-FMRP may be expressed in a minor fraction of cells, thus, leaky expression at low levels in the majority of cells is a major concern. However, leaving the Neo cassette in place is not expected to interfere with expression of wt FMRP from the cTAG allele, since Neo is downstream of the polyA site and transcription of Neo occurs in same direction as *Fmr1*. It is also unlikely that transcription of the GFP-tagged exon occurs from the Neo promoter, as we do not observe any aberrant short GFP-positive isoforms by Western. Finally, the Neo cassette will not interfere with expression of AcGFP-FMRP, as it will be floxed out upon Cre expression. Therefore, the Neo cassette was left in place in the final cTAG mouse.

Alternative splicing of *Fmr1* likely plays an important role in the function of FMRP. For example, exon 12, which encodes part of the KH2 domain critical for FMRP function, is alternatively spliced. In addition, exons 15 and 17 have three and two splice acceptor sites, respectively, and use of the downstream splice acceptor sites for exon 15 excludes FMRP's major phosphorylation site (Ser499 in mouse). Although AcGFP-FMRP typically appears as a single band on Western, multiple isoforms can be detected with use of commercial gradient gels (**Figure 42**). To characterize the splicing of *AcGFP-Fmr1*, RNA was prepared from cTAG/Y mice +/-Cre, as well as from wt mice. This allowed comparison of *AcGFP-Fmr1*, *Fmr1* expressed from the cTAG allele, and *Fmr1* expressed from the wt allele. Reverse transcribed products were PCR amplified as before using primers in exon 11 and either exon 17 (for the –Cre mice) or in AcGFP (for the +Cre mice, in order to select for *AcGFP-Fmr1* isoforms). Hot ^{32}P-dCTP was added in the final two cycles and products were separated by urea-PAGE for 5 hours. At least four

isoforms of in the expected size range of 580-780nt were observed (**Figure 45**). Reassuringly, all three forms of *Fmr1* mRNA, both tagged and untagged, had the same isoform expression pattern (*AcGFP-Fmr1* products were expected to be slightly larger due to downstream placement of the AcGFP-specific primer).

The best evidence that AcGFP-FMRP is functionally equivalent to wt FMRP would be to show using HITS-CLIP that mRNA binding activity is unaltered, both in terms of identities of targeted transcripts and binding distribution of AcGFP-FMRP on these transcripts. Pilot immunoprecipitations from cTAG/+ brain showed that AcGFP-FMRP was efficiently IPed under stringent wash conditions, while no wt FMRP was detectable (**Figure 46**). To compare mRNA association of AcGFP-FMRP and wt FMRP, HITS-CLIP was performed on AcGFP-FMRP from a +Cre, cTAG/+ brain using GFP antibodies and on FMRP from a wt brain using the 17722 FMRP antibody. CLIP was also performed on wt FMRP from a –Cre, cTAG/Y brain using the 17722 antibody, to show that FMRP expressed from the cTAG allele has normal mRNA associations. Finally, CLIP was performed on a wt brain using GFP antibodies, as a control to show that the signal in the GFP IPs was specific to the presence of GFP. Brains from the appropriate mice in the third postnatal week were rapidly minced under ice-cold buffer and immediately UV crosslinked. Homogenates were treated with DNAse and clarified. Supernatants were then subject to limited RNAse digestion prior to IP. IPs were stringently washed and RNAs were ligated to cold linker on-bead and subsequently ^{32}P labeled. Separation of labeled immunoprecipitates by SDS-PAGE and nitrocellulose transfer showed smears of protein:RNA complexes at the expected molecular weights above FMRP and AcGFP-FMRP protein bands, while no signal was observed for the control IP of GFP from wt lysate. RNA was cut from the nitrocellulose in the indicated regions (**Figure 47**) and further processed according to the standard HITS-CLIP protocol. Separation of products by urea-PAGE again showed RNA smears of expected sizes, while control lanes showed only discrete bands reflecting linker-linker ligation products that predominate in absence of IPed RNA (**Figure 47**). Final samples were sequenced by Illumina. Analysis of the data showed that the three experimental samples were extremely similar, both in terms of exonic tags per gene (all pairwise correlation

coefficients were at least 0.96 for the top 5000 targets, **Figure 48**) and in terms of tag distributions on target mRNAs (**Figure 49**). Finally, the number of exonic tags per gene measured in cTAG CLIP was extremely similar to that measured in FMRP CLIP in previous experiments (R2=0.94) (**Figure 48**). Together, these data provide strong evidence that AcGFP-FMRP is functionally equivalent to wt FMRP and that CLIP studies on the cTAG mouse should be successful.

Discussion:

HITS-CLIP has now been successfully performed on a number of RNA-binding proteins in brain, yielding a rich database of protein:RNA interaction maps ((Chi et al., 2009), (Licatalosi et al., 2008), (Darnell et al., 2011), (Polymenidou et al., 2011)). From these data, it is clear that RBPs extensively regulate neuronal mRNAs in a variety of ways, including splicing, alternative polyadenylation, translational expression and targeting by miRNAs. As informative as they are, these maps do not do justice to the rich complexity of molecular biology in the brain. We can already glimpse that some RBPs, such as Nova and FMRP, regulate networks of mRNAs with related functions. Yet our ability to perceive such networks is limited by experimental intermingling of mRNAs from all types of neurons inherent in whole brain analyses. Cell type-specific translational profiling experiments have begun to reveal the vast diversity of gene expression in different classes of neurons. The ability to perform cell type-specific HITS-CLIP on RBPs expressed from their native loci would dramatically improve our ability to understand the function of RBPs in local context.

To facilitate cell type-specific CLIP without disturbing native expression levels or patterns of FMRP, we have created a knock-in mouse model in which AcGFP-FMRP or wt FMRP can be conditionally driven from the same allele. In the presence of Cre, AcGFP-FMRP is expressed, while normal wt FMRP expression is maintained in surrounding cells in the absence of Cre. Inclusion of AcGFP provides a tag that can be IPed with high stringency and specificity, allowing HITS-CLIP analysis of discrete subpopulations of FMRP:RNA interactions. We have confirmed that both AcGFP-FMRP and wt FMRP expressed from the cTAG allele are expressed at normal levels

compared to FMRP expressed from the wt allele, and both products are of the expected sizes at the RNA and protein levels. AcGFP-FMRP and wt FMRP have identical distributions on sucrose gradients, indicating that AcGFP-FMRP associates normally with polysomes. In the absence of Cre, no AcGFP-FMRP can be detected in +Neo cTAG mice, indicating that the expression of AcGFP-FMRP is tightly restricted to the cell population of interest. Splicing of *AcGFP-FMRP* appears to be normal. Finally, parallel HITS-CLIP experiments performed on both AcGFP-FMRP and untagged FMRP (from both the cTAG and wt alleles) yielded near-identical results, providing final confirmation that use of AcGFP as an IPable CLIP tag is a viable strategy that does not interfere with the mRNA-binding function of FMRP. Overall, the cTAG mouse may be used to investigate FMRP function in any cell type of interest for which specific Cre drivers exist.

The most informative cell type-specific HITS-CLIP analyses will be those in which regulation of specific mRNAs can be linked to cell autonomous phenotypes relevant to neuronal biology and/or human disease. For example, cell autonomous loss of FMRP in Purkinje cells (PCs) has been shown to result in defects in mGluR-LTD at parallel fiber-PC synapses (Koekkoek et al., 2005) PCs are the sole mediators of signaling output from the cerebellum, providing tonic inhibitory feedback onto motor pathways, and specific loss of PCs during development results in impairment of motor learning (Chen et al., 1996). Individual PCs integrate excitatory input from hundreds of thousands of parallel fiber synapses and also receive strong excitatory input from climbing fiber synapses. mGluR-LTD at parallel fiber-PC synapses occurs when parallel fiber activity coincides with strong PC depolarization in response to climbing fiber activity, and results in relief of tonic inhibitory signaling by PCs (Linden, 1994). mGluR-LTD is central to motor learning tasks mediated by PCs, evidenced by impairment of conditioned eyeblink responses in global mGluR1 knockout mice that can be rescued by Purkinje cell-specific mGluR1 expression ((Aiba et al., 1994), (Kishimoto et al., 2002)). Eyeblink conditioning is a paradigm of associative motor learning that measures the ability of the subject to learn to blink in anticipation of an unpleasant stimulus (a puff of air on the eye) when it is preceded by a neutral stimulus (playing of a tone). Deficits in eyeblink conditioning are

observed in the PC-specific *Fmr1* KO, as well in human patients with FXS ((Koekkoek et al., 2005)). Protein synthesis is required for both parallel fiber-PC mGluR-LTD and motor learning of conditioned eyeblink responses ((Bracha et al., 1998), (Linden, 1996), (Karachot et al., 2001)), and postsynaptic signaling pathways that mediate parallel fiber-PC mGluR-LTD are likely to include a number of proteins whose expression is regulated by FMRP ((Ito, 2002), (Darnell et al., 2011)).

We propose to cross the *Fmr1* cTAG line to the Pcp2/L7 Cre line (Jackson labs #004146, Heiman et al 2008) used in the study by Koekkoek et al in order to perform AcGFP-FMRP HITS-CLIP in Purkinje neurons and gain insight into how loss of translational regulation of specific mRNAs leads to observed deficits in synaptic plasticity, spine morphogenesis and motor learning. Cre expression in the Pcp2/L7 line is detectible at P6 and is fully established 2-3 weeks after birth (Barski et al., 2000). HITS-CLIP will be performed in the third postnatal week, as this is a critical period of synaptogenesis during which FMRP is highly expressed, and again in adulthood, to correspond with the age at which cell autonomous *Fmr1* KO phenotypes were observed (Koekkoek et al., 2005). Intact cerebella will be crosslinked and HITS-CLIP will be performed on purified polysomes from according to previously established protocols. AcGFP-FMRP CLIP will also be performed on wt littermate controls to ensure that no signal is seen the absence of AcGFP. In the event that the amount of RNA recovered from these studies is low enough to cause linker-linker ligation products to predominate in the CLIP assay (an effect we routinely see when target RNA substrates are low), we will include biotinylated carrier RNA of known sequence in the linker ligation reactions. Carrier RNA will then be removed by streptavidin beads before PCR amplification of products, and the little that remains will be subtracted bioinformatically after sequencing. Specificity of Cre expression will be confirmed by performing immunofluorescence (IF) on AcGFP-FMRP. If this signal is not detectable, the Pcp2-Cre line will be crossed to the Rosa26R-lacZ reporter line (Jackson labs #003474) and Pcp2-Cre expression will be monitored using B-gal immunohistochemistry.

In previous FMRP CLIP experiments, specificity of FMRP:RNA interactions was demonstrated by correlation of CLIP data to mRNA abundance on polysomes as measured by exon array or to a published database of mRNA expression in neurons (Cahoy et al., 2008). While it was generally clear from these analyses that FMRP associates with a subset of mRNAs not correlated with mRNA abundance, a cell autonomous method of measuring mRNA translation levels would allow CLIP data from the proposed experiments to be accurately compared to the translational status of individual mRNAs for the first time. We propose to perform paired ribosome profiling assays using the RiboTag mouse, which expresses triple-HA tagged ribosomal protein L22 in a Cre-dependent manner (Jackson labs #011029). The RiboTag mouse was created using the same knock-in conditional tagging strategy as the FMRP cTAG mouse and can be crossed to the same Cre expression lines used in cell autonomous AcGFP-FMRP HITS-CLIP studies (Sanz et al., 2009). Ribosome profiling is a method of ascertaining mRNA translational status by high-throughput sequencing of mRNA tags protected from nuclease digest by ribosome binding. Ribosome profiling thus provides a direct readout of translational status, which is not necessarily correlated to mRNA abundance. Immunoprecipitation of HA-tagged ribosomes will allow recovery of mRNA tags specifically and cleanly from the cell type of interest, and these tags can be purified and processed via the same experimental pipeline used for CLIP.

Pairing cell autonomous HITS-CLIP and ribosomal profiling assays will allow pinpointing of the mRNAs most strongly regulated by FMRP in a known cell type that (at least for Purkinje neurons) is relatively easy to visualize by IF. This would offer a potential opportunity to detect protein-level changes in FMRP targets, a goal that has been largely elusive. IF will be performed for selected targets in cerebellar slices from FMRP/Pcp2-Cre/LacZ and FMRPcKO/Pcp2-Cre/LacZ littermates, normalizing IF signals to B-gal staining. If successful, these results would provide strong support for the model that FMRP inhibits the synthesis of specific proteins *in vivo*, and would provide independent validation of results from HITS-CLIP and puromycin runoff assays.

It is anticipated that the proposed experiments will reveal a narrowed list of mRNAs regulated by FMRP in Purkinje neurons. As discussed in the Introduction, some of these targets may be more directly responsible for demonstrated FMRP-mediated cell autonomous defects in Purkinje cell function than others, depending on the dosage sensitivity of the proteins in question and the relative influence of other pathways controlling protein expression. Proposed IF studies may provide some information as to which targets are most overexpressed in the absence of FMRP. Furthermore, examination of the literature may provide clues as to which FMRP targets are most likely to cause the observed phenotypes if overexpressed. For example, it is known that the mGluR-PLC-DAG-IP_3-PKC pathway is central to the expression of parallel fiber-PC mGluR-LTD, and many proteins supporting this pathway have been shown to be FMRP targets (Darnell et al., 2011). In order to directly demonstrate that translational control of particular mRNAs is responsible for cell autonomous loss-of-function phenotypes, phenotypic rescue could be attempted by lowering the dosage of particular FMRP target proteins, since FXS results from overexpression of these proteins. This may be most easily accomplished by crossing the conditional *Fmr1* KO to a conditional KO of the target in question. Such a cross would generate male pups that are -/Y for *Fmr1* and +/- for the target gene in +Cre cells, resulting in a Cre-dependent halving of the target gene dosage in the cell type where FMRP is absent. If a conditional KO mouse does not exist for the protein in question, protein expression could be knocked down by *in utero* electroporation of shRNAs against target mRNAs. Such a strategy would potentially allow the dosage of several proteins to be lowered simultaneously, which might be necessary to have an effect on phenotype if several proteins work in concert to achieve a function. However, shRNA-mediated knockdown would not be limited to the desired cell type.

Identification of FMRP targets most relevant for disease phenotypes has the potential to spur development of therapeutic drugs for treatment of patients with FXS. Encouragingly, FXS phenotypes have been shown to be both acutely inducible and acutely reversible in adult mice, in agreement with our finding of acute reversibility of FMRP-dependent ribosome stalling by kcRNA treatment in puromycin runoff assays.

The acute nature of FMRP regulation in adult mice was recently demonstrated by crossing both the *Fmr1* cKO and *Fmr1* cON lines with the tamoxifen-inducible Nestin-Cre driver line, allowing FMRP expression to be either turned off or turned on specifically in adult neural progenitor cells and their progeny (Guo et al., 2011). Conditional deletion of *Fmr1* in aNPCs in adult mice resulted in defects in the proliferation, differentiation and dendritic arbor complexity of these cells and impairment in behavioral assays designed to assess hippocampal-dependent learning. Conversely, conditional expression of *Fmr1* in aNPCs in an otherwise *Fmr1*-null background rescued these phenotypes. These results suggest that FXS results from ongoing (and therefore potentially treatable) misregulation of protein synthesis, and does not simply reflect irreversible consequences of loss of function during development. Connection of cell autonomous HITS-CLIP studies with these types of cell autonomous loss-of-function studies has the potential to significantly advance our understanding of FMRP function and to rationally guide development of therapies to treat FXS.

Figure 34. Construct design of the cTAG allele.

The terminal exon of *Fmr1* is flanked by lox sites so that Cre-dependent recombination results in expression of a downstream, AcGFP-tagged version of this same exon (including the entire 3'UTR). Thus, either wt FMRP or AcGFP-tagged FMRP can be expressed from the cTAG allele in a mutually exclusive fashion, dependent on Cre expression. AcGFP can then be used as an IP-able tag in cell type-specific CLIP experiments while maintaining normal wt FMRP expression in all cells not expressing Cre. LA=left homologous arm; RA=right homologous arm; Pfoot pA=Proudfoot consensus polyadenylation site; FNeoF= Frt-Neomycin-Frt cassette. Exon numbers indicated within rectangles; lox sites indicated by triangles.

A mouse model for cell-type specific FMRP function

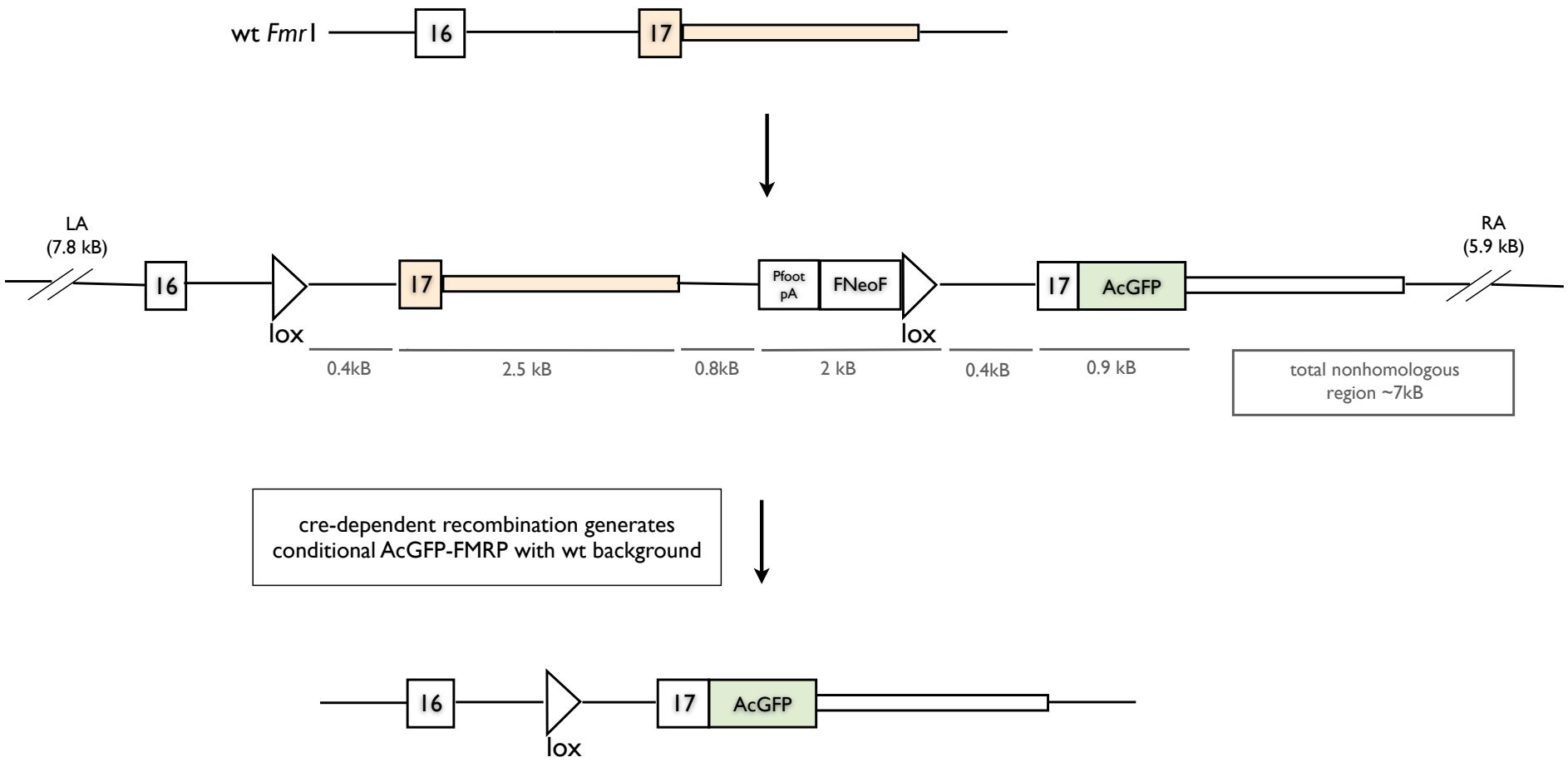

Figure 35. Polysome distribution of wt FMRP and C-terminally tagged AcGFP-FMRP in 293T cells.

Polysomes were fractionated from 293T cells transiently transfected with AcGFP-FMRP and fractions were analyzed by Western blot with FMRP antibody 17722, which recognizes both tagged (transfected) and untagged (endogenous) forms of FMRP. AcGFP adds approximately 30kD to the molecular weight of FMRP. Presence of the AcGFP tag did not alter the polysome distribution of FMRP. AcGFP-FMRP did not have multiple splice isoforms because it was expressed from a cDNA construct.

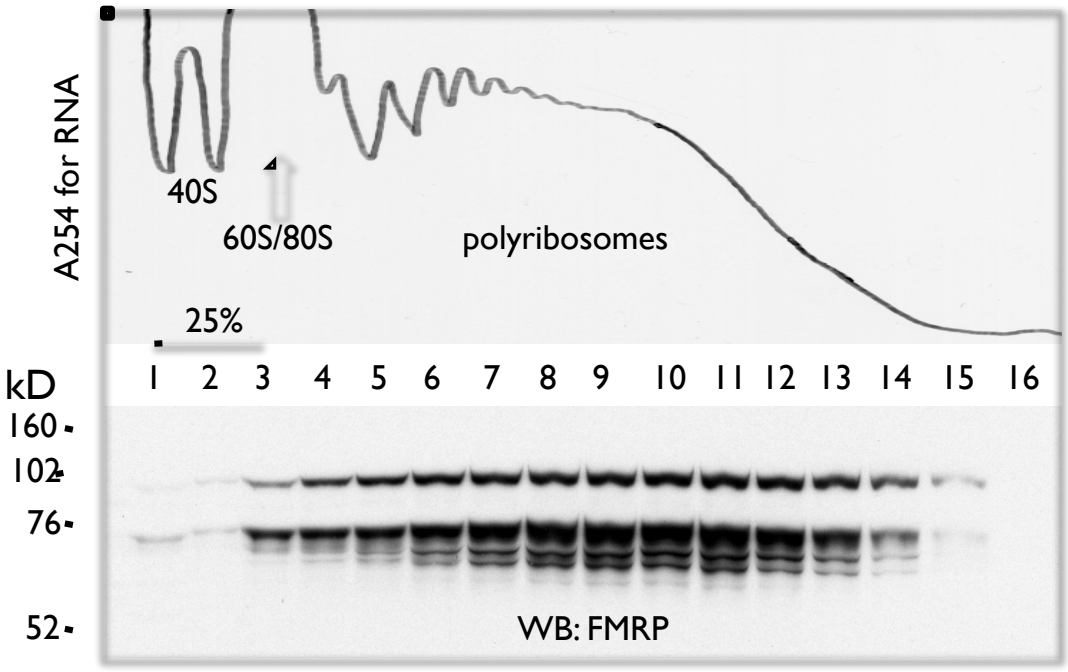
A254 for RNA
40S
60S/80S
polyribosomes
25%
kD
1 2 3 4 5 6 7 8 9 10 11 12 13 14 15 16
160
102
76
52
WB: FMRP

Figure 36. Retrieval of *Fmr1* sequence from BAC RP23-149C7 and targeting of upstream lox site.

14.3kB of sequence was retrieved from the BAC into linearized PL253 by homologous recombination at the pink and blue regions. A lox-neo-lox cassette was then amplified by PCR and targeted upstream of *Fmr1* exon 17 (the terminal exon) by homologous recombination at the green and purple regions. Finally, the lox-neo-lox cassette was reduced to a single lox site by arabinose induction of Cre.

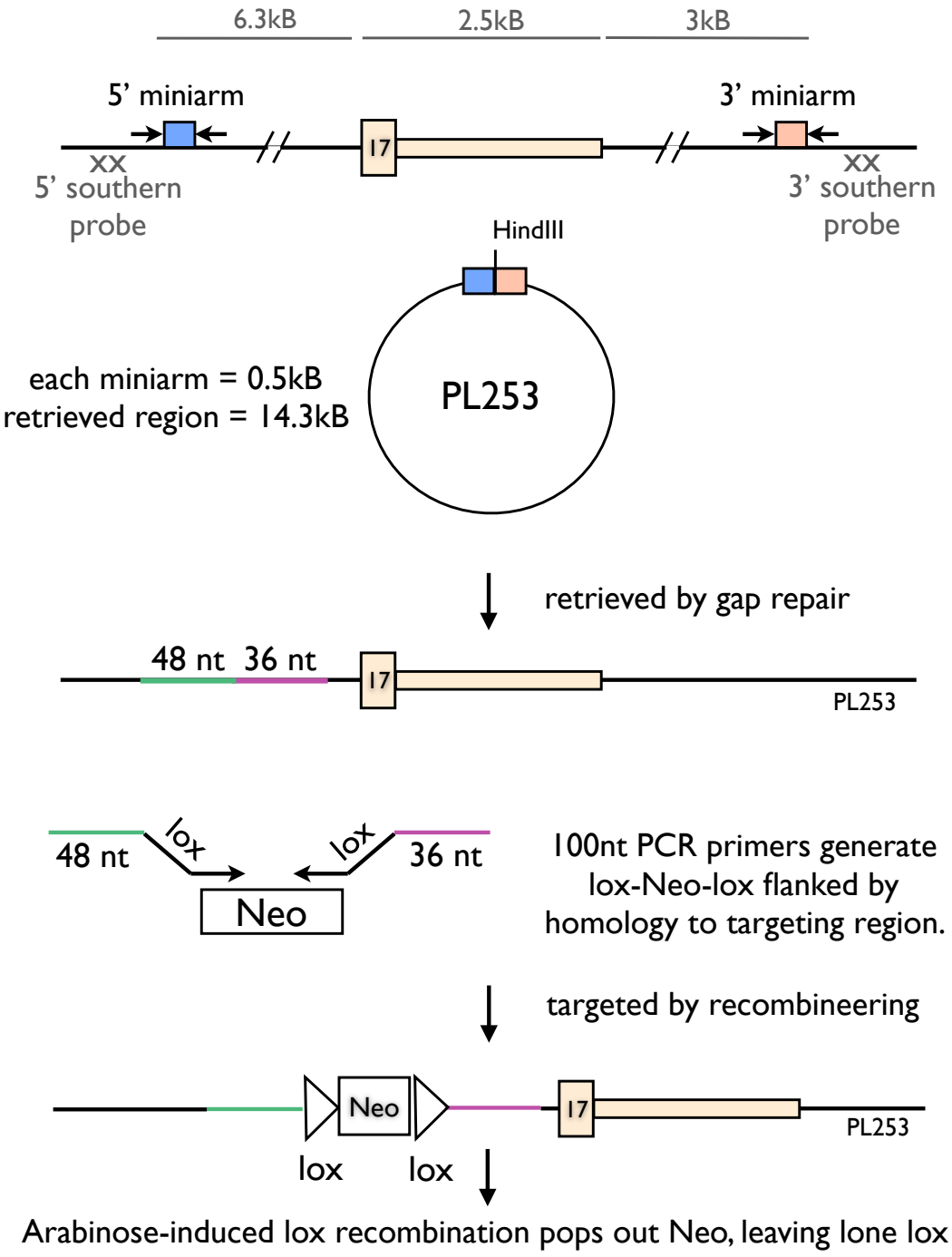
6.3kB
2.5kB
3kB
5' miniarm
3' miniarm
17
XX
5' southern probe
XX
3' southern probe
HindIII
each miniarm = 0.5kB
retrieved region = 14.3kB
PL253
retrieved by gap repair
48 nt
36 nt
17
PL253
48 nt
lox
lox
36 nt
Neo
100nt PCR primers generate lox-Neo-lox flanked by homology to targeting region.
targeted by recombineering
Neo
17
PL253
lox
lox
Arabinose-induced lox recombination pops out Neo, leaving lone lox

Figure 37. Final cloning of cTAG construct.

A Bsu36I-Proudfoot polyA-Frt-Neo-Frt-lox cassette was cloned upstream of AcGFP-tagged *Fmr1* exon 17 at the PacI site in pCR4-TOPO. The final cassette was then cloned into a native Bsu36I site downstream of *Fmr1* exon 17 in PL253. This strategy allowed uninterrupted homology downstream of AcGFP.

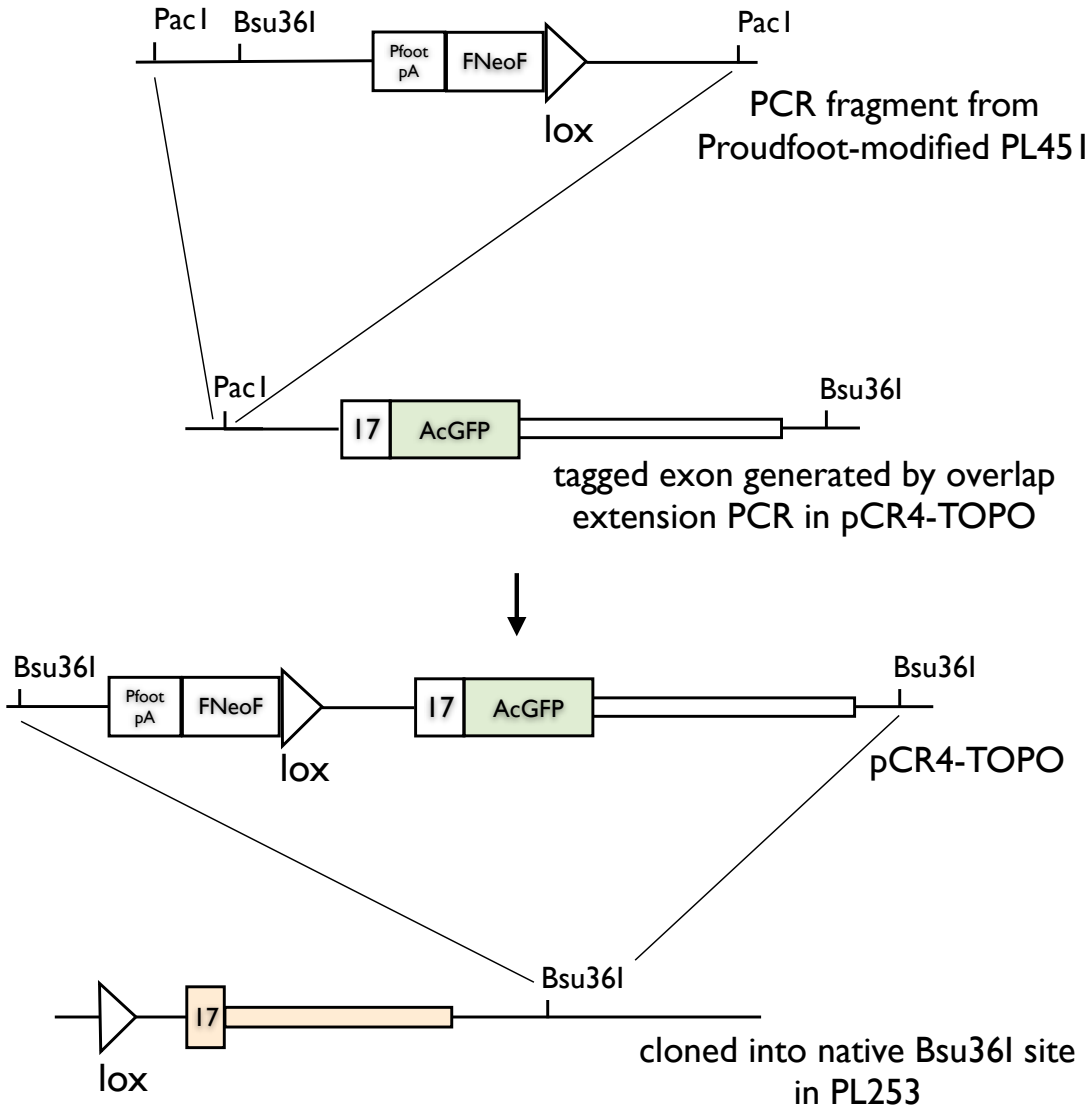
Pac I
Bsu36I
Pfoot pA
FNeoF
lox
Pac I
PCR fragment from Proudfoot-modified PL451
Pac I
17
AcGFP
Bsu36I
tagged exon generated by overlap extension PCR in pCR4-TOPO
Bsu36I
Pfoot pA
FNeoF
lox
17
AcGFP
Bsu36I
pCR4-TOPO
Bsu36I
17
lox
cloned into native Bsu36I site in PL253

Figure 38. Restriction digests confirming final cTAG construct.

Digests of the final cTAG construct in PL253 were performed with 2ug of DNA and 1uL of enzyme for 90 min. All bands were correct to high resolution except the 2.5kB PvuII band, which was expected to be 2.8kB. However, the affected fragment is entirely within the vector backbone and does not affect the construct.

PvuII expect: 0.5 - 0.8 - 1.3 - 2.2 - 2.8 - 3.2 - 3.4 - 5.2 - 6.6 kB
SpeI expect: 1.1 - 1.4 - 1.5 - 2.1 - 3.6 - 6.5 - 8.5 kB
XbaI expect: 0.8 - 1.1 - 1.2 - 1.5 - 2.9 - 3.6 - 7.3 - 7.5 kB

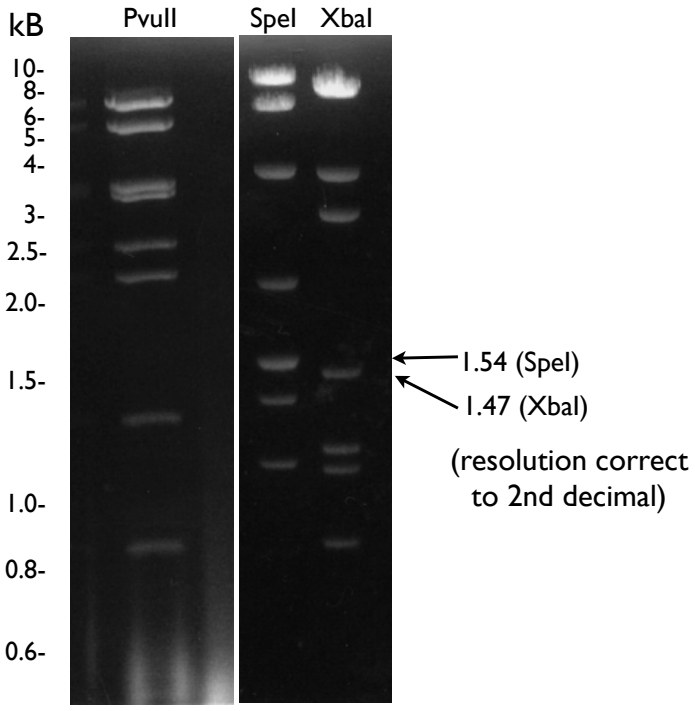
kB
PvuII
SpeI
XbaI
10-
8-
6-
5-
4-
3-
2.5-
2.0-
1.5-
1.0-
0.8-
0.6-
1.54 (SpeI)
1.47 (XbaI)
(resolution correct
to 2nd decimal)

Figure 39a. Primary Southern screen for presence of Neo cassette in ES cells injected with cTAG construct.

Southern blot was performed using NdeI digest and a 3' arm probe. The wt allele produces a 7.4kB band, while the correctly targeted allele produces a 10.1kB band due to an NdeI site engineered into the Proudfoot FNF-lox cassette. 7/200 clones contained the 10.1kB band.

Primary screen for correct targeting (Neo cassette present): NdeI digest with 3‘arm probe

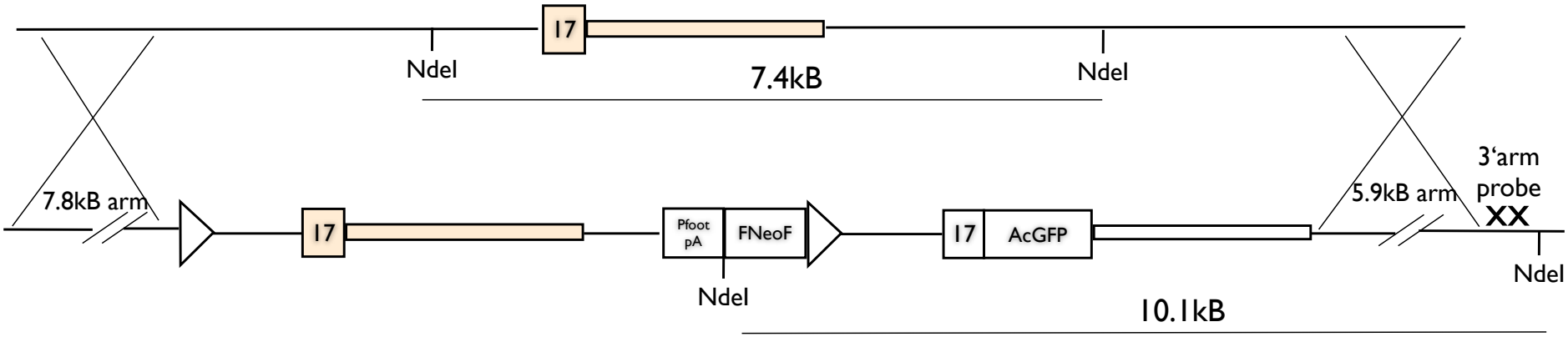

Figure 39b. Secondary Southern screen for presence of upstream lox site in ES cells injected with cTAG construct.

Southern blot was performed using EcoRI digest and a 5' arm probe. Homologous regions that have the potential to create unwanted crossovers are indicated in pink and blue. A 11.9 kB band is seen if the upstream lox site is absent (either in the wt allele or due to dropping during targeting), while the correctly targeted allele produces a 9.0kB band due to an EcoRI site engineered next to the lox site. Clones 70, 89, 103, 109 and 189 (band partially cut off) contain the upstream lox site, although clones 70 and 89 appear mixed with wt. Clones 100 and 127 appear to have dropped the upstream lox site from the targeted allele.

Check for incorrect targeting (upstream lox dropped): EcoRI digest with 5‘arm probe

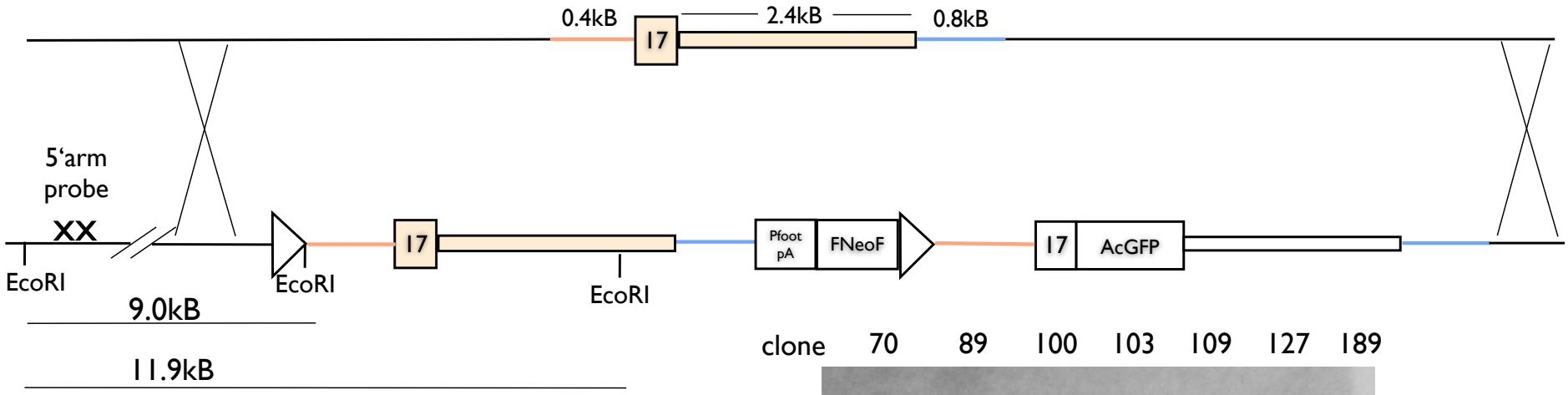

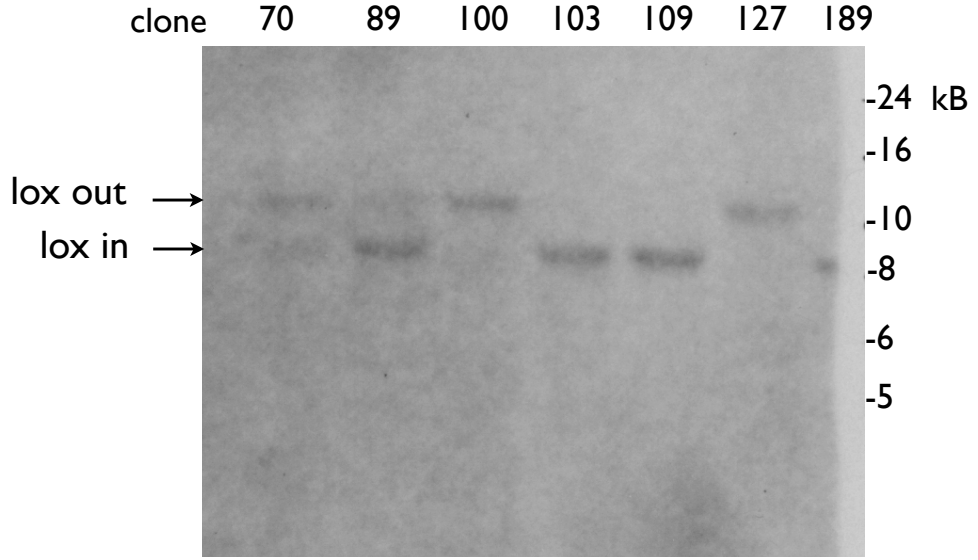

Figure 39c. Secondary Southern screen for presence of AcGFP in ES cells injected with cTAG construct.

Southern blot was performed using DraIII digest and a 3' arm probe. Homologous regions that have the potential to create unwanted crossovers are indicated in pink and blue. A 16.0 kB band is seen if AcGFP is dropped during targeting, while a 10.1kB band is generated from the wt allele. The correctly targeted allele produces a 9.5kB band due to an DraIII site present in AcGFP. Clones 70, 89, 100, 127 and 189 contain AcGFP, although clones 70 and 89 appear mixed with wt. Clones 103 and 109 appear to have dropped AcGFP from the targeted allele.

Check for incorrect targeting (GFP dropped): DraIII digest with 3‘arm probe

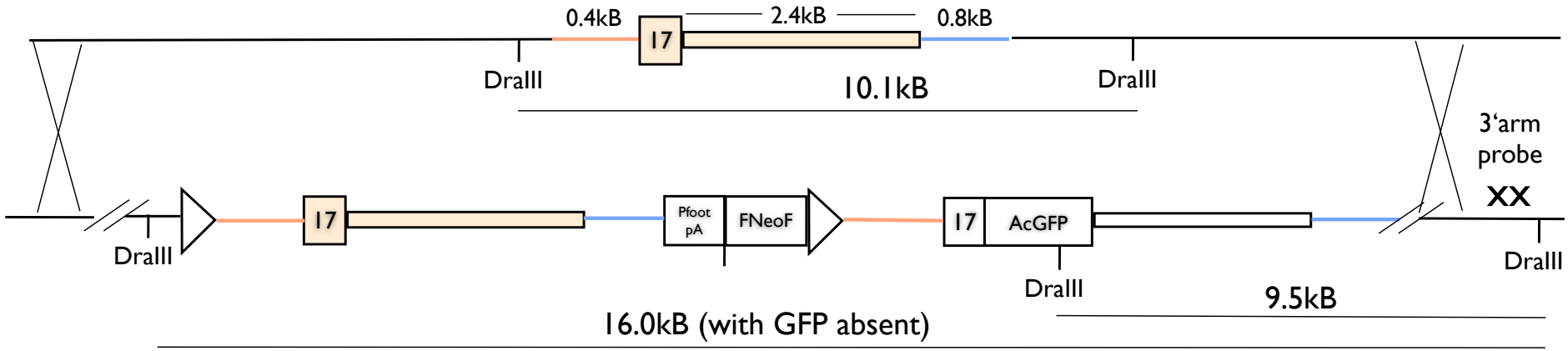

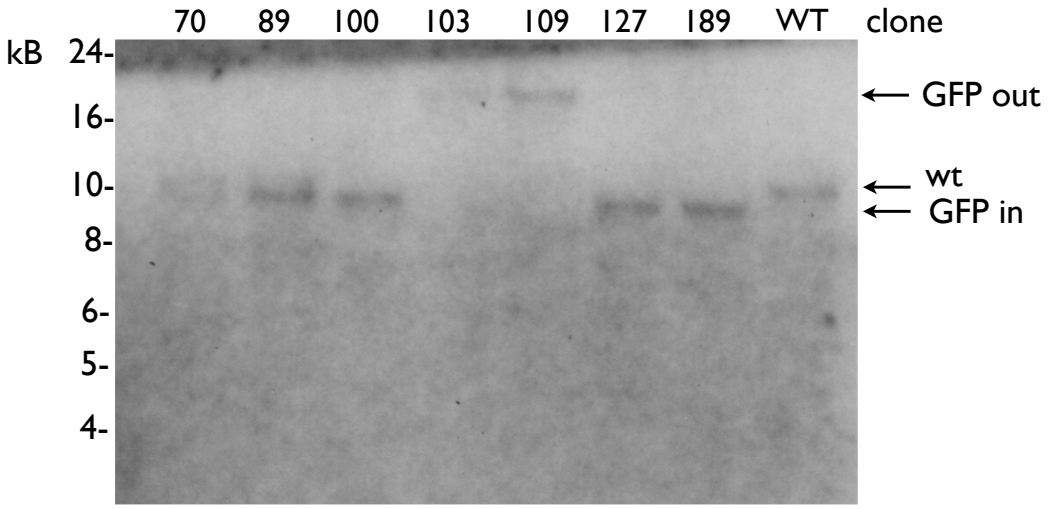

Figure 39d. Secondary Southern screen for presence of internal duplications, deletions or rearrangements in ES cells injected with cTAG construct.

Southern blot was performed using NdeI digest and an internal 3‘UTR probe. Homologous regions that have the potential to create unwanted crossovers are indicated in pink and blue. The correctly targeted allele produces both a 3.9kB band and a 10.1kB band due to an NdeI site engineered downstream of the Proudfoot sequence. All clones contain the 3.9kB band, although this band does not indicate whether the upstream lox site is present. Clones 70, 89, 100, 127 and 189 contain a downstream segment of the correct size, although clones 70 and 89 appear mixed with wt. The downstream segment of clones 103 and 109 is smaller because they have dropped AcGFP (see Fig 22c). Clone 127 has an unexpected band, which could indicate an unwanted event in the target allele, consistent with results from Fig 22e.

Check for duplications: NdeI digest with internal 3'UTR probe

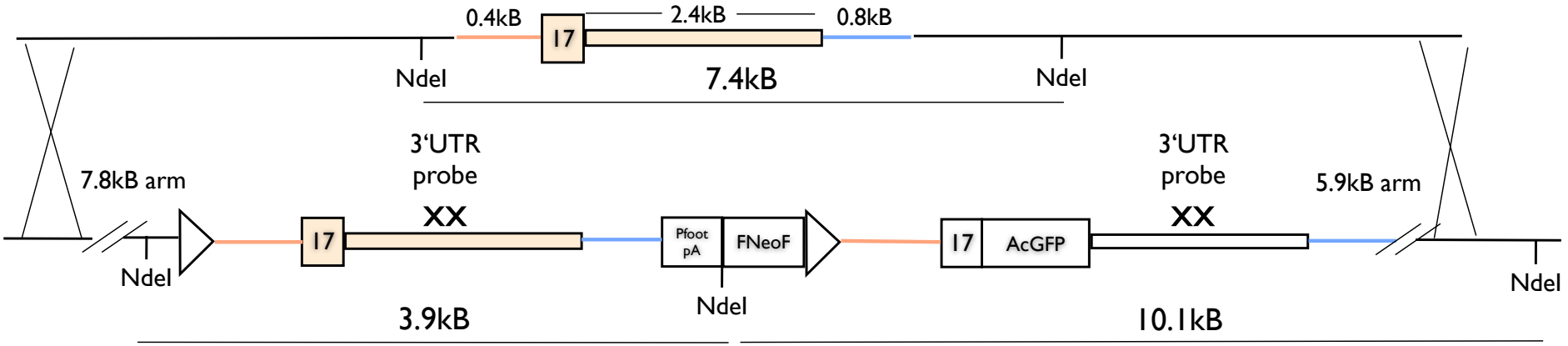

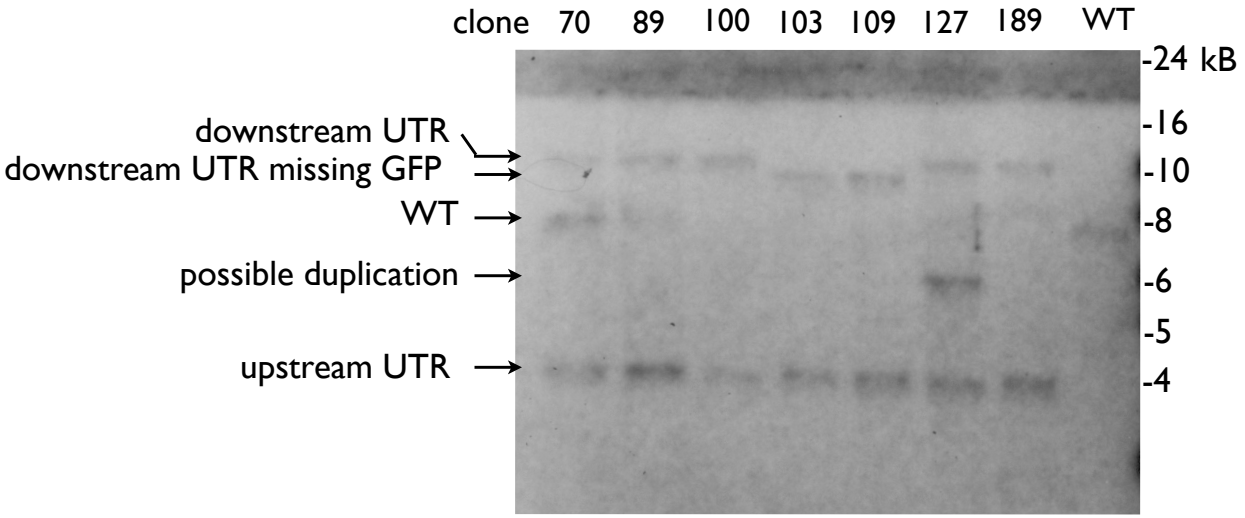

Figure 39e. Secondary Southern screen for presence of internal duplications, deletions or rearrangements in ES cells injected with cTAG construct.

Southern blot was performed using DraIII digest and an internal Neo probe. Homologous regions that have the potential to create unwanted crossovers are indicated in pink and blue. The correctly targeted allele produces 7.3kB band. If AcGFP is absent, a 16.0kB band will be observed. Clones 70, 100 and 189 contain a segment of the correct size, although clone 70 also contains an unexpected band. Clones 103 and 109 contain the 16.0kB band because they have dropped AcGFP (see Fig 22c). Clone 127 has an unexpected band, which could indicate an unwanted event in the target allele, consistent with results from Fig 22d.

Check for duplications: DraIII digest with internal Neo probe

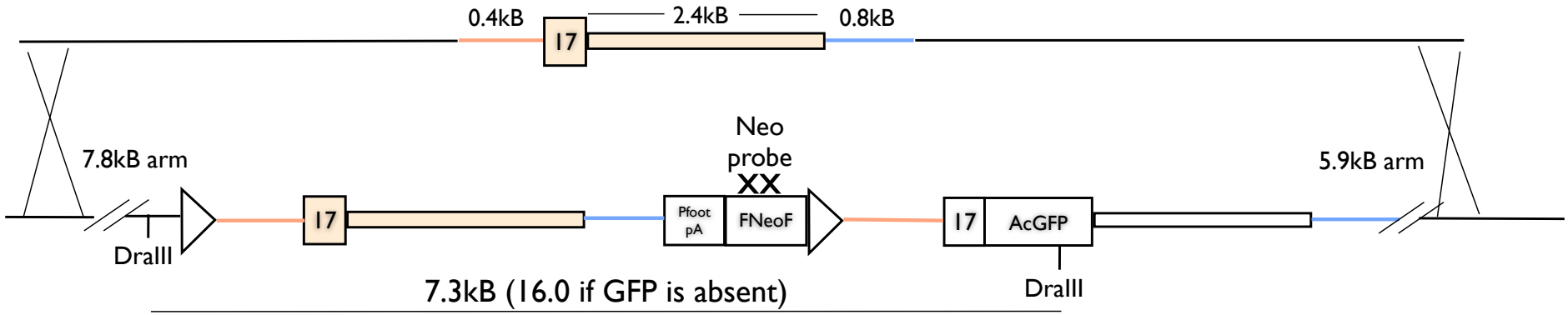

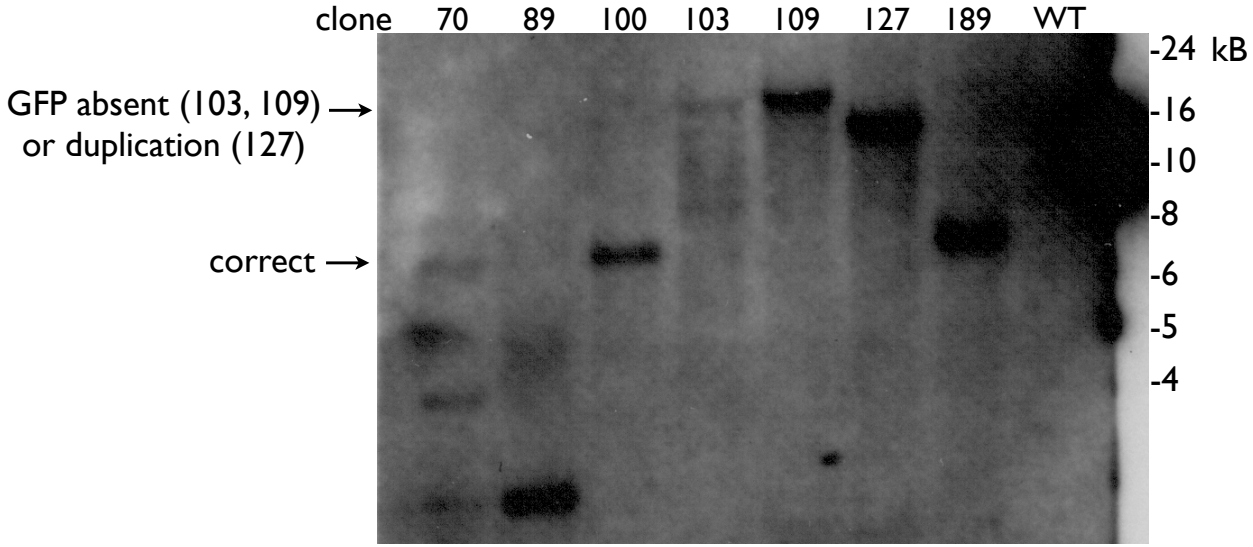

Figure 40. Expression of AcGFP-FMRP from the cTAG construct in ES cells.

ES cells from clone #189 were transfected with pPAC-Cre to induce expression of AcGFP-FMRP. One set of cells was selected with puromycin to enrich for Cre+ cells, since transfection rates of ES cells are typically around 1%. Presence of AcGFP-containing mRNA was detected by RT-PCR with primers in *Fmr1* exon 16 and 3'UTR, in which ^{32}P-dCTP was included in the final two cycles. Inclusion of AcGFP is indicated by an increase in product size from 0.6kB to 1.3kB.

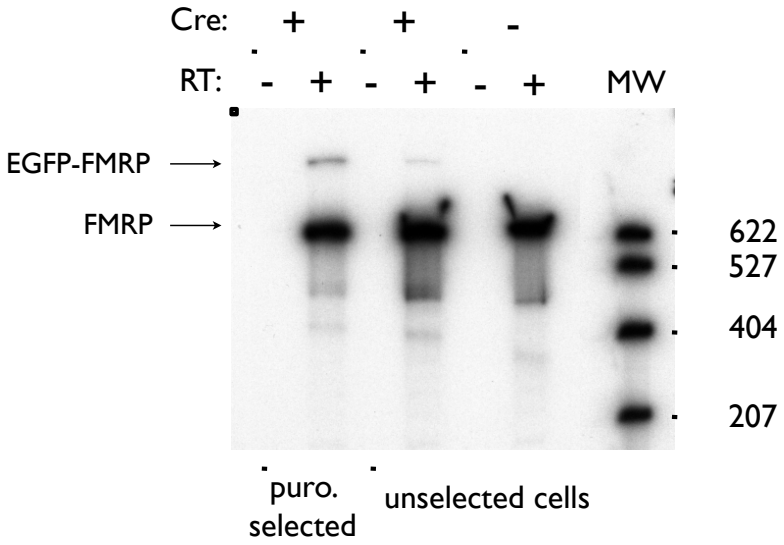
Cre: + + -
RT: - + - + - + MW
EGFP-FMRP
FMRP
622
527
404
207
puro. selected
unselected cells

Figure 41. cTAG breeding strategy.

Male albino B6 ES cells carrying the cTAG allele (derived from a B6 BAC) were combined with B6 blastocysts (non-albino). Resulting male chimeric mice were crossed with female B6 albinos. Albinism is a recessive trait, therefore if a pup resulting from this cross is albino, one set of chromosomes must have been derived from the ES cell. Since *Fmr1* is on the X chromosome, all white, female progeny from this cross should carry one copy of the cTAG allele and will be fully on the B6 background.

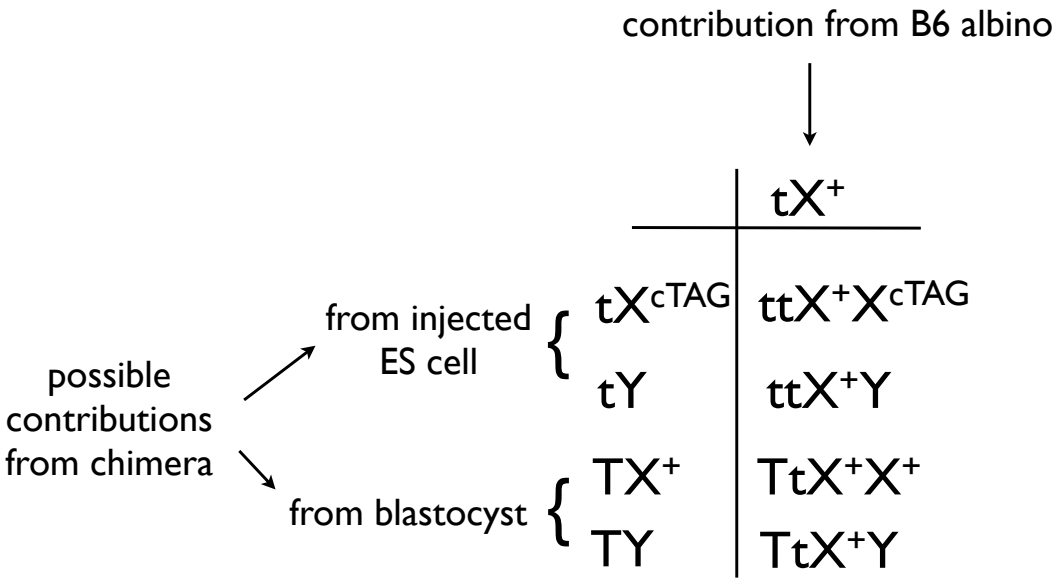

t = mutant tyrosinase gene, recessive for albinism
X^{cTAG} = X chromosome carrying cTAG allele
X^{+} = X chromosome carrying wt allele

Figure 42. Analysis of AcGFP-FMRP expression in cTAG/+ mice.

A) Western blots of brain lysate from a +Cre, cTAG/+ mouse and a –Cre, cTAG/+ mouse, blotted with FMRP antibody 17722 that recognizes both tagged and untagged forms of FMRP. AcGFP-FMRP expression was only detectable in +Cre mice and appeared at the expected molecular weight. Multiple splice isoforms of AcGFP-FMRP were detectable at the higher resolution provided by a gradient gel (right hand panel).

B) Presence of AcGFP-containing mRNA was detected by RT-PCR with primers in *Fmr1* exon 16 and 3'UTR, in which ^{32}P-dCTP was included in the final two cycles. Inclusion of AcGFP is indicated by an increase in product size from 0.6kB to 1.3kB.
In these experiments, two different Cre drivers were used: EIIA and Emx1. Both should drive Cre pan-neuronally but Emx1 is a more efficient driver.

A

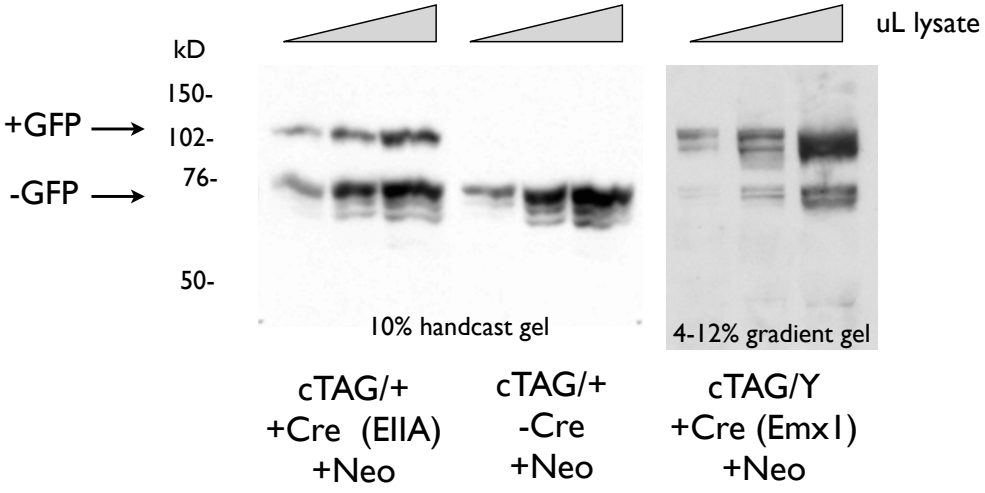
uL lysate
kD
150-
102-
76-
50-
+GFP
-GFP
10% handcast gel
4-12% gradient gel
cTAG/+
+Cre (EIIA)
+Neo
cTAG/+
-Cre
+Neo
cTAG/Y
+Cre (Emx1)
+Neo

B

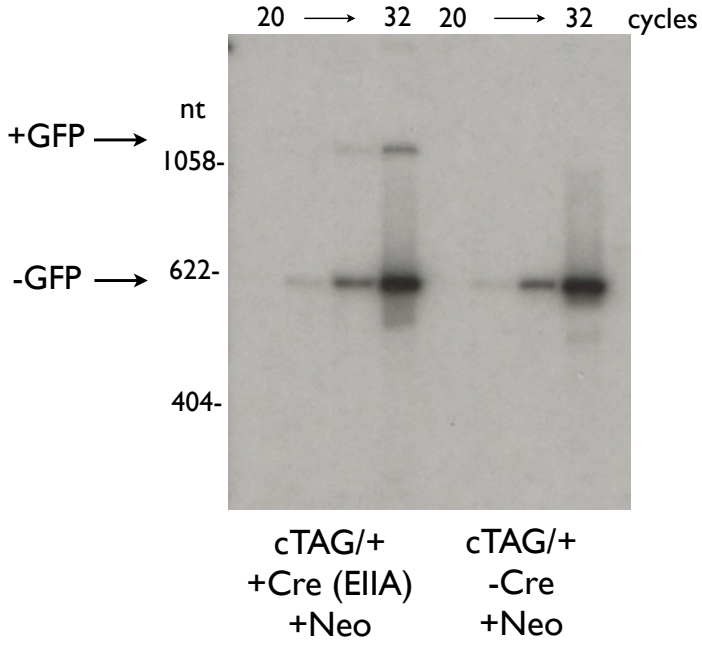
20 → 32 20 → 32 cycles
nt
1058-
622-
404-
+GFP
-GFP
cTAG/+
+Cre (EIIA)
+Neo
cTAG/+
-Cre
+Neo

Figure 43. Polysome distribution of wt FMRP and AcGFP-FMRP in –Cre, cTAG/+ and +Cre, cTAG/+ mouse brain.

Brain polysomes were separated over sucrose gradients and fractions were analyzed by Western blot with FMRP antibody 17722, which recognizes both tagged and untagged forms of FMRP. AcGFP adds approximately 30kD to the molecular weight of FMRP. No AcGFP-FMRP was detected in -Cre polysome fractions even after extended exposure. Presence of the AcGFP tag did not alter the polysome distribution of AcGFP-FMRP in brain.

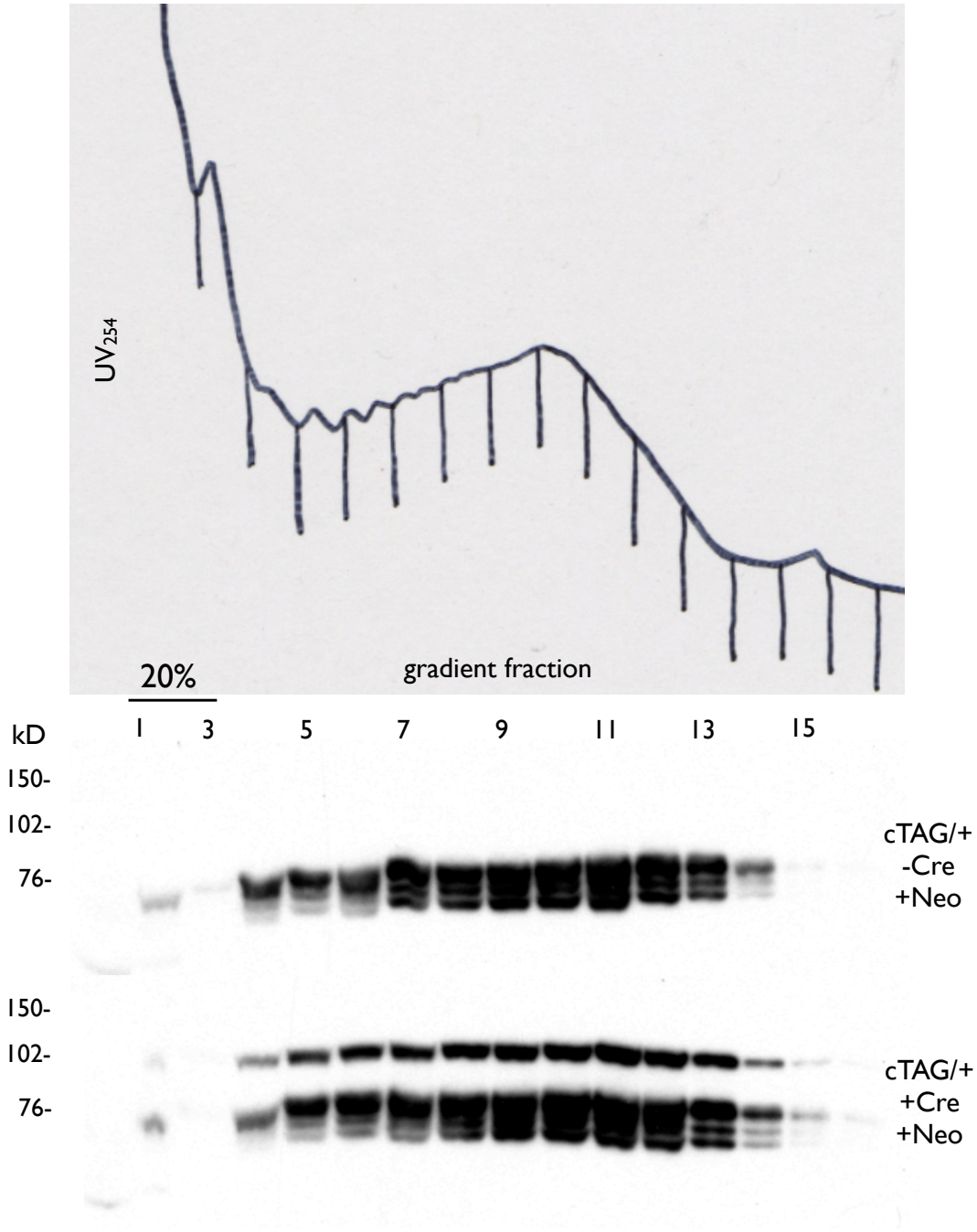
UV254
20%
gradient fraction
kD
1
3
5
7
9
11
13
15
150-
102-
76-
cTAG/+
-Cre
+Neo
150-
102-
76-
cTAG/+
+Cre
+Neo

Table 7: Mice used in characterization of cTAG allele.

Shown from left are: Mouse number, mouse genotype, presence of neomycin cassette, expression of Cre, Cre driver, and mouse age. Note: The EIIa male mice expressed Cre at extremely low levels, most likely due to mosaic expression of the driver.

Number	Genotype	Neo	Cre	Cre Driver	Age
1	+/Y	(+)	(–)		P17
2	cTAG/Y	(+)	(–)		P17
3	+Y	(–)	(–)		P17
4	cTAG/Y	(–)	(–)		P17
5	+/Y	(+)	(+)	EIIa (male)	P17
6	cTAG/Y	(+)	(+)	EIIa (male)	P17
7	+/Y	(–)	(–)		P23
8	cTAG/Y	(–)	(–)		P23
9	cTAG/Y	(–)	(–)		7wk
10	cTAG/Y	(–)	(–)		7wk
11	cTAG/+	(+)	(–)		P23
12	cTAG/+	(+)	(+)	EIIa (female)	P17
13	+/+	(+)	(+)	Emx1	P16
14	cTAG/+	(+)	(+)	Emx1	P16
15	+/Y	(+)	(+)	Emx1	P16
16	cTAG/Y	(+)	(+)	Emx1	P16

Figure 44. Analysis of AcGFP-FMRP expression at RNA and protein levels in panel of 16 mice (listed in Table 7).

The 16 mice vary in terms of presence of cTAG allele, presence of Neo cassette and expression of Cre. Protein and RNA was prepared from total brain.

Top panel: Western blot using FMRP antibody 17722 that recognizes both tagged and untagged forms of FMRP. Mice # 12, 14 and 16 express Cre. Degree of Cre expression was correlated to degree of AcGFP-FMRP expression. A small amount of leaky AcGFP-FMRP expression was observed in mice in which the Neo cassette was removed (#4, 8, 9 and 10).

Middle panels: Western blots using two different GFP antibodies (sc-9996 and 19C8) specifically detect AcGFP-FMRP.

Bottom panel: The ratio of *AcGFP-Fmr1* mRNA to wt *Fmr1* mRNA was determined for the 16 mice by QPCR using primers in *Fmr1* exon 16/exon 17 (to detect untagged *Fmr1* mRNA) and primers in exon 16/AcGFP (to detect tagged *AcGFP-Fmr1* mRNA). A small amount of leaky AcGFP-FMRP expression in the absence of the Neo cassette was also detected by QPCR. Therefore, the Neo cassette was left in place, since it did not appear to otherwise affect the expression of FMRP.

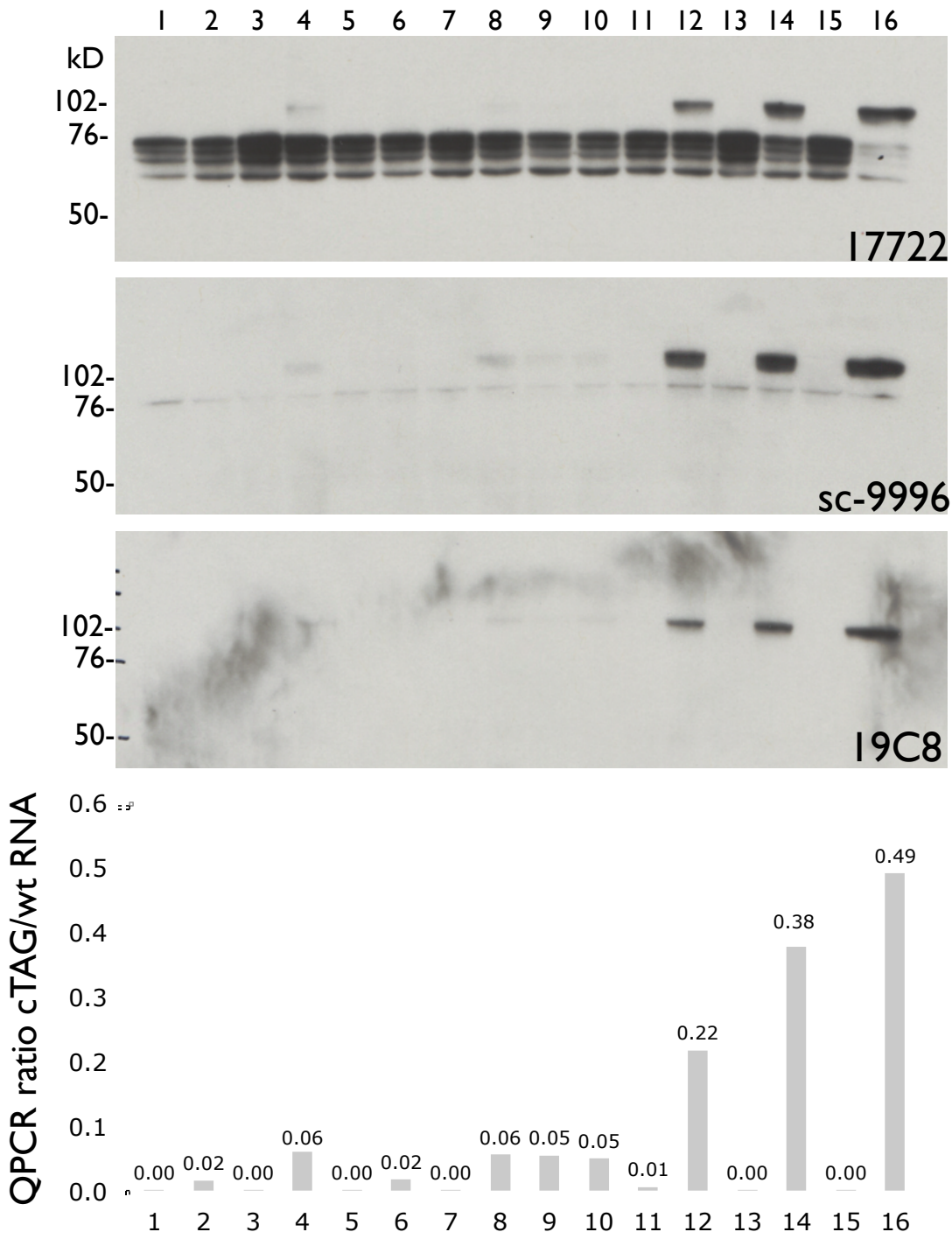
1 2 3 4 5 6 7 8 9 10 11 12 13 14 15 16
kD
102-
76-
50-
17722
102-
76-
50-
sc-9996
102-
76-
50-
19C8
QPCR ratio cTAG/wt RNA
0.6
0.5
0.4
0.3
0.2
0.1
0.0
0.00 0.02 0.00 0.06 0.00 0.02 0.00 0.06 0.05 0.05 0.01 0.22 0.00 0.38 0.00 0.49
1 2 3 4 5 6 7 8 9 10 11 12 13 14 15 16

Figure 45. Comparison of *Fmr1* splice isoforms.

A) Splice isoforms spanning exons 12-17 were detected by RT-PCR with primers in *Fmr1* exons 11/17 or exon 11/AcGFP, in which ^{32}P-dCTP was included in the final two cycles. From left to right: *Fmr1* expressed from the wt allele, *Fmr1* expressed from the cTAG allele, and *AcGFP-Fmr1* (these are mice #1, 2 and 16 from Table 7, respectively). Multiple splice isoforms appeared similar in all three samples (products amplified with exon 11/AcGFP primers were slightly larger because the AcGFP primer is positioned 44nt downstream of the exon 17 primer).

B) Cartoon showing relative positioning of FMRP exons and *Fmr1* splice isoforms, with known alternative splice isoforms indicated. Reproduced with permission from Steve Warren, from Bassell & Warren 2008.

A

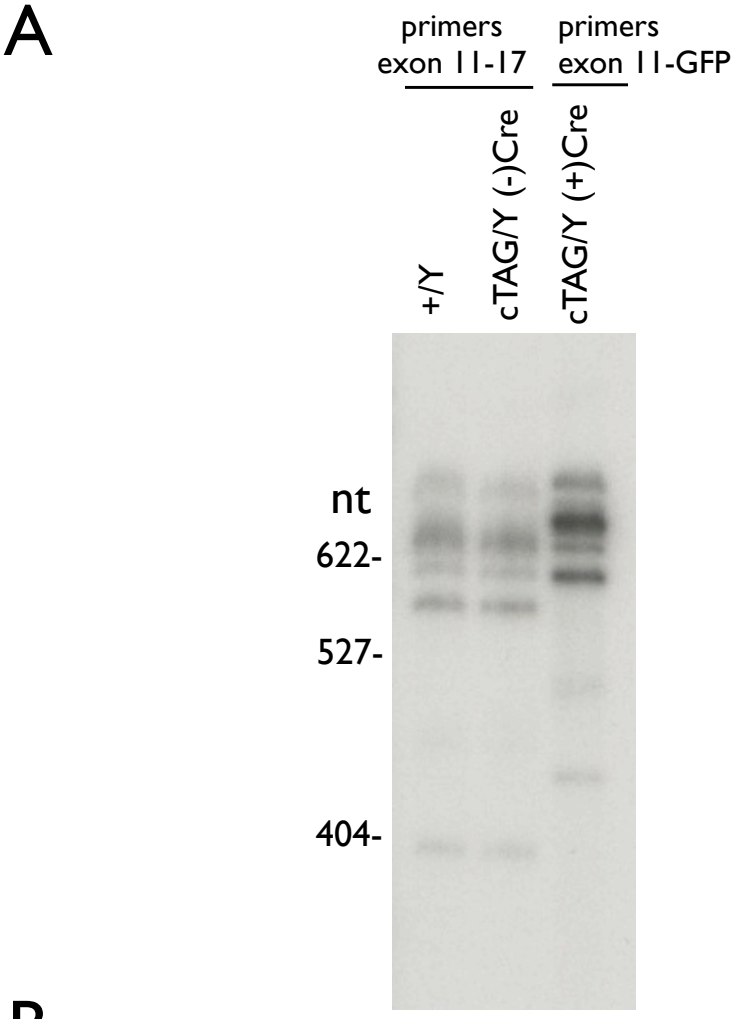
primers
exon 11-17
primers
exon 11-GFP
+/Y
cTAG/Y (-)Cre
cTAG/Y (+)Cre
nt
622-
527-
404-

B

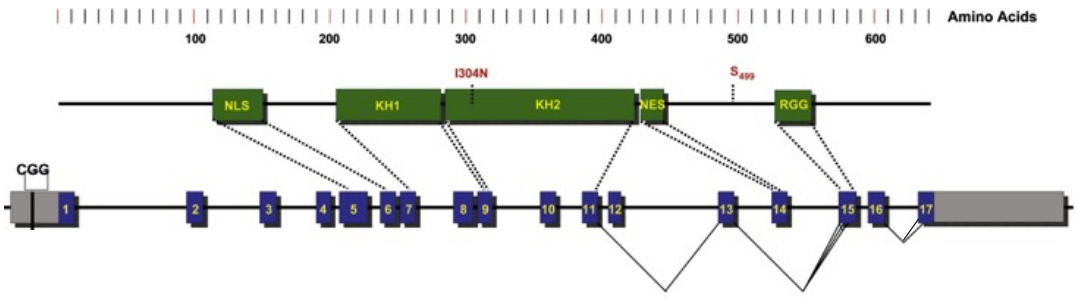
Amino Acids
100
200
300
400
500
600
I304N
S499
NLS
KH1
KH2
NES
RGG
CGG
1
2
3
4
5
6
7
8
9
10
11
12
13
14
15
16
17

Figure 46. Immunoprecipitation of AcGFP-FMRP from +Cre, cTAG/+ mouse brain.

Immunoprecipitations were performed using mixed GFP monoclonals 19C8 and 19F7 and standard CLIP conditions. Although the cTAG/+ mouse expressed both AcGFP-FMRP and wt FMRP, AcGFP-FMRP was specifically immunoprecipitated.

Upper panels: Western blot with GFP antibody sc-9996 showed successful depletion and IP of AcGFP-FMRP, with no signal detected in a control IP from a wt mouse (final lane).

Lower panels: Western blot with FMRP antibody 17722 (that recognizes both wt FMRP and AcGFP-FMRP) showed specific depletion and IP of AcGFP-FMRP, without detectible depletion or IP of wt FMRP. 5% of input/post-IP supernatants were loaded.

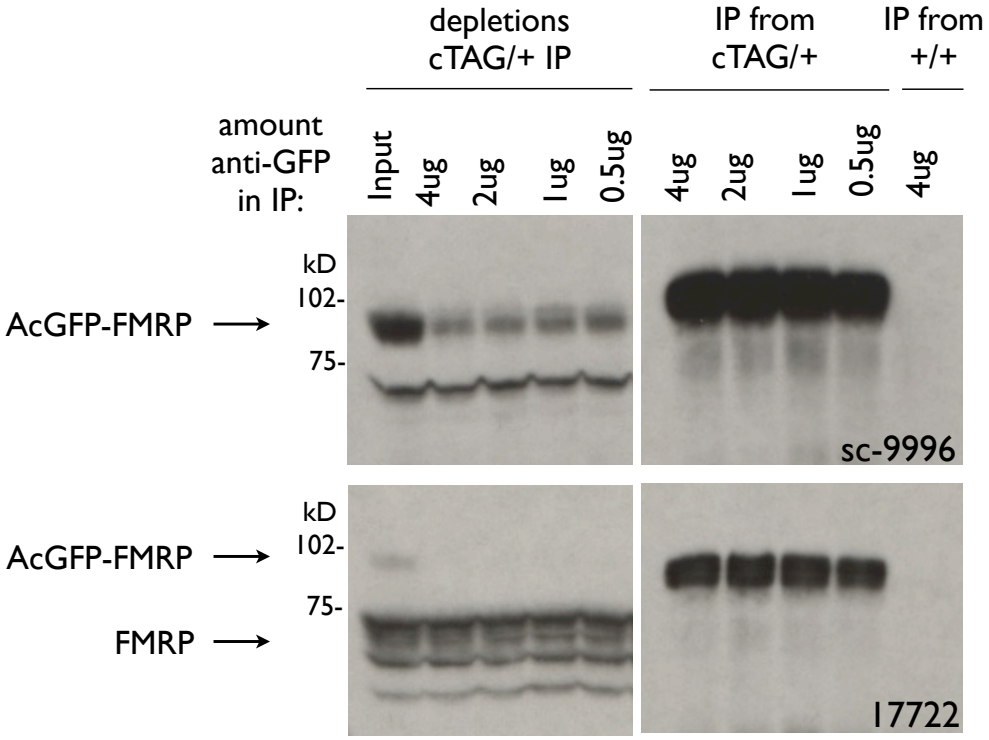
depletions
cTAG/+ IP
IP from
cTAG/+
IP from
+/+
amount
anti-GFP
in IP:
Input
4ug
2ug
1ug
0.5ug
4ug
2ug
1ug
0.5ug
4ug
kD
102-
75-
AcGFP-FMRP
sc-9996
kD
102-
75-
AcGFP-FMRP
FMRP
17722

Figure 47. AcGFP-FMRP CLIP of whole mouse brain.

A) Autoradiogram of labeled RNA:protein complexes immunoprecipitated from cTAG and wt mouse brains after RNAse digest. **Lane 1:** AcGFP-FMRP was IPed from brain lysate containing both wt FMRP and AcGFP-FMRP. **Lane 2:** FMRP was IPed from wt brain lysate. **Lane 3:** FMRP was IPed from brain lysate containing untagged FMRP expressed from the cTAG allele. **Lane 4:** Control IP performed with GFP antibodies on a wt lysate, showing that the signal in Lane 1 was specific to presence of GFP. Nitrocellulose membrane was cut out in regions indicated by dots.

B) RNAs purified from nitrocellulose were reverse transcribed, amplified by PCR and further purified by urea-PAGE . DNAs of correct size are visualized as a smear between 100-150nt. DNA was recovered from the gel cut at bracketed regions.

C) Agarose gel showing final CLIP DNA products.

A

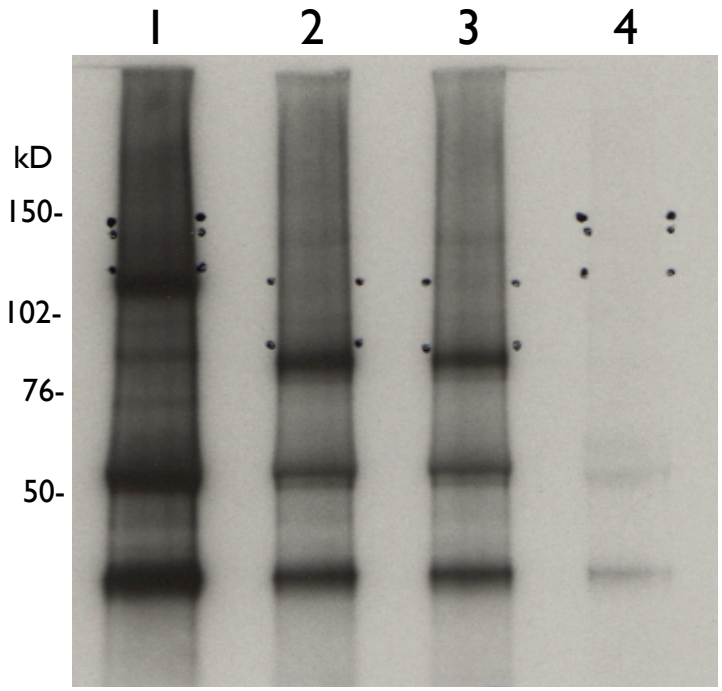

Lane 1: GFP antibody, +Cre, cTAG/+ lysate
Lane 2: FMRP antibody, wt lysate
Lane 3: FMRP antibody, -Cre, cTAG/Y lysate
Lane 4: GFP antibody, wt lysate

B

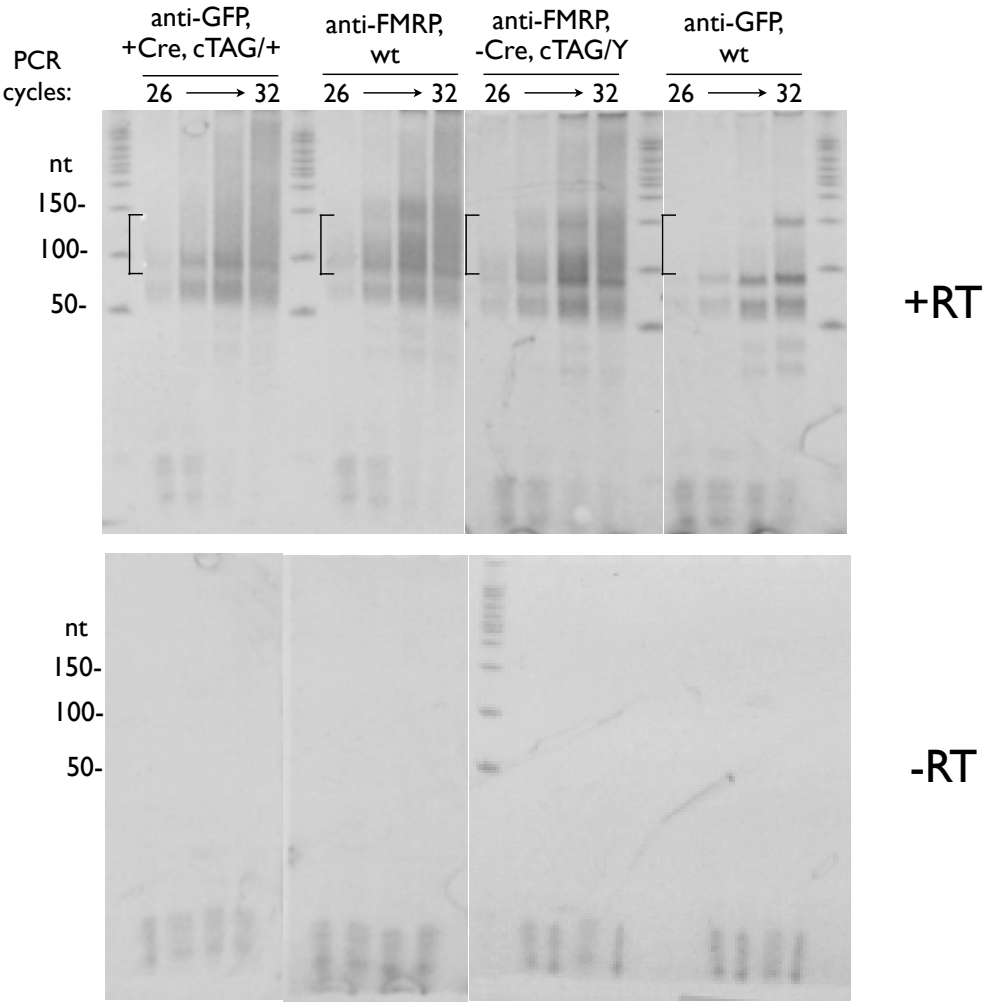
anti-GFP,
+Cre, cTAG/+
anti-FMRP,
wt
anti-FMRP,
-Cre, cTAG/Y
anti-GFP,
wt
PCR
cycles:
26 → 32
26 → 32
26 → 32
26 → 32
nt
150-
100-
50-
+RT
nt
150-
100-
50-
-RT

C

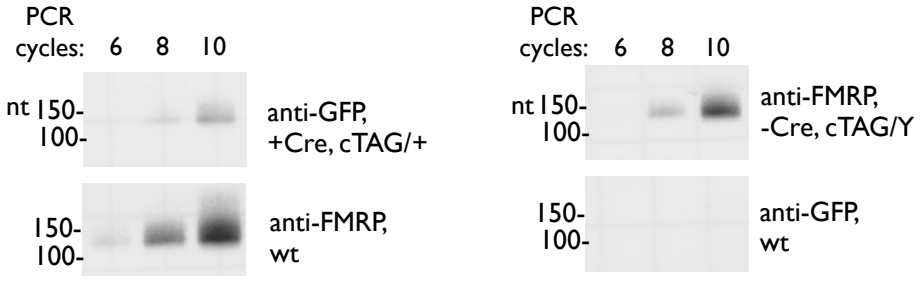
PCR
cycles: 6 8 10
nt 150-
100-
anti-GFP,
+Cre, cTAG/+
150-
100-
anti-FMRP,
wt
PCR
cycles: 6 8 10
nt 150-
100-
anti-FMRP,
-Cre, cTAG/Y
150-
100-
anti-GFP,
wt

Figure 48. Correlation of CLIP data from AcGFP-FMRP and wt FMRP mouse brains.

For each sample, the number of unique exonic CLIP tags mapping to each mRNA was plotted for the top 5000 targets. **A)** AcGFP-FMRP CLIP was highly correlated with wt FMRP CLIP performed in parallel. **B)** CLIP performed on FMRP expressed from the cTAG allele was highly correlated with CLIP performed on FMRP expressed from the endogenous allele, performed in parallel. **C)** AcGFP-FMRP CLIP was highly correlated with an earlier wt FMRP CLIP experiment.

A

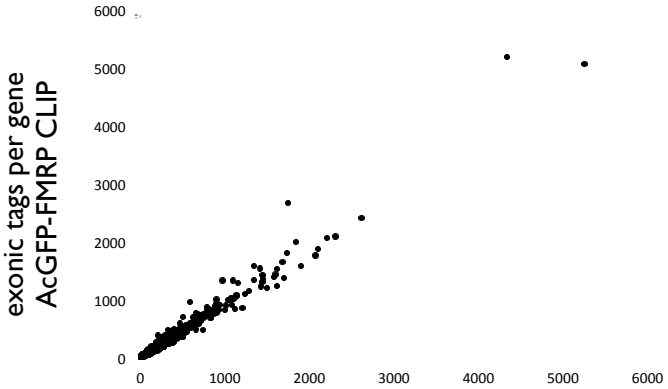

R^2=0.97

B

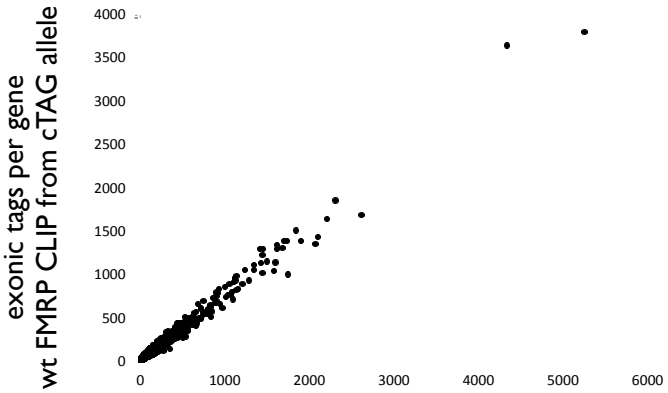

R^2=0.98

C

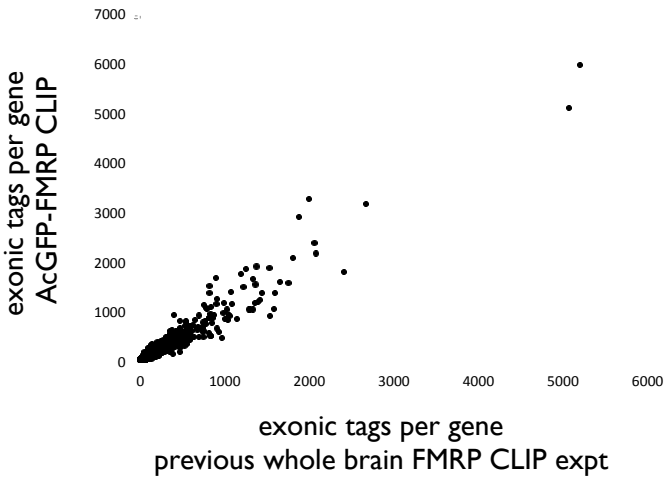

R^2=0.94

Figure 49. Comparison of tag distributions from wt FMRP and AcGFP-FMRP CLIP experiments.

The experimental tracks are represented in the following order: Upper track: FMRP CLIP from wt brain; middle track: FMRP CLIP from (-)Cre, cTAG/Y brain; lower track: AcGFP-FMRP CLIP from (+)Cre, cTAG/+ brain. Two gene examples are shown: *Bat2* (this page) and *Dlg4* (next page). Very similar tag numbers and distributions were observed in all three samples, indicating that the three forms of FMRP (AcGFP-FMRP, FMRP expressed from the cTAG allele, and FMRP expressed from the wt allele) are functionally equivalent.

Figure 49
pg 1 of 2

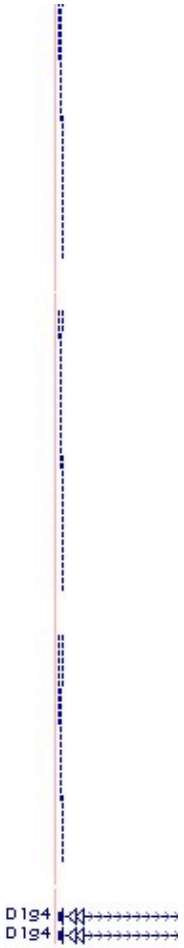
Dlg4
Dlg4

Chapter VI: General Discussion

We have shown that FMRP stalls ribosomes on a specific set of mRNAs previously identified as FMRP targets by HITS-CLIP. FMRP remains in dense fractions of sucrose gradients after treatment of brain lysates or cells with puromycin, a drug that causes translocating ribosomes to dissociate from mRNA. Since FMRP is well-characterized as a polysome-binding protein, this finding suggests that FMRP-associated mRNAs harbor nontranslocating ribosomes. FMRP loss-of-function in four different models was sufficient to increase the sensitivity of these nontranslocating ribosomes to puromycin, suggesting that FMRP is directly responsible for stalling these ribosomes and that loss of FMRP association with polysomes containing stalled ribosomes allows the stalled ribosomes to resume translocation. mRNAs that are not FMRP targets did not show this effect, providing further evidence that FMRP regulates the translation of specific target mRNAs. We have directly visualized FMRP-containing polysomes remaining in dense gradient fractions after both puromycin runoff and micrococcal nuclease treatment, lending support to a model in which FMRP-associated mRNAs contain multiple stalled, closely packed ribosomes. In an effort to address the origin of FMRP's target specificity, given that FMRP was observed to associate along the entire coding sequence length of its targets without discrete binding sites in polysome CLIP (Darnell 2011), we performed FMRP HITS-CLIP on total extracts and purified nuclear extracts from mouse brain. We did not find evidence of FMRP binding to intronic RNA or ncRNA, suggesting that the vast majority of FMRP appears to be associated with mature mRNA. However, our results did suggest that FMRP locally regulates translation of perinuclear mRNAs, a facet of FMRP biology that has received essentially no attention in the literature. We also performed FMRP HITS-CLIP on mice after seizure, and found that FMRP association with some mRNAs, including classical immediate-early genes such as c-fos, was altered after seizure compared to resting mice. This pilot experiment suggests future avenues for further research, such as an expanded timecourse of CLIP experiments after seizure and paired RNA-Seq profiling. Finally, we have designed a method of purifying membrane-associated and cytosolic polysomes from mouse brain, and have shown that FMRP-associated mRNAs are present in both compartments.

In order to refine our ability to understand how FMRP functions in diverse types of neurons, we have designed and generated a new knock-in mouse model, the FMRP conditional-tag (cTAG) mouse. In this mouse model, wt FMRP or AcGFP-tagged FMRP can be expressed from the same allele in a Cre-dependent, mutually exclusive fashion. AcGFP-FMRP is expressed in cells expressing Cre, while wt FMRP expression is maintained in all other cells. We have performed extensive analyses to confirm that the AcGFP tag does not alter the expression level or function of FMRP and that expression of the tagged isoform does not occur in the absence of Cre. Finally, we have shown that HITS-CLIP experiments performed using AcGFP-FMRP give near-identical results to CLIP experiments performed with wt FMRP. We plan to pair FMRP cTAG CLIP experiments with cell type-specific ribosome profiling experiments using the RiboTag mouse, which express HA-tagged ribosomes in a similar Cre-dependent manner. Together, these experiments will allow comprehension of translational regulation by FMRP with an unparalleled degree of specificity.

Section I: General model for FMRP function

Overall, the data presented here support a model in which FMRP inhibits translational elongation on specific mRNAs by stalling ribosomes. Although the canonical view has been that translational control occurs primarily at initiation, there are many examples in the literature of translational control during elongation. For example, the rate of ribosome progression can be slowed by mRNA pseudoknots (Somogyi et al., 1993), rare codons (Kimchi-Sarfaty et al., 2007), or interactions between the nascent polypeptide chain and the peptide exit tunnel (Fang et al., 2004). Ribosome stalling during elongation also occurs during targeting of mRNAs to the endoplasmic reticulum (ER) (Keenan et al., 2001). mRNAs encoding integral membrane or secreted proteins contain N-terminal signal sequences which, when translated, are bound by the signal recognition particle (SRP) as they emerge from the ribosome. This pauses ribosomal elongation until the SRP docks at the ER, at which point elongation resumes. Interestingly, the mechanistic basis for this elongational pausing was recently solved by crystallization of the SRP-80S ribosomal complex, in which it can be seen that the SRP is shaped like a telephone receiver, with one end binding the signal peptide near the ribosome exit channel and the

other end fitting into the intersubunit space where the elongation factor eEF2 usually binds (Wild et al., 2004). Although mRNAs associated with the ER are less sensitive to puromycin in runoff assays than free mRNAs ((Unsworth et al., 2010) and see discussion in previous chapter), we found that mRNA associations with the ER and with FMRP were not correlated; therefore, SRP stalling appears to be unrelated to FMRP function. Finally, two recent papers propose models in which 3'UTR-associated factors (hnRNPE1 or a Puf/Ago complex) inhibit activity of the elongation factor eEF1, thus stalling ribosomes shortly after elongation begins (Hussey et al., 2011), (Friend et al., 2012).

Interestingly, phospho-inhibition of the elongation factor eEF2 is emerging as an important element of translational control in neurons. Conceptually this makes some sense, as eEF2 kinase is a Ca^{2+}/calmodulin dependent kinase, and as such is poised to respond to neuronal activity. Phosphorylation of eEF2, which prevents its association with ribosomes and thus blocks ribosomal translocation, has long been a prominent example of nonspecific translational control during elongation. For example, phosphorylation of eEF2 is associated with decreased protein synthesis in the presence of intact polysomes during mitosis (Sivan et al., 2007). In neurons, eEF2 phosphoregulation has been shown to be locally and bidirectionally regulated in response to different forms of synaptic signaling (Sutton et al., 2007). Although eEF2 is a nonspecific elongation factor, synthesis of certain proteins actually increases when eEF2 is inhibited. For example, synthesis of the synaptic plasticity protein Arc in response to mGluR1 signaling was found to be dependent on both eEF2 phosphorylation and FMRP (Park et al., 2008). In another example, NMDAR activation and subsequent eEF2 phosphorylation resulted in increased translation of CamKIIa, and effect that was reproduced by low dose cycloheximide treatment, which limits elongation independently of eEF2 function (Scheetz et al., 2000). Both authors suggest that this paradoxical effect may be explained by inefficient initiation of affected transcripts. If competition for initiation factors is reduced by largescale reduction of translation, these mRNAs may be able to initiate more readily and achieve a modest level of translation even in the presence of phospho-eEF2. Such an effect was recently also found for Map1B, one of the top FMRP targets (personal communication, Nairn lab). However, given that Arc, CaMKIIa and Map1B are all

FMRP targets, it is tempting to speculate that FMRP and eEF2 might actually regulate elongation of separate sets of mRNAs, for example those coding for housekeeping genes versus those with synaptic functions.

Overall, it is clear there are a number of situations in which translational inhibition at elongation is important. In some of the above examples, translation of the nascent peptide is required to direct pausing as part of feedback inhibition loops or to target translation to certain compartments. More generally, inhibition of translation at elongation may markedly refine the temporal aspect of regulatory control. Translational pausing during elongation has the potential to provide instantaneous and rapidly reversible control on protein production. In contrast, inhibition at initiation provides less sharp temporal control, as ribosomes already in transit will still complete elongation and there will be a lag in protein synthesis when translation resumes, as ribosomes must translate the entire coding sequence from scratch before new protein is produced. Since initiation is usually considered the rate-limiting step of translation, translational pausing during elongation may also allow ribosomes to complete the time-consuming steps of initation during periods of low translational demand and then "wait in the wings" until new protein synthesis is needed. These benefits may be of greater magnitude for long mRNAs, and thus of particular relevance for some FMRP targets such as Bassoon.

In the case of FMRP, the even distribution of CLIP tags along the coding sequence of target mRNAs suggests that FMRP-directed ribosome stalling may occur randomly along the length of the coding sequence. Since CLIP tag maps represent FMRP:RNA interactions at the population level, individual transcripts could associate with single or multiple molecules of FMRP, and by extension could have single or multiple stalled ribosomes. *In vivo*, any ribosomes upstream of a stalled ribosome will eventually also become stalled. Stacking of multiple ribosomes with <30nt spacing has been observed when ribosomes are stalled *in vitro* (Wolin and Walter, 1988). Such a model is potentially consistent with our results showing that micrococcal nuclease treatment does not alter the size or physical appearance of polysomes that survive puromycin runoff. Together with results showing that little FMRP is released from these polysomes by

nuclease treatment, we suggest a model in which FMRP and ribosomes are tightly stacked together on stalled transcripts. One issue brought up by this model concerns the fact that we did not observe steady state differences in polysome size in the absence of FMRP, as might be expected if a stalled ribosome(s) was/were blocking passage of upstream ribosomes. One possible explanation for this result is that initiation could be secondarily inhibited, perhaps as a feedback response to elongational stalling. There are cases where concurrent phosphorylation of eEF2 and initiation factors has been observed (for example, (Kanhema et al., 2006)). However, it cannot be inferred in these cases whether initiation and elongation are inhibited on the same transcripts. Alternately, ribosome buildup behind a stalled ribosome might be balanced, on average, by ribosome runoff downstream of the stalled ribosome.

The fact that FMRP CLIP tags coat the coding sequence of target mRNAs without apparent discrete binding sites suggests the possibility that FMRP associates directly with ribosomes, traveling along and making close transient associations with the coding sequence during elongation. Although we cannot conclusively confirm such a model from our data, early studies did characterize FMRP as a ribosome-associated protein (Khandjian et al., 1996), (Siomi et al., 1996), (Eberhart et al., 1996), (Feng et al., 1997a). The acute reversibility of FMRP-mediated ribosome stalling demonstrated by kcRNA treatment during puromycin runoff suggests a model of dynamic ribosome stalling, perhaps in response to neuronal activity. It has been reported that unphosphorylated FMRP associates with more actively translating polysomes than a phosphomimetic form of FMRP (Ceman et al., 2003). Although this result could not be replicated in our lab, it suggests that ribosome stalling by FMRP could be phosphoregulated, for example in response to synaptic signaling. This conjecture is supported by the observation that the phosphorylated residue involved (Ser499 in mouse) is highly conserved, suggesting that phosphorylation at this site is likely important for FMRP function (Siomi et al., 2002). In such a model, derepression of FMRP-induced ribosome stalling would result in bursts of protein synthesis, thus tuning levels of specific proteins important for neuronal function in response to signaling. In the absence of FMRP, chronic overexpression of target proteins would uncouple synaptic signaling from dynamic responses in protein

expression and upset the finely controlled stoichiometry of synaptic proteins, leading to inappropriate expression of synaptic plasticity and subsequent defects in learning and memory.

Section II: Functional outcomes of FMRP regulation of target mRNAs

Role for FMRP in regulation of receptor signaling

The role of metabotropic glutamate receptors (mGluRs) in FXS has received a great deal of attention in the last decade. A link between FMRP and group I mGluRs was first suggested when *Fmr1* was identified as an mRNA present at synapses whose translation was upregulated in response to mGluR stimulation (Weiler et al., 1997). Although this finding suggested that mGluR-LTD might require FMRP and thus might fail to be expressed in the absence of FMRP, researchers were surprised to find that mGluR-LTD was in fact exaggerated in *Fmr1* KO mice (Huber et al., 2002). A model was formulated in which FMRP governs an inhibitory feedback loop that limits expression of mGluR-LTD, and it was suggested that this feedback might be particularly important during the critical period of synaptogenesis, when overexpression of LTD slows the process of synaptic maturation (Bear et al., 2004). Later it was found that in the absence of FMRP, mGluR-LTD no longer requires protein synthesis (Nosyreva and Huber, 2006). This finding suggested that in the absence of FMRP, proteins required for the expression of LTD are constitutively overexpressed, and thus additional synthesis is not required to facilitate LTD. Since this model was proposed, mGluR activity has been by far the most commonly used paradigm to assay the activity dependence of FMRP-mediated effects (Cruz-Martin et al., 2012), (Kao et al., 2010). Increased mGluR-LTD results in a long-term decrease in surface expression of postsynaptic AMPARs, which is associated with long thin spines and smaller PSDs (for review see (Luscher and Huber, 2010)). mGluRs mediate synaptic plasticity through a variety of mechanisms depending on cell type. In cerebellar parallel fiber-Purkinje cell synapses (the most well-studied mGluR-LTD system), mGluR activity is linked to phospholipase C hydrolysis of phosphoinositol, with subsequent release of intracellular calcium from the endoplasmic reticulum and activation of protein kinase C. This results in phosphorylation of AMPAR subunit GluR2, which

reduces its affinity for the postsynaptic scaffolding molecule GRIP and results in AMPAR endocytosis (Chung et al., 2003), (Steinberg et al., 2006). In contrast, mGluR-LTD in hippocampal region CA1, while less well characterized, does not require PKC and is thought to involve tyrosine dephosphorylation of AMPARs (Zhang et al., 2008), (Gladding et al., 2009). HITS-CLIP results show that mRNAs encoding mGluR subunits are targets of FMRP, suggesting that overexpression of mGluRs may contribute to enhanced mGluR-LTD expression in the *Fmr1* KO mouse.

Interestingly, FMRP also targets mRNAs encoding many other specific types of receptors, indicating that other forms of synaptic plasticity may also contribute to FXS. For example, the NMDA receptor and kainate receptor families are also highly targeted, while the AMPA receptor family, in contrast, is not. NMDA receptors induce plastic changes at synapses by passaging Ca^{2+} (in addition to Na^{+}) upon relief of a magnesium ion block of the channel pore during cellular depolarization. Crucially, the channel opens only when glutamate signaling corresponds with postsynaptic depolarization, signaling an effective correspondence between these two events. As is the case for mGluRs, changes in NMDAR activity mediate synaptic plasticity through modulation of postsynaptic AMPAR currents. The mechanistic details by which this occurs vary in different types of synapses; however, they are in general dependent on calcium and expressed through a combination of exocytotic changes in AMPAR surface expression, lateral diffusion of AMPARs between extrasynaptic sites and the PSD, and modulation of receptor conductance (for review see (Malenka and Bear, 2004)). Interestingly, a recent report found that NMDAR-LTP is enhanced upon loss of FMRP (Pilpel et al., 2009) and FMRP targets exhibit a high degree of overlap with the NMDAR-associated proteome (Darnell 2011). This suggests that the so-called "mGluR-LTD theory of FXS" in which chronic overexpression of "plasticity proteins" leads to exaggerated expression of synaptic plasticity may be a paradigm that applies to other forms of plasticity, including LTP.

FMRP also targets a number of other metabotropic receptors, many of which respond to stimuli other than glutamate. For example, latrophilins, which are brain-specific presynaptic adhesion-receptors, are very strongly targeted. Latrophilins are most well

known for binding to alpha-latrotoxin, a.k.a. black widow spider venom, which causes massive release of neurotransmitters. The teneuins, postsynaptic adhesion molecules with established roles in axon guidance and synaptogenesis, were recently identified as the endogenous ligands for latrophilins (Silva et al., 2011). Interestingly, teneuins are also FMRP targets. This suggests that the latrophilin-teneuin signaling axis may constitute an important facet of FMRP biology. In a second example, FMRP targets muscarinic acetylcholine receptors (mAChRs), which govern a form of protein-synthesis dependent LTD that is enhanced in the *Fmr1* KO (Volk et al., 2007). In a third example, FMRP targets certain receptor tyrosine kinases and phosphatases, a family of receptors that bind growth factors, cytokines and hormones and are linked to a variety of downstream signaling pathways including the PLC-IP_3, Ras-ERK and PI3K-Akt pathways (for review see (Dabrowski and Umemori, 2011)). Receptor tyrosine kinases dimerize upon ligand binding and each subunit's kinase domain phospho-activates the reciprocal subunit. Conversely, receptor tyrosine phosphatases dimerize in the resting state, occluding their phosphatase domains. Ligand binding causes monomerization, which exposes their phosphatase activity. Specifically, FMRP targets TrkB, TrkC and ephrin receptors, suggesting possible roles for FMRP in axon guidance and neurotrophic signaling. Interestingly, although the ErbB receptors are not strong targets, Erbb2ip, a PDZ domain-containing interacting protein for Erbb2 (otherwise known as HER2, a famous breast cancer oncogene) is a strong target, exemplifying that in general FMRP might modulate function of receptors even if the receptor genes themselves are not targeted. Finally, FMRP targets metabotropic GABA receptors ($GABA_B$ receptors), suggesting that its role is not exclusively limited to modulation of excitatory signaling.

Although FMRP does not broadly target ionotropic receptors, there are some prominent exceptions. Voltage gated calcium channel genes, especially those encoding the pore-forming α_1 subunits, are highly targeted. In particular, Cacna1e appears to be a major target. Cacna1e is present in postsynaptic spines and modulates plasticity through calcium-dependent activation of SK channels, which repolarizes the spine, reducing NMDAR activity (Bloodgood and Sabatini, 2009). Ligand gated calcium channels are also important targets, notably the inositol triphosphate (IP_3) and ryanodine receptors,

which release calcium from the endoplasmic reticulum in response to IP_3 and calcium, respectively. Finally, FMRP targets a few potassium and sodium channel genes, in particular the channel-forming subunit of the calcium-activated Big Potassium (BK) channel, Kcnma1, further underlining a major role for FMRP in regulation of calcium signaling.

Overall, HITS-CLIP data suggest that FMRP specifically targets metabotropic receptors and other non-conducting signaling receptors and receptors that either passage calcium or open in response to binding it. Most other monovalent cation channels are not significantly targeted. Inhibitory receptors such as glycine and GABA receptors are also not significantly targeted, with the exception of the metabotropic $GABA_B$ receptor. In general, this suggests that FMRP regulates the expression of a broad variety of receptors with specific roles in modulation of synaptic signaling, and future research into plasticity mechanisms in addition to mGluR-LTD may be productive.

Role for FMRP in regulation of synaptic plasticity pathways:

PSD proteins: Postsynaptic receptors are associated with a variety of signaling and scaffolding proteins clustered below the membrane, termed the postsynaptic density (PSD). Key roles of PSD proteins include anchoring receptors at the postsynaptic membrane and mediating signaling cascades initiated by the receptors (for review see (Feng and Zhang, 2009)). FMRP strongly targets members of the Dlg, Dlgap and Shank families of PSD proteins. All of these proteins contain PDZ domains, which facilitate scaffolding interactions, as well as numerous other protein-protein interaction domains, such as SH3 and GuK domains. The Dlg family, which includes the well-studied PSD-95, plays a critical role in clustering receptors, the canonical example being NMDARs, at the postsynaptic membrane (Gardoni et al., 2009). Interestingly, while FMRP strongly targets Dlg1, 2 and 4, it barely targets Dlg3, even through Dlg3 is the most abundant member of the family and clearly has an important role in synaptic function, especially in early postnatal development when FMRP function is at its peak (Zheng et al., 2010). The cTAG mouse should be useful in the resolution of such cases: by combining cell type-specific HITS-CLIP with cell type-specific ribosome profiling, it should be possible to

address whether lack of association between FMRP and Dlg3 is due to lack of coexpression in the same cells, or reflects functional discrimination by FMRP among Dlg family members. Dlgaps (a.k.a. SAPAPs) were originally identified as Dlg-binding proteins (Takeuchi et al., 1997) and were later shown to also bind to Shank proteins (Boeckers et al., 1999), which link to the actin cytoskeleton underlying the spine (Boeckers et al., 2002). Shanks also interact with mGluRs through another PSD protein, Homer (Hayashi et al., 2009). FMRP strongly targets all members of the Dlgap and Shank families, and members of both families have been strongly implicated in autism (Pinto et al., 2010) (Phelan and McDermid, 2012). It has been suggested that PSD proteins such as Dlgs constitute "slots" for receptor binding that determine how many receptors of a given type can occupy a synapse, even while individual receptors cycle in and out of the postsynaptic region (Malinow et al., 2000), (Schnell et al., 2002). Thus, FMRP's regulation of protein level of genes such as Dlg's is likely to have a direct impact on receptor signaling. Also, there is evidence that the relative stoichiometries of different PSD proteins is important; for example Shank and Homer appear to form a mesh-like structure in which Shank proteins form nodes connecting rod-like Homer proteins (Hayashi et al., 2009). Thus, FMRP could indirectly regulate the level of synaptic Homer proteins by controlling the amount of available Shank proteins. In contrast to the strong targeting of PSD proteins involved with NMDAR and mGluR signaling, FMRP does not target several PSD proteins that mediate AMPAR insertion and retention at the membrane, notably Grips, Grasp1 and Pick1 (Ye et al., 2000), (Kim et al., 2001), (Chung et al., 2000), consistent with AMPARs themselves not being FMRP targets.

Any discussion of the PSD inevitably includes CaMKIIa, by far the most abundant protein in the PSD and an important FMRP target (for review see (Lisman et al., 2012)). The CaMKIIa holoenzyme is a two-layer ring consisting of twelve subunits. Low levels of $Ca^{2+/}$calmodulin binding briefly activates CaMKIIa. However, if calmodulin binding is high enough that neighboring CamKIIa subunits are simultaneously bound, these subunits become autophosphorylated, extending the timecourse of activity even after calcium levels have returned to baseline. Thus, CamKIIa has properties that allow

integration of calcium signaling over time. The unusually high abundance of CaMKIIa at the PSD suggests a possible major structural role in addition to an enzymatic role. Coupled with CaMKIIa's ability to retain activity for extended periods, it suggests that CaMKIIa could coordinate long-lasting structural changes that could possibly be a substrate for memory storage. As discussed above, CaMKIIa translation increases under conditions in which global levels of translation decrease (Scheetz et al., 2000), suggesting that translational control is an important element in regulation of CaMKIIa expression.

Cytoskeletal proteins: Changes in synaptic plasticity are highly correlated with changes in spine shape and size: large spines tend to be more stable over time and have greater synaptic strength (expressing higher levels of AMPA receptors), while small spines tend to be weaker and more plastic (Kasai et al., 2003). It has long been recognized that FXS is associated with abnormal spine morphology in the form of long, thin, tortuous spines (Hinton et al., 1991), (Rudelli et al., 1985). Such changes in spine shape and size are primarily driven by actin dynamics. The actin network underlying spines is connected to various proteins in the PSD, such as Shanks, which allows transmission of information about signaling at the membrane to the underlying cytoskeleton (Boeckers et al., 2002). FMRP only weakly targets actin itself, but it does regulate several other cytoskeletal elements and regulatory proteins. For example, tropomodulins control rates of actin polymerization by capping the pointed ends of actin filaments. A mouse knockout of tropomodulin-2, a strong FMRP target, had enhanced LTP at Schaffer collateral synapses, demonstrating the necessity of proper actin polymerization for expression of synaptic plasticity (Cox et al., 2003). FMRP also targets ankyrins (which cluster membrane proteins such as receptors and adhesion molecules and anchor them to the actin/spectrin cytoskeleton), plakophilins (which link cadherins to intermediate filaments), and dystonin (which links intermediate filaments to actin). These molecules provide direct links between signaling proteins already shown to be FMRP targets and actin. Although cytoskeletal proteins are important for synaptic function, results from FMRP nuclear CLIP suggest that FMRP also locally regulates translation of cytoskeletal proteins around the nucleus. Therefore, translational control by FMRP of mRNAs

encoding cytoskeletal proteins likely has multiple functional outcomes, including but not limited to expression of synaptic plasticity.

Finally, six out of the top ten FMRP targets are involved with microtubule dynamics. Microtubules mediate fast transport of a variety of cellular components such as vesicles (for example synaptic vesicle precursors or vesicles carrying membrane receptors), mitochondria and translationally repressed RNA granules (for review see (Namba et al., 2011), (Kapitein and Hoogenraad, 2011), (Hirokawa, 2006). Transport is carried out by motor proteins in the kinesin and dynein families. Each member of these families has specificity for particular cargoes, facilitated by a variety of adaptor proteins. For example, rab GTPases are key mediators of vesicle transport, recruiting effector molecules that orchestrate motor-cargo assemby (Horgan and McCaffrey, 2011). Major FMRP targets include Maps (which bind and stabilize microtubules), kinesins and dyneins. Map1B is one of the few targets for which protein-level increases in whole cell lysate can be detected by Western blot after the loss of FMRP (Lu et al., 2004), (Zhang et al., 2001). Since the microtubule system trafficks key synaptic components such as receptors, a major facet of FMRP function appears to be downregulation of the delivery system for these components. This suggests that FMRP plays a role in cell-wide dampening of neuronal activity, by limiting the availability of "parts" for synaptic function.

cAMP signaling

Loss of FMRP has been linked to lowered cAMP levels in a variety of systems (Kelley et al., 2007), (Berry-Kravis and Huttenlocher, 1992), (Berry-Kravis and Sklena, 1993). cAMP is produced from ATP by adenylate cycles, which respond to G protein signaling from a variety of receptors. Consistent with lowered cAMP levels, FMRP targets Adcy1, 5 and 8, which are all calcium-sensitive adenylate cyclases. Synergistic response to G proteins and calcium positions adenylate cyclases as coincidence detectors for the activities of GPCRs and other receptors that admit calcium, such as NMDARs or calcium channels. Differing sensitivities to calcium can also tune different adenylate cyclases to varying stimulation thresholds; for example, Adcy1 reaches half maximal activity at

150nM Ca^{2+} (resting levels are 100nM), while Adcy8 is not half-active until 800nM Ca^{2+} (during activity, Ca^{2+} levels can locally approach 1-10uM (Banerjee and Hasan, 2005)) (Ferguson and Storm, 2004). FMRP also targets several phosphodiesterases, which hydrolyze cAMP, representing a counterbalance on the activity of adenylate cyclases.

cAMP stimulates members of the PKA family and the RapGEF Epac (discussed below in the section on small GTPase regulation). FMRP does not target any members of the PKA family. However, PKA activity is directed to particular microdomains by a diverse family of anchoring proteins known as AKAPs (Bauman et al., 2004). Interestingly, FMRP does target several of the AKAPs, including Akap6, which is a major target that anchors PKA to the nuclear envelope and whose mRNA was found to be associated with FMRP in the perinuclear compartment by FMRP nuclear CLIP. Modulation of PKA through cAMP is predicted to have broad effects on neuronal function; for example, PKA stimulates the transcription factor CREB, which upregulates important plasticity genes such as BDNF and secondary transcription factors such as c-fos, illustrating the potential complexity of downstream ripple effects of FMRP regulation.

Small GTPase signaling

Small GTPases are membrane-associated monomeric G proteins of 20-25kD that bind GTP in their active state. Regulation of small GTPase function is an essential component of FMRP biology (Darnell 2011). Several families of small GTPases including the Ras, Rho, Rab and Rheb families have been implicated in control of neuronal plasticity and memory (Ye and Carew, 2010), (Tolias et al., 2011), (Newey et al., 2005). The activity of small GTPases is controlled by accessory proteins called GAPs (GTP activating proteins) and GEFs (GTP exchange factors). GAPs reduce the activity of GTPases by promoting GTP hydrolysis, while GEFs activate GTPases by exchanging GDP for GTP. GEFs and GAPs are large multidomain proteins that interact with a wide variety of binding partners, allowing given GTPase activity to be tuned to particular localizations and inputs. Small GTPase signaling impinges on key cellular pathways including the MAPK/ERK and PI3K/AKT/mTOR pathways. Well-characterized downstream effects of GTPase signaling include actin remodeling (Rho family), membrane trafficking (Rab

family) and translational control (Rheb family). Small GTPase activity has profound consequences for cells (most prominently, excessive Ras signaling leads to overactive cell growth and tumorigenesis), so it is logical that their activity is under tight and complex regulation.

Most literature concerning FMRP's link to small GTPase activity has focused on Rac1 and actin remodeling, because FXS is associated with defects in spine morphogenesis. Some data show that phenotypes linked to loss of FMRP (enhanced mGluR LTD in mouse hippocampus; reduced dendritic branching in Drosophila) can be reversed by respectively inhibiting or overexpressing Rac1 (Bongmba et al., 2011), (Lee et al., 2003). This suggests that actin remodeling is important in the downstream expression of FMRP function, but does not show that FMRP directly regulates small GTPase activity. There is limited and conflicting data concerning direct effects of FMRP on Rac1 levels or activity (Bongmba et al., 2011), (Chen et al., 2010). The CLIP data shows that Rac1 is not a target of FMRP (in fact, as a general rule small GTPases themselves are not targeted by FMRP). However, a large number of GAPs and GEFs are strong FMRP targets, indicating that FMRP has a major and direct role in regulation of small GTPase activity, with implications for cytoskeletal remodeling and translational control (see section below).

Several major FMRP targets are GAPs or GEFs with functions at the PSD. These include syngap1, rapGEF4 (Epac2), kalirin and plexinB1. Syngap1 is a calcium-activated Ras GAP that is associated with Dlgs and NMDARs (Ye and Carew, 2010). Bidirectional manipulation of syngap1 expression affects AMPAR-mediated synaptic transmission, dependent on both PDZ and GAP domains (Rumbaugh et al., 2006). Epac2 is a cAMP-responsive RapGEF linked to spine remodeling (Woolfrey et al., 2009). Kalirin is a RhoGEF involved in spine formation and NMDAR-LTP (Ma et al., 2008), (Kiraly et al., 2011), (Lemtiri-Chlieh et al., 2011). PlexinB1 is a semaphorin receptor with a cytoplasmic Ras/Rap GAP domain (Bos and Pannekoek, 2012). Activation of Rap1 by plexinB1 requires both semaphorin binding and intracellular binding of a Rho GTPase next to the GAP domain (Oinuma et al., 2004). These targets exemplify the prominence

of small GTPase signaling at the synapse, although much work remains to better understand the steps between GTPase activity and downstream readouts such as spine remodeling or neurite outgrowth.

FMRP also strongly targets two GAPs that influence translational control through the mTOR pathway: NF1 and Tsc2. This is of particular interest because potential links between mTOR and FMRP have received a lot of attention (discussed further below). Both NF1 and Tsc2 are associated with diseases characterized by tumorigenesis (neurofibromatosis and tuberous sclerosis, respectively), due to overactivity of cellular growth pathways such as the PI3K/Akt/mTOR pathway (for review see (Hoeffer and Klann, 2010)). NF1 is a negative regulator of Ras (Cichowski and Jacks, 2001), while the Tsc1/2 complex is a negative regulator of Rheb (Huang and Manning, 2008). Both ultimately inhibit mTOR signaling and dampen translation (Johannessen et al., 2005), (Inoki et al., 2002); thus, targeting of NF1 and Tsc2 by FMRP would be predicted to increase global translation. This is contrary to the standard model of translational repression by FMRP, and complicated by the fact that FMRP also targets PIKE, PI3K, Akt, mTOR and the mTORC1 protein Raptor, which collectively would be predicted to have the opposite outcome (decreasing global translation). The paradox of why FMRP would target both positive and negative regulators of the same pathway may reflect an insufficiently subtle understanding of the situation, since FMRP may not target all of these mRNAs in every cell. The cTAG mouse could provide clarity in this case. Alternatively, NF1 and/or Tsc2 may participate in additional signaling pathways that are relevant FMRP biology. For example, NF1 het mice have elevated ERK activity, which is predicted to potentiate translation (Guilding et al., 2007).

Because most literature on Tsc2 and NF1 relates to oncogenesis, most of what is known about their function was deduced from non-neuronal systems. However, recent studies have demonstrated roles for Tsc2 in axonal pathfinding (Nie et al., 2010) and mGluR-LTD (Auerbach et al., 2011), both processes that require translation. The finding that *Tsc2*+/- mice have decreased mGluR-LTD was a surprise to the authors of the second study, who presumed that since loss of Tsc1/2 activity activates mTOR, which is

canonically considered to result in overactive translation, Tsc2 het mice might have *increased* mGluR-LTD like *Fmr1* KO mice, which also exhibit overactive translation. Instead, they found that *Tsc2*+/- mice had decreased mGluR-LTD and decreased *de novo* protein synthesis in hippocampal slices, both phenotypes opposite to what the authors observe in *Fmr1* KO mice. In fact, the effects caused by loss of Tsc2 are reversed if FMRP is also absent, which suggests that FMRP and Tsc2 normally counterbalance each other. One unresolved issue is why the rapamycin-dependent phenotypes in the Tsc2 het are linked to translational suppression. The authors suggest that if mTOR inhibits FMRP, then loss of Tsc2 would result in increased inhibition of FMRP, which could explain the repression of protein synthesis. However, they supply no evidence in support of this idea. As a side note, both *Tsc2*+/- and *Fmr1* KO mice displayed similar phenotypes at the behavioral level, despite opposing phenotypes at the biochemical and electrophysiological levels. Similar situations have been demonstrated by others, for example the *Syngap1* KO and the *PSD-95* KO have decreased/increased hippocampal LTP respectively, but both mice perform poorly in the Morris water maze (Komiyama et al., 2002), illustrating that behavioral readouts indicative of synaptic dysfunction are not always informative about the nature of the specific underlying molecular defect.

Translational control of presynaptic proteins

Overall, it is clear that FMRP regulates numerous mRNAs with well-characterized functions in synaptic signaling and synaptic plasticity. Local postsynaptic translation is necessary for the expression of several forms of plasticity including mGluR-LTD (Huber et al., 2000) and FMRP is present at synapses (Antar et al., 2005). Nonetheless, most FMRP is somatic and there are also a few reports of a role for FMRP in axons or at the presynaptic terminal. For example, Antar et al reports localization of FMRP in puncta in axons and growth cones of young (4 DIV) primary hippocampal neurons and that growth cones from *Fmr1* KO neurons have more filopodia and reduced motility (Antar et al., 2006). In addition, FMRP-containing granules (FXGs) have been found in axons of young neurons undergoing synaptogenesis, for example in olfactory bulb neurons (Christie et al., 2009). In agreement with the findings in growth cones, FXGs were more

abundant during periods of heightened synaptogenesis, for example in young mice or during reinnervation of the olfactory epithelium after injury. FMRP CLIP has revealed a number of targets classically associated with presynaptic functions. Several of these are involved with vesicle fusion and SNARE complex formation. However, the proteins that form the SNARE complex – syntaxin, synaptobrevin and SNAP-25 – are not strongly targeted even though they are highly abundant. Rather, several proteins with modulatory roles in SNARE complex formation are targeted. A key event in vesicle priming is the transition of syntaxin from a "closed" state, bound very strongly to munc18, to an "open" state capable of forming SNARE interactions (Dulubova et al., 1999). This transition is regulated by several FMRP targets, including munc13, syntaphilin, rabphilin3a, syntaxin binding protein-5 (tomosyn) and RIMs 1 and 2. Tomosyn and syntaphilin are both reported to bind to syntaxin and promote its association with the SNARE complex (Fujita et al., 1998), (Lao et al., 2000). Munc13 is reported to bind munc18, also promoting release of syntaxin from the closed state (Ma et al., 2011) (interestingly, munc13 is a diacylglycerol receptor, linking it to pathways highly targeted by FMRP as discussed above). In contrast, rabphilin is a negative regulator of vesicle release, binding SNAP-25 (Deak et al., 2006). RIMs are scaffolding proteins that bind a variety of presynaptic proteins; for example they are reported to activate munc13 by relieving autoinhibitory homodimerization (Deng et al., 2011). Overall, it seems that FMRP regulates vesicle exocytosis by means of targeting a number of modulatory proteins, a role that has received very little attention in the literature.

FMRP also plays a role in regulation of clathrin-mediated endocytosis, as revealed by targeting of synaptojanins and several of the adaptor-related protein complex (AP) genes, in particular the AP-2 subfamily. AP proteins are hubs that organize vesicle fusion, binding phosphoinositides, clathrin, and a variety of accessory factors (eg membrane deforming proteins and adaptors that recruit vesicle formation around particular membrane proteins) (Rodemer and Haucke, 2008). Synaptojanins are phosphatases that act on PIP_2 and PIP_3 to release and recycle AP-2 complexes and other factors involved with clathrin-mediated endocytosis (Cremona et al., 1999). While these processes are critical for recovery of vesicles into the presynaptic membrane after neurotransmitter

release, they may also play roles in postsynaptic endocytosis of receptors (Gong and De Camilli, 2008). By the same token, proteins involved in SNARE-mediated exocytosis could have postsynaptic roles, for example in vesicle-based delivery of receptors to the postsynaptic membrane. For example, tomosyn can be visualized on both sides of the synapse by electron micrograph (Fujita et al., 1998).

FMRP strongly targets Bassoon and Piccolo, two very large presynaptic proteins. Based on their size, one might conjecture a major structural role for these proteins. However, most synapses lacking Bassoon appear structurally normal by electron micrograph (Altrock et al., 2003), with the exception of unanchored ribbon synapses (specialized synapses that sustain slow, continuous vesicle release in response to "analog" variation in sensory input) (Lagnado, 2005). Nonetheless, truncation of most of Bassoon's protein sequence causes mice to have defects in vesicle release and to die of seizures, so Bassoon must play a more subtle but critical role in regulation of exocytosis (Altrock et al., 2003). Although Bassoon and Piccolo are major presynaptic proteins, they are translated somatically and axonally transported in Golgi-derived dense core vesicles (Dresbach et al., 2006), a model consistent with our finding that 92% of *Bsn* mRNA and 91% of *Pclo* mRNA is present on ER membranes. This mechanism might be a way to ensure that Bassoon and Piccolo avoid aggregation after translation since they are so large, or it could reflect a mechanism of pre-fabrication of proto-active zones that are then delivered to developing synapses. In any case, while targeting of Bassoon and Piccolo almost certainly indicates presynaptic consequences for FMRP function, it constitutes an example of somatic translational control of ER-associated mRNAs by FMRP.

Finally, FMRP targets several synaptic adhesion molecules, which occur in postsynaptic-presynaptic pairs and are of particular interest because some have been strongly linked to autism (Betancur et al., 2009). Neurexins, neuroligins, plexins and protocadherins are all important FMRP targets. These molecules make physical contact in pairs across the synaptic cleft (neurexins, which are presynaptic, bind neuroligins, which are postsynaptic; plexins bind semaphorins, which can be either secreted or membrane bound; protocadherins bind each other in homophilic or heterophilic interactions). The

diversity of adhesion molecules, both in terms of gene families and extensive alternative splicing, helps specify synaptic connections in a complex network environment (Ding et al., 2012). The best characterized of the adhesion molecules are the neuroligins and neurexins (Sudhof, 2008). The cytoplasmic portions of each bind to PDZ domain-containing proteins in the presynaptic active zone or PSD, harnessing a transsynaptic signaling complex that is essential for neuronal function; loss of neuroligins in mice is associated with severe defects in synaptic transmission (Varoqueaux et al., 2006) and mutations in either are strongly associated with autism (Betancur et al., 2009). Again, while we cannot infer local presynaptic translation of synaptic adhesion molecules from the CLIP data, FMRP clearly regulates targets with crucial functions on both sides of the synapse.

Meta-Regulation of Translational Control

FMRP directly regulates translation of specific mRNAs, as is evidenced by its RNA-dependent association with polysomes, its direct association with coding sequence as assayed by HITS-CLIP, its effect on the puromycin sensitivity of ribosomes associated with target mRNAs, and its effect on ^{35}S-methionine incorporation during translation of target mRNAs. However, a number of FMRP target mRNAs encode translation factors or proteins in signaling pathways that regulate translation. Therefore, regulation of these targets by FMRP is predicted to have secondary effects on global translation. FMRP has considerable specificity for particular translation factors. For example, of the myriad of initiation factors, FMRP strongly targets only one family, the eIF4Gs. The joining of eIF4G with eIF4E is a major control point of initiation, controlled by a family of 4E-binding proteins (4EBPs) that occlude eIF4G binding. Inhibition of eIF4G translation constitutes an alternate mechanism of limiting eIF4F assembly and illustrates a prime example of how FMRP can enforce secondary, nonspecific inhibition of translation.

FMRP is also predicted to have secondary effects on translational elongation. While there is a report that FMRP binds *eEF1* mRNA (Sung et al., 2003), this finding is based on interaction of *in vitro* transcribed message with recombinant FMRP under low salt conditions, all elements that reduce the probability that this is a specific interaction.

Furthermore, binding was not dependent on the I304 residue required for polysome binding that is central to FMRP function. However, the considerably more stringent CLIP assay shows that FMRP associates with *eEF2* mRNA to a much greater extent than with *eEF1* mRNA. However, inhibition of *eEF2* translation should not be construed as the primary mechanism by which FMRP acts, as this would be inconsistent with demonstrated direct FMRP association with hundreds of other target mRNAs. Nonetheless, downregulation of eEF2 protein levels by FMRP likely represents a secondary mode of translational control that may be important for neuronal function, since phospho-inhibition of eEF2 has been shown to occur in response to synaptic signaling (Scheetz et al., 2000), (Kanhema et al., 2006).

Another facet of translational control under secondary regulation by FMRP is the Argonaute/miRNA system. miRNAs are short, ~21nt long RNAs that, together with members of the Argonaute family and other factors, repress expression of target proteins. It is estimated that at least 60% of mammalian mRNAs are regulated by miRNAs (Bartel, 2009). miRNA processing begins in the nucleus, where the RNAse III enzyme Drosha trims out the miRNA hairpin loop from the larger RNA (multiple hairpin loops containing separate miRNA genes are often transcribed as a single unit). The hairpin loop is then exported to the cytoplasm, where the loop is cut off by another RNAse III enzyme, Dicer, leaving the stem as a short, double-stranded RNA. One strand of this intermediate is then assembled into a complex with Argonaute and other proteins, termed the RNA-induced silencing complex (RISC). The RISC then binds target mRNAs, guided by miRNA sequence complementarity and resulting in decreased protein production. Whether this occurs via translational suppression or mRNA degradation has been the subject of intense debate, but a reasonable current model is that initial steps of miRNA silencing involve inhibition of translational initiation, followed by targeting of the message to P-bodies, where deadenylases and decapping enzymes degrade the mRNA unless other pathways direct its release from P bodies (Djuranovic et al., 2011). However, much about this process remains to be resolved. For example, although miRNA binding sites are canonically thought to be located in 3'UTRs, more than 35% of Ago binding sites identified by CLIP are in introns or coding regions (Chi et al., 2009),

indicating the mechanism and/or scope of Ago function is not yet fully understood. FMRP targets all of the well-expressed Ago genes (Ago 1-3) as well as Dicer, suggesting that FMRP crosstalks with the Argonaute pathway and suppresses its function. This is in contradiction to suggestions in the literature that FMRP mediates its effects on translation *through* Ago. That this might be the case was originally suggested when large-scale purification of the RISC complex from *Drosophila* S2 cells revealed copurification of dfmr (Caudy et al., 2002). Because the HPLC-based purification scheme did not involve an antibody-based step, direct interaction of dfmr with RISC could not be proven. However, dfmr and Ago2 were subsequently coIPed (in the same cell system), using either TAP-tagged or T7 tagged (and overexpressed) dfmr (Caudy et al., 2002), (Ishizuka et al., 2002). While both authors claimed the associations were RNAse-resistant, data were either not shown (Caudy et al) or the association in fact appeared to be RNAse-sensitive (Ishizuka et al). This control is critical to show that dfmr and Ago2 directly interact and do not merely coexist on polysomes. Another issue with these experiments is that *Drosophila* Ago2 has no mammalian ortholog, so results are not necessarily translatable to mammalian Argonautes (mammalian Ago2 is orthologous to Drosophila Ago1). The coIP result was replicated in mammalian cells; however an *Fmr1* KO control was not included to demonstrate that (mammalian) Ago2 association was FMRP-dependent (Jin et al., 2004). This turned out to be a fatal flaw, as the antibody used (7G1-1) was later shown to indeed bind Ago2 in the absence of FMRP (oddly, this appeared to be due to contamination of the 7G1-1 clone with a separate monoclonal that recognized Ago2 (unpublished observation from our lab)). In addition, since we show in this thesis that polysome-associated FMRP appears to be largely inaccessible to antibodies (**Figure 11**), these coIPs may only capture the small portion of FMRP that is nonpolysomal *in vivo*. Another way to show that FMRP facilitates translational inhibition through Ago would be to show that knockdown of Ago2 results in translational derepression of FMRP target mRNAs. Such an experiment has not been published; instead, several attempts have been made to show the reverse – that knockdown or loss of FMRP reduces RNAi-mediated knockdown of reporter constructs (Ishizuka et al., 2002), (Caudy et al., 2002), (Plante et al., 2006), (Didiot et al., 2009). Results were mixed, with two of four groups finding that loss of FMRP reduced efficacy of RNAi. However, the reporters were not

FMRP targets and nonspecific binding may have occurred due to overexpression of the reporters. Finally, FMRP was not found in P bodies, which would be expected if FMRP-bound transcripts were entering the Ago pathway (Didiot et al., 2009). Together, these results do not provide sufficient evidence to conclude that FMRP induces translational repression by recruiting the RISC complex to target mRNAs. However, based on the CLIP results, we predict that FMRP may downregulate expression of Ago pathway components.

The mTOR and ERK pathways are important regulators of translational control that mediate the expression of several forms of protein synthesis-dependent synaptic plasticity, making their relationship to FMRP function the focus of intense study (Tang et al., 2002), (Richter and Klann, 2009), (Hoeffer and Klann, 2010). mTOR associates with two different complexes, mTORC1 and mTORC2, which direct mTOR activity towards particular substrates. The best-studied of these complexes, mTORC1, phosphorylates 4EBP1 and 4EBP2, relieving their inhibition of eIF4E and promoting translation. mTORC1 also phosphoactivates S6 kinases. S6 kinases phosphorylate ribosomal protein S6, which is associated with increased translation of messages containing 5' terminal polypyrimidine tracts in their UTRs. So-called 5'TOP mRNAs encode ribosomal proteins and translation factors, so activation of S6 kinase represents a second mechanism of eliciting a general increase in translation. Like mTOR, ERK also phosphorylates 4EBPs and S6 kinase. In addition, ERK can phosphoactivate eIF4E through Mnk1. These events are associated with a number of forms of synaptic plasticity (Richter and Klann, 2009), (Hoeffer and Klann, 2010). In particular, both mTOR and ERK signaling are required for hippocampal mGluR-LTD (Hou and Klann, 2004), (Banko et al., 2006), the form of synaptic plasticity most well-studied in FXS.

FMRP does not target MEK, ERK or Mnk mRNAs involved in the ERK pathway. In contrast, FMRP does target PIKE, PI3K, Akt, Tsc2, mTOR and Raptor, indicating a high level of control over the mTOR pathway. Except for Tsc2 (see above discussion), these results are consistent with a general downregulation of translation through limiting activity of the mTOR pathway. Literature supporting relationships between FMRP and

the mTOR pathway is complicated and conflicting. Before discussing it, it is worthwhile to consider the theoretical possibilities for FMRP interaction with the mTOR pathway. Following are three hypothetical scenarios:

FMRP could indirectly regulate the mTOR pathway by downregulating pathway components at the mRNA level. Based on CLIP data, this appears to be true, and should be expressed as an increase in these proteins in the *Fmr1* KO at least under some conditions, such as during mGluR5 activation.

FMRP could modulate the mTOR pathway at the protein level. For example, FMRP could dampen protein synthesis by binding/inhibiting mTORC1 or binding/activating the Tsc1/2 complex. If this were true, the mTOR pathway should be upregulated in the *Fmr1* KO, and treatment with rapamycin should mitigate KO phenotypes. Conversely, treatment of wt with rapamycin might have effects similar to FMRP overexpression, for example hypoactivity or increased anxiety (Peier et al., 2000). Although this scenario does not account for the importance of direct RNA binding in FMRP function, FMRP could theoretically have a secondary functional mode involving protein-protein interaction.

FMRP could be an effector of the mTOR pathway (meaning it acts directly on the translational machinery but is modulated by mTOR signaling). mTOR phosphorylation of FMRP could inhibit its catalytic activity, interfere with its binding activity/partners, or target it for degradation. If this were true, we would expect mTOR pathway activity to be unchanged in the *Fmr1* KO (excluding possible feedback effects). Treatment with rapamycin would be difficult to interpret because FMRP would not be the only mTOR effector.

Several studies have attempted to address whether or not the mTOR or ERK pathways are upregulated in the *Fmr1* KO, either basally or in response to mGluR activation by DHPG. In hippocampal slices, the ERK pathway was activated in response to DHPG (Banko et al., 2006), (Ronesi et al., 2012), (Osterweil et al., 2010), and the level of

activation was similar in wt and *Fmr1* KO (Ronesi et al., 2012), (Osterweil et al., 2010). There is a report of aberrant ERK signaling in *Fmr1* KO cortical synaptoneurosomes correlated with increased protein phosphatase 2A (PP2A) activity (Kim et al., 2008). The protein phosphatase genes Ppp2r2c and Ppp2r5b are strong FMRP targets, so increased PP2A activity in the *Fmr1* KO is consistent with CLIP results. However, the bulk of the evidence, including the fact that FMRP does not target members of the ERK pathway, indicates that ERK signaling acts independently of FMRP.

Results concerning the mTOR pathway are more complicated, and appear to depend in part on whether hippocampal slices are rested before assaying. In non-rested slices, basal mTOR signaling was increased in the *Fmr1* KO; upon DHPG stimulation mTOR signaling increased in wt but remained saturated in the KO (Sharma et al., 2010). This group also found upregulation at the protein level of PIKE, one of the top FMRP targets. Since PIKE is an upstream driver of the mTOR pathway, increased synthesis of PIKE in the *Fmr1* KO could explain the overall increased activity of the pathway (Sharma et al., 2010), (Gross et al., 2011). These results are consistent with an earlier report that mTOR signaling was upregulated in response to DHPG (Hou and Klann, 2004). In contrast, Osterweil et al found that the mTOR pathway was basally unchanged in the *Fmr1* KO and not inducible by DHPG in either wt or KO (Osterweil et al., 2010). However, the slices used in this experiment were rested for four hours prior to assay; if non-rested slices were used the mTOR pathway was basally upregulated in the *Fmr1* KO, consistent with Sharma et al. Which result is correct is unclear – freshly dissected slices may better represent the *in vivo* state, or they may be more subject to transient stresses induced in preparation. Finally, a third group reported that the mTOR pathway was upregulated in wt but not *Fmr1* KO in response to DHPG (in rested slices (Ronesi et al., 2012)). However, this interpretation is unclear because data are normalized to the baseline state. If basal mTOR signaling is upregulated in the *Fmr1* KO and not further increased by DHPG as seen by Sharma et al, this would be plotted as a *lack of* rather than a *saturation of* mTOR signaling in the KO – very opposite conclusions based on what could be similar results.

The above results are insufficient to allow firm conclusions about whether FMRP affects mTOR signaling, either as a modulator or an effector, although together with the CLIP results they do suggest that FMRP at least has an indirect effect on the pathway through translational inhibition of its components. However, one report does attempt to address whether FMRP is directly affected by mTOR and/or ERK signaling (ie, whether FMRP is a downstream effector). The authors found that basal FMRP phosphorylation was absent in the *S6K1* KO hippocampus, and that stimulation of primary neurons with DHPG resulted in increased S6 and FMRP phosphorylation over similar timecourses, which could be attenuated by mTOR and ERK inhibitors (Narayanan et al., 2008). Together, these results suggest that both mTOR and ERK activate S6K1, which then phosphorylates FMRP. Phosphorylation of FMRP has been reported to result in decreased translation of its targets (Narayanan et al., 2008), (Ceman et al., 2003). The finding that mGluR-LTD was correlated with increased phosphorylation of S6K1 but remained expressed in *S6K1* KO mice seems to suggest that S6K1 is not a central player in the expression of mGluR-LTD (Antion et al., 2008). However, these results could be consistent with a model in which S6K1 phosphorylates FMRP (causing translational suppression) during mGluR-LTD in order to maintain expression of LTD within normal limits. Loss of S6K1 and subsequent dephosphorylation of FMRP would be predicted to result in translational derepression of FMRP targets. Since loss of FMRP increases expression of mGluR-LTD, inactivation of FMRP by dephosphorylation might be expected to similarly increase mGluR-LTD. Thus, mGluR-LTD would continue to be expressed in the *S6K1* KO, as observed.

Overall, it is clear that FMRP can indirectly affect translational control via several avenues. Interestingly, FMRP does not target mRNAs coding for ribosomal or proteasomal proteins, even though many of these mRNAs are very abundant and this would represent a very direct route of secondary control over protein homeostasis. Instead, FMRP appears to indirectly tune global translation by controlling levels of select translation factors and signaling pathways. However, it is also possible that seemingly nonspecific translational control could in fact preferentially affect FMRP target mRNAs (Hay and Sonenberg, 2004). For example, it has been suggested that since eIF4A is a

helicase, decreased formation of the eIF4F complex (as caused by FMRP inhibition of eIF4G expression) might preferentially inhibit translation of mRNAs with long and/or highly structured 5'UTRs, which tends to be the case for FMRP target mRNAs (personal communication, Chaolin Zhang).

Summary

Overall, FMRP clearly regulates coherent functional modules of genes with critical roles in neuronal function. For example, FMRP regulates multiple mRNAs required for the expression of synaptic plasticity at many levels, including those encoding receptors, scaffolding proteins, signaling molecules and cytoskeletal modulators. Interestingly, a general theme emerges from this analysis: that FMRP appears to target modulators rather than core effectors. For example, FMRP targets metabotropic receptors and certain calcium-responsive or calcium-passaging channels but does not target most monovalent ionotropic channels such as AMPARs that actually mediate the bulk of depolarization. Additionally, FMRP targets a number of genes that regulate formation of the SNARE complex, but only weakly targets the core SNARE components themselves. In a third example, FMRP targets several proteins that modulate actin polymerization or link actin filaments to receptors, but only weakly targets actin itself. In a fourth example, FMRP strongly targets several PKA anchoring proteins, but does not target PKA. Finally, FMRP strongly targets a large number of GAPs and GEFs but does not regulate the expression of small GTPases directly. This suggests that a major role for FMRP is to regulate the expression of a diverse range of modulator proteins that control core features of neuronal function.

Taken together, the data suggest a model in which FMRP regulates the translation of specific mRNAs by stalling ribosomes during elongation. Ribosome stalling was acutely reversible *in vitro*, suggesting that regulation of FMRP activity *in vivo* may constitute a highly reactive means by which to adjust the expression of specific proteins important for neuronal function. The HITS-CLIP data suggest that FMRP regulates hundreds, if not a few thousand, of mRNAs in this manner, and examination of the functional roles of FMRP targets makes it clear that much of FMRP's functional biology remains

unexplored. The newly developed cTAG mouse provides a valuable tool to perform focused studies of FMRP function in specific cells and circuits relevant to FXS phenotypes. In particular, I plan to continue these studies by performing parallel cell autonomous HITS-CLIP and ribosome profiling assays in Purkinje neurons, with the goal of defining which mRNA targets of FMRP are most responsible for the defects in spine dysmorphogenesis, parallel fiber:PC mGluR-LTD and eyeblink conditioning observed when FMRP is specifically knocked out in these cells. These studies will provide the first high-resolution view of FMRP function in a single cell type and will begin to paint a more detailed picture of how loss of FMRP results in complex neurological dysfunction.

References

Abul-Husn NS, Bushlin I, Moron JA, Jenkins SL, Dolios G, Wang R, Iyengar R, Ma'ayan A, Devi LA (2009) Systems approach to explore components and interactions in the presynapse. Proteomics **9:** 3303–3315

Adegbola A, Gao H, Sommer S, Browning M (2008) A novel mutation in JARID1C/SMCX in a patient with autism spectrum disorder (ASD). Am J Med Genet A **146A:** 505–511

Aiba A, Kano M, Chen C, Stanton ME, Fox GD, Herrup K, Zwingman TA, Tonegawa S (1994) Deficient cerebellar long-term depression and impaired motor learning in mGluR1 mutant mice. Cell **79:** 377–388

Albrethsen J, Knol JC, Jimenez CR (2009) Unravelling the nuclear matrix proteome. J Proteomics **72:** 71–81

Altrock WD, tom Dieck S, Sokolov M, Meyer AC, Sigler A, Brakebusch C, Fassler R, Richter K, Boeckers TM, Potschka H, Brandt C, Loscher W, Grimberg D, Dresbach T, Hempelmann A, Hassan H, Balschun D, Frey JU, Brandstatter JH, Garner CC, Rosenmund C, Gundelfinger ED (2003) Functional inactivation of a fraction of excitatory synapses in mice deficient for the active zone protein bassoon. Neuron **37:** 787–800

Antar LN, Dictenberg JB, Plociniak M, Afroz R, Bassell GJ (2005) Localization of FMRP-associated mRNA granules and requirement of microtubules for activity-dependent trafficking in hippocampal neurons. Genes Brain Behav **4:** 350–359

Antar LN, Li C, Zhang H, Carroll RC, Bassell GJ (2006) Local functions for FMRP in axon growth cone motility and activity-dependent regulation of filopodia and spine synapses. Mol Cell Neurosci **32:** 37–48

Antion MD, Hou L, Wong H, Hoeffer CA, Klann E (2008) mGluR-dependent long-term depression is associated with increased phosphorylation of S6 and synthesis of elongation factor 1A but remains expressed in S6K-deficient mice. Mol Cell Biol **28:** 2996–3007

Auerbach BD, Osterweil EK, Bear MF (2011) Mutations causing syndromic autism define an axis of synaptic pathophysiology. Nature **480:** 63–68

Bakker CE, de Diego Otero Y, Bontekoe C, Raghoe P, Luteijn T, Hoogeveen AT, Oostra BA, Willemsen R (2000) Immunocytochemical and biochemical characterization of FMRP, FXR1P, and FXR2P in the mouse. Exp Cell Res **258:** 162–170

Banerjee S, Hasan G (2005) The InsP3 receptor: its role in neuronal physiology and neurodegeneration. Bioessays **27:** 1035–1047

Bangash MA, Park JM, Melnikova T, Wang D, Jeon SK, Lee D, Syeda S, Kim J, Kouser M, Schwartz J, Cui Y, Zhao X, Speed HE, Kee SE, Tu JC, Hu JH, Petralia RS, Linden DJ, Powell CM, Savonenko A, Xiao B, Worley PF (2011) Enhanced polyubiquitination of Shank3 and NMDA receptor in a mouse model of autism. Cell **145:** 758–772

Banko JL, Hou L, Poulin F, Sonenberg N, Klann E (2006) Regulation of eukaryotic initiation factor 4E by converging signaling pathways during metabotropic glutamate receptor-dependent long-term depression. J Neurosci **26:** 2167–2173

Banko JL, Poulin F, Hou L, DeMaria CT, Sonenberg N, Klann E (2005) The translation repressor 4E-BP2 is critical for eIF4F complex formation, synaptic plasticity, and memory in the hippocampus. J Neurosci **25:** 9581–9590

Bardoni B, Castets M, Huot ME, Schenck A, Adinolfi S, Corbin F, Pastore A, Khandjian EW, Mandel JL (2003) 82-FIP, a novel FMRP (fragile X mental retardation protein) interacting protein, shows a cell cycle-dependent intracellular localization. Hum Mol Genet **12:** 1689–1698

Bardoni B, Schenck A, Mandel JL (1999) A novel RNA-binding nuclear protein that interacts with the fragile X mental retardation (FMR1) protein. Hum Mol Genet **8:** 2557–2566

Barski JJ, Dethleffsen K, Meyer M (2000) Cre recombinase expression in cerebellar Purkinje cells. Genesis **28:** 93–98

Bartel DP (2009) MicroRNAs: target recognition and regulatory functions. Cell **136:** 215–233

Basu SN, Kollu R, Banerjee-Basu S (2009) AutDB: a gene reference resource for autism research. Nucleic Acids Res **37:** D832–6

Bauman AL, Goehring AS, Scott JD (2004) Orchestration of synaptic plasticity through AKAP signaling complexes. Neuropharmacology **46:** 299–310

Bear MF, Huber KM, Warren ST (2004) The mGluR theory of fragile X mental retardation. Trends Neurosci **27:** 370–377

Bechara EG, Didiot MC, Melko M, Davidovic L, Bensaid M, Martin P, Castets M, Pognonec P, Khandjian EW, Moine H, Bardoni B (2009) A novel function for fragile X mental retardation protein in translational activation. PLoS Biol **7:** e16

Berry-Kravis E, Huttenlocher PR (1992) Cyclic AMP metabolism in fragile X syndrome. Ann Neurol **31:** 22–26

Berry-Kravis E, Sklena P (1993) Demonstration of abnormal cyclic AMP production in platelets from patients with fragile X syndrome. Am J Med Genet **45:** 81–87

Betancur C, Sakurai T, Buxbaum JD (2009) The emerging role of synaptic cell-adhesion pathways in the pathogenesis of autism spectrum disorders. Trends Neurosci **32:** 402–412

Bingol B, Schuman EM (2006) Activity-dependent dynamics and sequestration of proteasomes in dendritic spines. Nature **441(7097):** 1144–1148

Bliss TV, Lomo T (1973) Long-lasting potentiation of synaptic transmission in the dentate area of the anaesthetized rabbit following stimulation of the perforant path. J Physiol **232:** 331–356

Blonden L, van 't Padje S, Severijnen LA, Destree O, Oostra BA, Willemsen R (2005) Two members of the Fxr gene family, Fmr1 and Fxr1, are differentially expressed in Xenopus tropicalis. Int J Dev Biol **49:** 437–441

Bloodgood BL, Sabatini BL (2009) NMDA Receptor-Mediated Calcium Transients in Dendritic Spines. **Biology of the NMDA Receptor:**

Boeckers TM, Bockmann J, Kreutz MR, Gundelfinger ED (2002) ProSAP/Shank proteins - a family of higher order organizing molecules of the postsynaptic density with an emerging role in human neurological disease. J Neurochem **81:** 903–910

Boeckers TM, Winter C, Smalla KH, Kreutz MR, Bockmann J, Seidenbecher C, Garner CC, Gundelfinger ED (1999) Proline-rich synapse-associated proteins ProSAP1 and ProSAP2 interact with synaptic proteins of the SAPAP/GKAP family. Biochem Biophys Res Commun **264:** 247–252

Bongmba OY, Martinez LA, Elhardt ME, Butler K, Tejada-Simon MV (2011) Modulation of dendritic spines and synaptic function by Rac1: a possible link to Fragile X syndrome pathology. Brain Res **1399:** 79–95

Bos JL, Pannekoek WJ (2012) Semaphorin signaling meets rap. Sci Signal **5:** pe6

Bottai D, Guzowski JF, Schwarz MK, Kang SH, Xiao B, Lanahan A, Worley PF, Seeburg PH (2002) Synaptic activity-induced conversion of intronic to exonic sequence in Homer 1 immediate early gene expression. J Neurosci **22:** 167–175

Bracha V, Irwin KB, Webster ML, Wunderlich DA, Stachowiak MK, Bloedel JR (1998) Microinjections of anisomycin into the intermediate cerebellum during learning affect the acquisition of classically conditioned responses in the rabbit. Brain Res **788:** 169–178

Brakeman PR, Lanahan AA, O'Brien R, Roche K, Barnes CA, Huganir RL, Worley PF (1997) Homer: a protein that selectively binds metabotropic glutamate receptors. Nature **386:** 284–288

Brown V, Jin P, Ceman S, Darnell JC, O'Donnell WT, Tenenbaum SA, Jin X, Feng Y, Wilkinson KD, Keene JD, Darnell RB, Warren ST (2001) Microarray identification of FMRP-associated brain mRNAs and altered mRNA translational profiles in fragile X syndrome. Cell **107:** 477–487

Buckanovich RJ, Darnell RB (1997) The neuronal RNA binding protein Nova-1 recognizes specific RNA targets in vitro and in vivo. Mol Cell Biol **17:** 3194–3201

Bureau I, Shepherd GM, Svoboda K (2008) Circuit and plasticity defects in the developing somatosensory cortex of FMR1 knock-out mice. J Neurosci **28:** 5178–5188

Bushey D, Tononi G, Cirelli C (2011) Sleep and synaptic homeostasis: structural evidence in Drosophila. Science **332:** 1576–1581

Cahoy JD, Emery B, Kaushal A, Foo LC, Zamanian JL, Christopherson KS, Xing Y, Lubischer JL, Krieg PA, Krupenko SA, Thompson WJ, Barres BA (2008) A transcriptome database for astrocytes, neurons, and oligodendrocytes: a new resource for understanding brain development and function. J Neurosci **28:** 264–278

Cajigas IJ, Will T, Schuman EM (2010) Protein homeostasis and synaptic plasticity. EMBO J **29:** 2746–2752

Caudy AA, Myers M, Hannon GJ, Hammond SM (2002) Fragile X-related protein and VIG associate with the RNA interference machinery. Genes Dev **16:** 2491–2496

Ceman S, O'Donnell WT, Reed M, Patton S, Pohl J, Warren ST (2003) Phosphorylation influences the translation state of FMRP-associated polyribosomes. Hum Mol Genet **12:** 3295–3305

Chang YF, Imam JS, Wilkinson MF (2007) The nonsense-mediated decay RNA surveillance pathway. Annu Rev Biochem **76:** 51–74

Chen A, Muzzio IA, Malleret G, Bartsch D, Verbitsky M, Pavlidis P, Yonan AL, Vronskaya S, Grody MB, Cepeda I, Gilliam TC, Kandel ER (2003a) Inducible enhancement of memory storage and synaptic plasticity in transgenic mice expressing an inhibitor of ATF4 (CREB-2) and C/EBP proteins. Neuron **39:** 655–669

Chen L, Bao S, Lockard JM, Kim JK, Thompson RF (1996) Impaired classical eyeblink conditioning in cerebellar-lesioned and Purkinje cell degeneration (pcd) mutant mice. J Neurosci **16:** 2829–2838

Chen L, Yun SW, Seto J, Liu W, Toth M (2003b) The fragile X mental retardation protein binds and regulates a novel class of mRNAs containing U rich target sequences. Neuroscience **120:** 1005–1017

Chen LY, Rex CS, Babayan AH, Kramar EA, Lynch G, Gall CM, Lauterborn JC (2010) Physiological activation of synaptic Rac>PAK (p-21 activated kinase) signaling is defective in a mouse model of fragile X syndrome. J Neurosci **30:** 10977–10984

Chi SW, Zang JB, Mele A, Darnell RB (2009) Argonaute HITS-CLIP decodes microRNA-mRNA interaction maps. Nature **460:** 479–486

Christie SB, Akins MR, Schwob JE, Fallon JR (2009) The FXG: a presynaptic fragile X granule expressed in a subset of developing brain circuits. J Neurosci **29:** 1514–1524

Christov CP, Gardiner TJ, Szuts D, Krude T (2006) Functional requirement of noncoding Y RNAs for human chromosomal DNA replication. Mol Cell Biol **26:** 6993–7004

Chung HJ, Steinberg JP, Huganir RL, Linden DJ (2003) Requirement of AMPA receptor GluR2 phosphorylation for cerebellar long-term depression. Science **300:** 1751–1755

Chung HJ, Xia J, Scannevin RH, Zhang X, Huganir RL (2000) Phosphorylation of the AMPA receptor subunit GluR2 differentially regulates its interaction with PDZ domain-containing proteins. J Neurosci **20:** 7258–7267

Cichowski K, Jacks T (2001) NF1 tumor suppressor gene function: narrowing the GAP. Cell **104:** 593–604

Coffee RLJ, Williamson AJ, Adkins CM, Gray MC, Page TL, Broadie K (2012) In vivo neuronal function of the fragile X mental retardation protein is regulated by phosphorylation. Hum Mol Genet **21:** 900–915

Cole AJ, Abu-Shakra S, Saffen DW, Baraban JM, Worley PF (1990) Rapid rise in transcription factor mRNAs in rat brain after electroshock-induced seizures. J Neurochem **55:** 1920–1927

Collingridge GL, Peineau S, Howland JG, Wang YT (2010) Long-term depression in the CNS. Nat Rev Neurosci **11:** 459–473

Copeland NG, Jenkins NA, Court DL (2001) Recombineering: a powerful new tool for mouse functional genomics. Nat Rev Genet **2:** 769–779

Corbin F, Bouillon M, Fortin A, Morin S, Rousseau F, Khandjian EW (1997) The fragile X mental retardation protein is associated with poly(A)+ mRNA in actively translating polyribosomes. Hum Mol Genet **6:** 1465–1472

Cox PR, Fowler V, Xu B, Sweatt JD, Paylor R, Zoghbi HY (2003) Mice lacking Tropomodulin-2 show enhanced long-term potentiation, hyperactivity, and deficits in learning and memory. Mol Cell Neurosci **23:** 1–12

Cremona O, Di Paolo G, Wenk MR, Luthi A, Kim WT, Takei K, Daniell L, Nemoto Y, Shears SB, Flavell RA, McCormick DA, De Camilli P (1999) Essential role of phosphoinositide metabolism in synaptic vesicle recycling. Cell **99:** 179–188

Croning MD, Marshall MC, McLaren P, Armstrong JD, Grant SG (2009) G2Cdb: the Genes to Cognition database. Nucleic Acids Res **37:** D846–51

Cruz-Martin A, Crespo M, Portera-Cailliau C (2012) Glutamate induces the elongation of early dendritic protrusions via mGluRs in wild type mice, but not in fragile X mice. PLoS One **7:** e32446

Dabrowski A, Umemori H (2011) Orchestrating the synaptic network by tyrosine phosphorylation signalling. J Biochem **149:** 641–653

Darnell JC, Fraser CE, Mostovetsky O, Darnell RB (2009) Discrimination of common and unique RNA-binding activities among Fragile X mental retardation protein paralogs. Hum Mol Genet **18:** 3164–3177

Darnell JC, Fraser CE, Mostovetsky O, Stefani G, Jones TA, Eddy SR, Darnell RB (2005a) Kissing complex RNAs mediate interaction between the Fragile-X mental retardation protein KH2 domain and brain polyribosomes. Genes Dev **19:** 903–918

Darnell JC, Jensen KB, Jin P, Brown V, Warren ST, Darnell RB (2001) Fragile X mental retardation protein targets G quartet mRNAs important for neuronal function. Cell **107:** 489–499

Darnell JC, Mostovetsky O, Darnell RB (2005b) FMRP RNA targets: identification and validation. Genes Brain Behav **4:** 341–349

Darnell JC, Van Driesche SJ, Zhang C, Hung KY, Mele A, Fraser CE, Stone EF, Chen C, Fak JJ, Chi SW, Licatalosi DD, Richter JD, Darnell RB (2011) FMRP stalls ribosomal translocation on mRNAs linked to synaptic function and autism. Cell **146:** 247–261

Davidovic L, Bechara E, Gravel M, Jaglin XH, Tremblay S, Sik A, Bardoni B, Khandjian EW (2006) The nuclear microspherule protein 58 is a novel RNA-binding protein that interacts with fragile X mental retardation protein in polyribosomal mRNPs from neurons. Hum Mol Genet **15:** 1525–1538

Davidovic L, Huot ME, Khandjian EW (2005) Lost once, the Fragile X Mental Retardation protein is now back onto brain polyribosomes. RNA Biol **2:** 1–3

De Boulle K, Verkerk AJ, Reyniers E, Vits L, Hendrickx J, Van Roy B, Van den Bos F, de Graaff E, Oostra BA, Willems PJ (1993) A point mutation in the FMR-1 gene associated with fragile X mental retardation. Nat Genet **3:** 31–35

de Petris S (1970) Electron microscopy of polyribosomes synthesizing immunoglobulin chains. Comparison with sizes determined by density-gradient-sedimentation data. Biochem J **118:** 385–389

Deak F, Shin OH, Tang J, Hanson P, Ubach J, Jahn R, Rizo J, Kavalali ET, Sudhof TC (2006) Rabphilin regulates SNARE-dependent re-priming of synaptic vesicles for fusion. EMBO J **25:** 2856–2866

Deng L, Kaeser PS, Xu W, Sudhof TC (2011) RIM proteins activate vesicle priming by reversing autoinhibitory homodimerization of Munc13. Neuron **69:** 317–331

Dictenberg JB, Swanger SA, Antar LN, Singer RH, Bassell GJ (2008) A direct role for FMRP in activity-dependent dendritic mRNA transport links filopodial-spine morphogenesis to fragile X syndrome. Dev Cell **14:** 926–939

Didiot MC, Subramanian M, Flatter E, Mandel JL, Moine H (2009) Cells lacking the fragile X mental retardation protein (FMRP) have normal RISC activity but exhibit altered stress granule assembly. Mol Biol Cell **20:** 428–437

Didiot MC, Tian Z, Schaeffer C, Subramanian M, Mandel JL, Moine H (2008) The G-quartet containing FMRP binding site in FMR1 mRNA is a potent exonic splicing enhancer. Nucleic Acids Res **36:** 4902–4912

Diehn M, Bhattacharya R, Botstein D, Brown PO (2006) Genome-scale identification of membrane-associated human mRNAs. PLoS Genet **2:** e11

Ding JB, Oh WJ, Sabatini BL, Gu C (2012) Semaphorin 3E-Plexin-D1 signaling controls pathway-specific synapse formation in the striatum. Nat Neurosci **15:** 215–223

Diribarne G, Bensaude O (2009) 7SK RNA, a non-coding RNA regulating P-TEFb, a general transcription factor. RNA Biol **6:** 122–128

Djuranovic S, Nahvi A, Green R (2011) A parsimonious model for gene regulation by miRNAs. Science **331:** 550–553

Dodge-Kafka KL, Bauman A, Kapiloff MS (2008) A-kinase anchoring proteins as the basis for cAMP signaling. Handb Exp Pharmacol 3–14

Dolen G, Osterweil E, Rao BS, Smith GB, Auerbach BD, Chattarji S, Bear MF (2007) Correction of fragile X syndrome in mice. Neuron **56:** 955–962

Doyle JP, Dougherty JD, Heiman M, Schmidt EF, Stevens TR, Ma G, Bupp S, Shrestha P, Shah RD, Doughty ML, Gong S, Greengard P, Heintz N (2008) Application of a translational profiling approach for the comparative analysis of CNS cell types. Cell **135:** 749–762

Dresbach T, Torres V, Wittenmayer N, Altrock WD, Zamorano P, Zuschratter W, Nawrotzki R, Ziv NE, Garner CC, Gundelfinger ED (2006) Assembly of active zone precursor vesicles: obligatory trafficking of presynaptic cytomatrix proteins Bassoon and Piccolo via a trans-Golgi compartment. J Biol Chem **281:** 6038–6047

Duffy C, Teyler TJ, Shashoua VE (1981) Long-term potentiation in the hippocampal slice: evidence for stimulated secretion of newly synthesized proteins. Science **212:** 1148–1151

Dulubova I, Sugita S, Hill S, Hosaka M, Fernandez I, Sudhof TC, Rizo J (1999) A conformational switch in syntaxin during exocytosis: role of munc18. EMBO J **18:** 4372–4382

Eberhart DE, Malter HE, Feng Y, Warren ST (1996) The fragile X mental retardation protein is a ribonucleoprotein containing both nuclear localization and nuclear export signals. Hum Mol Genet **5:** 1083–1091

Edbauer D, Neilson JR, Foster KA, Wang CF, Seeburg DP, Batterton MN, Tada T, Dolan BM, Sharp PA, Sheng M (2010) Regulation of synaptic structure and function by FMRP-associated microRNAs miR-125b and miR-132. Neuron **65:** 373–384

Ehlers MD (2003) Activity level controls postsynaptic composition and signaling via the ubiquitin-proteasome system. Nat Neurosci **6:** 231–242

Fagan RJ, Lazaris-Karatzas A, Sonenberg N, Rozen R (1991) Translational control of ornithine aminotransferase. Modulation by initiation factor eIF-4E. J Biol Chem **266:** 16518–16523

Fang P, Spevak CC, Wu C, Sachs MS (2004) A nascent polypeptide domain that can regulate translation elongation. Proc Natl Acad Sci U S A **101:** 4059–4064

Feng W, Zhang M (2009) Organization and dynamics of PDZ-domain-related supramodules in the postsynaptic density. Nat Rev Neurosci **10:** 87–99

Feng Y, Absher D, Eberhart DE, Brown V, Malter HE, Warren ST (1997a) FMRP associates with polyribosomes as an mRNP, and the I304N mutation of severe fragile X syndrome abolishes this association. Mol Cell **1:** 109–118

Feng Y, Gutekunst CA, Eberhart DE, Yi H, Warren ST, Hersch SM (1997b) Fragile X mental retardation protein: nucleocytoplasmic shuttling and association with somatodendritic ribosomes. J Neurosci **17:** 1539–1547

Ferguson GD, Storm DR (2004) Why calcium-stimulated adenylyl cyclases? Physiology (Bethesda) **19:** 271–276

FLEXNER JB, FLEXNER LB, STELLAR E (1963) Memory in mice as affected by intracerebral puromycin. Science **141:** 57–59

Forte GM, Pool MR, Stirling CJ (2011) N-terminal acetylation inhibits protein targeting to the endoplasmic reticulum. PLoS Biol **9:** e1001073

Fridell RA, Benson RE, Hua J, Bogerd HP, Cullen BR (1996) A nuclear role for the Fragile X mental retardation protein. EMBO J **15:** 5408–5414

Friend K, Campbell ZT, Cooke A, Kroll-Conner P, Wickens MP, Kimble J (2012) A conserved PUF-Ago-eEF1A complex attenuates translation elongation. Nat Struct Mol Biol **19:** 176–183

Fuchs G, Stein AJ, Fu C, Reinisch KM, Wolin SL (2006) Structural and biochemical basis for misfolded RNA recognition by the Ro autoantigen. Nat Struct Mol Biol **13:** 1002–1009

Fujita Y, Shirataki H, Sakisaka T, Asakura T, Ohya T, Kotani H, Yokoyama S, Nishioka H, Matsuura Y, Mizoguchi A, Scheller RH, Takai Y (1998) Tomosyn: a syntaxin-1-binding protein that forms a novel complex in the neurotransmitter release process. Neuron **20:** 905–915

Gabel LA, Won S, Kawai H, McKinney M, Tartakoff AM, Fallon JR (2004) Visual experience regulates transient expression and dendritic localization of fragile X mental retardation protein. J Neurosci **24:** 10579–10583

Gardoni F, Marcello E, Di Luca M (2009) Postsynaptic density-membrane associated guanylate kinase proteins (PSD-MAGUKs) and their role in CNS disorders. Neuroscience **158:** 324–333

Giorgi C, Yeo GW, Stone ME, Katz DB, Burge C, Turrigiano G, Moore MJ (2007) The EJC factor eIF4AIII modulates synaptic strength and neuronal protein expression. Cell **130:** 179–191

Gladding CM, Collett VJ, Jia Z, Bashir ZI, Collingridge GL, Molnar E (2009) Tyrosine dephosphorylation regulates AMPAR internalisation in mGluR-LTD. Mol Cell Neurosci **40:** 267–279

Gong LW, De Camilli P (2008) Regulation of postsynaptic AMPA responses by synaptojanin 1. Proc Natl Acad Sci U S A **105:** 17561–17566

Greer PL, Hanayama R, Bloodgood BL, Mardinly AR, Lipton DM, Flavell SW, Kim TK, Griffith EC, Waldon Z, Maehr R, Ploegh HL, Chowdhury S, Worley PF, Steen J, Greenberg ME (2010) The Angelman Syndrome protein Ube3A regulates synapse development by ubiquitinating arc. Cell **140:** 704–716

Gross C, Yao X, Pong DL, Jeromin A, Bassell GJ (2011) Fragile X mental retardation protein regulates protein expression and mRNA translation of the potassium channel Kv4.2. J Neurosci **31:** 5693–5698

Guilding C, McNair K, Stone TW, Morris BJ (2007) Restored plasticity in a mouse model of neurofibromatosis type 1 via inhibition of hyperactive ERK and CREB. Eur J Neurosci **25:** 99–105
Guo W, Allan AM, Zong R, Zhang L, Johnson EB, Schaller EG, Murthy AC, Goggin SL, Eisch AJ, Oostra BA, Nelson DL, Jin P, Zhao X (2011) Ablation of Fmrp in adult neural stem cells disrupts hippocampus-dependent learning. Nat Med **17:** 559–565
Guzowski JF, McNaughton BL, Barnes CA, Worley PF (1999) Environment-specific expression of the immediate-early gene Arc in hippocampal neuronal ensembles. Nat Neurosci **2:** 1120–1124
Hagerman R, Hoem G, Hagerman P (2010) Fragile X and autism: Intertwined at the molecular level leading to targeted treatments. Mol Autism **1:** 12
Harlow EG, Till SM, Russell TA, Wijetunge LS, Kind P, Contractor A (2010) Critical period plasticity is disrupted in the barrel cortex of FMR1 knockout mice. Neuron **65:** 385–398
Hay N, Sonenberg N (2004) Upstream and downstream of mTOR. Genes Dev **18:** 1926–1945
Hayashi MK, Tang C, Verpelli C, Narayanan R, Stearns MH, Xu RM, Li H, Sala C, Hayashi Y (2009) The postsynaptic density proteins Homer and Shank form a polymeric network structure. Cell **137:** 159–171
He M, Liu Y, Wang X, Zhang MQ, Hannon GJ, Huang ZJ (2012) Cell-type-based analysis of microRNA profiles in the mouse brain. Neuron **73:** 35–48
Hegde AN (2010) The ubiquitin-proteasome pathway and synaptic plasticity. Learn Mem **17:** 314–327
Heiman M, Schaefer A, Gong S, Peterson JD, Day M, Ramsey KE, Suarez-Farinas M, Schwarz C, Stephan DA, Surmeier DJ, Greengard P, Heintz N (2008) A translational profiling approach for the molecular characterization of CNS cell types. Cell **135:** 738–748
Hinton VJ, Brown WT, Wisniewski K, Rudelli RD (1991) Analysis of neocortex in three males with the fragile X syndrome. Am J Med Genet **41:** 289–294
Hirokawa N (2006) mRNA transport in dendrites: RNA granules, motors, and tracks. J Neurosci **26:** 7139–7142
Hoeffer CA, Klann E (2010) mTOR signaling: at the crossroads of plasticity, memory and disease. Trends Neurosci **33:** 67–75
Horgan CP, McCaffrey MW (2011) Rab GTPases and microtubule motors. Biochem Soc Trans **39:** 1202–1206
Hou L, Antion MD, Hu D, Spencer CM, Paylor R, Klann E (2006) Dynamic translational and proteasomal regulation of fragile X mental retardation protein controls mGluR-dependent long-term depression. Neuron **51:** 441–454
Hou L, Klann E (2004) Activation of the phosphoinositide 3-kinase-Akt-mammalian target of rapamycin signaling pathway is required for metabotropic glutamate receptor-dependent long-term depression. J Neurosci **24:** 6352–6361
Huang da W, Sherman BT, Lempicki RA (2009) Bioinformatics enrichment tools: paths toward the comprehensive functional analysis of large gene lists. Nucleic Acids Res **37:** 1–13
Huang J, Manning BD (2008) The TSC1-TSC2 complex: a molecular switchboard controlling cell growth. Biochem J **412:** 179–190
Huber KM, Gallagher SM, Warren ST, Bear MF (2002) Altered synaptic plasticity in a mouse model of fragile X mental retardation. Proc Natl Acad Sci U S A **99:** 7746–7750
Huber KM, Kayser MS, Bear MF (2000) Role for rapid dendritic protein synthesis in hippocampal mGluR-dependent long-term depression. Science **288:** 1254–1257
Hussey GS, Chaudhury A, Dawson AE, Lindner DJ, Knudsen CR, Wilce MC, Merrick WC, Howe PH (2011) Identification of an mRNP complex regulating tumorigenesis at the translational elongation step. Mol Cell **41:** 419–431
Iacoangeli A, Rozhdestvensky TS, Dolzhanskaya N, Tournier B, Schutt J, Brosius J, Denman RB, Khandjian EW, Kindler S, Tiedge H (2008) On BC1 RNA and the fragile X mental retardation protein. Proc Natl Acad Sci U S A **105:** 734–739
Ingolia NT, Lareau LF, Weissman JS (2011) Ribosome profiling of mouse embryonic stem cells reveals the complexity and dynamics of mammalian proteomes. Cell **147:** 789–802
Inoki K, Li Y, Zhu T, Wu J, Guan KL (2002) TSC2 is phosphorylated and inhibited by Akt and suppresses mTOR signalling. Nat Cell Biol **4:** 648–657
Iossifov I, Ronemus M, Levy D, Wang Z, Hakker I, Rosenbaum J, Yamrom B, Lee YH, Narzisi G, Leotta A, Kendall J, Grabowska E, Ma B, Marks S, Rodgers L, Stepansky A, Troge J, Andrews P, Bekritsky M, Pradhan K, Ghiban E, Kramer M, Parla J, Demeter R, Fulton LL,

Fulton RS, Magrini VJ, Ye K, Darnell JC, Darnell RB, Mardis ER, Wilson RK, Schatz MC, McCombie WR, Wigler M (2012) De novo gene disruptions in children on the autistic spectrum. Neuron **74:** 285–299

Ishizuka A, Siomi MC, Siomi H (2002) A Drosophila fragile X protein interacts with components of RNAi and ribosomal proteins. Genes Dev **16:** 2497–2508

Ito M (1986) Long-term depression as a memory process in the cerebellum. Neurosci Res **3:** 531–539

Ito M (2002) Historical review of the significance of the cerebellum and the role of Purkinje cells in motor learning. Ann N Y Acad Sci **978:** 273–288

Jensen KB, Darnell RB (2008) CLIP: crosslinking and immunoprecipitation of in vivo RNA targets of RNA-binding proteins. Methods Mol Biol **488:** 85–98

Jensen KB, Musunuru K, Lewis HA, Burley SK, Darnell RB (2000) The tetranucleotide UCAY directs the specific recognition of RNA by the Nova K-homology 3 domain. Proc Natl Acad Sci U S A **97:** 5740–5745

Jin P, Zarnescu DC, Ceman S, Nakamoto M, Mowrey J, Jongens TA, Nelson DL, Moses K, Warren ST (2004) Biochemical and genetic interaction between the fragile X mental retardation protein and the microRNA pathway. Nat Neurosci **7:** 113–117

Johannessen CM, Reczek EE, James MF, Brems H, Legius E, Cichowski K (2005) The NF1 tumor suppressor critically regulates TSC2 and mTOR. Proc Natl Acad Sci U S A **102:** 8573–8578

Kadota Y, Niiya A, Masaki R, Yamamoto A, Araki M, Taketani S (1997) A newly identified membrane protein localized exclusively in intracellular organelles of neurons. Brain Res Mol Brain Res **46:** 265–273

Kallappagoudar S, Varma P, Pathak RU, Senthilkumar R, Mishra RK (2010) Nuclear matrix proteome analysis of Drosophila melanogaster. Mol Cell Proteomics **9:** 2005–2018

Kammermeier PJ, Worley PF (2007) Homer 1a uncouples metabotropic glutamate receptor 5 from postsynaptic effectors. Proc Natl Acad Sci U S A **104:** 6055–6060

Kang H, Schuman EM (1996) A requirement for local protein synthesis in neurotrophin-induced hippocampal synaptic plasticity. Science **273:** 1402–1406

Kanhema T, Dagestad G, Panja D, Tiron A, Messaoudi E, Havik B, Ying SW, Nairn AC, Sonenberg N, Bramham CR (2006) Dual regulation of translation initiation and peptide chain elongation during BDNF-induced LTP in vivo: evidence for compartment-specific translation control. J Neurochem **99:** 1328–1337

Kano M, Hashimoto K, Tabata T (2008) Type-1 metabotropic glutamate receptor in cerebellar Purkinje cells: a key molecule responsible for long-term depression, endocannabinoid signalling and synapse elimination. Philos Trans R Soc Lond B Biol Sci **363:** 2173–2186

Kao DI, Aldridge GM, Weiler IJ, Greenough WT (2010) Altered mRNA transport, docking, and protein translation in neurons lacking fragile X mental retardation protein. Proc Natl Acad Sci U S A **107:** 15601–15606

Kapitein LC, Hoogenraad CC (2011) Which way to go? Cytoskeletal organization and polarized transport in neurons. Mol Cell Neurosci **46:** 9–20

Karachot L, Shirai Y, Vigot R, Yamamori T, Ito M (2001) Induction of long-term depression in cerebellar Purkinje cells requires a rapidly turned over protein. J Neurophysiol **86:** 280–289

Kasai H, Matsuzaki M, Noguchi J, Yasumatsu N, Nakahara H (2003) Structure-stability-function relationships of dendritic spines. Trends Neurosci **26:** 360–368

Keenan RJ, Freymann DM, Stroud RM, Walter P (2001) The signal recognition particle. Annu Rev Biochem **70:** 755–775

Kelleher RJr, Govindarajan A, Jung HY, Kang H, Tonegawa S (2004) Translational control by MAPK signaling in long-term synaptic plasticity and memory. Cell **116:** 467–479

Kelley DJ, Davidson RJ, Elliott JL, Lahvis GP, Yin JC, Bhattacharyya A (2007) The cyclic AMP cascade is altered in the fragile X nervous system. PLoS One **2:** e931

Khandjian EW, Corbin F, Woerly S, Rousseau F (1996) The fragile X mental retardation protein is associated with ribosomes. Nat Genet **12:** 91–93

Khandjian EW, Huot ME, Tremblay S, Davidovic L, Mazroui R, Bardoni B (2004) Biochemical evidence for the association of fragile X mental retardation protein with brain polyribosomal ribonucleoparticles. Proc Natl Acad Sci U S A **101:** 13357–13362

Kim CH, Chung HJ, Lee HK, Huganir RL (2001) Interaction of the AMPA receptor subunit GluR2/3 with PDZ domains regulates hippocampal long-term depression. Proc Natl Acad Sci U S A **98:** 11725–11730

Kim JH, Liao D, Lau LF, Huganir RL (1998) SynGAP: a synaptic RasGAP that associates with the PSD-95/SAP90 protein family. Neuron **20:** 683–691

Kim M, Bellini M, Ceman S (2009) Fragile X mental retardation protein FMRP binds mRNAs in the nucleus. Mol Cell Biol **29:** 214–228

Kim SH, Markham JA, Weiler IJ, Greenough WT (2008) Aberrant early-phase ERK inactivation impedes neuronal function in fragile X syndrome. Proc Natl Acad Sci U S A **105:** 4429–4434

Kimchi-Sarfaty C, Oh JM, Kim IW, Sauna ZE, Calcagno AM, Ambudkar SV, Gottesman MM (2007) A "silent" polymorphism in the MDR1 gene changes substrate specificity. Science **315:** 525–528

Kiraly DD, Lemtiri-Chlieh F, Levine ES, Mains RE, Eipper BA (2011) Kalirin binds the NR2B subunit of the NMDA receptor, altering its synaptic localization and function. J Neurosci **31:** 12554–12565

Kishimoto Y, Fujimichi R, Araishi K, Kawahara S, Kano M, Aiba A, Kirino Y (2002) mGluR1 in cerebellar Purkinje cells is required for normal association of temporally contiguous stimuli in classical conditioning. Eur J Neurosci **16:** 2416–2424

Klemmer P, Meredith RM, Holmgren CD, Klychnikov OI, Stahl-Zeng J, Loos M, van der Schors RC, Wortel J, de Wit H, Spijker S, Rotaru DC, Mansvelder HD, Smit AB, Li KW (2011) Proteomics, ultrastructure, and physiology of hippocampal synapses in a fragile X syndrome mouse model reveal presynaptic phenotype. J Biol Chem **286:** 25495–25504

Koekkoek SK, Yamaguchi K, Milojkovic BA, Dortland BR, Ruigrok TJ, Maex R, De Graaf W, Smit AE, VanderWerf F, Bakker CE, Willemsen R, Ikeda T, Kakizawa S, Onodera K, Nelson DL, Mientjes E, Joosten M, De Schutter E, Oostra BA, Ito M, De Zeeuw CI (2005) Deletion of FMR1 in Purkinje cells enhances parallel fiber LTD, enlarges spines, and attenuates cerebellar eyelid conditioning in Fragile X syndrome. Neuron **47:** 339–352

Komiyama NH, Watabe AM, Carlisle HJ, Porter K, Charlesworth P, Monti J, Strathdee DJ, O'Carroll CM, Martin SJ, Morris RG, O'Dell TJ, Grant SG (2002) SynGAP regulates ERK/MAPK signaling, synaptic plasticity, and learning in the complex with postsynaptic density 95 and NMDA receptor. J Neurosci **22:** 9721–9732

Kondrashov N, Pusic A, Stumpf CR, Shimizu K, Hsieh AC, Xue S, Ishijima J, Shiroishi T, Barna M (2011) Ribosome-mediated specificity in Hox mRNA translation and vertebrate tissue patterning. Cell **145:** 383–397

Kozak M (2006) Rethinking some mechanisms invoked to explain translational regulation in eukaryotes. Gene **382:** 1–11

Kraut-Cohen J, Gerst JE (2010) Addressing mRNAs to the ER: cis sequences act up! Trends Biochem Sci **35:** 459–469

Laggerbauer B, Ostareck D, Keidel EM, Ostareck-Lederer A, Fischer U (2001) Evidence that fragile X mental retardation protein is a negative regulator of translation. Hum Mol Genet **10:** 329–338

Lagnado L (2005) Ribbon synapses: anchors away for a fishy tale. Curr Biol **15:** R102–5

Lao G, Scheuss V, Gerwin CM, Su Q, Mochida S, Rettig J, Sheng ZH (2000) Syntaphilin: a syntaxin-1 clamp that controls SNARE assembly. Neuron **25:** 191–201

Lee A, Li W, Xu K, Bogert BA, Su K, Gao FB (2003) Control of dendritic development by the Drosophila fragile X-related gene involves the small GTPase Rac1. Development **130:** 5543–5552

Lee HY, Ge WP, Huang W, He Y, Wang GX, Rowson-Baldwin A, Smith SJ, Jan YN, Jan LY (2011) Bidirectional regulation of dendritic voltage-gated potassium channels by the fragile X mental retardation protein. Neuron **72:** 630–642

Lemtiri-Chlieh F, Zhao L, Kiraly DD, Eipper BA, Mains RE, Levine ES (2011) Kalirin-7 is necessary for normal NMDA receptor-dependent synaptic plasticity. BMC Neurosci **12:** 126

Lerner RS, Seiser RM, Zheng T, Lager PJ, Reedy MC, Keene JD, Nicchitta CV (2003) Partitioning and translation of mRNAs encoding soluble proteins on membrane-bound ribosomes. RNA **9:** 1123–1137

Levitt N, Briggs D, Gil A, Proudfoot NJ (1989) Definition of an efficient synthetic poly(A) site. Genes Dev **3:** 1019–1025

Lewis HA, Musunuru K, Jensen KB, Edo C, Chen H, Darnell RB, Burley SK (2000) Sequence-specific RNA binding by a Nova KH domain: implications for paraneoplastic disease and the fragile X syndrome. Cell **100:** 323–332

Li L, Haynes MP, Bender JR (2003) Plasma membrane localization and function of the estrogen receptor alpha variant (ER46) in human endothelial cells. Proc Natl Acad Sci U S A **100:** 4807–4812

Li L, Rutlin M, Abraira VE, Cassidy C, Kus L, Gong S, Jankowski MP, Luo W, Heintz N, Koerber HR, Woodbury CJ, Ginty DD (2011) The functional organization of cutaneous low-threshold mechanosensory neurons. Cell **147:** 1615–1627

Li Z, Zhang Y, Ku L, Wilkinson KD, Warren ST, Feng Y (2001) The fragile X mental retardation protein inhibits translation via interacting with mRNA. Nucleic Acids Res **29:** 2276–2283

Liao L, Park SK, Xu T, Vanderklish P, Yates JRr (2008) Quantitative proteomic analysis of primary neurons reveals diverse changes in synaptic protein content in fmr1 knockout mice. Proc Natl Acad Sci U S A **105:** 15281–15286

Licatalosi DD, Mele A, Fak JJ, Ule J, Kayikci M, Chi SW, Clark TA, Schweitzer AC, Blume JE, Wang X, Darnell JC, Darnell RB (2008) HITS-CLIP yields genome-wide insights into brain alternative RNA processing. Nature **456:** 464–469

Lin Y, Bloodgood BL, Hauser JL, Lapan AD, Koon AC, Kim TK, Hu LS, Malik AN, Greenberg ME (2008) Activity-dependent regulation of inhibitory synapse development by Npas4. Nature **455:** 1198–1204

Linden DJ (1994) Long-term synaptic depression in the mammalian brain. Neuron **12:** 457–472

Linden DJ (1996) A protein synthesis-dependent late phase of cerebellar long-term depression. Neuron **17:** 483–490

Lisman J, Yasuda R, Raghavachari S (2012) Mechanisms of CaMKII action in long-term potentiation. Nat Rev Neurosci **13:** 169–182

Lu R, Wang H, Liang Z, Ku L, O'donnell WT, Li W, Warren ST, Feng Y (2004) The fragile X protein controls microtubule-associated protein 1B translation and microtubule stability in brain neuron development. Proc Natl Acad Sci U S A **101:** 15201–15206

Luscher C, Huber KM (2010) Group 1 mGluR-dependent synaptic long-term depression: mechanisms and implications for circuitry and disease. Neuron **65:** 445–459

Lyford GL, Yamagata K, Kaufmann WE, Barnes CA, Sanders LK, Copeland NG, Gilbert DJ, Jenkins NA, Lanahan AA, Worley PF (1995) Arc, a growth factor and activity-regulated gene, encodes a novel cytoskeleton-associated protein that is enriched in neuronal dendrites. Neuron **14:** 433–445

Lynch MA (2004) Long-term potentiation and memory. Physiol Rev **84:** 87–136

Ma C, Li W, Xu Y, Rizo J (2011) Munc13 mediates the transition from the closed syntaxin-Munc18 complex to the SNARE complex. Nat Struct Mol Biol **18:** 542–549

Ma XM, Kiraly DD, Gaier ED, Wang Y, Kim EJ, Levine ES, Eipper BA, Mains RE (2008) Kalirin-7 is required for synaptic structure and function. J Neurosci **28:** 12368–12382

Malenka RC, Bear MF (2004) LTP and LTD: an embarrassment of riches. Neuron **44:** 5–21

Malinow R, Mainen ZF, Hayashi Y (2000) LTP mechanisms: from silence to four-lane traffic. Curr Opin Neurobiol **10:** 352–357

Maroney PA, Yu Y, Fisher J, Nilsen TW (2006) Evidence that microRNAs are associated with translating messenger RNAs in human cells. Nat Struct Mol Biol **13:** 1102–1107

Marrone DF, Schaner MJ, McNaughton BL, Worley PF, Barnes CA (2008) Immediate-early gene expression at rest recapitulates recent experience. J Neurosci **28:** 1030–1033

Mathews, M., Sonenberg, N., and Hershey, J.W.B. (2007). Translational Control in Biology and Medicine (Cold Spring Harbor, N.Y.: Cold Spring Harbor Laboratory Press)

Melner MH, Haas AL, Klein JM, Brash AR, Boeglin WE, Nagdas SK, Winfrey VP, Olson GE (2006) Demonstration of ubiquitin thiolester formation of UBE2Q2 (UBCi), a novel ubiquitin-conjugating enzyme with implantation site-specific expression. Biol Reprod **75:** 395–406

Mili S, Steitz JA (2004) Evidence for reassociation of RNA-binding proteins after cell lysis: implications for the interpretation of immunoprecipitation analyses. RNA **10:** 1692–1694

Miller S, Yasuda M, Coats JK, Jones Y, Martone ME, Mayford M (2002) Disruption of dendritic translation of CaMKIIalpha impairs stabilization of synaptic plasticity and memory consolidation. Neuron **36:** 507–519

Miyashiro KY, Beckel-Mitchener A, Purk TP, Becker KG, Barret T, Liu L, Carbonetto S, Weiler IJ, Greenough WT, Eberwine J (2003) RNA cargoes associating with FMRP reveal deficits in cellular functioning in Fmr1 null mice. Neuron **37:** 417–431

Muddashetty RS, Kelic S, Gross C, Xu M, Bassell GJ (2007) Dysregulated metabotropic glutamate receptor-dependent translation of AMPA receptor and postsynaptic density-95 mRNAs at synapses in a mouse model of fragile X syndrome. J Neurosci **27:** 5338–5348

Muddashetty RS, Nalavadi VC, Gross C, Yao X, Xing L, Laur O, Warren ST, Bassell GJ (2011) Reversible inhibition of PSD-95 mRNA translation by miR-125a, FMRP phosphorylation, and mGluR signaling. Mol Cell **42:** 673–688

Nalavadi VC, Muddashetty RS, Gross C, Bassell GJ (2012) Dephosphorylation-induced ubiquitination and degradation of FMRP in dendrites: a role in immediate early mGluR-stimulated translation. J Neurosci **32:** 2582–2587

Namba T, Nakamuta S, Funahashi Y, Kaibuchi K (2011) The role of selective transport in neuronal polarization. Dev Neurobiol **71:** 445–457

Napoli I, Mercaldo V, Boyl PP, Eleuteri B, Zalfa F, De Rubeis S, Di Marino D, Mohr E, Massimi M, Falconi M, Witke W, Costa-Mattioli M, Sonenberg N, Achsel T, Bagni C (2008) The fragile X syndrome protein represses activity-dependent translation through CYFIP1, a new 4E-BP. Cell **134:** 1042–1054

Narayanan U, Nalavadi V, Nakamoto M, Pallas DC, Ceman S, Bassell GJ, Warren ST (2007) FMRP phosphorylation reveals an immediate-early signaling pathway triggered by group I mGluR and mediated by PP2A. J Neurosci **27:** 14349–14357

Narayanan U, Nalavadi V, Nakamoto M, Thomas G, Ceman S, Bassell GJ, Warren ST (2008) S6K1 phosphorylates and regulates fragile X mental retardation protein (FMRP) with the neuronal protein synthesis-dependent mammalian target of rapamycin (mTOR) signaling cascade. J Biol Chem **283:** 18478–18482

Nelson MD, Fitch DH (2011) Overlap extension PCR: an efficient method for transgene construction. Methods Mol Biol **772:** 459–470

Newey SE, Velamoor V, Govek EE, Van Aelst L (2005) Rho GTPases, dendritic structure, and mental retardation. J Neurobiol **64:** 58–74

Nie D, Di Nardo A, Han JM, Baharanyi H, Kramvis I, Huynh T, Dabora S, Codeluppi S, Pandolfi PP, Pasquale EB, Sahin M (2010) Tsc2-Rheb signaling regulates EphA-mediated axon guidance. Nat Neurosci **13:** 163–172

Niere F, Wilkerson JR, Huber KM (2012) Evidence for a fragile X mental retardation protein-mediated translational switch in metabotropic glutamate receptor-triggered Arc translation and long-term depression. J Neurosci **32:** 5924–5936

Nosyreva ED, Huber KM (2006) Metabotropic receptor-dependent long-term depression persists in the absence of protein synthesis in the mouse model of fragile X syndrome. J Neurophysiol **95:** 3291–3295

Nottrott S, Simard MJ, Richter JD (2006) Human let-7a miRNA blocks protein production on actively translating polyribosomes. Nat Struct Mol Biol **13:** 1108–1114

O'Donnell WT, Warren ST (2002) A decade of molecular studies of fragile X syndrome. Annu Rev Neurosci **25:** 315–338

Ocampo J, Mondragon R, Roa-Espitia AL, Chiquete-Felix N, Salgado ZO, Mujica A (2005) Actin, myosin, cytokeratins and spectrin are components of the guinea pig sperm nuclear matrix. Tissue Cell **37:** 293–308

Ogawa M, Mizugishi K, Ishiguro A, Koyabu Y, Imai Y, Takahashi R, Mikoshiba K, Aruga J (2008) Rines/RNF180, a novel RING finger gene-encoded product, is a membrane-bound ubiquitin ligase. Genes Cells **13:** 397–409

Oinuma I, Ishikawa Y, Katoh H, Negishi M (2004) The Semaphorin 4D receptor Plexin-B1 is a GTPase activating protein for R-Ras. Science **305:** 862–865

Osterweil EK, Krueger DD, Reinhold K, Bear MF (2010) Hypersensitivity to mGluR5 and ERK1/2 leads to excessive protein synthesis in the hippocampus of a mouse model of fragile X syndrome. J Neurosci **30:** 15616–15627

Pante N, Kann M (2002) Nuclear pore complex is able to transport macromolecules with diameters of about 39 nm. Mol Biol Cell **13:** 425–434

Park S, Park JM, Kim S, Kim JA, Shepherd JD, Smith-Hicks CL, Chowdhury S, Kaufmann W, Kuhl D, Ryazanov AG, Huganir RL, Linden DJ, Worley PF (2008) Elongation factor 2 and fragile X mental retardation protein control the dynamic translation of Arc/Arg3.1 essential for mGluR-LTD. Neuron **59:** 70–83

Peier AM, McIlwain KL, Kenneson A, Warren ST, Paylor R, Nelson DL (2000) (Over)correction of FMR1 deficiency with YAC transgenics: behavioral and physical features. Hum Mol Genet **9:** 1145–1159

Peier AM, Nelson DL (2002) Instability of a premutation-sized CGG repeat in FMR1 YAC transgenic mice. Genomics **80:** 423–432

Phan AT, Kuryavyi V, Darnell JC, Serganov A, Majumdar A, Ilin S, Raslin T, Polonskaia A, Chen C, Clain D, Darnell RB, Patel DJ (2011) Structure-function studies of FMRP RGG peptide recognition of an RNA duplex-quadruplex junction. Nat Struct Mol Biol **18:** 796–804

Phelan K, McDermid HE (2012) The 22q13.3 Deletion Syndrome (Phelan-McDermid Syndrome). Mol Syndromol **2:** 186–201

Pilpel Y, Kolleker A, Berberich S, Ginger M, Frick A, Mientjes E, Oostra BA, Seeburg PH (2009) Synaptic ionotropic glutamate receptors and plasticity are developmentally altered in the CA1 field of Fmr1 knockout mice. J Physiol **587:** 787–804

Pinto D, Pagnamenta AT, Klei L, Anney R, Merico D, Regan R, Conroy J, Magalhaes TR, Correia C, Abrahams BS, Almeida J, Bacchelli E, Bader GD, Bailey AJ, Baird G, Battaglia A, Berney T, Bolshakova N, Bolte S, Bolton PF, Bourgeron T, Brennan S, Brian J, Bryson SE, Carson AR, Casallo G, Casey J, Chung BH, Cochrane L, Corsello C, Crawford EL, Crossett A, Cytrynbaum C, Dawson G, de Jonge M, Delorme R, Drmic I, Duketis E, Duque F, Estes A, Farrar P, Fernandez BA, Folstein SE, Fombonne E, Freitag CM, Gilbert J, Gillberg C, Glessner JT, Goldberg J, Green A, Green J, Guter SJ, Hakonarson H, Heron EA, Hill M, Holt R, Howe JL, Hughes G, Hus V, Igliozzi R, Kim C, Klauck SM, Kolevzon A, Korvatska O, Kustanovich V, Lajonchere CM, Lamb JA, Laskawiec M, Leboyer M, Le Couteur A, Leventhal BL, Lionel AC, Liu XQ, Lord C, Lotspeich L, Lund SC, Maestrini E, Mahoney W, Mantoulan C, Marshall CR, McConachie H, McDougle CJ, McGrath J, McMahon WM, Merikangas A, Migita O, Minshew NJ, Mirza GK, Munson J, Nelson SF, Noakes C, Noor A, Nygren G, Oliveira G, Papanikolaou K, Parr JR, Parrini B, Paton T, Pickles A, Pilorge M, Piven J, Ponting CP, Posey DJ, Poustka A, Poustka F, Prasad A, Ragoussis J, Renshaw K, Rickaby J, Roberts W, Roeder K, Roge B, Rutter ML, Bierut LJ, Rice JP, Salt J, Sansom K, Sato D, Segurado R, Sequeira AF, Senman L, Shah N, Sheffield VC, Soorya L, Sousa I, Stein O, Sykes N, Stoppioni V, Strawbridge C, Tancredi R, Tansey K, Thiruvahindrapduram B, Thompson AP, Thomson S, Tryfon A, Tsiantis J, Van Engeland H, Vincent JB, Volkmar F, Wallace S, Wang K, Wang Z, Wassink TH, Webber C, Weksberg R, Wing K, Wittemeyer K, Wood S, Wu J, Yaspan BL, Zurawiecki D, Zwaigenbaum L, Buxbaum JD, Cantor RM, Cook EH, Coon H, Cuccaro ML, Devlin B, Ennis S, Gallagher L, Geschwind DH, Gill M, Haines JL, Hallmayer J, Miller J, Monaco AP, Nurnberger JIJ, Paterson AD, Pericak-Vance MA, Schellenberg GD, Szatmari P, Vicente AM, Vieland VJ, Wijsman EM, Scherer SW, Sutcliffe JS, Betancur C (2010) Functional impact of global rare copy number variation in autism spectrum disorders. Nature **466:** 368–372

Plante I, Davidovic L, Ouellet DL, Gobeil LA, Tremblay S, Khandjian EW, Provost P (2006) Dicer-derived microRNAs are utilized by the fragile X mental retardation protein for assembly on target RNAs. J Biomed Biotechnol **2006:** 64347

Plath N, Ohana O, Dammermann B, Errington ML, Schmitz D, Gross C, Mao X, Engelsberg A, Mahlke C, Welzl H, Kobalz U, Stawrakakis A, Fernandez E, Waltereit R, Bick-Sander A, Therstappen E, Cooke SF, Blanquet V, Wurst W, Salmen B, Bosl MR, Lipp HP, Grant SG, Bliss TV, Wolfer DP, Kuhl D (2006) Arc/Arg3.1 is essential for the consolidation of synaptic plasticity and memories. Neuron **52:** 437–444

Polymenidou M, Lagier-Tourenne C, Hutt KR, Huelga SC, Moran J, Liang TY, Ling SC, Sun E, Wancewicz E, Mazur C, Kordasiewicz H, Sedaghat Y, Donohue JP, Shiue L, Bennett CF, Yeo GW, Cleveland DW (2011) Long pre-mRNA depletion and RNA missplicing contribute to neuronal vulnerability from loss of TDP-43. Nat Neurosci **14:** 459–468

Porter K, Komiyama NH, Vitalis T, Kind PC, Grant SG (2005) Differential expression of two NMDA receptor interacting proteins, PSD-95 and SynGAP during mouse development. Eur J Neurosci **21:** 351–362

Potter MD, Nicchitta CV (2000) Regulation of ribosome detachment from the mammalian endoplasmic reticulum membrane. J Biol Chem **275:** 33828–33835

Price DK, Zhang F, Ashley CTJ, Warren ST (1996) The chicken FMR1 gene is highly conserved with a CCT 5'-untranslated repeat and encodes an RNA-binding protein. Genomics **31:** 3–12

Qin M, Kang J, Burlin TV, Jiang C, Smith CB (2005) Postadolescent changes in regional cerebral protein synthesis: an in vivo study in the FMR1 null mouse. J Neurosci **25:** 5087–5095

Rabani M, Levin JZ, Fan L, Adiconis X, Raychowdhury R, Garber M, Gnirke A, Nusbaum C, Hacohen N, Friedman N, Amit I, Regev A (2011) Metabolic labeling of RNA uncovers principles of RNA production and degradation dynamics in mammalian cells. Nat Biotechnol **29:** 436–442

Ramamoorthi K, Fropf R, Belfort GM, Fitzmaurice HL, McKinney RM, Neve RL, Otto T, Lin Y (2011) Npas4 regulates a transcriptional program in CA3 required for contextual memory formation. Science **334:** 1669–1675

Ray RS, Corcoran AE, Brust RD, Kim JC, Richerson GB, Nattie E, Dymecki SM (2011) Impaired respiratory and body temperature control upon acute serotonergic neuron inhibition. Science **333:** 637–642

Richter JD, Klann E (2009) Making synaptic plasticity and memory last: mechanisms of translational regulation. Genes Dev **23:** 1–11

Rodemer C, Haucke V (2008) Clathrin/AP-2-dependent endocytosis: a novel playground for the pharmacological toolbox? Handb Exp Pharmacol 105–122

Ronesi JA, Collins KA, Hays SA, Tsai NP, Guo W, Birnbaum SG, Hu JH, Worley PF, Gibson JR, Huber KM (2012) Disrupted Homer scaffolds mediate abnormal mGluR5 function in a mouse model of fragile X syndrome. Nat Neurosci **15:** 431–40, S1

Rudelli RD, Brown WT, Wisniewski K, Jenkins EC, Laure-Kamionowska M, Connell F, Wisniewski HM (1985) Adult fragile X syndrome. Clinico-neuropathologic findings. Acta Neuropathol **67:** 289–295

Rumbaugh G, Adams JP, Kim JH, Huganir RL (2006) SynGAP regulates synaptic strength and mitogen-activated protein kinases in cultured neurons. Proc Natl Acad Sci U S A **103:** 4344–4351

Sanz E, Yang L, Su T, Morris DR, McKnight GS, Amieux PS (2009) Cell-type-specific isolation of ribosome-associated mRNA from complex tissues. Proc Natl Acad Sci U S A **106:** 13939–13944

Scheetz AJ, Nairn AC, Constantine-Paton M (2000) NMDA receptor-mediated control of protein synthesis at developing synapses. Nat Neurosci **3:** 211–216

Schenck A, Bardoni B, Moro A, Bagni C, Mandel JL (2001) A highly conserved protein family interacting with the fragile X mental retardation protein (FMRP) and displaying selective interactions with FMRP-related proteins FXR1P and FXR2P. Proc Natl Acad Sci U S A **98:** 8844–8849

Schnell E, Sizemore M, Karimzadegan S, Chen L, Bredt DS, Nicoll RA (2002) Direct interactions between PSD-95 and stargazin control synaptic AMPA receptor number. Proc Natl Acad Sci U S A **99:** 13902–13907

Schratt GM, Tuebing F, Nigh EA, Kane CG, Sabatini ME, Kiebler M, Greenberg ME (2006) A brain-specific microRNA regulates dendritic spine development. Nature **439:** 283–289

Schutt J, Falley K, Richter D, Kreienkamp HJ, Kindler S (2009) Fragile X mental retardation protein regulates the levels of scaffold proteins and glutamate receptors in postsynaptic densities. J Biol Chem **284:** 25479–25487

Seiser RM, Nicchitta CV (2000) The fate of membrane-bound ribosomes following the termination of protein synthesis. J Biol Chem **275:** 33820–33827

Sharma A, Hoeffer CA, Takayasu Y, Miyawaki T, McBride SM, Klann E, Zukin RS (2010) Dysregulation of mTOR signaling in fragile X syndrome. J Neurosci **30:** 694–702

Sharova LV, Sharov AA, Nedorezov T, Piao Y, Shaik N, Ko MS (2009) Database for mRNA half-life of 19 977 genes obtained by DNA microarray analysis of pluripotent and differentiating mouse embryonic stem cells. DNA Res **16:** 45–58

Shashoua VE (1976) Identification of specific changes in the pattern of brain protein synthesis after training. Science **193:** 1264–1266

Silva JP, Lelianova VG, Ermolyuk YS, Vysokov N, Hitchen PG, Berninghausen O, Rahman MA, Zangrandi A, Fidalgo S, Tonevitsky AG, Dell A, Volynski KE, Ushkaryov YA (2011) Latrophilin 1 and its endogenous ligand Lasso/teneurin-2 form a high-affinity transsynaptic receptor pair with signaling capabilities. Proc Natl Acad Sci U S A **108:** 12113–12118

Siomi H, Matunis MJ, Michael WM, Dreyfuss G (1993a) The pre-mRNA binding K protein contains a novel evolutionarily conserved motif. Nucleic Acids Res **21:** 1193–1198

Siomi H, Siomi MC, Nussbaum RL, Dreyfuss G (1993b) The protein product of the fragile X gene, FMR1, has characteristics of an RNA-binding protein. Cell **74:** 291–298

Siomi MC, Higashijima K, Ishizuka A, Siomi H (2002) Casein kinase II phosphorylates the fragile X mental retardation protein and modulates its biological properties. Mol Cell Biol **22:** 8438–8447

Siomi MC, Zhang Y, Siomi H, Dreyfuss G (1996) Specific sequences in the fragile X syndrome protein FMR1 and the FXR proteins mediate their binding to 60S ribosomal subunits and the interactions among them. Mol Cell Biol **16:** 3825–3832

Sivan G, Kedersha N, Elroy-Stein O (2007) Ribosomal slowdown mediates translational arrest during cellular division. Mol Cell Biol **27:** 6639–6646

Soden ME, Chen L (2010) Fragile X protein FMRP is required for homeostatic plasticity and regulation of synaptic strength by retinoic acid. J Neurosci **30:** 16910–16921

Somogyi P, Jenner AJ, Brierley I, Inglis SC (1993) Ribosomal pausing during translation of an RNA pseudoknot. Mol Cell Biol **13:** 6931–6940

Spencer CM, Serysheva E, Yuva-Paylor LA, Oostra BA, Nelson DL, Paylor R (2006) Exaggerated behavioral phenotypes in Fmr1/Fxr2 double knockout mice reveal a functional genetic interaction between Fragile X-related proteins. Hum Mol Genet **15:** 1984–1994

Stanton PK, Sarvey JM (1984) Blockade of long-term potentiation in rat hippocampal CA1 region by inhibitors of protein synthesis. J Neurosci **4:** 3080–3088

Stebbins-Boaz B, Cao Q, de Moor CH, Mendez R, Richter JD (1999) Maskin is a CPEB-associated factor that transiently interacts with elF-4E. Mol Cell **4:** 1017–1027

Stefani G, Fraser CE, Darnell JC, Darnell RB (2004) Fragile X mental retardation protein is associated with translating polyribosomes in neuronal cells. J Neurosci **24:** 7272–7276

Steinberg JP, Takamiya K, Shen Y, Xia J, Rubio ME, Yu S, Jin W, Thomas GM, Linden DJ, Huganir RL (2006) Targeted in vivo mutations of the AMPA receptor subunit GluR2 and its interacting protein PICK1 eliminate cerebellar long-term depression. Neuron **49:** 845–860

Steward O, Bakker CE, Willems PJ, Oostra BA (1998a) No evidence for disruption of normal patterns of mRNA localization in dendrites or dendritic transport of recently synthesized mRNA in FMR1 knockout mice, a model for human fragile-X mental retardation syndrome. Neuroreport **9:** 477–481

Steward O, Wallace CS, Lyford GL, Worley PF (1998b) Synaptic activation causes the mRNA for the IEG Arc to localize selectively near activated postsynaptic sites on dendrites. Neuron **21:** 741–751

Sudhof TC (2008) Neuroligins and neurexins link synaptic function to cognitive disease. Nature **455:** 903–911

Sung YJ, Dolzhanskaya N, Nolin SL, Brown T, Currie JR, Denman RB (2003) The fragile X mental retardation protein FMRP binds elongation factor 1A mRNA and negatively regulates its translation in vivo. J Biol Chem **278:** 15669–15678

Sutton MA, Taylor AM, Ito HT, Pham A, Schuman EM (2007) Postsynaptic decoding of neural activity: eEF2 as a biochemical sensor coupling miniature synaptic transmission to local protein synthesis. Neuron **55:** 648–661

Takeuchi M, Hata Y, Hirao K, Toyoda A, Irie M, Takai Y (1997) SAPAPs. A family of PSD-95/SAP90-associated proteins localized at postsynaptic density. J Biol Chem **272:** 11943–11951

Tamanini F, Van Unen L, Bakker C, Sacchi N, Galjaard H, Oostra BA, Hoogeveen AT (1999) Oligomerization properties of fragile-X mental-retardation protein (FMRP) and the fragile-X-related proteins FXR1P and FXR2P. Biochem J **343 Pt 3:** 517–523

Tang SJ, Reis G, Kang H, Gingras AC, Sonenberg N, Schuman EM (2002) A rapamycin-sensitive signaling pathway contributes to long-term synaptic plasticity in the hippocampus. Proc Natl Acad Sci U S A **99:** 467–472

Tarn WY, Chang TH (2009) The current understanding of Ded1p/DDX3 homologs from yeast to human. RNA Biol **6:** 17–20

Teplova M, Malinina L, Darnell JC, Song J, Lu M, Abagyan R, Musunuru K, Teplov A, Burley SK, Darnell RB, Patel DJ (2011) Protein-RNA and protein-protein recognition by dual KH1/2 domains of the neuronal splicing factor Nova-1. Structure **19:** 930–944

Thermann R, Hentze MW (2007) Drosophila miR2 induces pseudo-polysomes and inhibits translation initiation. Nature **447:** 875–878

Tierney E, Nwokoro NA, Kelley RI (2000) Behavioral phenotype of RSH/Smith-Lemli-Opitz syndrome. Ment Retard Dev Disabil Res Rev **6:** 131–134

Tierney E, Nwokoro NA, Porter FD, Freund LS, Ghuman JK, Kelley RI (2001) Behavior phenotype in the RSH/Smith-Lemli-Opitz syndrome. Am J Med Genet **98:** 191–200

Todd PK, Mack KJ, Malter JS (2003) The fragile X mental retardation protein is required for type-I metabotropic glutamate receptor-dependent translation of PSD-95. Proc Natl Acad Sci U S A **100:** 14374–14378

Tolias KF, Duman JG, Um K (2011) Control of synapse development and plasticity by Rho GTPase regulatory proteins. Prog Neurobiol **94:** 133–148

Trinh, M.A., Kaphzan, H., Wek, R.C., Pierre, P., Cavener, D.R., Klann, E. (2012). Brain-Specific Disruption of the eIF2a Kinase PERK Decreases ATF4 Expression and Impairs Behavioral Flexibility, Cell Reports , doi:10.1016/j.celrep.2012.04.010

Turrigiano GG (2008) The self-tuning neuron: synaptic scaling of excitatory synapses. Cell **135:** 422–435

Unsworth H, Raguz S, Edwards HJ, Higgins CF, Yague E (2010) mRNA escape from stress granule sequestration is dictated by localization to the endoplasmic reticulum. FASEB J **24:** 3370–3380

Vandesompele J, De Preter K, Pattyn F, Poppe B, Van Roy N, De Paepe A, Speleman F (2002) Accurate normalization of real-time quantitative RT-PCR data by geometric averaging of multiple internal control genes. Genome Biol **3:** RESEARCH0034

Varoqueaux F, Aramuni G, Rawson RL, Mohrmann R, Missler M, Gottmann K, Zhang W, Sudhof TC, Brose N (2006) Neuroligins determine synapse maturation and function. Neuron **51:** 741–754

Vattem KM, Wek RC (2004) Reinitiation involving upstream ORFs regulates ATF4 mRNA translation in mammalian cells. Proc Natl Acad Sci U S A **101:** 11269–11274

Vazdarjanova A, McNaughton BL, Barnes CA, Worley PF, Guzowski JF (2002) Experience-dependent coincident expression of the effector immediate-early genes arc and Homer 1a in hippocampal and neocortical neuronal networks. J Neurosci **22:** 10067–10071

Visa N, Alzhanova-Ericsson AT, Sun X, Kiseleva E, Bjorkroth B, Wurtz T, Daneholt B (1996) A pre-mRNA-binding protein accompanies the RNA from the gene through the nuclear pores and into polysomes. Cell **84:** 253–264

Voeltz GK, Rolls MM, Rapoport TA (2002) Structural organization of the endoplasmic reticulum. EMBO Rep **3:** 944–950

Volk LJ, Pfeiffer BE, Gibson JR, Huber KM (2007) Multiple Gq-coupled receptors converge on a common protein synthesis-dependent long-term depression that is affected in fragile X syndrome mental retardation. J Neurosci **27:** 11624–11634

Wallace CS, Lyford GL, Worley PF, Steward O (1998) Differential intracellular sorting of immediate early gene mRNAs depends on signals in the mRNA sequence. J Neurosci **18:** 26–35

Wan L, Dockendorff TC, Jongens TA, Dreyfuss G (2000) Characterization of dFMR1, a Drosophila melanogaster homolog of the fragile X mental retardation protein. Mol Cell Biol **20:** 8536–8547

Wang DO, Martin KC, Zukin RS (2010) Spatially restricting gene expression by local translation at synapses. Trends Neurosci **33:** 173–182

Wang H, Dictenberg JB, Ku L, Li W, Bassell GJ, Feng Y (2008) Dynamic association of the fragile X mental retardation protein as a messenger ribonucleoprotein between microtubules and polyribosomes. Mol Biol Cell **19:** 105–114

Wang H, Iacoangeli A, Lin D, Williams K, Denman RB, Hellen CU, Tiedge H (2005) Dendritic BC1 RNA in translational control mechanisms. J Cell Biol **171:** 811–821

Wang H, Ku L, Osterhout DJ, Li W, Ahmadian A, Liang Z, Feng Y (2004) Developmentally-programmed FMRP expression in oligodendrocytes: a potential role of FMRP in regulating translation in oligodendroglia progenitors. Hum Mol Genet **13:** 79–89

Waung MW, Pfeiffer BE, Nosyreva ED, Ronesi JA, Huber KM (2008) Rapid translation of Arc/Arg3.1 selectively mediates mGluR-dependent LTD through persistent increases in AMPAR endocytosis rate. Neuron **59:** 84–97

Weiler IJ, Irwin SA, Klintsova AY, Spencer CM, Brazelton AD, Miyashiro K, Comery TA, Patel B, Eberwine J, Greenough WT (1997) Fragile X mental retardation protein is translated near synapses in response to neurotransmitter activation. Proc Natl Acad Sci U S A **94:** 5395–5400

Wild K, Halic M, Sinning I, Beckmann R (2004) SRP meets the ribosome. Nat Struct Mol Biol **11:** 1049–1053

Willemsen R, Bontekoe C, Tamanini F, Galjaard H, Hoogeveen A, Oostra B (1996) Association of FMRP with ribosomal precursor particles in the nucleolus. Biochem Biophys Res Commun **225:** 27–33

Wolin SL, Walter P (1988) Ribosome pausing and stacking during translation of a eukaryotic mRNA. EMBO J **7:** 3559–3569

Woolfrey KM, Srivastava DP, Photowala H, Yamashita M, Barbolina MV, Cahill ME, Xie Z, Jones KA, Quilliam LA, Prakriya M, Penzes P (2009) Epac2 induces synapse remodeling and depression and its disease-associated forms alter spines. Nat Neurosci **12:** 1275–1284

Xiao B, Tu JC, Petralia RS, Yuan JP, Doan A, Breder CD, Ruggiero A, Lanahan AA, Wenthold RJ, Worley PF (1998) Homer regulates the association of group 1 metabotropic glutamate receptors with multivalent complexes of homer-related, synaptic proteins. Neuron **21:** 707–716

Yamagata K, Kaufmann WE, Lanahan A, Papapavlou M, Barnes CA, Andreasson KI, Worley PF (1994a) Egr3/Pilot, a zinc finger transcription factor, is rapidly regulated by activity in brain neurons and colocalizes with Egr1/zif268. Learn Mem **1:** 140–152

Yamagata K, Sanders LK, Kaufmann WE, Yee W, Barnes CA, Nathans D, Worley PF (1994b) rheb, a growth factor- and synaptic activity-regulated gene, encodes a novel Ras-related protein. J Biol Chem **269:** 16333–16339

Ye B, Liao D, Zhang X, Zhang P, Dong H, Huganir RL (2000) GRASP-1: a neuronal RasGEF associated with the AMPA receptor/GRIP complex. Neuron **26:** 603–617

Ye X, Carew TJ (2010) Small G protein signaling in neuronal plasticity and memory formation: the specific role of ras family proteins. Neuron **68:** 340–361

Yeo GW, Coufal NG, Liang TY, Peng GE, Fu XD, Gage FH (2009) An RNA code for the FOX2 splicing regulator revealed by mapping RNA-protein interactions in stem cells. Nat Struct Mol Biol **16:** 130–137

Young KG, Kothary R (2005) Spectrin repeat proteins in the nucleus. Bioessays **27:** 144–152

Young KG, Kothary R (2008) Dystonin/Bpag1 is a necessary endoplasmic reticulum/nuclear envelope protein in sensory neurons. Exp Cell Res **314:** 2750–2761

Young KG, Pinheiro B, Kothary R (2006) A Bpag1 isoform involved in cytoskeletal organization surrounding the nucleus. Exp Cell Res **312:** 121–134

Zalfa F, Adinolfi S, Napoli I, Kuhn-Holsken E, Urlaub H, Achsel T, Pastore A, Bagni C (2005) Fragile X mental retardation protein (FMRP) binds specifically to the brain cytoplasmic RNAs BC1/BC200 via a novel RNA-binding motif. J Biol Chem **280:** 33403–33410

Zalfa F, Eleuteri B, Dickson KS, Mercaldo V, De Rubeis S, di Penta A, Tabolacci E, Chiurazzi P, Neri G, Grant SG, Bagni C (2007) A new function for the fragile X mental retardation protein in regulation of PSD-95 mRNA stability. Nat Neurosci **10:** 578–587

Zalfa F, Giorgi M, Primerano B, Moro A, Di Penta A, Reis S, Oostra B, Bagni C (2003) The fragile X syndrome protein FMRP associates with BC1 RNA and regulates the translation of specific mRNAs at synapses. Cell **112:** 317–327

Zang JB, Nosyreva ED, Spencer CM, Volk LJ, Musunuru K, Zhong R, Stone EF, Yuva-Paylor LA, Huber KM, Paylor R, Darnell JC, Darnell RB (2009) A mouse model of the human Fragile X syndrome I304N mutation. PLoS Genet **5:** e1000758

Zhang C, Frias MA, Mele A, Ruggiu M, Eom T, Marney CB, Wang H, Licatalosi DD, Fak JJ, Darnell RB (2010) Integrative modeling defines the Nova splicing-regulatory network and its combinatorial controls. Science **329:** 439–443

Zhang Y, O'Connor JP, Siomi MC, Srinivasan S, Dutra A, Nussbaum RL, Dreyfuss G (1995) The fragile X mental retardation syndrome protein interacts with novel homologs FXR1 and FXR2. EMBO J **14:** 5358–5366

Zhang Y, Venkitaramani DV, Gladding CM, Zhang Y, Kurup P, Molnar E, Collingridge GL, Lombroso PJ (2008) The tyrosine phosphatase STEP mediates AMPA receptor endocytosis after metabotropic glutamate receptor stimulation. J Neurosci **28:** 10561–10566

Zhang YQ, Bailey AM, Matthies HJ, Renden RB, Smith MA, Speese SD, Rubin GM, Broadie K (2001) Drosophila fragile X-related gene regulates the MAP1B homolog Futsch to control synaptic structure and function. Cell **107:** 591–603

Zhao W, Chuang SC, Bianchi R, Wong RK (2011) Dual regulation of fragile X mental retardation protein by group I metabotropic glutamate receptors controls translation-dependent epileptogenesis in the hippocampus. J Neurosci **31:** 725–734

Zheng CY, Petralia RS, Wang YX, Kachar B, Wenthold RJ (2010) SAP102 is a highly mobile MAGUK in spines. J Neurosci **30:** 4757–4766